POLITECNICO DI MILANO

ENERGY DEPARTMENT

DOCTORAL PROGRAM IN:

ENERGY AND NUCLEAR SCIENCE AND TECHNOLOGY

Optimal Operation of Microgrids and Multi-Energy Systems Accounting for Forecast Uncertainty

Author: Luca Moretti

Supervisor: Giampaolo Manzolini

Co-Supervisor: Emanuele Martelli

Tutor: Stefano Campanari

2019 – XXXI Cycle

Abstract

Microgrids and Multi-Energy Systems (MES) are emerging more and more as fundamental elements in the undergoing transition towards cleaner and more sustainable energy systems. The key feature that makes microgrids and MES appealing is that they can harvest in a capillary way the degrees of freedom offered by Distributed Energy Resources (DER), to coordinately manage them in order to improve overall system efficiency. Furthermore, in virtue of their operational flexibility, microgrids are particularly suited for the integration of non-dispatchable Renewable Energy Sources (RES) in the generation mix, since they can more effectively cope with their intermittent nature.

This thesis focuses on the development of optimization algorithms, based on Mixed Integer Linear Programming (MILP), for the central strategic controller of microgrids and MES, often referred to as Energy Management System (EMS). Formal scheduling optimization, based on the forecasts of load and RES generation, is very effective in reducing the system overall operating cost and in allowing for higher renewable penetration. On the other hand, predictive scheduling optimization must account for the non-deterministic nature of forecasts, to ensure safe real-time system operation. Two alternative MILP formulations of the scheduling problem are therefore proposed and numerically tested: a deterministic formulation, indirectly accounting for forecast uncertainty through the introduction of spinning reserve constraints, and a more advanced formulation based on the Affinely Adjustable Robust Optimization (AARO) theory, which explicitly addresses uncertainty by defining optimal decision rules that prescribe adjustments to the dispatch solution as a function of the observed forecast errors.

The two formulations are compared in an extensive numerical analysis, accounting for three real-life case studies representative of on- and off-grid systems. Different EMS featuring the two formulations are proposed and numerically tested, under various assumptions on the capabilities and the architecture of the control system. The comparison highlights how the AARO formulation is particularly suited for applications where forecast uncertainty is high and the possibility of modifying commitment decisions during real-time operation is limited.

Based on the developed deterministic problem formulation, a two-layers EMS is proposed for off-grid electric hybrid microgrids, comprising a set of dispatchable generators, a battery stack, and a PV field. The EMS is suited for the minute-by-minute microgrid control, featuring a second layer compatible with direct implementation on the system Programmable Logic Controller (PLC). The proposed EMS is compared with an EMS provided by the industrial partner ENGIE Eps, demonstrating its potential in attaining better economic performance while at the same time increasing the share of renewable energy generation.

Finally, a MILP-based algorithm for the optimal design and management of off-grid microgrids is proposed, for application to regional electrification planning. The algorithm identifies the best microgrid design by selecting components from a discrete catalog of models, accounting for their expected optimal scheduling profiles and considering the effect of dispatch decisions on components wearing. The comparison with a heuristic algorithm developed by the MIT Universal Energy Lab confirms once more the potential of the MILP-based approach, both in terms of cost reduction and renewable penetration increase.

Sommario

Le microreti e i sistemi Multi-Energy (SME) si stanno affermando sempre di più come potenziali elementi chiave nella transizione verso un sistema energetico più pulito e sostenibile. La caratteristica fondamentale di microreti e SME è la possibilità di sfruttare in maniera capillare i gradi di libertà offerti dalle Risorse Energetiche Distribuite (RED), controllandole in maniera coordinata al fine di migliorare l'efficienza complessiva del sistema. Inoltre, grazie alla loro flessibilità operativa, le microreti sono particolarmente adatte per l'integrazione nel mix energetico di Fonti di Generazione Rinnovabile (FGR) non controllabili, poichè possono più efficacemente gestire la loro natura intermittente.

Questo lavoro di Tesi tratta lo sviluppo di algoritmi di ottimizzazione basati sulla Programmazione Mista Lineare Intera (PMLI), da integrarsi nel controllore strategico centrale di microreti e SME, normalmente definito Energy Management System (EMS). L'ottimizzazione formale della gestione di risorse, basata sulle previsioni di generazione da FGR e di carico, può garantire significative vantaggi in termini di riduzione dei costi operativi, e può consentire il raggiungimento di più alti livelli di penetrazione da rinnovabile. L'ottimizzazione predittiva della gestione deve però fare i conti con la natura non deterministica delle previsioni, in modo da garantire un affidabile funzionamento del sistema. Per questa ragione, due formulazioni PMLI alternative del problema di pianificazione della gestione sono proposte e testate numericamente: una formulazione deterministica, che considera in maniera indiretta l'incertezza attraverso l'adizione di vincoli di riserva, e una formulazione più avanzata basata sulla tecnica dell'ottimizzazione robusta affine, che tratta esplicitamente l'incertezza identificando delle regole di correzione per adattare i profili di dispacciamento a seconda degli errori di previsione osservati.

Le due formulazioni sono confrontate per mezzo di una estesa campagna di simulazioni, considerando tre casi studio rappresentativi di sistemi reali, sia in isola che connessi alla rete. Diversi EMS basati sulle due formulazioni sono proposti e testati numericamente, considerando una varietà di assunzioni sulle capacità e sulla struttura del sistema di controllo. Il confronto dimostra come la formulazione robusta è particolarmente adatta ad applicazioni in cui l'incertezza delle previsioni è alta, e dove la possibilità di modificare in tempo reale lo stato operativo delle unità è limitata.

Sulla base della formulazione deterministica sviluppata, si è poi proposto un EMS a due livelli per la gestione di microreti elettriche ibride. L'EMS proposto è stato confrontato con un EMS fornito dal partner industriale ENGIE Eps, dimostrando come il primo sia potenzialmente in grado di garantire un miglior risultato economico e di aumentare allo stesso tempo la penetrazione da fonte rinnovabile.

Infine, si è sviluppato un algoritmo basato su PMLI per l'ottimizzazione del design e della gestione di microreti in isola, da utilizzarsi nel contesto della pianificazione dell'elettrificazione di regioni. L'algoritmo è in grado di indentificare il miglior progetto di microrete selezionando i componenti da un catalogo discreto di modelli, considerando il loro profilo atteso di funzionamento e l'effetto delle decisioni di dispacciamento sull'usura di alcuni dei componenti. L'algoritmo è stato confrontato con un analogo euristico sviluppato dal MIT Universal Energy Access Lab, confermando ancora una volta il potenziale dell'approccio PMLI sia in termidi di riduzione di costo che di aumento della penetrazione rinnovabile.

Acknowledgments

I would like to thank the following people, who significantly contributed to this work. My supervisor Prof. Giampaolo Manzolini, for his advice and for granting me full liberty of pursuing my research interests, and my co-supervisor Prof. Emanuele Martelli, for his precious support and vast experience on the mathematical subjects. Dr. Pietro Raboni and the industrial partner ENGIE Eps, who supported the research activities and provided invaluable data and technical experience. The industrial partner SIRAM, for their support on the CHP case studies. Prof. Ignacio Perez-Arriaga, for hosting me at the MIT Universal Energy Access Lab, and Dr. Claudio Vergara, with whom was a pleasure to collaborate while in Boston. The Rocca Foundation, for sponsoring the visiting period at MIT.

And then, I would like to thank all the amazing people I had the privilege to meet and work with during these years. My office mates, without whom everything would have been simpler and extremely boring, with a special mention to Sonia, her snacks drawer, and her capacity to listen. Simone and Lorenzo, amazing co-workers and supportive friends. Asto, Bino and the fabulous Joster, for the free and vital therapy sessions. The Gechini and the entire GECOS group. And finally, the most important acknowledgment goes to my parents, for coping with me and my work stress and for always having my back.

It has been fun. Let’s not do this again.

CONTENTS

1 INTRODUCTION 11
2 MICROGRIDS AND MULTI-ENERGY SYSTEMS 15
2.1 Off-grid Microgrids 16
2.2 On-grid Microgrids 17
2.3 Microgrids Control 18
2.4 Centralized approaches to microgrid management 20
2.5 Scheduling Optimization based on Mixed Integer Linear Programming 21
3 DETERMINISTIC SCHEDULING PROBLEM FORMULATION 24
3.1 Problem Statement 24
3.2 Multi-Energy System Architecture 26
3.3 Objective function 26
3.4 Components Modeling 27
3.4.1 Controllable units 27
3.4.2 Non-dispatchable Units 32
3.4.3 Storages 32
3.4.4 Networks 34
3.4.5 Connectors 34
3.4.6 Loads and Generation Balance 35
3.5 Reserve Constraints 37
3.6 Topology 38
3.7 System modeling example: household featuring Solar Assisted Heat Pump 38
4 AFFINELY ADJUSTABLE ROBUST SCHEDULING PROBLEM FORMULATION 42
4.1 Problem Statement 43
4.2 Adjustable Robust Problem Formulation 45
4.2.1 Uncertain data: energy demand and non-dispatchable production 45
4.2.2 Controllable machines 46
4.2.3 Energy storages and networks: 46
4.2.4 Energy balance 47
4.2.5 Objective function: 48

4.3 Tractable Reformulation of AARC 50
4.3.1 Deterministic constraints 53
4.3.2 Uncertain Equalities 54
4.3.3 Uncertain Inequalities 54
4.4 Uncertainty set definition 55
4.5 Limitations of the Affine Decision Rules 56
4.5.1 Improper modeling of recursive battery efficiency 57
4.5.2 Over-conservative decision rules for poly-generation units 58
4.5.3 Use of quick-start units 61
4.5.4 Dynamic Constraints 61
4.6 Model Adjustments 62
4.6.1 Partial-past recourse 62
4.6.2 Uncertainty factors aggregation 63
5 DAY-AHEAD OPERATION SCHEDULING 66
5.1 Test Cases Definition 68
5.2 Forecast Profiles and Uncertainty Characterization 70
5.3 Deterministic Problem Formulation 72
5.4 Rule-based Second Layer EMS 72
5.4.1 Rule-based second layer algorithm for off-grid microgrid 73
5.4.2 Rule-based second layer algorithm for grid-connected multi-energy systems 75
5.4.3 Off-Grid Electric Microgrid Results 76
5.4.4 Grid-Connected CHP Systems Results 79
5.5 MILP-based Second Layer EMS 85
5.5.1 Second Layer MILP Formulation 86
5.5.2 Robust and Deterministic Model Adaptations for Quick-Start Units 89
5.5.3 Off-Grid Electric Microgrid Results 91
5.5.4 Hospital Results 95
5.5.5 Campus Results 100
5.6 Conclusions 103
6 OPERATION SCHEDULING ACCORDING TO ROLLING HORIZON APPROACH 105

6.1 Case Study Definition 106
6.2 Introduction of Variable Time Mesh 108
6.3 Wind Forecast and Uncertainty 109
6.4 Simulation Results 111
6.5 Conclusions 114
7 TWO LAYERS DETERMINISTIC EMS FOR REAL-TIME CONTROL OF HYBRID OFF GRID ELECTRIC MICROGRIDS 115
7.1 Microgrid Architecture 116
7.2 Hierarchical EMS Structure 117
7.2.1 Forecast Generation Module 117
7.3 First Layer: Optimal Unit Commitment 118
7.3.1 Modeling Assumptions 118
7.3.2 First layer output 120
7.3.3 Second Layer: Dispatch Update 120
7.4 Heuristic EMS 122
7.4.1 Comparison with HOMER Load Following strategy 123
7.5 Case Study Definition 124
7.5.1 Microgrid Characteristics 124
7.5.2 Forecasting Methods 126
7.5.3 Economic Performance Indexes 128
7.6 Simulation Results 129
7.6.1 Hierarchical Control Testing 129
7.6.2 Garowe Current Design 130
7.6.3 New Design 132
7.7 Conclusions 135
8 DESIGN OPTIMIZATION OF RURAL OFF-GRID MICROGRIDS 137
8.1 Microgrid Design optimization algorithms 138
8.2 Hybrid Microgrid Architecture 140
8.3 Microgrid design optimization 143
8.3.1 Design objective function 145

8.4 MILP Design Problem Formulation 146
8.4.1 Annuitization of variable life-time components in PA 146
8.4.2 Modeling Assumptions 147
8.4.3 Spinning reserve requirements 152
8.5 PA Operation sub-problem 153
8.6 Heuristic design algorithm (HA) 153
8.7 Comparison of HA and PA design and operation 155
8.8 Conclusions 160
9 CONCLUSIONS 162
9.1 Future works 165
10 REFERENCES 167

1 INTRODUCTION

The threat posed by climate change to the environmental stability of our Planet is becoming more and more apparent as years go by. The alarming reports of the International Panel on Climate Change [1], collecting all scientific findings that indicate the anthropogenic cause of climate change and describing the expected effects of global warming, well attest the urgency for an immediate and effective transition to a cleaner and sustainable economy.

The scenarios [2] that aim at limiting the average planet temperature increase below 2°C (the threshold above which most of the severe consequences of climate change turn from likely to almost certain [3]) call for a dramatic reduction in the emission of greenhouse gases, to be achieved within a few decades from now. This implies a disruptive reshape of the primary energy supply mix, with a phase-out of fossil fuels in favor of zero-emissions technologies and Renewable Energy Sources (RES) which should affect all sectors of energy consumption. A major contribution is also expected from improvements in energy conversion and utilization efficiency, which already have a fundamental role in reducing the impact of yearly energy demand increase: according to the International Energy Agency [2], improvements in energy efficiency already have the merit of cutting by 50% the expansion rate of global primary energy demand, which is nevertheless predicted to grow by 25% within 2040. In fully developed economies, improvements in the efficiency of energy production and usage have already stabilized primary energy demand, decoupling economic growth indexes and gross energy consumption [2]. New regulations on energy efficiency and the adoption of more advanced technological solutions have been the keys in attaining this important result. Energy consumption increase is therefore mainly driven by developing countries where per capita energy consumption is still very low [4]. India leads the ranks, with the country primary energy demand that is expected to more than double by 2040, while China follows close behind, although its need for additional energy is growing at a slowing pace [2]. In third place for expected primary energy consumption increase is Africa, where the industrialization rate has yet to fully trigger. Supporting in a sustainable way the socio-economical and industrial growth of developing countries will, therefore, be one of the huge challenges of this century: as opposed to developed nations, which can now aim at cutting emissions after a century of unregulated and fossil fuel-based industrial development, developing nations will rapidly need to find a balance between supporting their economic expansion and dealing with the consequences of environmentally non-sustainable development.

The power sector is expected to lead the energy decarbonization process. Currently, electricity generation accounts for about one-third of global CO2 emissions, and about 40% of global primary energy consumption [5]. This share appears to be destined to grow, as electricity might become a preferential vector to meet final energy needs, primarily as a consequence of the electrification of the transports sector [6].

The interest in RES as a potential solution to reduce the environmental impact of the power sector, and the substantial investments that have been directed to research and development of RES technologies, has led in the last decade to a sharp decrease in their cost. According to IRENA [7] the Levelized Cost of Electricity from most RES is already competitive with or even lower than generation cost from fossil fuels, without

accounting for governmental economic incentives. The cost reduction trend is impressive: in the period 2010-2017 the LCOE from utility-scale projects has dropped by 73% for solar PV systems, and by 23% for onshore wind generation, and it is expected to decrease even further in the next years. In 2018, half of the total growth in installed electric generation capacity came from wind and solar [5], demonstrating that, although still marginal in the overall energy generation balance, RES are destined to be the key of the near future power sector evolution.

Once their installment cost has been accounted, RES virtually produce energy at no cost, but without massive investments in storage systems they are not capable of consistently meeting the energy demand, since the generation potential of most RES is determined by non-controllable environmental factors that might not always ensure sufficient energy production to supply the electric demand. The main obstacle to attaining very high RES penetration is therefore posed by their non-controllable nature, which complicates their large-scale integration in the electricity generation system. The drop in RES installment cost has on the other hand been recently followed by a reduction in the cost of electrochemical storage systems, both because of their application in combination with RES and because of the rise of electric mobility. Lithium-ion batteries, which in 2017 covered for about 60% of the total installed electrochemical storage capacity, reduced of an order of magnitude their price in less than a decade, going from an average battery pack cost of 1160 $/kWh in 2010 to 176 $/kWh in 2018 [8]. This has opened a completely new perspective on the potential role of electrochemical storage in the power sector, that goes beyond off-grid applications. Utility-scale storage Battery Energy Storage Systems (BESS) to provide ancillary services to the electric grid are already economically viable, and interesting business models based on the coordinated management of behind-the-meter batteries for demand-side response are being proposed [9].

The undergoing Digital Revolution represents an opportunity in terms of emerging technological resources that can contribute to putting into effect the described energy transition. Digitalization refers to the increasingly pervasive role that Information and Communication Technologies (ICT) have in most modern technological systems. The practical effects of digitalization are an easiness in collecting data that has no precedents, and more importantly the possibility of establishing advanced digital networks, comprising a variety of interconnected technological devices communicating with one another. Although always characterized by the use of digital technologies, digitalization of energy systems has accelerated at an astounding rate: global investment in digital electricity infrastructure and software has grown by over 20% annually since 2014, reaching USD 47 billion in 2016 [10]. Specifically, system digitalization provides many opportunities for increasing energy efficiency and reducing costs in domestic and industrial systems. Smart HVAC systems for buildings allow to better modulate the supply of heating and cooling services, adapting to the behavior of the users and offering the possibility of implementing demand-side response actions to price signals from the electric grid. Similarly, an increase in the flexibility of industrial production processes and better management of energy generation and consumption units can improve productivity while reducing energy consumption.

The increasing need of extensive RES deployment, combined with the opportunities deriving from systems digitalization and the need for a more efficient energy consumption paves the way for the rise of distributed

smart energy systems, interconnecting a variety of DER (including non-controllable RES) and coordinating their operation along with any opportunity for demand-side response to attain systemic energetic and economical operational advantages. In this scenario, the development of advanced optimization algorithms that fully exploit the opportunities offered by decentralized and coordinated DER control is an essential step of the energy transition.

Scope of Work

This thesis addresses the definition of mathematical optimization techniques for the efficient predictive management of distributed smart energy systems, often referred to as M*icrogrids* or more broadly *Multi-Energy Systems*. The application of the proposed algorithms is numerically assessed on real-life test cases, characterized based on datasets of demand and RES generation potential profiles provided by industrial partners. The case studies encompass both grid-connected and off-grid applications of the concept of microgrid, deployed both in developing and developed countries. Particular attention is paid to systems featuring a high penetration of RES, which are therefore more affected by the intermittency of RES power output, in addition to the stochasticity of load profiles. The thesis is structured in the following Chapters:

- **Chapter 1** depicts the role of Microgrids and Multi-Energy Systems in the current energy scenario, discussing their potential application as grid-connected and off-grid systems;
- **Chapter 2** examines the solutions that have been proposed in the literature for the optimal management of microgrids, with a particular focus on optimization techniques based on Mixed Integer Linear Programming (MILP);
- **Chapter 3** and **Chapter 4** propose two alternative MILP formulations for the optimal scheduling problem of a generic Multi-Energy System, characterized by a different approach to RES generation and load uncertainty;
- **Chapter 5** and **Chapter 6** compare the performance of the two proposed formulation, integrating the optimization models in the EMS of three real-life microgrids: different EMS architectures are proposed and numerically tested, accounting for the effect of uncertainty on system operation;
- **Chapter 7** proposes and numerically evaluates an advanced two-layers predictive EMS for the minute-by-minute management of hybrid off-grid microgrids, based on the scheduling problem formulation presented in Chapter 3;
- **Chapter 8** develops an adaptation of the scheduling problem formulation introduced in Chapter 3, to tackle the problem of optimal discrete components selection for off-grid hybrid microgrids;
- **Chapter 9** summarizes the findings of the doctoral thesis and outlines future developments connected to this work.

Publications

The papers included in this thesis are Paper I, Paper II and Paper III of the list below. With regard to these, I am the first author, responsible of the modeling, the simulations and part of the writing. Significant parts of the Chapters 4, 5, 7 and 8 are self-citations from previous mentioned papers. As reported in Elsevier

policy, as author of these articles, I retain the right to include the journal article, full or in part, in a thesis or dissertation without any permission. Starting from the results shown in Chapter 6 a fourth Paper is currently under writing.

Paper I

L. Moretti, S. Polimeni, L. Meraldi, P. Raboni, S. Leva, and G. Manzolini, "*Assessing the impact of a two-layer predictive dispatch algorithm on design and operation of off-grid hybrid microgrids*," *Renewable Energy*, vol. 143, pp 1439-1453, May 2019

Paper II

L. Moretti, M. Astolfi, C. Vergara, E. Macchi, J. I. Pérez-Arriaga, and G. Manzolini, "*A design and dispatch optimization algorithm based on mixed integer linear programming for rural electrification*," *Applied Energy*, vol. 233–234, pp. 1104–1121, Jan. 2019

Paper III

L. Moretti, E. Martelli, G. Manzolini, "*An efficient robust optimization model for the unit commitment and dispatch of multi-energy systems and microgrids", Submitted to Applied Energy*

2 MICROGRIDS AND MULTI-ENERGY SYSTEMS

This Chapter introduces the concept of Microgrid and Multi-Energy System (MES) and discusses their role in today's energy systems. Practical examples of real-life systems are identified and discussed, relevant for both off-grid and grid-connected applications. The typical hierarchical structure of the control system overseeing the operation of a microgrid (normally referred to as Energy Management System, or EMS) is presented, identifying the control levels that will be developed in the present work. Different approaches to microgrid management are discussed, focusing on centralized EMS featuring mathematical optimization of strategic scheduling decisions. Three alternative approaches have been proposed in literature for the formulation of the optimal scheduling problem for microgrids and MES, based on the Mixed Integer Linear Programming technique: deterministic, stochastic and robust formulation. The objective of this thesis is to formulate two alternative versions of the scheduling problem for a general MES or multi-good microgrid, respectively based on the deterministic and robust approach, and to compare the performance of EMS respectively featuring the former and the latter.

The US Department of Energy defines a microgrid as "a group of interconnected loads and Distributed Energy Resources (DER) within clearly defined electrical boundaries that acts as a single controllable entity with respect to the grid. A microgrid can connect and disconnect from the grid to enable it to operate in both grid-connected or island mode." [11]. DER include both controllable and non-controllable generation units (e.g. internal combustion generators, PhotoVoltaic (PV) arrays) and any type of storage systems (e.g. batteries, compressed air systems). This definition is targeting a specific declination of the concept of microgrid, identifying the large subset of electric microgrids which operate in parallel with the national electric network. A microgrid might, on the other hand, not be designed to operate independently from the main network, or equivalently not foresee a connection with any external electrical system. Furthermore, although the presence of the electric energy vector is a fundamental characteristic of most real-world microgrids, often these systems are dedicated also to the supply of different forms of energy other than electricity, such as heating and/or cooling. Indeed, the management of multiple energy vectors and energy-related services (e.g. internal production processes, transport services) can be effectively integrated within a microgrid, exchanging within its boundaries a multitude of physical and virtual goods and interacting with a variety of external systems other than the national grid. This broader management approach allows to exploit synergies in the energy conversion processes, as well as to efficiently plan activities within the microgrid to increase system reliability and economic performance. The described integrated systems are referred to as Multi-Energy Systems (MES) or Multi-Energy Micro-Grids (MEMG) [12].

Indeed, the key features defining an MES are:

1) The presence within the MES of an arbitrary combination of DER and loads, interconnected by local distribution networks dealing different forms of energy, and potentially interacting with external networks (e.g. main grid, district heating, other MES);
2) The presence of a local control system, overseeing the internal management of all units and defining the interaction of the MES seen as a single entity with all external systems;

Therefore, MES constitute decentralized control hubs, capable of efficiently tapping the internal degrees of freedom offered by the local DERs to supply all internal demands and maximize the economic advantage for its users, by also accounting for the interaction of the MES with external systems. The proposed definition encompasses a multitude of practical systems, that can potentially play a key role in the undergoing evolution of the energy system, both in developed and developing countries.

2.1 Off-grid Microgrids

The oldest example of electric off-grid microgrids is constituted by the first electric DC systems, starting to emerge around the world in the late XIX century [13]. The first European power plant dates to 1883 and was built in Milan (right beside the city Cathedral), to power the newly installed electric lighting of the Teatro Alla Scala and the surrounding shops. Similarly, all the initial applications of electric generators were constituted by local electrical systems independent one from the other. The electric services industry then started to expand in national transmission networks under a state-regulated monopoly market, interconnecting the various electric islands and originating national grids as we know it today. Independent electrical systems though still constitute the only way of supplying electricity to remote locations which cannot be connected to the main grid, such as geographical islands or remote communities. The archipelago of Hawaii is a good example of electrical system still based on independent microgrids, due to its geographical characteristics. Its islands are divided into different electric districts, not connected one another, relying on local power plants to supply the energy demand [14]. Each district must ensure its own electric stability, and this poses significant obstacles in the envisioned transition to a 100% renewable generation portfolio by 2045 [15] from the current electricity generation mix primarily based on imported fossil fuels, which makes the state of Hawaii the US state with the highest electricity cost [16].

Off-grid microgrids still represent an alternative to grid extension for the electrification of rural regions, in countries where the main grid is still not thoroughly expanded or provides very low service reliability to its customers. Access to affordable electricity supply is widely viewed as a key requirement to drive human development and diminish poverty levels worldwide. For this reason, the United Nations have set as part of the 2030 Agenda for Sustainable Development the ambitious goal of reaching universal energy access by 2030 [17]. Local governments and regulators in many developing countries, supported by international cooperation agencies, are therefore working on programs to extend energy access for the population in a cost-effective manner [18]. At the same time, in the last decade, the technological cost to supply rural communities through local renewable energy sources (RES) such as wind and photovoltaic has dramatically dropped [7], making off-grid systems an increasingly attractive alternative to grid extension [19]. In many cases, microgrids and standalone systems have the potential to be a cost-effective solution to provide electricity access in areas sparsely covered by the national grid. Furthermore, they constitute the only viable electrification strategy for remote communities, which would otherwise unlikely be included in grid extension plans [20]. The national grid still offers electricity at a cheaper price than installing and operating an off-grid system, but its extension involves relevant costs for erecting new transmission lines and, in developing countries, is a solution that generally suffers from significant transmission losses and is associated to poor reliability [21], attributable to weaknesses in the national power sector management. On the contrary,

microgrids have the potential to constitute reliable local supply systems, which can potentially work both in parallel with the national grid or independently from it. Furthermore, the local management of non-dispatchable generators and the cost-effective inclusion of large storage systems can allow for very high penetration of renewable sources, contributing to lower the environmental impact of the increase in energy consumption due to the electrification of new customers, putting the basis for the development of a national electric system which is both economically [22] and environmentally [23] sustainable.

Diesel Internal Combustion Engines (ICE) represent the traditional generation choice for small-scale off-grid systems, in virtue of their high operational flexibility, high reliability, and low complexity and cost. On the other hand, they pose a problem both in terms of environmental impact and final cost of electricity. Diesel generators produce nitrogen oxides and particulate matter, that affect air quality and might cause health problem to the local population. Furthermore, they are associated with high levels of specific CO2 emissions. Finally, the cost of diesel, increased by the fact that it needs to be shipped to these remote locations, results in an extremely high LCOE, mainly attributable to the fuel cost. Both for environmental and economic reasons, modern off-grid microgrids aim at reaching very high penetration from distributed RES, supported by storage systems, to reduce as much as possible diesel consumption. A practical example of large-scale off-grid microgrid is represented by the town of Garowe, Somalia [24], where the community energy needs are supplied by a combination of diesel ICEs, a 750 kW wind farm and a 1.5MW solar field, supported by a lead-acid battery stack. The system is managed by our industrial partner ENGIE Eps, and load and RES generation profiles are used to characterize the case studies in Chapters 5 and 6.

2.2 On-grid Microgrids

Microgrids have plenty of potential applications also in the grid-connected world. A significant number of behind-the-meter DER owned by medium- and small-scale consumers is already present in the power system. Cost-effective on-grid distributed generation has traditionally been associated to Combined Heat and Power (CHP) systems: these systems recover waste heat produced as a by-product from fuel-based electricity generation and make use of it to supply a thermal load. If most of the recovered heat is used, CHP dramatically increases overall system efficiency, allowing to exploit most of the primary energy provided by burning fuel: normally, CHP generators can recover 85-90% of the chemical energy stored in the combustible. A large fraction of energy end-users, such as industries, offices, and households which together account for about 50% of total European primary energy consumption, require the supply of both heat and electricity. Energy-intensive consumers (e.g. industries with thermal production processes, large offices, hospitals, and campuses) can attain significant cost savings by installing CHP generators to provide part or all of the energy demand, as opposed to separately purchasing electric energy from the grid and producing heat with natural gas-fired boilers.

Microgrids capability of serving as a local balancing point, integrating the management of dispatchable DERs and non-dispatchable RES, makes them capable of playing a fundamental role in fully developed power systems. They can contribute in limiting the impact of increasing distributed RES installation within their boundaries, by exploiting the internal degrees of freedom offered by DERs and demand-side response

capacity to control the entity of fluctuations in the energy exchange with the national grid, or even provide balancing services to the grid by responding to external load variation signals. In this perspective, the concept of Virtual Power Plant (VPP) has been recently proposed [25], signifying the idea that microgrids can behave, at their connection point with the national grid, equivalently to a conventional power plant, by tapping the dispatchability of their DER to yield a controllable net effect on the network. The idea of VPP goes beyond the physical definition of microgrid boundaries, as the capacity of a common EMS to coordinate the operation of DERs can extend through communication networks to aggregate DERs that are geographically located in different areas [26].

2.3 Microgrids Control

Determining the optimal scheduling of microgrids and Multi Energy Systems is no easy task. Off-grid microgrids and on-grid microgrids required to operate in islanded mode must be able to guarantee adequate power quality to their customers without relying on the electric stability provided by the main grid. At the same time, it is necessary for systems with high renewable penetration to maximize the advantages of renewable energy production, minimizing generation potential curtailment: to optimally achieve this objective often depends on effectively planning the energy storage state of charge evolution, accounting for the expected short-term RES production to schedule the commitment of dispatchable generators. Similarly, complex MES featuring many poly-generation units and intertwined internal energy balances can supply a given set of loads in a multitude of ways, and it is generally hard to establish a-priory management approaches that consistently ensure optimal system performance. Additionally, grid-connected microgrids might gain substantial economic benefits by planning in advance their interaction with the national grid through the internal scheduling of production and consumption, by supplying ancillary services to the grid or by simply adapting to variable price signals.

It is therefore apparent how the microgrid scheduling problem is generally a complex optimization problem, affected by dynamic phenomena acting on diverse temporal scales. To separately tackle the various temporal dimensions of microgrid control, a multi-level control system architecture is generally proposed in literature [27][28], addressing specific aspects of the management problem in a hierarchical fashion. With specific reference to electric systems, which are the most complex in terms of phenomena associated with diverse temporal resolutions, Olivares [29] identifies the following three control levels:

***Primary control*:** it is the lowest control level, acting on the fastest dynamics (e.g. voltage and frequency regulation, 1 – 10 ms). Since speed and reliability are the main concerns, this level is directly addressed by Local Controllers (LC), that act based on local system status measurements. This avoids delays and potential faults associated with communications with other microgrid elements. Droop control [30] is a typical solution to cope with instantaneous fluctuations of net demand, which represent the most critical example of fast response requirement.

***Secondary control*:** it is responsible for frequency and voltage restoration as well as for the identification of the optimal Unit Commitment (UC) and Economic Dispatch (ED) solution, based on the observed (and in some cases predicted) values of demand and non-dispatchable production. The microgrid UC is the

operating status plan of each unit, defining when the unit must be switched on or off, whereas the ED is the combination of operating setpoints for the active units that minimize the overall operating cost. Since it is acting on a slower time frame, secondary control can be based on more complex calculation, and it is therefore suited for implementation on a Microgrid Central Controller (MGCC), which collects information about the system status and identifies the optimal management solution in the perspective of overall system performance. This intermediate control level is referred to by Olivares as the *Energy Management System* (EMS).

***Tertiary control*:** it is the highest control level in the hierarchical structure depicted by Olivares, and it is the level taking the strategic management decisions related to the interactions with external systems (e.g. supply of ancillary services to the grid, bidding in the day-ahead energy market by participating as Virtual Power Plant) and on the medium to long term evolution of exogenous factors affecting the optimal microgrid management (e.g. renewable production potential, energy price profiles, expected demand).

Although useful in identifying a reference hierarchical control structure, the proposed definition of the control levels should be considered flexible: tertiary control might be the level in charge of defining the microgrid UC, particularly in the presence of non-flexible units which start-up must be planned well in advance. A longer-term perspective might also be important for the definition of the reference storage state of charge trajectory, to better account for its economic and operating effect on the microgrid management strategy. Finally, MES that integrate the management of different goods and services will need a hierarchical control structure suited to effectively deal with the temporal scale characterizing the dynamic behavior of each internal energy vector.

This work is focused on the definition of optimization algorithms to address the two higher levels of the described control structure. In our definition, we consider as microgrid (or MES) EMS the combination of secondary and tertiary control, although the EMSs proposed in this work are indeed structured in a hierarchical two-levels subdivision which is consistent with the classification proposed by Olivares.

Two major EMS paradigms have been proposed in literature: decentralized and centralized EMSs [31]. In decentralized EMSs [32] decision making is performed by the LC of each unit, which establishes its optimal dispatch strategy based on the system condition parameters that can be observed in its surroundings (e.g. local voltage and frequency levels, unit current and past status). In some cases, decentralized EMSs can be based on the interactions between neighboring LCs and the MGCC. The most popular paradigm of decentralized microgrid EMSs proposed in recent years is agent-based control systems (or Multi-Agent System, MAS) [33]. MAS is based on the idea that LCs interact via distributed communication networks, exchanging biddings based on decentralized artificial intelligence algorithms which account for the behavior of neighboring agents and on the evolution of the environmental boundary conditions [34][35]. Decentralized control algorithms appeal consists in the creation of a resilient communication network, that can effectively address system control also in case of failure of one of its parts. Information is also exchanged in a more capillary and effective way between agents, rather than in the case of a radial information flow towards a central control entity. Finally, distributed control algorithms might be well suited for fluid distributed

networks comprising multiple private independent customers, which can connect and disconnect from the network and aim at the maximization of their own profit rather than of the overall performance [36]. On the other hand, giving up a centralized supervision of the general system status does not allow to perform an optimal coordinated decision-making process on the operating plan of all DERs, at the price of overall performance reduction. Furthermore, centralized EMSs are easier to deploy in most practical cases, and for microgrids with a single owner or constituted by independent DER owners that give up the full control of their units to a central coordinator (e.g. aggregators), centralized EMSs are considered the most effective control solution.

2.4 Centralized approaches to microgrid management

As already described, centralized microgrid management is overseen by a central controller (MGCC) that:

1) monitors the overall system status (namely all relevant information regarding microgrid DERs and loads);
2) is informed about the technical characteristics of the microgrid and of its units;
3) often communicates with external systems providing information useful for the identification of the optimal microgrid operating strategy (e.g. RES generation and internal loads forecast profiles, price signals from the network).

The MGCC then communicates the reference operating plan to the LCs, continuously updating its decisions to account for the actual system evolution with respect to the original plan.

Several techniques have been proposed to address the MGCC decision making process. The simplest approach relies on the definition of fixed scheduling policies, that define the scheduling plan as a function of the observed system status (e.g. load demand / RES contribution, storage charge status) and exogenous boundary conditions (e.g. network energy prices). The scheduling policy can be based on dispatch priority lists [37], or feature more complex evaluations that also account for the system evolution history. This is the case of the well-known Cycle Charge and Load Following management strategies for off-grid microgrids [38], which constitute a benchmark for the evaluation management algorithms in virtue of their good performance and easy on-field implementation. A different class of approaches is based on the adoption of metaheuristics, algorithms that perform a heuristic search of the space encompassing all feasible scheduling solutions to identify the optimal management strategy. These methods can be used to formulate predictive instances of the scheduling optimization problem, accounting for forecasts of load and RES generation in the definition of the commitment and dispatch plan. Metaheuristic techniques adopted in literature include Genetic Algorithms (GA) [39][40], Particle Swarm Optimization (PSO) [41][42] and Ant Colony Optimization (ACO) [43]. These methods have the advantage of introducing no restrictions on the complexity of the system operation modeling. On the other hand, they identify a solution which has no guarantee of global optimality, which constitutes a relevant limitation especially for complex microgrid architectures where the optimal dispatch problem is characterized by a large number of local minima. Furthermore, they are associated with long computational times and inconsistent optimization outcomes due to the inherently stochastic behavior of their solution process [27].

One of the most successful techniques reported in the literature to tackle the optimal microgrid scheduling problem is constituted by Mixed Integer Linear Programming (MILP). The MILP framework requires that the scheduling problem is formulated resorting only to linear equations, linking the problem optimization variables and defining the problem objective function. On the other hand, thanks to its structure the optimization problem can be solved by means of efficient solution algorithms, which can rapidly solve extremely complicated problems providing a solution with a certificate of global optimality. Several formulations of the scheduling problem based on the MILP framework have been proposed in literature, dealing in different ways with the problem of forecast uncertainty. The following Paragraph presents a detailed review of these formulations.

2.5 Scheduling Optimization based on Mixed Integer Linear Programming

As explained in the previous Paragraph, predictive scheduling optimization relies on the forecast of exogenous factors, such as load and RES non-dispatchable generation potential, to identify the optimal system operating plan. On the other hand, in real-life application it is essential to account for the non-deterministic nature of forecasts, since the actual profiles of predicted parameters will generally deviate from their expected behavior, hindering the optimality of the solution associated to the forecasted profiles, and even leading to service outages in case of wrong and non-modifiable operating decision. This requirement is particularly critical for isolated electric microgrids featuring a high installed capacity of intermittent renewables, which cannot rely on the national grid to balance instantaneous fluctuations of electric net demand, and/or for systems with limited operational flexibility (units affected by limited ramp rates, long start-up times, and/or poor turndown ratio), for which the actuation of corrective measures to the planned course of operation might be costly or technically unfeasible. As far as MILP-based approaches are concerned, different techniques have been proposed to cope with this issue, which can be classified into three main categories: deterministic formulations with reserve requirements, stochastic programming, and robust optimization.

Deterministic MILP formulations account for a single nominal forecast scenario and do not explicitly consider the effect of forecast errors. Deviation from forecast must thus be addressed by the lower level of the control system. A degree of conservativeness is imposed in the nominal solution by introducing reserve constraints, which require that the identified optimal scheduling ensures operating margins for real-time dispatch corrections. Reserve constraints, particularly in the context of electrical systems, are often referred to as *spinning reserve* requirements since they imply that the committed units (readily available for setpoint adjustments) provide enough generation capacity to compensate potential net demand deviations from forecast. Examples of deterministic formulation of the scheduling problem are [44], where the approach is adopted for the optimal management off-grid hybrid microgrid, and [45], where a MILP-based deterministic optimization model is proposed for the optimal scheduling of Combined Cooling Heating and Power (CCHP) systems. Despite being an extremely simple approach, it has the merit of allowing for the definition of very complex and detailed system models, which would imply an excessive computational complexity if replicated resorting to the other formulation approaches. Furthermore, its conservativeness can be tuned

by acting on the spinning reserve requirements. Finally, by frequently updating the scheduling solution and, if possible, the forecasts input, forecast errors can be identified and addressed.

Stochastic programming defines instead a family of potential manifestations of the uncertain problem parameters (e.g. realizations of demand and RES generation), each associated with a probability of occurrence. The optimal solution minimizes the expected value of the operating cost accounting for all considered scenarios [46]. Most stochastic formulations proposed in literature resort to a two-stage formulation, which divides problem variables into two groups. "Here and now" variables are decided before observing the actual realization of uncertain profiles, and their value is set regardless of the actual uncertainty manifestation. These variables include the definition of the UC plan and the operating set points of non-flexible units. "Wait and see" variables are on the other hand scenario-dependent, and they are optimized based on the actual scenario realization. Alipour et al. [47] propose a two-stage stochastic integer program for the optimal scheduling of CHP systems integrated with a thermal storage and subject to market and load uncertainties. Martinez et al. [48] developed a two-stage stochastic programming formulation for grid-connected microgrids where first-stage decisions are the conventional generation schedules and load set points, while second-stage decisions are electricity exchanges with the main grid as well as load adjustments. Cardoso et al. [49] propose a two-stage Stochastic Linear Programming model for battery scheduling of a microgrid. The robustness and the average performance of the solutions identified through stochastic programming are on the other hand closely affected by the number and the representativeness of the selected scenarios. To obtain a robust and effective solution, a large number of scenarios must be considered which increases the computational complexity of the stochastic program, calling for advanced decomposition techniques (e.g. Benders' decomposition). Furthermore, in order to properly generate the scenarios and characterize their likelihood, it is necessary to know the statistical distribution of all uncertainty factors, which is not always available.

Robust optimization [17], as opposed to stochastic optimization, defines uncertainty as a mathematical space (called *uncertainty set*), and therefore as all infinite potential realizations within the uncertainty set, regardless of their likelihood. The identified solution is feasible for all possible realizations encompassed by the uncertainty space, consistently ensuring safe system operation. Majidi et al. [18] apply the robust approach proposed by Bertsimas and Sim [19] for discrete optimization problems to the optimal scheduling of CHP systems with demand response programs, considering uncertain electric demand and energy prices. To reduce the solution conservativeness and improve performances, a two-stage problem formulation (referred to as Adjustable Robust Optimization, ARO) can be adopted, by accounting for corrective measures to the first stage solution which depend on the uncertainty manifestation [20]. Two main families of ARO approaches have been presented in the literature. In the first family of approaches (referred to as "fully adaptive"), the ARO problem is solved according to a bi-level algorithm: the upper-level problem is associated to first stage decisions (e.g. commitment variables), while the lower-level addresses the "maximin" dispatch problem associated to the worst-case uncertainty realization. Iterating between the two levels, either using dual information and a Benders-like algorithm [21] or imposing KKT conditions on the lower level problem and using the column-and-constraints generation algorithm [22], it is possible to refine first

stage decisions until the robust optimal commitment is identified. This kind of approach has been recently applied to the optimal day-ahead scheduling of electric microgrids [23][24] and MES [25], showing how the robust formulation can ensure higher system reliability and lower objective function volatility with respect to both deterministic and stochastic optimization methods. In the second family of approaches, second stage variables are expressed as a priori defined functions (*decision rule*) of the realization of uncertainty [26]. Expressing second stage variables according to predefined mathematical functions limits the space of possible recourse actions with respect to the previous family of approaches. On the other hand, it provides decision rules which could be effectively used to cope with the realization of the uncertainty factors during the real-time operation of the systems while preserving feasibility. Affine decision rules (e.g. linear with respect to uncertainty) are normally adopted to ensure problem tractability, although they may lead to a sub-optimal solution in comparison with fully adaptive formulations [27]. Bertsimas and Goyal [28] have on the other hand shown that piece-wise linear decision rules are optimal for adaptive optimization problems. Concerning the operation of energy systems, Zugno et al. [29] proposed an Affinely ARO (AARO) formulation featuring piece-wise decision rules, for the optimal commitment of CHP power plants subject to uncertain head demand and electricity price. Results show that, compared to the stochastic programming approach, the AARO formulation can guarantee zero outages (heat demand not served) with a limited revenue reduction due to the additional solution conservativeness. Attarha et al. [30] demonstrates the direct applicability of AARO decision rules as bidding strategy for a grid connected PV-BESS system subject to uncertain solar generation potential and energy prices. Lorca et al. thoroughly explore the application of AARO to the UC of large-scale power systems with uncertain nodal power injection, proposing improved solution algorithms to deal with the complexity of the problem. To the author's knowledge though, there is no evidence in the literature for an AARO formulation explicitly considering MES subject to multiple uncertain demands (e.g., electricity and heat) and RES production.

The present work is dedicated to the development and comparison of two alternative MILP formulations of the optimal scheduling problem, for a generic MES or Multi-Good MicroGrid (MEMG). Specifically, the two general formulations presented in Chapter 3 and Chapter 4 are respectively based on the deterministic and the affinely adjustable robust approaches, to compare a very simple yet effective approach to predictive scheduling optimization with a complex mathematical instrument focused on ensuring service reliability in all scenarios. Various declinations of two-layers EMS are defined in the following Chapters, and the adoption of the two formulations in different contexts is discussed by means of an extensive numerical campaign exploring different off-grid and grid-connected real-life case studies.

3 DETERMINISTIC SCHEDULING PROBLEM FORMULATION

This Chapter introduces a general deterministic MILP formulation of the Unit Commitment (UC) and Economic Dispatch (ED) optimization problem for a generic Multi Energy System (MES). The formulation allows to flexibly represent a wide variety of potential applications, through the definition of classes of components that encompass most of the units generally installed in real systems. Starting from a basic description of the standard modeling approach for each component class, different declinations of the approach are discussed, to depict a general modeling strategy that can be adapted according to the specific characteristics of potential real-life problem instances. Scheduling optimization is based on the expected values of all exogenous factors that affect system operation (e.g. load consumption pattern, environmental conditions) over the optimization planning window. Uncertainty is accounted for by means of spinning reserve constraints, that increase solution conservativeness and ensure margins for real-time corrections. An example of a practical system modeled by means of the proposed methodology is discussed at the end of the Chapter.

In this Chapter, a purely deterministic MILP formulation of the scheduling problem of a generic MES is presented. A general schematization of an MES is obtained by grouping the components in classes of elements, for which a set of modeling equations is presented and discussed. The deterministic approach does not directly address the problem of forecast accuracy related to the non-deterministic nature of the exogenous factors expected profiles. Modifications to the scheduling solution made necessary by forecast errors are addressed by the lower levels of the control system. The introduction of constraints to increase the conservativeness of the nominal solution and ensure margins for real-time corrections is discussed in Paragraph 3.5, while the lower level adjustment strategies that are required to adjust the solution during real-time operation are discussed at length in the following Chapters.

3.1 Problem Statement

The set of components constituting a generic MES comprise of:

- the set of controllable units $\boldsymbol{\mathcal{M}}$: $\boldsymbol{\mathcal{M}}$ can be split in units $\boldsymbol{\mathcal{F}}$ that consume external inputs (or *fuels*) and units $\boldsymbol{\mathcal{B}}$ that consume inputs produced within the MES itself;
- the set of non-controllable units (e.g., intermittent renewable sources) $\boldsymbol{\mathcal{ND}}$;
- the set of storage systems $\boldsymbol{\mathcal{S}}$;
- the set of loads $\boldsymbol{\mathcal{L}}$, partitionable in controllable loads $\boldsymbol{\mathcal{L}}^d$ and non-controllable loads $\boldsymbol{\mathcal{L}}^{nd}$
- the set of external networks $\boldsymbol{\mathcal{N}}$ which can mono- or bi-directionally trade goods with the MES.

A schematic representation of the general MES is depicted in Figure 1.

Energy demand profiles and the profiles of environmental conditions, which among other things determine the generation potential of non-dispatchable sources $\boldsymbol{\mathcal{ND}}$, represent the problem exogenous variables, in the sense that they are part of the boundary conditions defining the optimal dispatch problem and with respect to which the optimal solution is identified. Environmental conditions might also influence how some of the MES components operate (e.g. ambient temperature affecting the performance of a gas turbine).

Forecast profiles for all non-controllable exogenous factors, therefore, constitute a necessary input that must be defined in order to address the optimal dispatch problem. Several techniques (e.g., physical models [55], machine learning [56][57] or statistical techniques [58]) are available for this task. Forecasts are necessary to fully define the problem, in order to identify the optimal scheduling (UC and ED) of the MES.

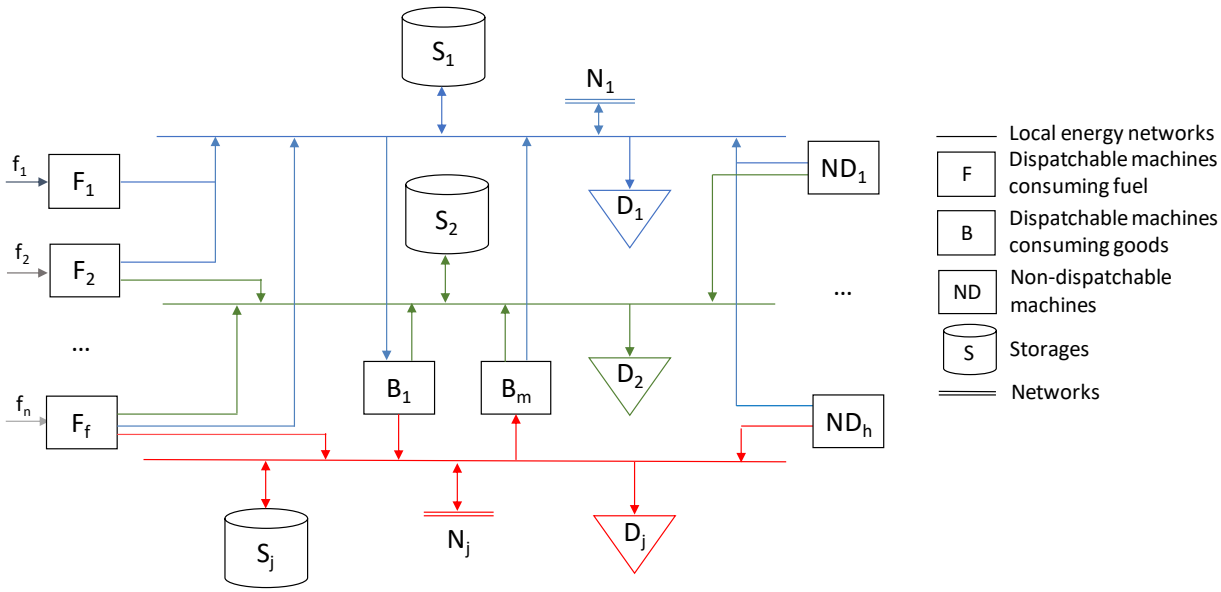

Figure 1: MES general scheme

The optimal scheduling problem can be defined as follows. Based on:

- Forecasted demand profile of each internal microgrid good;
- Forecasted generation potential profile of all non-dispatchable units;
- Technical constraints and part-load performance maps of controllable units;
- Technical parameters, including capacity and charge/discharge efficiency, defining all storage systems;
- Transmission capacity of connections to external networks, and purchase/selling price profiles;

the objective is to determine the optimal system operating schedule over the simulation time horizon, comprising commitment status and operating setpoint of all controllable units. More specifically, problem optimization variables include:

- Input consumption profile for all dispatchable machines $\boldsymbol{\mathcal{F}} \cup \boldsymbol{\mathcal{B}}$;
- Charge/discharge profiles for all storage systems $\boldsymbol{\mathcal{S}}$;
- Exchange profiles with all external networks $\boldsymbol{\mathcal{N}}$;
- Production curtailment profiles for all non-dispatchable units $\boldsymbol{\mathcal{ND}}$;
- Supply profile of all dispatchable goods $\boldsymbol{\mathcal{L}}^d$;
- Non-served load profile for all microgrid loads $\boldsymbol{\mathcal{L}}$;

The optimization objective function is to minimize the overall expected microgrid operating cost, accounting for:

- Cost of consumed fuels by machines $\mathcal{F}$;
- Operation and Maintenance (O&M) costs for all units;
- Costs/revenues connected to trading with external networks $\mathcal{N}$;
- Cost of non-served demand for all loads $\mathcal{L}$;
- Any virtual costs defined to represent desirable solution characteristics.

3.2 Multi-Energy System Architecture

As already mentioned, the general MES representation shown in Figure 1 is suited for modeling a wide range of applications, that can be schematized in a modular way starting from the following elemental component classes:

- **Controllable units $\mathcal{M}$**: units that convert an input into output/s, according to an operating space map linking the consumption rate of the input to the production rate of the output/s. When the unit is active, the management system can move its operating point within the operating space, while subject to all technical limitations specified for the unit. The consumed input can either be an internal microgrid good (machines subset $\mathcal{B}$) or an external *fuel* (machines subset $\mathcal{F}$), purchased at a known price which can be time-dependent;
- **Non-controllable units $\mathcal{ND}$**: all generation units which operating point cannot be controlled freely by the management system, since it is mainly determined by exogenous factors. The management system might still be able to connect/disconnect the unit and/or to curtail part of its maximum generation potential;
- **Storages $\mathcal{S}$**: all units capable of storing an internal MES good according to storage charge/discharge/self-discharge efficiencies;
- **Networks $\mathcal{N}$**: all external systems capable of trading goods with the MES. According to their direction, exchanges are associated with a purchase/selling price, which can be time-dependent;
- **Loads $\mathcal{L}$**: internal consumption points, requesting the supply of goods according to a reference consumption profile which can, in the case of dispatchable loads $\mathcal{L}^d$, be influenced by the EMS;
- **Connectors $\mathcal{C}$**: elements representing directional transferring connections, converting one microgrid good to another according to its transfer efficiency.

The set of all goods exchanged within the microgrid is defined as $\mathcal{G}$. Some goods in $\mathcal{G}$ might not be associated with an internal load, or conversely, be associated with a set of loads $\mathcal{L}_j \subseteq \mathcal{L}$.

Each of the presented elements is represented by means of a standard set of constraints, which may be adapted according to the representation choices best suited for the specific unit/problem instance. All constraints defining the modeling approach for each element class are presented in detail in Paragraph 3.4, specifying in detail which are the optimization variables and the parameters associated with each unit.

3.3 Objective function

The optimization process aims at minimizing the overall MES cost function, or *objective function*. Different objective functions can be defined, according to the target of the optimization process (e.g. fuel cost,

limitation of control variables deviations with respect to the scheduled plan, pollutants emissions). In this work the objective function is defined as an equivalent cost index, comprising all operating costs associated to the microgrid units, the value of trades with all external networks, and the penalization associated to failing at supplying internal demands. In addition to these physical cost indexes, a series of virtual cost terms is also introduced, which serve the function of discerning among otherwise equivalent solutions the one best suited for practical implementation. Virtual cost terms comprise setpoint variation penalty, dissipation penalization, and final storage charge valorization:

$$OF = \sum_{t\in\mathcal{T}} \left[\sum_{i\in\mathcal{F}} c_{i,t}^{f} + \sum_{i\in\mathcal{M}\cup\mathcal{S}} c_{i,t}^{O\&M} + \sum_{i\in\mathcal{N}} c_{i,t}^{net} + \sum_{i\in\mathcal{L}} c_{i,t}^{UM} + \sum_{i\in\mathcal{M}} c_{i,t}^{\Delta P} + \sum_{i\in\mathcal{G}} c_{i,t}^{diss} \right] \widetilde{\Delta t} - \sum_{i\in\mathcal{S}} v_i^{end} \tag{1}$$

Where:

- $c_{i,t}^{f}$ is the fuel cost for machine $i \in \mathcal{F}$;
- $c_{i,t}^{O\&M}$ is the operation and maintenance cost for machines and storages $i \in \mathcal{M} \cup \mathcal{S}$;
- $c_{i,t}^{net}$ is the cost/revenue associated with trades with network $i \in \mathcal{N}$;
- $c_{i,t}^{UM}$ is the penalty for the unmet demand from load $i \in \mathcal{L}$;
- $c_{i,t}^{\Delta P}$ is the virtual set-point variation cost for machine $i \in \mathcal{M}$;
- $c_{i,t}^{diss}$ is the virtual dissipation cost for good $i \in \mathcal{G}$;
- v_i^{end} is the virtual final charge valorization for storage $i \in \mathcal{S}$.

Virtual cost terms have an impact on the overall objective function that is tuned according to the importance attributed to the characteristics they represent. As a general rule, their impact on the objective function should be marginal with respect to the physical cost terms.

3.4 Components Modeling

3.4.1 Controllable units

The set of controllable units $\mathcal{M}$ is divided into machines consuming external inputs (i.e. fuels) $\mathcal{F}$, and machines consuming inputs produced internally $\mathcal{B}$ (Figure 1). Only single-input / multiple-outputs machines accounted for in the formulation presented in this Chapter (e.g. single degree of freedom units), but the modeling approach can be extended to account for units with multiple degrees of freedom [59]. The decision variables defining the operating status of each dispatchable machine in each problem timestep t are:

- Binary commitment variable z_t, equal to 1 when the machine is in operation;
- Input consumption rate in_t
- Output production rate $\boldsymbol{o}_t \in \mathbb{R}^{j}$, where j is the number of machine outputs.

The key element in the representation of a controllable machine is its part load curve, indicating the input-output functional dependency that describes all possible operating points for the unit. For machines with a

single degree of freedom, the production rate of all outputs is univocally determined as function of the input consumption rate, according to the part-load curve $f_{\boldsymbol{\Theta}_t}(in)$:

$$\boldsymbol{o}_t = f_{\boldsymbol{\Theta}_t}(in_t) \qquad \forall t \in \boldsymbol{\mathcal{T}} \qquad (2)$$

As indicated in Eq.(2), the shape of the input – output off-design curve $f_{\boldsymbol{\Theta}_t}$ might depend on the environmental conditions $\boldsymbol{\Theta}_t$ (e.g. ambient temperature, radiation, humidity, etc.). Provided that the expected profile of $\boldsymbol{\Theta}_t$ and its effect on function $f_{\boldsymbol{\Theta}_t}$ are both known, the part-load curve can be adapted in each time-step, to account for changes in the machine input – output relation.

In general, function $f_{\boldsymbol{\Theta}_t}$ is not linear, and therefore cannot be directly introduced in the MILP formulation. On the other hand, a non-linear function can be approximated by a piece-wise linear function, constituted by a series of consecutive linear segments. Given the set of discretization points $\boldsymbol{\mathcal{P}}$, which must include the boundaries of the off-design curve, any operating point laying on one of the segments of the piece-wise linear representation of $f_{\boldsymbol{\Theta}_t}$ can be obtained as a weighted average of its vertexes. To each point $p \in \boldsymbol{\mathcal{P}}$ is therefore associated with a time-dependent weight $\alpha_{p,t}$, and in all instants consumption and production of the dispatchable unit are obtained as a linear combination of all discretization point n-tuples ($\widetilde{in}_{p,t}$, $\tilde{o}_{p,j,t}$):

$$in_t = \sum_p \widetilde{in}_{p,t} \cdot \alpha_{p,t} \qquad \forall t \in \boldsymbol{\mathcal{T}} \qquad (3)$$

$$o_{j,t} = \sum_p \tilde{o}_{p,j,t} \cdot \alpha_{p,t} \qquad \forall t \in \boldsymbol{\mathcal{T}} \qquad (4)$$

The time dependency of discretization point coefficients $\widetilde{in}_{p,t}$ and $\tilde{o}_{p,j,t}$ allows accounting for the effect of environmental conditions on the shape of the machine operating curve. Based on the estimated profile of ambient conditions vector $\boldsymbol{\Theta}_t$ the correct adaptation of $f_{\boldsymbol{\Theta}_t}$ can be calculated for each timestep t, and the coefficients of each discretization point can be modified accordingly.

The summation of linear combination weights $\alpha_{p,t}$ must be equal to 1 when the machine is on, while it must be zero otherwise. It is therefore linked to the commitment variable z_t:

$$\sum_p \alpha_{p,t} = z_t \qquad \forall t \in \boldsymbol{\mathcal{T}} \qquad (5)$$

Constraints (3)-(5) bound the operating point within the convex hull of discretization set $\boldsymbol{\mathcal{P}}$. The operating point must on the other hand fall on one of the linear segments $k \in [1..N_p - 1]$ connecting adjacent couples of discretization points in $\boldsymbol{\mathcal{P}}$, where N_p is the cardinality of set $\boldsymbol{\mathcal{P}}$. Binary variables β_k enforce that only the weights $\alpha_{k,t}/\alpha_{k+1,t}$, vertexes of segment k, can be active at a given time:

$$\sum_{k \in [1..N_p - 1]} \beta_{k,t}(t) = 1 \qquad \forall t \in \boldsymbol{\mathcal{T}} \qquad (6)$$

$$\begin{aligned} \alpha_{p,t} &\leq \beta_{p-1,t} + \beta_{p,t} && \forall t \in \boldsymbol{\mathcal{T}}, p \in \boldsymbol{\mathcal{P}} \\ \alpha_{1,t} &\leq \beta_{1,t} && \forall t \in \boldsymbol{\mathcal{T}} \end{aligned} \qquad (7)$$

$$\alpha_{n,t} \leq \beta_{n-1,t}$$

The described representation methodology allows dealing with characteristic curves of any shape. The accuracy of the piece-wise approximant can be controlled by increasing the number of discretization points N_p (Figure 2 – left). On the other hand, increasing N_p leads to a sensible increase in the number of problem variables. Furthermore, binary variables $\beta_{k,t}$ sensibly slow down the MILP solution algorithm, affecting the solution branch and bound stage.

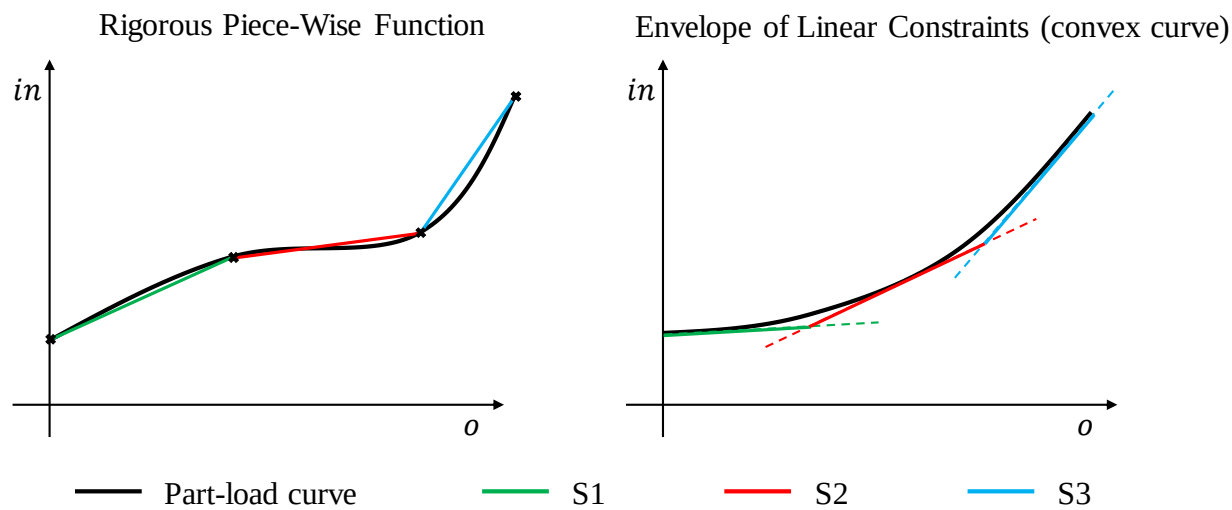

Figure 2: three-segment piece-wise representation of non-linear part-load curves. For non-convex curves (right) the formal piece-wise definition must be implemented. Convex curves (left) can be approximated by a family of linear constraints each associated to a segment of the PWL approximant.

An alternative and more computationally effective representation can be formulated for machines with convex off-design curves in the hyperspace $(in - \boldsymbol{o})$ (Figure 2 – right). In this case, the part-load curve can be represented via a family of linear constraints $c \in \boldsymbol{\mathcal{LC}}_i$, defined by coefficients $m_{c,j,t}$ and $q_{c,j,t}$ $\forall c \in \boldsymbol{\mathcal{LC}}_i$. Each constraint sets a lower bound to input consumption rate as a function of machine output production:

$$in \geq \tilde{m}_{c,j,t} o_{j,t} + \tilde{q}_{c,j,t} z_t \qquad \forall t \in \boldsymbol{\mathcal{T}} \qquad (8)$$

Due to the convexity of the part-load curve, only the linear constraint of the family which lays the closest to the original non-linear curve will set the most restrictive bound in any point of the operating space. Given that a cost is associated with input consumption, the optimality of the solution will imply an input rate as low as possible, making the operating point fall on the piece-wise maximum envelope of $\boldsymbol{\mathcal{LC}}_i$.

The simplified approach for convex off-design curves drastically reduces the computational burden, at the expense of potential misrepresentations of the machine operating curve. In particular, the operating space allowed by this representation corresponds to the entire region laying above the piece-wise representation of the characteristic curve. Although in most cases optimality will push the operating points on the lower boundary of this region (e.g. the characteristic curve itself), in some cases this condition might be bypassed to avoid violation of other constraints, on the machine or on the system (e.g. ramp down constraints, constraints on maximum dissipation). The approximated representation for convex operating curves should,

therefore, be adopted only when no other constraints might be bypassed because of the described relaxation of the input – output function.

The load of all units, while in operation, is bounded by their maximum and minimum operating points:

$$z_t \widetilde{in}^{min} \leq in_t \leq z_t \widetilde{in}^{max} \qquad \forall t \in \boldsymbol{\mathcal{T}} \qquad (9)$$

Where $\widetilde{in}^{min}$ and $\widetilde{in}^{max}$ are respectively associated with minimum / maximum machine load.

The operating region in the case of the α / β representation, when the machine is active, is always bounded within the extreme points in $\boldsymbol{\mathcal{P}}$ (highest / lowest $\widetilde{in}_{p,t}$). Tighter limitations on maximum / minimum power output can be enforced through constraint (9).

Unit setpoint variations can also be limited by upwards and downwards ramping constraints:

$$-z_t \widetilde{rd} - \widetilde{in}^{max,SD}(1 - z_t) \leq in_t - in_{t-1} \leq z_{t-1} \widetilde{ru} + \widetilde{in}^{max,SU}(1 - z_{t-1}) \qquad \forall t \in \boldsymbol{\mathcal{T}} \qquad (10)$$

Where $\widetilde{rd}$ and $\widetilde{ru}$ are respectively the maximum ramp-down and ramp-up rate while in operation, $\widetilde{in}^{max,SU}$ is the maximum load which can be reached within the first time-step the machine is put in operation, and $\widetilde{in}^{max,SD}$ is the maximum load below which it is possible to shut down the machine. The value of all three parameters must be set in accordance with the problem temporal resolution. The ramp-down limitation is bypassed during shut-downs due to the term $\widetilde{in}^{max,SD}(1 - z_t)$, allowing for downwards set-point deviations up to $\widetilde{in}^{max,SD}$ when z_t is zero. According to the value of z_{t-1}, stating whether the machine was already on or is potentially turning on during timestep t, the correct upper limit to load variation is set either to $\widetilde{ru}$ or to $\widetilde{in}^{max,SU}$.

Time-steps during which a start-up occurs are identified by the binary start-up variable δ_t, equal to 1 when the machine is started-up. Its value is bounded by the variation of commitment variable z_t:

$$z_t - z_{t-1} \leq \delta_t \leq \frac{z_t - z_{t-1} + 1}{2} \qquad \forall t \in \boldsymbol{\mathcal{T}} \qquad (11)$$

Changes in the commitment status can be limited by technical requirements on minimum up/downtimes, imposing that as after a start-up / shut-down the on/off status is not modified before the time interval T^{UT}/T^{DT} has elapsed:

$$z_\tau \geq z_t - z_{t-1} \qquad \forall t \in \boldsymbol{\mathcal{T}}, \tau \in [t..t + T^{UT}] \qquad (12)$$

$$1 - z_\tau \geq z_{t-1} - z_t \qquad \forall t \in \boldsymbol{\mathcal{T}}, \tau \in [t..t + T^{DT}] \qquad (13)$$

Up/downtimes are relevant both to limit frequent changes in the commitment, which might be harmful to the machine and to account technical constraints on the actuation of the start-up/shut-down command. Start-ups can also be associated with an additional input consumption $\widetilde{in}^{SU}$, and/or to a penalization/increase on machine outputs $\tilde{o}_j^{SU}$, which accounted for through the start-up variable:

$$in_t^{TOT} = in_t + \delta_t \widetilde{in}^{SU} \qquad \forall t \in \boldsymbol{\mathcal{T}} \qquad (14)$$

$$o_{j,t}^{TOT} = o_{j,t} + \delta_t \tilde{o}_j^{SU} \qquad \forall t \in \boldsymbol{\mathcal{T}} \qquad (15)$$

While the consumption penalty $\widetilde{in}^{SU}$ is always positive, output modification due to start-up $\tilde{o}_j^{SU}$ can either be positive or negative, according to the effect that the start-up has on the production of output *j*.

A particular type of controllable units is represented by on/off units, whose only degree of freedom is their commitment status and are characterized by a single operating point, which can still depend on environmental conditions $\boldsymbol{\Theta}_t$. For these units, the discretization set $\boldsymbol{\mathcal{P}}$ collapses to a single time-dependent n-tuple, and constraints (3)-(11) reduce to:

$$in_t = \widetilde{in}_t z_t \qquad \forall t \in \boldsymbol{\mathcal{T}} \qquad (16)$$

$$o_{j,t} = \tilde{o}_{j,t} z_t \qquad \forall t \in \boldsymbol{\mathcal{T}} \qquad (17)$$

Constraints on start-up/shut-down limitations, (eq (12)(13)) as well as input / output modifications due to start-ups (eq. (14)-(15)), are still enforced by the same formulation.

Some units might be able to function according to a variety of potential operating modes, each associated with a different characteristic curve $f_{\boldsymbol{\Theta}}$. These units can be modeled as a set of mutually exclusive virtual machines $\boldsymbol{\mathcal{ME}}_g$, comprising the independent technological definition of each operating mode. A constraint on the commitment variables of the machines in the set ensures that only one operating mode can be active at a time:

$$\sum_{i \in \boldsymbol{\mathcal{ME}}_g} z_{i,t} \leq 1 \qquad \forall g, t \in \boldsymbol{\mathcal{T}} \qquad (18)$$

The physical costs indexes for controllable machines comprise purchase expense for external inputs of machines $\boldsymbol{\mathcal{F}}$ and operation and maintenance cost for all machines $\boldsymbol{\mathcal{M}}$:

$$c_{i,t}^{f} = \left(in_{i,t}^{TOT} \tilde{c}_{i,t}^{f,buy}\right) \qquad \forall\, i \in \boldsymbol{\mathcal{F}}, t \in \boldsymbol{\mathcal{T}} \qquad (19)$$

$$c_{i,t}^{O\&M} = z_{i,t} \tilde{c}_i^{OMxh} + in_{i,t} \tilde{c}_i^{OMxE} + \delta_{i,t} \tilde{c}_i^{SU} \qquad \forall\, i \in \boldsymbol{\mathcal{M}}, t \in \boldsymbol{\mathcal{T}} \qquad (20)$$

Operation and maintenance costs $c_{i,t}^{O\&M}$ can either be proportional to the operating hours $\tilde{c}_i^{OMxh}$, to the fuel consumption rate $\tilde{c}_i^{OMxE}$, or to both, according to the specific machine technology. Furthermore, wearing due to machine start-up can be directly accounted for by means of the start-up cost $\tilde{c}_i^{SU}$. Fuels are assumed to be available with no limitations and purchased at the price $\tilde{c}_{i,t}^{f,buy}$.

In addition to physical costs (19)-(20), a virtual set point variation cost is introduced in the objective function, indicating how easily a machine can modify its load within its technical limits. The penalty is proportional to the absolute value of the deviation, defined as:

$$\Delta in_{i,t} \geq in_{i,t} - in_{i,t-1} \qquad i \in \boldsymbol{\mathcal{M}}, t \in \boldsymbol{\mathcal{T}} \qquad (21)$$

$$\Delta in_{i,t} \geq in_{i,t-1} - in_{i,t} \qquad i \in \boldsymbol{\mathcal{M}}, t \in \boldsymbol{\mathcal{T}} \qquad (22)$$

Multiple penalty bands can be defined, attributing an increasing specific penalty cost to more abrupt set-point modifications. This way, a cost dead band can also be included, associating no penalization to

variations within a certain threshold. If n_i^{bands} is the number of penalization bands for set point variation curve of machine i, each characterized by an increasing specific deviation cost $\tilde{c}_{i,b}^{\Delta P}$ and a validity threshold $\widetilde{th}_{i,b}^{\Delta P}$, overall deviation cost is lower bounded by the family of linear constraints:

$$c_{i,t}^{\Delta P} \geq \Delta in_{i,t} \tilde{c}_{i,b}^{\Delta P} + \tilde{q}_{i,b}^{\Delta P} \qquad i \in \boldsymbol{\mathcal{M}}, b \in [1..n_i^{bands}] \qquad (23)$$

$$\tilde{q}_{i,b}^{\Delta P} = \widetilde{th}_{i,b-1}^{\Delta P}\left(\tilde{c}_{i,b}^{\Delta P} - \tilde{c}_{i,b-1}^{\Delta P}\right) + \tilde{q}_{i,b-1}^{\Delta P} \qquad i \in \boldsymbol{\mathcal{M}}, b \in [2..n_i^{bands}] \qquad (24)$$

$$\tilde{q}_{i,1}^{\Delta P} = 0 \qquad i \in \boldsymbol{\mathcal{M}} \qquad (25)$$

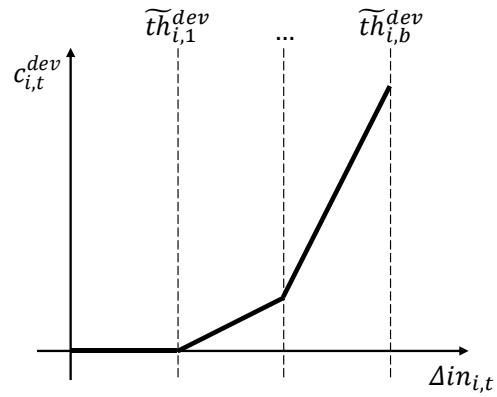

Figure 3: band-dependent set point variation cost as function of set point variation $\Delta in_{i,t}$

3.4.2 Non-dispatchable Units

Non-dispatchable units mainly represent RES, which do not consume any fuel and provide an output which is only a function of the environmental conditions. These units can still be represented as dispatchable units, if they can be connected/disconnected from the system (on/off dispatchable units), or if they are equipped with a control system capable of reducing their output from the maximum potential (e.g. PV panels equipped with a Reduced Power Point Tracking module, RPPT). The output of RES which cannot be controlled in any way can be, in principle, directly discounted from the demand profiles to obtain the net demand. It is often important though to keep track of the isolated contribution of each RES, to define for example reserve requirements that account for source-wise generation stability. To this end, a generation profile is defined for each RES included in the non-controllable units set $\boldsymbol{\mathcal{ND}}$:

$$o_{i,j,t} = \tilde{o}_{i,j,t} \qquad \forall t \in \boldsymbol{\mathcal{T}}, i \in \boldsymbol{\mathcal{ND}} \qquad (26)$$

Non-controllable units can still provide more than one output (e.g. thermal-PV).

3.4.3 Storages

The general representation of a storage system is equivalent to the model of a tank, varying its content level according to the exchanges with the energy network to which it is connected. The decision variables defining the operating and internal status of each storage $s \in \boldsymbol{\mathcal{S}}$ at time t are:

- Storage bus exchange rate $sp_{s,t}$, split into charging and discharging components $sp_{s,t}^{ch}$ / $sp_{s,t}^{disch}$;
- Storage content level $C_{s,t}$.

Storage bus exchange $sp_{s,t}$, positive when the flux is directed from the storage to the bus, negative otherwise, is yield by the difference between the strictly positive charge/discharge components $sp_{s,t}^{ch}$ and $sp_{s,t}^{disch}$, accounting for charge/discharge efficiencies $\tilde{\eta}_s^{ch}$ / $\tilde{\eta}_s^{disch}$:

$$sp_{s,t} = sp_{s,t}^{disch}\,\tilde{\eta}_s^{disch} - \frac{sp_{s,t}^{ch}}{\tilde{\eta}_s^{ch}} \qquad \forall t \in \boldsymbol{\mathcal{T}}, s \in \boldsymbol{\mathcal{S}} \qquad (27)$$

Storage content can degrade in time, such as in the case of thermal storages losing heat to the environment or the self-discharge of electrochemical storages due to internal reactions. In both cases, charge loss is proportional to the charge level. The dynamic equation expressing the evolution in time of storage content $C_{s,t}$ is expressed as:

$$C_{s,t+1} = C_{s,t}\left(1 - \tilde{\eta}_s^{sd}\widetilde{\Delta t}\right) + \left(sp_{s,t}^{ch} - sp_{s,t}^{disch}\right)\widetilde{\Delta t} \qquad \forall t \in \boldsymbol{\mathcal{T}}, s \in \boldsymbol{\mathcal{S}} \qquad (28)$$

where: $\tilde{\eta}_s^{sd}$ is the storage self-discharge rate and $\widetilde{\Delta t}$ is the time-step duration. At all times, storage charge is bounded within maximum and minimum capacity:

$$\tilde{C}_s^{min} \leq C_{s,t} \leq \tilde{C}_s^{max} \qquad \forall t \in \boldsymbol{\mathcal{T}}, s \in \boldsymbol{\mathcal{S}} \qquad (29)$$

Case-specific detailed linear models can be adopted for storage technologies that exhibit more complex dynamic behavior. This is the case of lead-acid batteries, for which the "two-tanks" Kinetic Battery Model (KiBaM [60]) has been implemented in the model design adaptation described in Chapter 8.

Splitting net storage power into its inwards / outwards positive components is necessary to separately account for storage charge/discharge efficiencies. When losses caused by either process represent an incontrovertible penalization to the overall performance, the solution optimality will inevitably imply that in each time step only one of the two fluxes will be different from zero. Nevertheless, in the presence of constraints that account for the consequences of production surplus, a storage status variable $s_{s,t}$ should be introduced, to prevent charge/discharge components from being different from zero at the same time, leading to losses overestimate which might be used to dissipate the production excess. In this case, storage charge and discharge power are limited by storage power rating $\widetilde{sp}_s^{ch,max}$ / $\widetilde{sp}_s^{disch,max}$, as well as by the charge/discharge status variable $s_{s,t}$, equal to 1 when the storage is charging:

$$0 \leq sp_{s,t}^{ch} \leq \widetilde{sp}_s^{ch,max} s_{s,t} \qquad \forall t \in \boldsymbol{\mathcal{T}}, s \in \boldsymbol{\mathcal{S}} \qquad (30)$$

$$0 \leq sp_{s,t}^{disch} \leq \widetilde{sp}_s^{disch,max}\,(1 - s_{s,t}) \qquad \forall t \in \boldsymbol{\mathcal{T}}, s \in \boldsymbol{\mathcal{S}} \qquad (31)$$

Variable $s_{s,t}$, can be removed from the constraints if losses overestimate is not considered a problem.

Operation and maintenance costs for storage systems $c_{s,t}^{O\&M}$ quantifies the cost of storage wearing and is therefore proportional to storage usage, in terms of energy throughput. Wearing costs $\tilde{c}_s^{OMxTP}$ is entirely allocated on the storage discharge component, firstly because it is conceptually more similar to attributing a marginal dispatch cost to energy drawn from the storage, and secondly to avoid potential situations in which dissipating production excess is more convenient in terms of global objective function than charging the storage.

$$c_{s,t}^{O\&M} = sp_{s,t}^{disch} \tilde{c}_s^{OMxTP} \qquad \forall t \in \boldsymbol{\mathcal{T}}, s \in \boldsymbol{\mathcal{S}} \qquad (32)$$

Since the optimization foresight is limited to the horizon time, no information is available to determine the value of any residual storage charge at the end of the simulation period. A common solution to prevent complete storage depletion within the simulation horizon is to impose a cyclic storage charge constraint (e.g. final condition equal to starting condition). An alternative, that avoids binding final storage capacity to a fixed value, is to associate a valorization v_i^{end} to the final storage content $C_{s,T}$:

$$v_i^{end} = C_{s,T} \tilde{v}_i^C \qquad \forall s \in \boldsymbol{\mathcal{S}} \qquad (33)$$

The specific residual charge value $\tilde{v}_i^C$ should be equal to the expected avoided cost that a higher starting capacity would ensure in the following solution instance of the optimization problem, starting at the end of the present horizon time. In other terms, the final storage valorization is related to the marginal production cost below which it is optimal to produce to charge the storage, as well as the threshold above which (accounting for the effect of round-trip efficiency) it is convenient to use the storage instead of a less cost-effective production unit.

3.4.4 Networks

External networks connected to the MES behave like sources/sink that can bi-directionally exchange with the microgrid according to inwards/outwards flux limitations. Time-dependent purchase/selling price profiles allow for an economic valorization of trades. The decision variables defining the exchange status with a network at time t are:

- Net exchange rate $np_{s,t}$, split into the purchase and selling components $np_{s,t}^{pur}$ / $np_{s,t}^{sell}$.

As seen for storages, net network exchange, positive when the flux is directed from the network to the microgrid, negative otherwise, is yield by the difference between the strictly positive purchase/selling components, on which separate maximum limitations are enforced:

$$np_{n,t} = np_{n,t}^{pur} - sp_{n,t}^{sell} \qquad \forall t \in \boldsymbol{\mathcal{T}}, n \in \boldsymbol{\mathcal{N}} \qquad (34)$$

$$0 \leq np_{n,t}^{pur} \leq \widetilde{np}_n^{pur,max} \qquad \forall t \in \boldsymbol{\mathcal{T}}, n \in \boldsymbol{\mathcal{N}} \qquad (35)$$

$$0 \leq np_{n,t}^{sell} \leq \widetilde{np}_n^{sell,max} \qquad \forall t \in \boldsymbol{\mathcal{T}}, n \in \boldsymbol{\mathcal{N}} \qquad (36)$$

Net trading value is calculated according to the purchase/selling prices $\tilde{c}_{n,t}^{pur}$ / $\tilde{c}_{n,t}^{sell}$:

$$c_{n,t}^{net} = np_{n,t}^{pur} \tilde{c}_{n,t}^{pur} - np_{n,t}^{sell} \tilde{c}_{n,t}^{sell} \qquad \forall t \in \boldsymbol{\mathcal{T}}, n \in \boldsymbol{\mathcal{N}} \qquad (37)$$

In this case, it is not necessary to introduce a binary variable imposing that a given time only net flux component is different from zero since the effect on the objective function of a simultaneous purchase/selling is unambiguously negative (as long as the selling price is lower than the purchase price). Therefore, solution optimality will always imply the required condition.

3.4.5 Connectors

Microgrid goods $\boldsymbol{\mathcal{G}}$ can represent either distinct physical goods which differ because of their physical nature (e.g. heat and electricity in CHP systems) or virtual goods, which are differentiated in order to represent the

microgrid topological characteristics. Specifically, a purely electric microgrid with different buses and transmission lines can be modeled as a multi-good microgrid by associating to each bus a different good. In this perspective, transmission lines can be represented as components converting one good into another. Connectors can be mono- or bi-directional, and each connection converting good i in good j is characterized by a transmission efficiency $\tilde{\eta}_{i,j}$. Defining as $\boldsymbol{\mathcal{C}}$ the set of ordinated couples (i,j) indicating a connection converting good i in good $j \in \boldsymbol{\mathcal{G}}$, the directional non-negative flux across the connection is limited by connector capacity $\tilde{p}_{i,j}^{conn,max}$:

$$0 \leq p_{i,j,t}^{conn} \leq \tilde{p}_{i,j}^{conn,max} \qquad \forall t \in \boldsymbol{\mathcal{T}}, (i,j) \in \boldsymbol{\mathcal{C}} \qquad (38)$$

As already seen in the case of storages, if the connection is bidirectional and does not have bi-directional unit efficiency, the connector will be able to introduce an artificial dissipation on either one of its ends. If excess production of either good i or good j might cause violating some constraints, it is therefore necessary to introduce a binary variable preventing a simultaneous transfer in both directions:

$$0 \leq p_{i,j,t}^{conn} \leq \tilde{p}_{i,j}^{conn,max} c_{ij} \qquad \forall t \in \boldsymbol{\mathcal{T}}, (i,j) \in \boldsymbol{\mathcal{C}} \qquad (39)$$

$$0 \leq p_{j,i,t}^{conn} \leq \tilde{p}_{j,i}^{conn,max} (1 - c_{ij}) \qquad \forall t \in \boldsymbol{\mathcal{T}}, (i,j) \in \boldsymbol{\mathcal{C}} \qquad (40)$$

3.4.6 Loads and Generation Balance

Loads $\boldsymbol{\mathcal{L}}$ can be divided into two categories: non-deferrable loads $\boldsymbol{\mathcal{L}}_j^{nd}$ and deferrable loads $\boldsymbol{\mathcal{L}}_j^{d}$.

Non-deferrable loads do not offer any exploitable degree of freedom in the optimization process, and simply constitute a fixed demand profile that must be satisfied by the system. Failing at providing the instantaneous demand of a non-deferrable load is normally associated with a penalty cost. Each non-deferrable load $l \in \boldsymbol{\mathcal{L}}_j^{nd}$ is therefore associated with a reference demand profile $\tilde{d}_{l,t}$, and to an unmet demand $\sigma_{l,t}$ such that:

$$0 \leq \sigma_{l,t} \leq \tilde{d}_{l,t} \qquad \forall t \in \boldsymbol{\mathcal{T}}, s \in \boldsymbol{\mathcal{S}} \qquad (41)$$

Deferrable loads $l \in \boldsymbol{\mathcal{L}}_j^{d}$ on the other hand, accept a decoupling between actual supply profile $d_{l,t}^{d}$and reference demand profile $\tilde{d}_{l,t}^{d}$. The cumulated good supply must be equivalent to the reference cumulated demand over given temporal windows $w \in \boldsymbol{\mathcal{W}}_l$, with a tolerance that can depend on time (Eq.(43)).

A demand – production balance is enforced for all MES internal goods $\boldsymbol{\mathcal{G}}$ in each timestep, accounting for production and consumption contributions:

$$\sum_{i \in \boldsymbol{\mathcal{M}}} o_{i,j,t}^{TOT} - \sum_{i \in \boldsymbol{\mathcal{B}}_j} in_{i,t}^{TOT} + \sum_{s \in \boldsymbol{\mathcal{S}}_j} sp_{s,t} + \sum_{n \in \mathcal{N}_j} np_{n,t} + \sum_{i \in \boldsymbol{\mathcal{ND}}_j} \tilde{o}_{i,j,t}^{TOT} \sum_{(i,j) \in \boldsymbol{\mathcal{C}}} p_{i,j,t}^{conn} \tilde{\eta}_{i,j} - \sum_{(j,i) \in \boldsymbol{\mathcal{C}}} p_{j,i,t}^{conn} = \sum_{l \in \boldsymbol{\mathcal{L}}_j^{nd}} \left(\tilde{d}_{l,t} - \sigma_{l,t}\right) + \sum_{l \in \boldsymbol{\mathcal{L}}_j^{d}} d_{l,t}^{d} + p_{j,t}^{diss} \qquad \forall j \in \boldsymbol{\mathcal{G}}, \; t \in \boldsymbol{\mathcal{T}} \qquad (42)$$

$$\sum_{w} \left(\tilde{d}_{l,w}^{d} - \sigma_{l,w}\right)\left(1 - \widetilde{Th}_{l,w}^{DWN}\right) \leq \sum_{w} d_{l,w}^{d} \leq \sum_{w} \left(\tilde{d}_{l,w}^{d} - \sigma_{l,w}\right)\left(1 + \widetilde{Th}_{l,w}^{UP}\right) \qquad \forall j \in \mathcal{G}, \; l \in \boldsymbol{\mathcal{L}}_j^{d}, \; w \in \boldsymbol{\mathcal{W}}_l \qquad (43)$$

Where:

- $\sum_{i \in \boldsymbol{\mathcal{M}}_j} o_{i,j,t}^{TOT}$ is the overall production of good j from dispatchable producers $\boldsymbol{\mathcal{M}}_j$ producing j
- $\sum_{i \in \boldsymbol{\mathcal{B}}_j} in_{i,j,t}^{TOT}$ is the overall consumption of good j from dispatchable consumers $\boldsymbol{\mathcal{B}}_j$ consuming j
- $\sum_{i \in \boldsymbol{\mathcal{S}}_j} sp_{s,t}$ is the net bus exchange with the storage systems $\boldsymbol{\mathcal{S}}_j$ storing good j
- $\sum_{i \in \boldsymbol{\mathcal{N}}_j} np_{n,t}$ is the net exchange with the network $\boldsymbol{\mathcal{N}}_j$ trading good j
- $\sum_{i \in \boldsymbol{\mathcal{ND}}_j} \tilde{o}_{i,j,t}^{TOT}$ is the overall production of good j from non-dispatchable machines $\boldsymbol{\mathcal{ND}}_j$ producing j
- $\sum_{(i,j) \in \boldsymbol{\mathcal{C}}} p_{i,j,t}^{conn} \tilde{\eta}_{i,j}$ is the overall inwards flux from all connectors $\boldsymbol{\mathcal{C}}_j^{\leftarrow}$ directed to j
- $\sum_{(j,i) \in \boldsymbol{\mathcal{C}}} p_{j,i,t}^{conn}$ is the overall outwards flux to all connectors $\boldsymbol{\mathcal{C}}_j^{\rightarrow}$ converting good j
- $\sum_{l \in \boldsymbol{\mathcal{L}}_j} \left(\tilde{d}_{l,t} - \sigma_{l,t}\right)$ is the served non-flexible demand of good j at time t, obtained subtracting from reference demand $\tilde{d}_{l,t}$ of non-dispatchable load $l \in \boldsymbol{\mathcal{L}}_j^{nd}$ the non-served demand $\sigma_{l,t}$
- $p_{j,t}^{diss}$ is the overall dissipated production excess of good j at time t
- $\sum_w \left(\tilde{d}_{l,w}^{d} - \sigma_{l,w}\right)$ is the served dispatchable demand over time - window $w \in \boldsymbol{\mathcal{W}}_l$

Physical limits in the dissipation of excess production (e.g. nominal power of electric dump-load, heat rejection system, etc.) can be accounted for by introducing an upper limitation on $p_{j,t}^{diss}$:

$$0 \leq p_{j,t}^{diss} \leq \tilde{p}_{j,t}^{diss,max} \qquad \forall j \in \boldsymbol{\mathcal{G}}, t \in \boldsymbol{\mathcal{T}} \qquad (44)$$

Unmet demand is associated in any case to a specific penalty cost, which must quantify the damage of not supplying the required demand. The penalty cost can be an actual cost (e.g. contractual penalty for service interruption) or a virtual cost proportional to the entity of consequences following unbalances (e.g. black-out due to insufficient generation capacity in off-grid electrical systems). Each load $l \in \boldsymbol{\mathcal{L}}_j$, regardless of whether it is deferrable or not, is therefore associated with a specific unmet penalty $\tilde{c}_l^{\sigma}$, which contributes to the overall unmet cost $c_{j,t}^{UM}$ for good $j \in \boldsymbol{\mathcal{G}}$ at time t:

$$c_{j,t}^{UM} = \sum_{l \in \boldsymbol{\mathcal{L}}_j} \sigma_{l,t} \cdot \tilde{c}_l^{\sigma} \qquad \forall j \in \boldsymbol{\mathcal{G}}, t \in \boldsymbol{\mathcal{T}} \qquad (45)$$

Identifying separate non-deferrable loads profiles, instead of working directly with an aggregate non-deferrable load, is useful to distinguish loads that are associated with different levels of priority, quantified by the load-specific unmet penalty $\tilde{c}_l^{\sigma}$.

It is often useful to associate a virtual cost also to excess production dissipation $p_{j,t}^{diss}$. Although solution optimality ensures that no unnecessary dissipation takes place, if no cost is associated to dissipation it is not relevant from the point of view of the optimization when the dissipation takes place, as long as the optimal overall amount of production is curtailed. In reality, due to the non-deterministic nature of non-dispatchable generation potential and of demand, it is always preferable to differentiate among equivalent solutions the one that postpone dissipation of excess production, whenever possible, as long as possible, so

that if the excess production has been overestimated (e.g. higher demand, renewable production lower than forecast) generation potential can be increased by avoiding dissipation in later times. This preferential selection among otherwise equivalent solutions can be introduced in the formulation by defining a virtual time-dependent dissipation cost $c_{j,t}^{diss}$ for each good $j \in \boldsymbol{\mathcal{G}}$:

$$c_{j,t}^{diss} = p_{j,t}^{diss} \cdot \tilde{c}_{j,t}^{diss} \qquad \forall j \in \boldsymbol{\mathcal{G}}, t \in \boldsymbol{\mathcal{T}} \qquad (46)$$

Where $\tilde{c}_{j,t}^{diss}$ is the specific dissipation cost for good $j \in \boldsymbol{\mathcal{G}}$ at time t. To postpone production curtailment, dissipation cost $\tilde{c}_{j,t}^{diss}$ must decrease in time.

3.5 Reserve Constraints

The deterministic scheduling problem formulation presented in this Chapter assumes that forecast profiles of demand and non-dispatchable generation are certain and does not account for the effect of their potential deviation from their nominal profile. These deviations are thus managed by lower control levels, which will be discussed at length in the following Chapters. Therefore, it is often necessary to impose a level of conservativeness to the deterministic scheduling solution, to ensure that real-time corrections to the dispatch profiles can actually be implemented by the system. To this end, reserve constraints can be added in the formulation: they require that the maximum generation potential from storage systems and active generators is enough to compensate the maximum potential net demands increase:

$$\sum_{s \in \boldsymbol{\mathcal{S}}} sp_{s,t}^{res} + \sum_{i \in \boldsymbol{\mathcal{M}}} p_{i,j,t}^{res} z_{i,t} \geq \tilde{d}_{j,t}(1 + \Delta \tilde{d}_{j,t}^{\%}) - \sum_{i \in UP} \widetilde{up}_{i,t}(1 - \Delta \widetilde{up}_{i,t}^{\%}) \qquad \forall t \in \boldsymbol{\mathcal{T}} \qquad (47)$$

The reserve contribution from generators $p_{i,j,t}^{res}$ is bounded by either the maximum load or the ramping limitations:

$$p_{i,j,t}^{res} = \min\left(\tilde{p}_{i,j}^{max}, p_{i,j,t} + \widetilde{ru}_{i,j}^{lim}\right) \qquad \forall t \in \boldsymbol{\mathcal{T}} \qquad (48)$$

The reserve contribution from the storage system is bounded by either the maximum storage power or minimum storage charge:

$$sp_{s,t}^{res} \leq \min\left(\widetilde{sp}_{s}^{max}; \frac{C_{s,t} - \tilde{C}_{s}^{min}}{\widetilde{\Delta t}}\right) \qquad \forall t \in \boldsymbol{\mathcal{T}} \qquad (49)$$

Note that within the day-ahead planning MILP the limitation on reserve contribution deriving from the minimum storage charge constraint is enforced with respect to the expected storage content $C_{s,t}$. During real-time operation though, if the storage system compensates net demand forecast errors the storage charge trajectory will be different from its expected profile (computed by the scheduling MILP). This might hinder the ability of the storage system to provide reserve power, particularly in later timesteps, when the build-up effect of forecast errors is more significant. Therefore, an additional "energy reserve" constraint is added, to impose that the planned storage charge is enough to provide the reserve contribution for the future $\tilde{T}^{res}$ time steps:

$$\sum_{\tau=t}^{t+\tilde{T}^{res}} sp_{s,\tau}^{res}\widetilde{\Delta t} \leq C_{s,t} - \tilde{C}_s^{min} \qquad \forall t \in \mathcal{T} \qquad (50)$$

Although the constraint does not account for the actual storage charge evolution, the conservativeness of the deterministic planning solution can be increased by increasing the energy reserve duration $\tilde{T}^{res}$, as well as the power deviation thresholds $\Delta\widetilde{up}_{i,t}^{\%}$ and $\Delta\tilde{d}_{j,t}^{\%}$.

3.6 Topology

The modeling approach presented can also be used to introduce the effect of topology in systems where loads and units are located in different areas connected by internal distribution networks. This can be done by defining nodes associated with a virtual good, whose balance will only be directly affected by those units connected to the node. The nodes can be then linked by connectors, creating an oriented graph which is representative of the physical connections within the system. This topological model is valid as long as the distribution system is not characterized by strong dynamic behavior.

3.7 System modeling example: household featuring Solar Assisted Heat Pump

A practical example of a complex system which optimal management problem was tackled according to the proposed formulation is the system for the domestic supply of electricity, sanitary hot water, and heating shown in Figure 4.

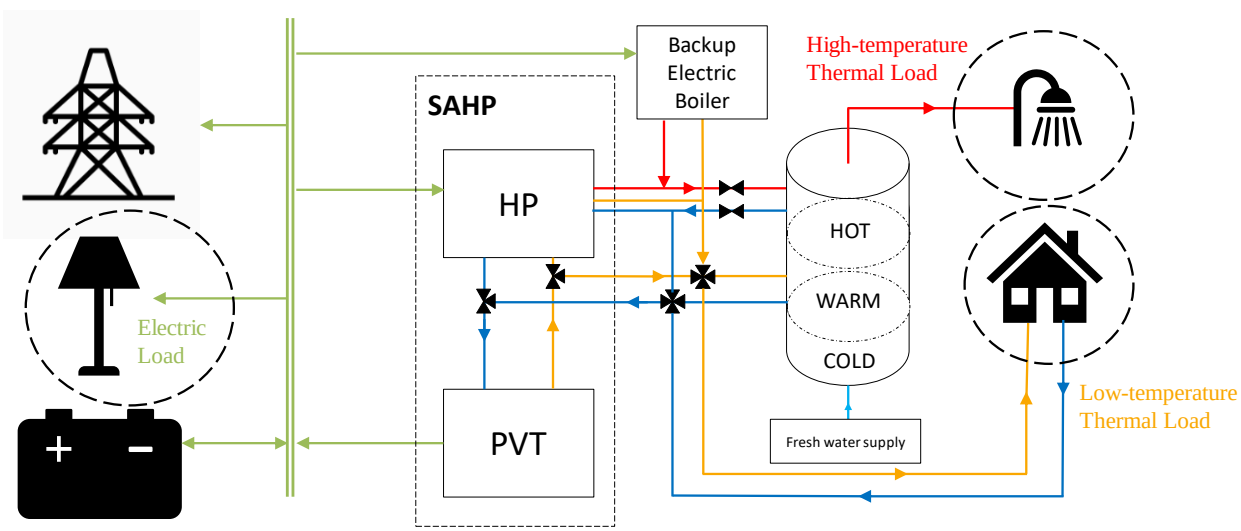

Figure 4: scheme of the system for the domestic supply of electricity, heating and sanitary hot water featuring a Solar-Assisted Heat Pump

The system features a Solar Assisted Heat Pump (SAHP), a unit comprising a traditional Heat Pump (HP) and a Photo-Voltaic Thermal (PVT) panel array, which is a PV array featuring an internal cooling system. Its thermal output that can be used to enhance the performances of the HP or to supply a low-temperature thermal load. The SAHP is supported in supplying the thermal load by a backup electric boiler. This system has been the object of a doctoral thesis [61], in which the MILP model was used to assess its optimal performance. It is here presented only as an example of complex system that can be tackled with the

proposed formulation: the results of the calculations go beyond the scope of this thesis and are not here reported. Results can be found in [61] and in [62].

Both the SAHP and the electric boiler can produce at two temperature levels, associated to the requirements for sanitary water supply (high-temperature thermal load) and for the house radiant floor heating system (low-temperature thermal load). The PVT heat production is only compatible with the low-temperature thermal load. Additionally, the system features a battery, to increase self-consumption of the electricity produced by the PVT panels and limit the dependency from the grid, and a hot water tank, where the fresh water supply from the central water system is heated up to reach the temperature target required by the high-temperature thermal load.

The different colors in Figure 4 indicate the various forms of energy that are exchanged within the microgrid, and constitute the set of microgrid goods $\boldsymbol{\mathcal{G}}$: electricity, and low-temperature heat and high-temperature heat. Each good $j \in \boldsymbol{\mathcal{G}}$ is in this case associated with a single load $\boldsymbol{\mathcal{L}}_j$: electricity and sanitary hot water represent non-dispatchable loads, as their demand must be immediately served. On the other hand, low-temperature heat for household heating is provided by a radiant floor system, connected to the low-temperature water circuit. Due to the considerable thermal inertia of the radiant floor system, deviations from the reference heat supply profile are allowed, as long as an equivalent energy supply over periodic time windows is provided. Low-temperature heat can, therefore, be treated as a deferrable load, imposing the equivalence between the energy supply profile integral and the low-temperature heat reference demand profile, over time windows $w \in \boldsymbol{\mathcal{W}}_{LTH}$, as represented by Eq.(43). The allowed thermal shift between consecutive windows can be controlled by tuning parameters $\widetilde{Th}^{DWN}_{LTH,w}$ and $\widetilde{Th}^{UP}_{LTH,w}$.

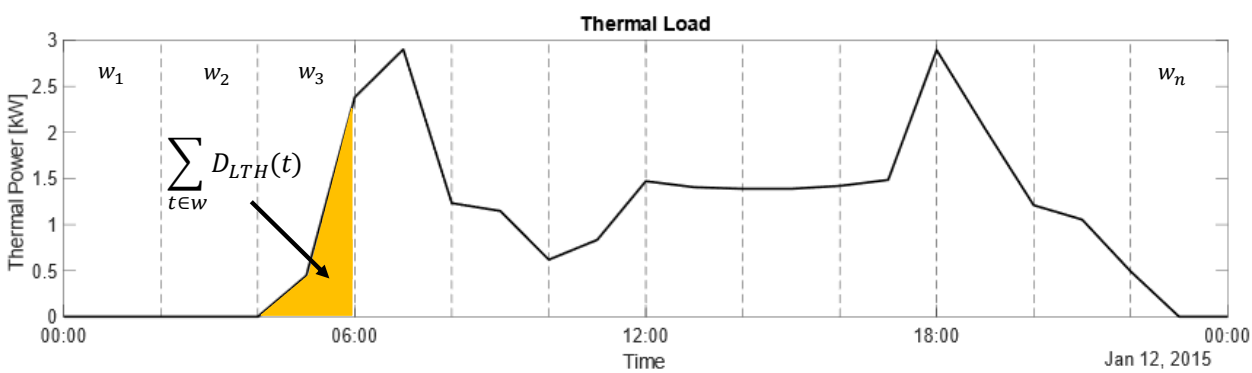

Figure 5: reference low-temperature heat profile and energy integral imposed for time window w3.

To account for the various potential operating modes of the SAHP, associated to the opening and closing of the valves shown in Figure 4 and to the different temperature setpoints of the heat pump, the SAHP is modeled as four mutually exclusive machines, corresponding to the various SAHP operating modes shown in Figure 6. These units constitute the group of mutually exclusive units $\boldsymbol{\mathcal{ME}}_{SAHP}$. Only one SAHP operating mode can thus be active at a given time. The same approach is used to model the alternative operating modes of the electric boiler. Part-load curves are defined as piece-wise functions, parameterized according to two time-dependent environmental factors $\boldsymbol{\Theta}_t$: ambient temperature and solar radiation.

The lithium-Ion battery and the coupling with the national grid can be modeled according to the methodologies described respectively in 3.4.3 and 3.4.4. The open-circuit hot water tank, on the other hand, represents an example of a component that does not fit in the general approach described above. For such components, an ad-hoc set of constraints was defined to represent its operation in the MILP dispatch problem formulation. The modeling strategy adopted for the open-loop storage can be found in [62].

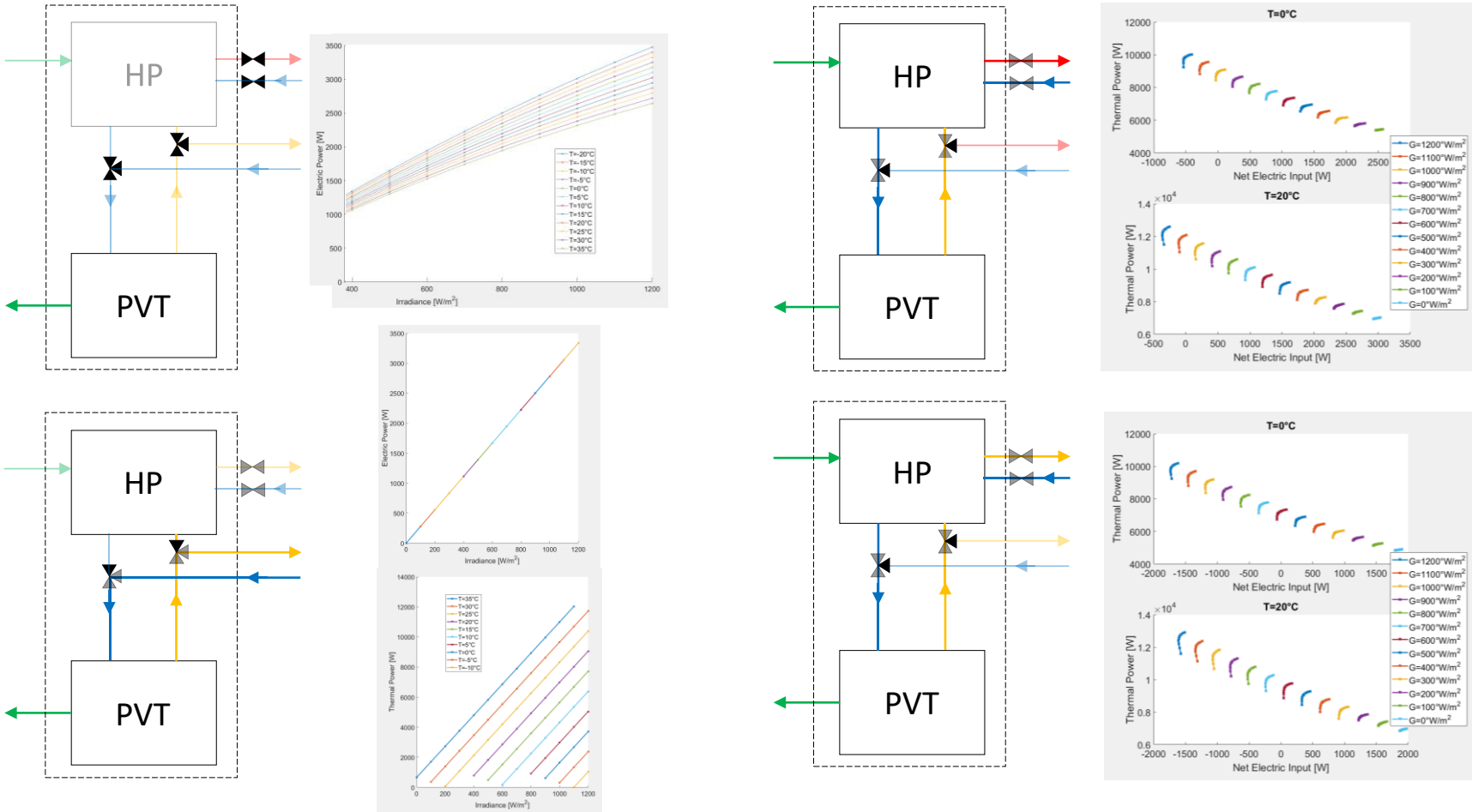

Figure 6: SAHP operating modes, associated to virtual mutually exclusive dispatchable units, and relevant part-load curves, as function of ambient paramters

4 AFFINELY ADJUSTABLE ROBUST SCHEDULING PROBLEM FORMULATION

This Chapter proposes an alternative MILP formulation of the scheduling problem presented in Chapter 3, based on the Affinely Adjustable Robust Optimization (AARO) theory. Uncertainty of forecast profiles is explicitly addressed by defining a mathematical uncertainty space, encompassing all potential manifestations of uncertain parameters. In addition to the nominal solution, that represents the operating schedule in case forecasts are not affected by errors, the approach yields optimal decision rules as linear functions of forecast errors manifestations, which indicate how to adjust the operating load of the units to adapt the dispatch solution to the uncertainty manifestation. The optimal problem solution, comprising both nominal scheduling and dispatch adjustment policies, ensures operation feasibility for any manifestation of forecast errors included in the uncertainty space. The AARO formulation is on the other hand associated to limitations in the capacity of dealing with system non-linearities, due to the functional form of decision rules, and to a significant increase in the problem computational complexity with respect to the deterministic formulation of Chapter 3. Furthermore, the AARO solution approach pursued in this thesis, based on the derivation of a tractable robust counterpart reformulation by exploiting the strong duality theorem, must deal with the impossibility of defining integer recourse variables. This limitation introduces inaccuracies in the mathematical definition of the recursive actions, such as underestimate of storage recursive efficiency and over-conservative optimal decision rules. These limits are thoroughly examined by means of practical examples.

The scheduling problem formulation proposed in Chapter 3 is deterministic, in the sense that it only accounts for uncertainty in the input profiles of exogenous factors (demand profiles, non-dispatchable generation potential profiles) by enforcing reserve constraints (Paragraph 3.5), but does not explicitly account for manifestations of the forecasted uncertain parameters different from their nominal profiles. The system response to all deviations of exogenous parameters from forecast is left to the lower-level management algorithms. This Chapter presents an alternative formulation of the deterministic UC and ED problem defined in Chapter 3, based on the Affinely Adjustable Robust Optimization (AARO) framework. The model is developed for a generic MES subject to multiple uncertain demands and non-dispatchable generators. The mathematical structure of the adopted robust formulation is incompatible with some of the representation techniques introduced in the previous Chapter for the deterministic MILP formulation (e.g. piece-wise linearization of part-load curves). The AARO model here presented is, therefore, less adaptable to general systems that feature strong non-linearities.

The model is *two-stage*, meaning that two different hierarchical levels are identified in the formulation. The first layer is associated with the optimal "*nominal*" UC and ED corresponding to the nominal forecasts of demand and non-dispatchable generation. First stage variables are referred to as "*here and now* decisions" since they must be defined ahead of the operation time. The first layer output corresponds to the nominal operating schedule defined by the deterministic formulation of Chapter 3. Second stage variables are conversely referred to as "*wait and see* decisions": instead of assuming a unique value regardless of the specific

uncertainty manifestation, they are defined in the form of functions (*decision rules*) depending on the actual observations of all uncertain parameters. Based on the observed values of demand and non-dispatchable generation (or equivalently on the observed forecast errors history), second stage variables are therefore adjusted, adapting to each specific scenario. In the UC and ED problem, second stage variables include setpoint corrections for all dispatchable units, storages, and network exchanges. The problem second stage is also referred to as "*recourse"* with respect to the *nominal* first stage solution, and second stage variables are also called *recursive decisions*. The model is formulated for both off-grid and grid-connected systems. In systems interacting with external networks, particular attention is paid to the evaluation of the effect that decision rules have on the economic interaction with the networks. Compared to previous works using AARO approaches (e.g., [54][53]), the proposed model features:

- Uncertainty affecting two or more demands of energy (e.g., electricity and heat);
- The accurate modeling of the costs/revenues associated with the recourse adjustments of the energy exchanges with external energy networks (e.g., national grid);
- An ad hoc formulation of the uncertainty set allowing appreciable performance improvements with respect to the traditional Γ-robustness approach [63];
- Simplified decision rules (here called "partial recourse memory"), attaining good system performance while considerably reducing the computational time.

The conceptual advantages and limits of the proposed formulation are discussed and analyzed in Paragraph 4.5, by means of simple synthetic test cases. The adoption of the formulation is then compared with the deterministic approach of Chapter 3 in Chapters 5 and 6, analyzing three different real-world test cases under various operating scenarios.

Although we limit our attention to electric and CHP systems, it is worth noting that the proposed model could be applied more in general to complex MES.

4.1 Problem Statement

As depicted in Chapter 3, the generic MES comprises a set of dispatchable and non-dispatchable units (e.g., intermittent renewable sources), and is potentially connected to energy storage systems and external energy networks. For the sake of simplicity, and in accordance with the test cases presented in the following Chapters, in this Chapter we limit the attention to systems that only have one non-dispatchable load per each microgrid internal good, and that feature single-output non-dispatchable generators. The model could, on the other hand, be extended to feature multiple loads and poly-generation non-dispatchable units, to get to a more general system schematization as done for the deterministic formulation in Chapter 3. A schematic representation of the MES to which the AARO formulation refers is depicted in Figure 7, highlighting with dashed circles the accounted sources of uncertainty.

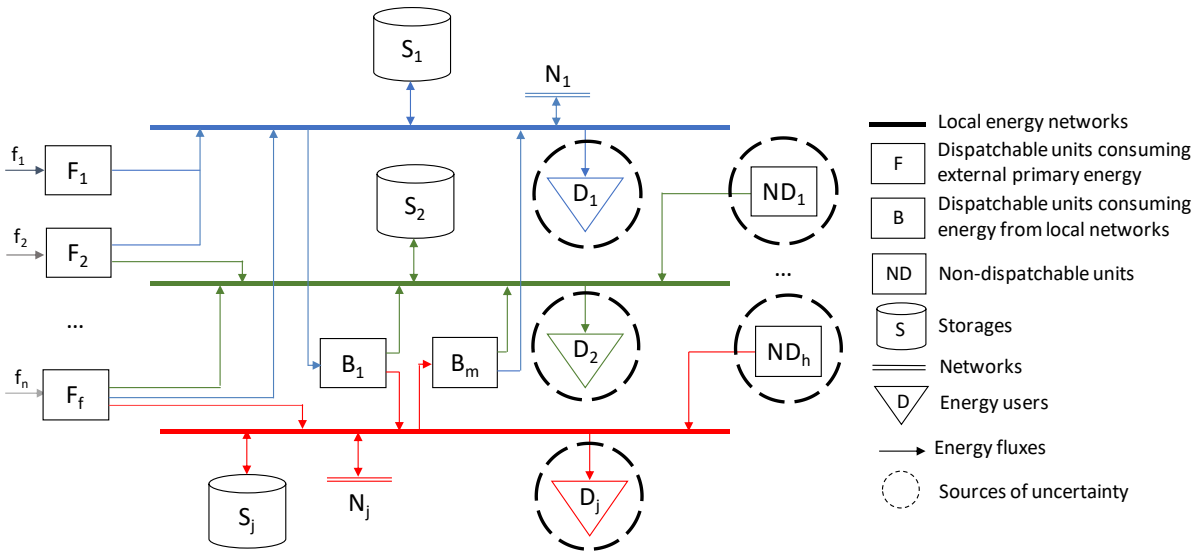

Figure 7: MES subject to multiple uncertainty factors.

Energy demand profiles and generation potential profiles of non-dispatchable units were, in the deterministic formulation, only characterized by their nominal forecast. Due to the stochastic nature of environmental conditions and to the unpredictable decisions of the MES users influencing the energy demand patterns, forecasts are on the other hand affected by uncertainty (i.e., the reference profiles will be affected by errors). These potential deviations from forecasts are accounted by the deterministic formulation through the definition of reserve constraints. The robust formulation adopts a more systematic approach to uncertainty: uncertain parameters are defined by a mathematical description of the potential errors associated with their nominal forecast profiles. The mathematical space that bounds the potential uncertainty manifestations (e.g. the actual values assumed by uncertain parameters as opposed to their forecast), is referred to as *uncertainty set* $\boldsymbol{\mathcal{U}}$.

The scheduling problem tackled through the robust formulation proposed in this Chapter can be stated as follows. Given:

- forecasts of power generation from non-dispatchable units and energy demand profiles;
- uncertainty space encompassing all possible forecast errors;
- operating limits and part-load performance maps of dispatchable units;
- forecasted generation potential of non-dispatchable units (e.g., solar, wind);
- charge/discharge efficiency of storage systems;
- transmission losses and maximum transmission capacity of networks;

we aim at determining:

- the nominal commitment and dispatch solution (i.e., here and now decisions) to be taken sufficiently ahead of the operation time (e.g., 24 hours ahead) based on the available forecast;

- the optimal decision rules that set how to adjust units setpoints, storage charge/discharge and exchanges with energy networks during real-time operation, while minimizing the expected operating cost (nominal costs plus the expected cost of recursive decisions).

The identified solution must guarantee operational feasibility for any possible uncertainty realization (i.e., forecast error) within the uncertainty space $\boldsymbol{\mathcal{U}}$.

This last feature is the essential appeal of the robust formulation: once a conservativeness level is defined by tuning the definition of the uncertainty set, the solution yield by the formulation comes with a guarantee that, as long as the units are regulated according to the optimal decision rules and the observed forecast errors are encompassed by the uncertainty set, service continuity is enforced with a mathematical guarantee.

4.2 Adjustable Robust Problem Formulation

This Paragraph presents the uncertain formulation of the scheduling problem for the general system depicted in Figure 7. Forecasts uncertainty is represented by unknown deviations from the nominal forecast of all MES internal demands $\delta\boldsymbol{d}$ and of the generation potential from all non-controllable units $\delta\boldsymbol{up}$. Parameters and variables which assume a different value according to the uncertainty manifestation are indicated with the superscript $^{\delta}$. In general, variables vector $\boldsymbol{x}^{\delta}$ comprises a nominal (first stage) value $\boldsymbol{x}$ and a recursive (second stage) correction $\Delta\boldsymbol{x}^{\delta}$ which depends on the uncertainty manifestation:

$$\boldsymbol{x}^{\delta} = \boldsymbol{x} + \Delta\boldsymbol{x}^{\delta} \tag{51}$$

4.2.1 Uncertain data: energy demand and non-dispatchable production

The uncertain exogenous factors accounted in the model are the profiles of energy demands $\boldsymbol{\mathcal{D}}$ internal to the MES and production potential from all installed non-dispatchable units.

The uncertain demand $\tilde{d}_{j,t}^{\delta}$ of each form of energy $j \in \boldsymbol{\mathcal{D}}$ at time $t \in \boldsymbol{\mathcal{T}}$ is composed of its nominal forecasted value $\tilde{d}_{j,t}$, and of the uncertain deviation from it $\delta\tilde{d}_{j,t}$:

$$\tilde{d}_{j,t}^{\delta} = \tilde{d}_{j,t} + \delta\tilde{d}_{j,t} \qquad \forall\, j \in \boldsymbol{\mathcal{D}}, t \in \boldsymbol{\mathcal{T}} \tag{52}$$

Where $\boldsymbol{\mathcal{T}}$ is the set of simulation time steps and $\boldsymbol{\mathcal{D}}$ is the set of internal energy demands.

Similarly, the uncertain generation potential $\widetilde{up}_{i,t}^{\delta}$ from each non-dispatchable unit (e.g., solar PV panels, wind turbine) $i \in \boldsymbol{\mathcal{ND}}$ at time t is defined by a nominal value (forecast) $\widetilde{up}_{i,t}$ and an uncertain deviation $\delta\widetilde{up}_{i,t}$:

$$\widetilde{up}_{i,t}^{\delta} = \widetilde{up}_{i,t} + \delta\widetilde{up}_{i,t} \qquad \forall\, i \in \boldsymbol{\mathcal{ND}}, t \in \boldsymbol{\mathcal{T}} \tag{53}$$

Where $\boldsymbol{\mathcal{ND}}$ is the set of installed non-dispatchable units. The representation of non-dispatchable generators adopted in this formulation corresponds to the modeling approach depicted in Paragraph 3.4.2, accounting for an uncertain generation potential.

4.2.2 Controllable machines

The necessity of following purely linear decision rules implies that the part-load performance map of each controllable unit $i \in \boldsymbol{\mathcal{M}}$ must be approximated by means of a single linear relation between uncertain machine input $f_{i,t}^{\delta}$ and production $p_{i,j,t}^{\delta}$ of machine output $j \in \boldsymbol{\mathcal{O}}_i$, where $\boldsymbol{\mathcal{M}}$ is the set of dispatchable machines within the microgrid and $\boldsymbol{\mathcal{O}}_i$ is the set of energy outputs yield by machine $i \in \boldsymbol{\mathcal{M}}$. Piece-wise representations of the operating curve, as described in Paragraph 3.4.1, cannot be implemented, as purely linear adjustments to the unit setpoint might violate the non-linear relation represented by the piece-wise part-load map. The uncertain load of each unit $f_{i,t}^{\delta}$ comprises a nominal value $f_{i,t}$ (first stage decision) associated with a perfect forecast scenario and a real-time correction $\Delta f_{i,t}^{\delta}$ (second stage recourse) depending on uncertainty:

$$f_{i,t}^{\delta} = f_{i,t} + \Delta f_{i,t}^{\delta} \qquad \forall\, i \in \boldsymbol{\mathcal{M}}, t \in \boldsymbol{\mathcal{T}} \qquad (54)$$

$$p_{i,j,t}^{\delta} = f_{i,t}^{\delta} \widetilde{m}_{i,j} + z_{i,t} \tilde{q}_{i,j} \qquad \forall\, i \in \boldsymbol{\mathcal{M}}, t \in \boldsymbol{\mathcal{T}}, j \in \boldsymbol{\mathcal{O}}_i \qquad (55)$$

The constants $\widetilde{m}_{i,j}$ and $\tilde{q}_{i,j}$ are obtained by regressing the part-load map of the unit while $z_{i,t}$ is the binary variable indicating the on/off status of the unit. For units characterized by particularly slow start-up and/or ramp rates, real-time corrections may not be possible: if this is the case, their load includes only the nominal component (first stage decision).

Constraints (9) and (10) accounting for maximum/minimum operating load, and start-up/shut-down/operating ramping limitations are enforced on the machine uncertain operating point:

$$z_{i,t} \tilde{f}_i^{min} \leq f_{i,t}^{\delta} \leq z_{i,t} \tilde{f}_i^{max} \qquad \forall\, i \in \boldsymbol{\mathcal{M}}, t \in \boldsymbol{\mathcal{T}} \qquad (56)$$

$$\begin{aligned} -\widetilde{rd}_i^{lim} z_{i,t} - \tilde{f}_i^{max,SD}\left(1 - z_{i,t}\right) \leq f_{i,t}^{\delta} - f_{i,t-1}^{\delta} \\ \leq \widetilde{ru}_i^{lim} z_{i,t-1} + \tilde{f}_i^{max,SU}(1 - z_{i,t-1}) \end{aligned} \qquad \forall\, i \in \boldsymbol{\mathcal{M}}, t \in \boldsymbol{\mathcal{T}} \qquad (57)$$

Constraints (56)-(57), and in general all uncertain constraints, must be valid for any uncertainty manifestation, that is for any potential recursive correction $\Delta f_{i,t}^{\delta}$ to the nominal input value $f_{i,t}$.

All constraints involving the commitment status of dispatchable machines (minimum up/downtime, start-up consumption penalty) are included in the robust formulation equivalently as done for the deterministic formulation in Chapter 3. Since the commitment is not adjusted adaptively, these constraints are identical to the deterministic constraints (11)-(13).

4.2.3 Energy storages and networks:

The definition of the uncertain net exchange and its relevant directional components defining the interactions with storages and networks are analogous to Chapter 3, but account for the uncertain recursive correction of power components:

$$sp_{s,t}^{\delta} = dp_{s,t}^{\delta} \tilde{\eta}_s^{dis} - \frac{cp_{s,t}^{\delta}}{\tilde{\eta}_s^{ch}} \qquad \forall\, s \in \boldsymbol{\mathcal{S}}, t \in \boldsymbol{\mathcal{T}} \qquad (58)$$

$$0 \leq dp_{s,t}^{\delta} \leq \widetilde{dp}_{s,t}^{max};\ 0 \leq cp_{s,t}^{\delta} \leq \widetilde{cp}_{s,t}^{max} \qquad \forall\, s \in \boldsymbol{\mathcal{S}}, t \in \boldsymbol{\mathcal{T}} \qquad (59)$$

$$np_{n,t}^{\delta} = imp_{n,t}^{\delta} - exp_{n,t}^{\delta} \qquad \forall\, n \in \boldsymbol{\mathcal{N}}, t \in \boldsymbol{\mathcal{T}} \qquad (60)$$

$$0 \leq imp_{s,t}^{\delta} \leq \widetilde{imp}_{s,t}^{max};\ 0 \leq exp_{s,t}^{\delta} \leq \widetilde{exp}_{s,t}^{max} \qquad \forall\, n \in \boldsymbol{\mathcal{N}}, t \in \boldsymbol{\mathcal{T}} \qquad (61)$$

$$C_{s,t+1}^{\delta} = C_{s,t}^{\delta}(1 - \tilde{\varepsilon}_s^{SD}\widetilde{\Delta t}) + \left[cp_{s,t}^{\delta} - dp_{s,t}^{\delta}\right]\widetilde{\Delta t} \qquad \forall\, s \in \boldsymbol{\mathcal{S}}, t \in \boldsymbol{\mathcal{T}} \qquad (62)$$

$$\tilde{C}_s^{min}. \leq C_{s,t}^{\delta} \leq \tilde{C}_s^{max}. \qquad \forall\, s \in \boldsymbol{\mathcal{S}}, t \in \boldsymbol{\mathcal{T}} \qquad (63)$$

Due to the uncertain nature of actual net storage power, and to its potential inversion as a consequence of decision rules, a binary storage variable preventing simultaneous charge/discharge of the storage system can be included only on nominal exchange components $dp_{s,t}$ and $cp_{s,t}$, as shown in Eq.(30)-(31). Recursive discharge/charge fluxes $dp_{s,t}^{\delta}$ and $cp_{s,t}^{\delta}$ might therefore be (and often are) both different from zero at the same time. As explained more in detail in Paragraph 0, this can cause an overestimate of losses due to storage round-trip efficiency in the recourse energy balance.

The dynamic storage charge evolution is defined by the uncertain equivalents of constraints (28)-(29), accounting for charge/discharge fluxes ad self-discharge losses:

$$C_{s,t+1}^{\delta} = C_{s,t}^{\delta}(1 - \tilde{\varepsilon}_s^{SD}\widetilde{\Delta t}) + \left[cp_{s,t}^{\delta} - dp_{s,t}^{\delta}\right]\widetilde{\Delta t} \qquad \forall\, s \in \boldsymbol{\mathcal{S}}, t \in \boldsymbol{\mathcal{T}} \qquad (64)$$

$$\tilde{C}_s^{min}. \leq C_{s,t}^{\delta} \leq \tilde{C}_s^{max}. \qquad \forall\, s \in \boldsymbol{\mathcal{S}}, t \in \boldsymbol{\mathcal{T}} \qquad (65)$$

It must be noted that uncertain storage charge $C_{s,t}^{\delta}$ will depend on the entire uncertain exchange history $sp_{s,\tau}^{\delta}$, with $\tau \in [1..t]$.

4.2.4 Energy balance

For each form of energy $j \in \boldsymbol{\mathcal{D}}$ (e.g., heating, cooling, electricity) and time step $t \in \boldsymbol{\mathcal{T}}$, the uncertain energy balance requires that the sum of users' uncertain energy demand $\tilde{d}_{j,t}^{\delta}$, recursive energy consumption $f_{b,t}^{\delta}$ from units $b \in \boldsymbol{\mathcal{B}}_j$ (the subset of $\boldsymbol{\mathcal{M}}$ including machines consuming the form of energy *j*) and recursive dissipated excess production $p_{j,t}^{diss,\delta}$ is equal to the sum of recursive energy production $p_{i,t}^{\delta}$ from dispatchable units $i \in \boldsymbol{\mathcal{M}}_j$ (the subset of $\boldsymbol{\mathcal{M}}$ including machines producing the form of energy *j*), uncertain generation potential $\widetilde{up}_{l,t}^{\delta}$ from non-dispatchable units $l \in \boldsymbol{\mathcal{ND}}_j$ (the subset of $\mathcal{ND}$ including non-dispatchable units producing the form of energy *j*), recursive net energy exchange $sp_{s,t}^{\delta}$ with storages $s \in \boldsymbol{\mathcal{S}}_j$ (the subset of $\boldsymbol{\mathcal{S}}$ including storage systems for the form of energy *j*) and recursive net energy exchange $np_{n,t}^{\delta}$ with external networks $n \in \boldsymbol{\mathcal{N}}_j$ (the subset of $\boldsymbol{\mathcal{N}}$ including networks trading the form of energy *j*):

$$\tilde{d}_{j,t}^{\delta} + \sum_{b \in \boldsymbol{\mathcal{B}}_j} f_{b,t}^{TOT\delta} + p_{j,t}^{diss,\delta} = \sum_{i \in \boldsymbol{\mathcal{M}}_j} p_{i,j,t}^{\delta} + \sum_{l \in \boldsymbol{\mathcal{ND}}_j} \widetilde{up}_{l,t}^{\delta} + \sum_{s \in \boldsymbol{\mathcal{S}}_j} sp_{s,t}^{\delta} + \sum_{n \in \boldsymbol{\mathcal{N}}_j} np_{n,t}^{\delta} \qquad \forall\, j \in \boldsymbol{\mathcal{D}}, t \in \boldsymbol{\mathcal{T}} \qquad (66)$$

$$p_{j,t}^{diss,\delta} \geq 0 \qquad \forall j \in \boldsymbol{\mathcal{D}}, t \in \boldsymbol{\mathcal{T}} \qquad (67)$$

No unmet demand is included in the balance, as the objective of the robust formulation is to avoid it in all potential scenarios. Generation curtailment from all non-dispatchable generators is aggregated in the dissipation term $p_{j,t}^{diss,\delta}$, which is always greater or equal than zero (although its recursive correction component

$\Delta p_{j,t}^{diss,\delta}$ can be either positive or negative, representing an increase/reduction of the overall generation curtailment).

4.2.5 Objective function:

The objective function is to minimize the expected total operating cost of the MES, comprising fuel cost, and the value of trades with external energy networks, as shown in Eq.(68).

$$\sum_{\tau=1}^{T}\left[\sum_{i\in F}\left(f_{i,t}^{TOT}+\mathbb{E}\left[\Delta f_{i,t}^{\delta}\right]\widetilde{w}^{\Delta}\right)\tilde{c}_{fuel,i,t}+\sum_{n\in N}\left(imp_{n,t}\tilde{c}_{n,t}^{imp}-exp_{n,t}\tilde{c}_{n,t}^{exp}+\mathbb{E}\left[\Delta c_{n,t}^{np}\right]\widetilde{w}^{\Delta}\right)\right] \tag{68}$$

Each cost term comprises a component associated with its nominal operation (decided beforehand based on the available forecast) and a component connected to the recursive corrections. In general, it is worth noting that the expected value (denoted with the operator $\mathbb{E}$) of this recursive cost correction may be non-zero, either because the average value of the forecast error is not zero, and/or because different decision rules are defined according to the sign of the deviation from forecast (positive or negative). The relative importance of the expected recursive cost correction with respect to the nominal cost index is controlled by a weight parameter $\widetilde{w}^{\Delta}$, reducing the impact of recursive cost terms on the objective function with respect to first-stage decisions. This has both the effect of avoiding situations in which, due to pathological shapes of the uncertainty set, nominal cost terms are even out or even fully compensated by recursive cost corrections, and of giving preference to the optimization of the nominal (no error) dispatch solution. Hourly and start-up O&M can be easily included as shown in Chapter 3, since they only depend on fist stage non-adaptive commitment variables, while O&M proportional to second stage variables must be split in their nominal and recursive components.

The term $\mathbb{E}\left[\Delta c_{n,t}^{nP}\right]$ in Eq.(68) represents the economic valorization of the expected network exchange once it deviates from its nominal value $np_{n,t}$ due to the expected recursive corrections. It is not trivial to calculate its value, because of the difference between selling and purchasing prices typically affecting energy trading with the external networks (the selling price is typically appreciably lower than the purchase price). Depending on the nominal value of energy import $np_{n,t}$ and the expected value of its recourse corrections $\mathbb{E}\left[\Delta np_{n,t}^{\delta}\right]$, six scenarios (depicted in Figure 8) can be identified:

1) **Nominal import and expected import increase in the recourse:** $\begin{cases} np_{n,t}>0 \\ \mathbb{E}\left[\Delta np_{n,t}^{\delta}\right]>0 \end{cases}$

$$\mathbb{E}\left[\Delta c_{n,t}^{np}\right]=\mathbb{E}\left[\Delta np_{n,t}^{\delta}\right]\tilde{c}_{n,t}^{imp} \tag{69}$$

The expected correction leads to an increase in the energy import which is univocally associated with an additional cost accounted for at the energy purchase price $\tilde{c}_{n,t}^{imp}$.

2) **Nominal export and expected export increase in the recourse:** $\begin{cases} np_{n,t}<0 \\ \mathbb{E}\left[\Delta np_{n,t}^{\delta}\right]<0 \end{cases}$

$$\mathbb{E}\left[\Delta c_{n,t}^{np}\right]=\mathbb{E}\left[\Delta np_{n,t}^{\delta}\right]\tilde{c}_{n,t}^{exp} \tag{70}$$

The expected correction leads to an increase in the energy export which is univocally associated with an additional revenue accounted for at the energy selling price $\tilde{c}_{n,t}^{exp}$.

3) Nominal export to network and export reduction in the recourse: $\begin{cases} np_{n,t} < 0 \\ \mathbb{E}[\Delta np_{n,t}^{\delta}] > 0 \end{cases}$

$$\text{a)} \quad if\ |np_{n,t}| \geq |\mathbb{E}[\Delta np_{n,t}^{\delta}]| \Rightarrow \mathbb{E}[\Delta c_{n,t}^{np}] = \mathbb{E}[\Delta np_{n,t}^{\delta}]\tilde{c}_{n,t}^{exp} \tag{71}$$

The expected correction leads to a decrease of the energy export which does not exceed the value planned in the nominal solution: thus, the value of the expected recourse is a missed revenue accounted for at the energy selling price $\tilde{c}_{n,t}^{exp}$.

$$\text{b)} \quad if\ |np_{n,t}| < |\mathbb{E}[\Delta np_{n,t}^{\delta}]| \Rightarrow \mathbb{E}[\Delta c_{n,t}^{np}] = -np_{n,t}\tilde{c}_{n,t}^{exp} + (np_{n,t} + \mathbb{E}[\Delta np_{n,t}^{\delta}])\tilde{c}_{n,t}^{imp} \tag{72}$$

The expected correction leads to a decrease of the energy export which exceeds the value planned in the nominal solution, and causes the inversion of the exchange direction: thus, a fraction of the exchange deviation $\mathbb{E}[\Delta np_{n,t}^{\delta}]$ corresponding to the nominal energy export $np_{n,t}$ (negative since sold to the network) is associated with a missed revenue accounted for at the energy selling price $\tilde{c}_{n,t}^{exp}$, while the remainder $(np_{n,t} + \mathbb{E}[\Delta np_{n,t}^{\delta}])$ is associated with an additional cost accounted for at the purchase price $\tilde{c}_{n,t}^{imp}$.

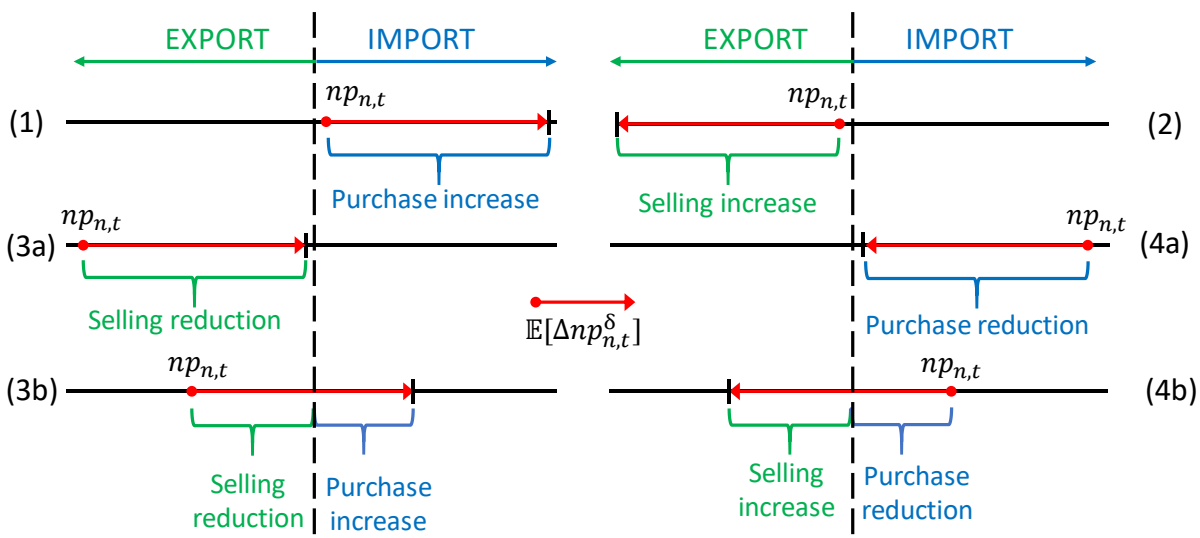

Figure 8: scenarios for the valorization of the expected network exchange deviation $\mathbb{E}[\Delta np_{n,t}^{\delta}]$:depending on the amplitude of the deviation and on the nominal operating condition, the appropriate valorization must be considered

4) Nominal import and expected import decrease in the recourse: $\begin{cases} np_{n,t} > 0 \\ \mathbb{E}[\Delta np_{n,t}^{\delta}] < 0 \end{cases}$

$$\text{a)} \quad if\ |np_{n,t}| \geq |\mathbb{E}[\Delta np_{n,t}^{\delta}]| \Rightarrow \mathbb{E}[\Delta c_{n,t}^{np}] = \mathbb{E}[\Delta np_{n,t}^{\delta}]\tilde{c}_{n,t}^{imp} \tag{73}$$

The expected correction leads to a decrease of the energy import which does not exceed the value planned in the nominal solution: thus, the value of the expected recourse is a cost reduction accounted for at the energy purchase price $\tilde{c}_{n,t}^{imp}$.

$$\text{b)} \quad if\ |np_{n,t}| < |\mathbb{E}[\Delta np_{n,t}^{\delta}]| \Rightarrow \mathbb{E}[\Delta c_{n,t}^{np}] = -np_{n,t}\tilde{c}_{n,t}^{imp} + (np_{n,t} + \mathbb{E}[\Delta np_{n,t}^{\delta}])\tilde{c}_{n,t}^{exp} \tag{74}$$

The expected correction leads to a decrease of the energy import which exceeds the value planned in the nominal solution, and causes the inversion of the exchange direction: thus, a fraction of the exchange deviation $\mathbb{E}\left[\Delta np_{n,t}^{\delta}\right]$ corresponding to the nominal energy export $np_{n,t}$ (positive since purchased from the network) is associated with a missed cost accounted for at the energy purchase price $\tilde{c}_{n,t}^{imp}$, while the remainder $\left(np_{n,t} + \mathbb{E}\left[\Delta np_{n,t}^{\delta}\right]\right)$ is associated with an additional revenue accounted for at the energy selling price $\tilde{c}_{n,t}^{exp}$.

The value of the expected cost term $\mathbb{E}\left[\Delta c_{n,t}^{np}\right]$ is therefore determined based on a set of constraints identifying the correct scenario:

$$\mathbb{E}\left[\Delta c_{n,t}^{np}\right] = \left(\mathbb{E}\left[\Delta imp_{n,t}^{\delta}\right]^{+} - \mathbb{E}\left[\Delta exp_{n,t}^{\delta}\right]^{+}\right)\tilde{c}_{n,t}^{imp} + \left(\mathbb{E}\left[\Delta imp_{n,t}^{\delta}\right]^{-} - \mathbb{E}\left[\Delta exp_{n,t}^{\delta}\right]^{-}\right)\tilde{c}_{n,t}^{exp} \tag{75}$$

$$\begin{aligned}
&0 \leq \mathbb{E}\left[\Delta imp_{n,t}^{\delta}\right]^{-} \leq exp_{n,t} \\
&\mathbb{E}\left[\Delta imp_{n,t}^{\delta}\right]^{-} \leq \mathbb{E}\left[\Delta imp_{n,t}^{\delta}\right] \\
&\mathbb{E}\left[\Delta imp_{n,t}^{\delta}\right]^{+} = \mathbb{E}\left[\Delta imp_{n,t}^{\delta}\right] - \mathbb{E}\left[\Delta imp_{n,t}^{\delta}\right]^{-} \\
&0 \leq \mathbb{E}\left[\Delta exp_{n,t}^{\delta}\right]^{+} \leq imp_{n,t} \\
&\mathbb{E}\left[\Delta exp_{n,t}^{\delta}\right]^{+} \leq \mathbb{E}\left[\Delta exp_{n,t}^{\delta}\right] \\
&\mathbb{E}\left[\Delta exp_{n,t}^{\delta}\right]^{-} = \mathbb{E}\left[\Delta exp_{n,t}^{\delta}\right] - \mathbb{E}\left[\Delta exp_{n,t}^{\delta}\right]^{+}
\end{aligned} \tag{76}$$

All uncertain constraints described in this Paragraph must be enforced for any potential manifestation of uncertainty, that is for any potential set of recursive variable corrections $\Delta \boldsymbol{x}^{\delta}$ to first stage decisions $\boldsymbol{x}$. Effectively, this implies that each uncertain constraint corresponds to an infinitude of constraints, associated with all infinite potential uncertainty manifestations encompassed by the uncertainty set.

4.3 Tractable Reformulation of AARC

Since all the above-listed constraints and objective function are linear, the adjustable robust optimization problem can be written as follows:

$$\begin{aligned}
&\min_{\boldsymbol{x}^{\delta}}\left\{\mathbb{E}\left[\tilde{\boldsymbol{c}}^{\mathrm{T}}\boldsymbol{x}^{\delta}\right] : \ \forall \tilde{\boldsymbol{\delta}} \in \mathcal{U} \ \ \tilde{A}^{e}\boldsymbol{x}^{\delta} = \tilde{\boldsymbol{b}}_{\delta}^{e} \wedge \tilde{A}^{i}\boldsymbol{x}^{\delta} \leq \tilde{\boldsymbol{b}}_{\delta}^{i}\right\} \\
&\tilde{\boldsymbol{b}}_{\delta}^{e} = \tilde{H}^{e}\tilde{\boldsymbol{\delta}} + \tilde{\boldsymbol{h}}^{e} \\
&\tilde{\boldsymbol{b}}_{\delta}^{i} = \tilde{H}^{i}\tilde{\boldsymbol{\delta}} + \tilde{\boldsymbol{h}}^{i}
\end{aligned} \tag{77}$$

where the vector $\boldsymbol{x}^{\delta}$ denotes the optimization variables, $\tilde{\boldsymbol{c}}$ is the vector of cost coefficients, $\tilde{A}^{e}$ and $\tilde{A}^{i}$ are the left-hand side matrixes of equality and inequality constraints, $\tilde{\boldsymbol{b}}_{\delta}^{e}$ and $\tilde{\boldsymbol{b}}_{\delta}^{i}$ are the right-hand side vectors respectively, $\tilde{\boldsymbol{\delta}}$ is the perturbation vector and $\tilde{H}^{e}$ and $\tilde{H}^{i}$ are incidence matrixes associating each element to the corresponding uncertain data. As indicated in Eq. (77), according to the assumption of limiting uncertainty to the forecast of energy demands and non-dispatchable generation potential, the cost vector and the coefficients of the constraints left-hand side matrixes are certain. Uncertainty only affects the constraint right-hand side vectors $\tilde{\boldsymbol{b}}_{\delta}^{e}$ and $\tilde{\boldsymbol{b}}_{\delta}^{i}$, which depend affinely on forecast errors of energy demands and generation potential from non-dispatchable units, and in turn decision variables $\boldsymbol{x}^{\delta}$, through the recursive corrections $\boldsymbol{\Delta x}^{\delta}$. These two features make the problem a particular type of adjustable robust optimization problem called “fixed recourse” [50].

To preserve tractability and linearity of the robust counterpart, in this work, the uncertainty set $\boldsymbol{\mathcal{U}}$ is represented as a bounded polyhedron defined by a set of linear constraints, described by a matrix $\tilde{L}$ and right-hand side vector $\tilde{\boldsymbol{l}}$:

$$\boldsymbol{\mathcal{U}} = \{\tilde{\boldsymbol{\delta}} : \tilde{L}\tilde{\boldsymbol{\delta}} \leq \tilde{\boldsymbol{l}}\} \tag{78}$$

For the same reason, recursive variable adjustment $\boldsymbol{\Delta x}^{\delta}$ are modeled as linear decision rules with respect to uncertainty vector $\tilde{\boldsymbol{\delta}}$. According the definition provided in Eq.(51), variable vector $\boldsymbol{x}^{\delta}$ is split in two groups:

- *First stage* ("here and now" / "nominal") variables, $\boldsymbol{x}$, to be decided ahead of the operation time. The vector $\boldsymbol{x}$ includes $f_{i,t}$, $z_{i,t}$, $p_{i,j,t}$, $np_{n,t}$, $exp_{n,t}$, $imp_{n,t}$, $p_{i,j,t}^{diss}$, $sp_{s,t}$, $dp_{s,t}$, $cp_{s,t}$.
- *Second stage* ("recursive" / "adjustment") variables $\Delta\boldsymbol{x}^{\delta}$ are defined as piecewise linear functions of $\tilde{\boldsymbol{\delta}}$ so that their value adapts based on the observed values of $\tilde{\boldsymbol{\delta}}$ during actual operation. $\Delta\boldsymbol{x}^{\delta}$ includes $\Delta f_{i,t}^{\delta}$, $\Delta p_{i,j,t}^{\delta}$, $\Delta np_{n,t}^{\delta}$, $\Delta exp_{n,t}^{\delta}$, $\Delta imp_{n,t}^{\delta}$, $\Delta p_{j,t}^{diss,\delta}$, $\Delta sp_{s,t}^{\delta}$, $\Delta dp_{s,t}^{\delta}$, $\Delta cp_{s,t}^{\delta}$.

It is worth noting that binary on/off variables $z_{i,t}$ are not adjustable, and the commitment decisions are assumed to be univocally taken in the first stage (e.g., no integer recourse). Similarly, the loads of the units which cannot be adjusted during real-time operation are defined only in the first stage.

The coefficients defining the affine decision rules are grouped in the coefficients matrix Y.

$$\boldsymbol{x}^{\delta} = \begin{bmatrix} \boldsymbol{x} \\ \Delta\boldsymbol{x}^{\delta} \end{bmatrix}, \qquad \text{where } \Delta\boldsymbol{x}_{\delta} = Y\tilde{\boldsymbol{\delta}} \tag{79}$$

The elements of the recourse coefficient matrix Y are the optimization variables through which the affine decision rules are optimized. In this formulation, for the variables $\boldsymbol{x}$ which are non-adjustable (i.e., the binary on/off variables of all units and, possibly, the loads of the non-flexible units whose load cannot be adjusted on a real-time basis), the corresponding coefficients of the recourse matrix Y are zero. Moreover, to ensure practical applicability, it is necessary to enforce non-anticipativity for the decision rules, meaning that second stage real-time corrections $\Delta\boldsymbol{x}^{\delta}$ at any time t can only depend on the previous observations of forecast errors (i.e. on manifestations of $\tilde{\boldsymbol{\delta}}$ occurred before or during t**)**. Considering the recursive adjustment $\Delta x_{i,k,t}^{\delta}$ of variable i as a function of uncertainty factor $k \in \boldsymbol{\mathcal{K}}$ (e.g., electricity demand, PV production) at time t, matrix $Y_{i,k,t,\tau}$ in the time-indexes space (where the pair (t,τ) identifies correction at time t as function of observation at time τ) is lower triangular, as indicated in Eq.(80):

$$\begin{aligned} \Delta x_{i,k,t}^{\delta} &= \sum_{\tau} Y_{i,k,t,\tau}\delta_{\tau} \\ Y_{i,k,t,\tau} &= 0 \qquad\qquad \forall i,k \in \boldsymbol{\mathcal{K}}, t \in \boldsymbol{\mathcal{T}}, \tau > t \end{aligned} \tag{80}$$

Where $\boldsymbol{\mathcal{K}}$ is the set of all uncertain parameters affecting system operation.

To maximize the operational flexibility of the system, piece-wise linear decision rules with a breakpoint in $\tilde{\boldsymbol{\delta}} = \mathbf{0}$ are adopted [54]. Uncertain parameters $\tilde{\boldsymbol{\delta}}$ are therefore split in their positive and negative components, for which different decision rules are defined by means of specific coefficient matrixes Y^{+} and Y^{-}:

$$\widetilde{\boldsymbol{\delta}} = \widetilde{\boldsymbol{\delta}}^{+} - \widetilde{\boldsymbol{\delta}}^{-} \tag{81}$$

$$\widetilde{\boldsymbol{\delta}}^{+}, \widetilde{\boldsymbol{\delta}}^{-} \geq \mathbf{0} \tag{82}$$

$$\Delta \boldsymbol{x}^{\delta} = Y^{+}\widetilde{\boldsymbol{\delta}}^{+} - Y^{-}\widetilde{\boldsymbol{\delta}}^{-} = \begin{bmatrix} Y^{+} & \mathbf{0} \\ \mathbf{0} & Y^{-} \end{bmatrix} \begin{bmatrix} \widetilde{\boldsymbol{\delta}}^{+} \\ \widetilde{\boldsymbol{\delta}}^{-} \end{bmatrix} \tag{83}$$

A practical example of the importance of defining different correction policies according to the sign of forecast errors is shown in Figure 9: in virtue of having separately defined coefficient matrixes Y^{+} and Y^{-}, a decrease in electricity demand can be recursively met by decreasing the ICE set-point (therefore attaining an expected fuel saving), while an increase in electricity demand is balanced by increasing the battery discharge flow. If a single matrix Y was defined, responding with a reduction of the ICE set-point when the demand is lower than forecasted would imply increasing the ICE load when the demand is higher than expected (continuous slope of decision rules shown in Figure 9). As a consequence, the nominal operating load p_{ICE} would be necessarily bounded to a value lower than its maximum $\tilde{p}_{ICE}^{MAX}$ to avoid violating the maximum load constraint due to the recursive correction Δp_{ICE}^{δ}.

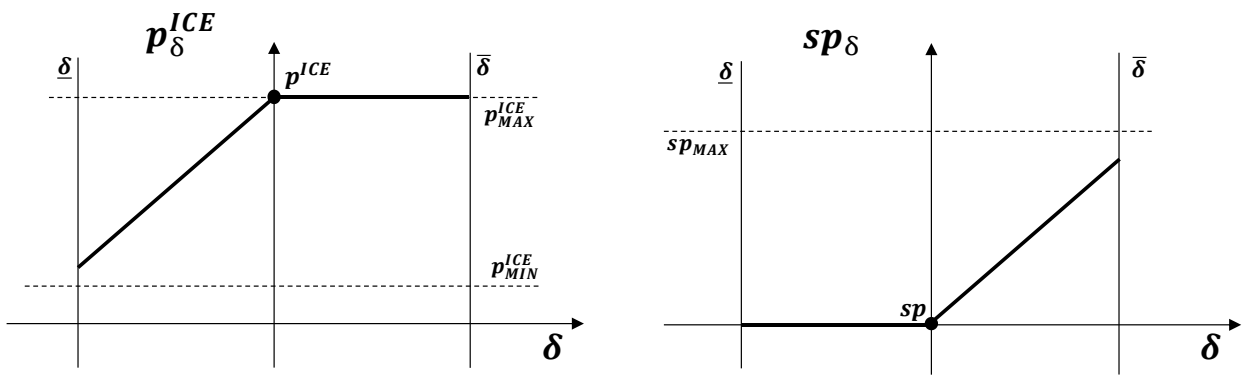

Figure 9: Example of possible decision rules for the load of an ICE, enabled by piece-wise affine recourse. In the first stage solution, the nominal electricity (or heat) demand is produced by the ICE operating at maximum load. A positive perturbation of demand (positive δ) wrt forecast is met by increasing the power discharged from the storage, while a negative perturbation can be met by decreasing the ICE load.

Separately accounting for positive/negative error components $\tilde{\delta}^{+}$ and $\tilde{\delta}^{-}$sensibly increases the flexibility of decision rules and in turn the feasible space for first stage variables. On the other hand, any net forecast error $\tilde{\delta}$ can be associated with a variety of $\tilde{\delta}^{+}/\tilde{\delta}^{-}$ combinations yielding the same net result. Due to the absence of binary uncertain variables, the polyhedral definition of the uncertainty space does not prohibit the simultaneous occurrence of both error components. If the corrective actions prescribed by Y^{+} and Y^{-} push towards opposite directions (e.g. decreasing ICE load if demand has been overestimated, increasing it otherwise), this does not represent a problem, since the most extreme uncertainty realization for each constraint will correspond to considering only one error component different from zero and as high as possible (largest deviation from nominal). Otherwise, the sum of the setpoint corrections calculated separately as function of $\tilde{\delta}^{+}$ and $\tilde{\delta}^{-}$ could lead to an overall correction higher than what should be accounted for, if only the positive or negative part of $\tilde{\delta}$ was different from zero at a given time.

Problem (77) can be rewritten as an Affinely Adjustable Robust Counterpart (AARC) problem:

$$\min_{\boldsymbol{x},Y}\left\{\mathbb{E}\left[\tilde{\boldsymbol{c}}\begin{bmatrix}\boldsymbol{x}\\ Y\tilde{\boldsymbol{\delta}}\end{bmatrix}\right]:\ \forall\tilde{\boldsymbol{\delta}}\in\mathcal{U}\ \ \tilde{A}^e\begin{bmatrix}\boldsymbol{x}\\ Y\tilde{\boldsymbol{\delta}}\end{bmatrix}=\tilde{H}^e\tilde{\boldsymbol{\delta}}+\tilde{\boldsymbol{h}}^e,\tilde{A}^i\begin{bmatrix}\boldsymbol{x}\\ Y\tilde{\boldsymbol{\delta}}\end{bmatrix}\leq\tilde{H}^i\tilde{\boldsymbol{\delta}}+\tilde{\boldsymbol{h}}^i\right\} \tag{84}$$

Once again, it is worth noting that the problem features an infinite number of constraints since each one must be enforced for any possible realization of the uncertain parameter vector $\tilde{\boldsymbol{\delta}}$.

The left-hand side constraint matrixes $\tilde{A}^e$ and $\tilde{A}^i$ can be partitioned into two blocks: the first block contains the columns associated with first stage variables and it is typically called "technology matrix" $\tilde{T}$, while the second block, associated with recourse variables, is called "recourse matrix" $\tilde{W}$:

$$\begin{aligned}\tilde{A}^e&=\left[\tilde{T}^e\ \tilde{W}^e\right]\\ \tilde{A}^i&=\left[\tilde{T}^i\ \tilde{W}^i\right]\end{aligned} \tag{85}$$

$$\min_{\boldsymbol{x},Y}\left\{\mathbb{E}\left[\tilde{\boldsymbol{c}}\begin{bmatrix}\boldsymbol{x}\\ Y\tilde{\boldsymbol{\delta}}\end{bmatrix}\right]:\ \forall\tilde{\boldsymbol{\delta}}\in\mathcal{U}\,,\qquad \tilde{T}^e\boldsymbol{x}+\tilde{W}^eY\tilde{\boldsymbol{\delta}}=\tilde{H}^e\tilde{\boldsymbol{\delta}}+\tilde{\boldsymbol{h}}^e\,,\tilde{T}^i\boldsymbol{x}+\tilde{W}^iY\tilde{\boldsymbol{\delta}}\leq\tilde{H}^i\tilde{\boldsymbol{\delta}}+\tilde{\boldsymbol{h}}^i\right\} \tag{86}$$

As far as uncertain inequality constraints are concerned, it is possible to enforce the feasibility under any possible manifestation of $\tilde{\boldsymbol{\delta}}$ through a row-wise max operator acting independently on each constraint, as indicated below:

$$\min_{\boldsymbol{x},Y}\tilde{\boldsymbol{c}}\begin{bmatrix}\boldsymbol{x}\\ Y\hat{\mathbb{E}}[\tilde{\boldsymbol{\delta}}]\end{bmatrix} \tag{87}$$

$$s.t.\ \left(\tilde{W}^eY-\tilde{H}^e\right)\tilde{\boldsymbol{\delta}}=\tilde{\boldsymbol{h}}^e-\tilde{T}^e\boldsymbol{x}\qquad\forall\boldsymbol{\delta}\in\mathcal{U} \tag{88}$$

$$\max_{\boldsymbol{\delta}\in\mathcal{U}}\left[\left(\tilde{W}^iY-\tilde{H}^i\right)\tilde{\boldsymbol{\delta}}\right]\leq\tilde{\boldsymbol{h}}^i-\tilde{T}^i\boldsymbol{x} \tag{89}$$

Constraints (88)-(89) must be valid for any potential manifestation of $\tilde{\boldsymbol{\delta}}$ within $\mathcal{U}$.

The optimization problem as expressed by Eq. (87)-(89) is a semi-infinite problem, which cannot be solved directly. On the other hand, since (i) $\tilde{\boldsymbol{b}}^e_\delta$ and $\tilde{\boldsymbol{b}}^i_\delta$ are affine functions of $\tilde{\boldsymbol{\delta}}$**,** (ii) $\mathcal{U}$ is polyhedral, (iii) the problem features fixed recourse, the AARC can be converted into a deterministic equivalent with a finite number of variables and constraints called the *tractable robust counterpart reformulation* [50]. To this end, problem constraints can be divided into three categories:

1) Purely deterministic constraints (e.g. $\left(\tilde{W}Y-\tilde{H}\right)=0$)
2) Uncertain equalities (Eq. (88))
3) Uncertain inequalities (Eq. (89))

4.3.1 Deterministic constraints

Purely deterministic constraints do not involve uncertain parameters but only first-stage variables (i.e., for such constraints the corresponding coefficients of matrices $\tilde{W}^e$, $\tilde{W}^i$ and $\tilde{H}^e$, $\tilde{H}^i$ are zero), and they can, therefore, be directly included in the robust counterpart. These constraints are, for instance, all constraints for dispatchable units involving only first stage variable $z_{i,t}$ (i.e. minimum up/downtime, start-up penalization), or constraints (75)-(76) defining the accurate economic valorization of expected recursive network exchange deviation $\mathbb{E}\left[\Delta np^{\delta}_{n,t}\right]$.

4.3.2 Uncertain Equalities

Uncertain equalities involve both first and second stage variables, as well as uncertain parameters. Each equality constraint must, therefore, be valid for any potential combination of values that the elements of $\widetilde{\boldsymbol{\delta}}$ can assume within $\mathcal{U}$. The feasibility requirement over the entire space $\mathcal{U}$ implies that the constraint must be also valid when $\widetilde{\boldsymbol{\delta}} = \mathbf{0}$. This means that the right-hand side of (88) must be identically zero:

$$\tilde{T}^e \boldsymbol{x} = \widetilde{\boldsymbol{h}}^e \tag{90}$$

Consequently, the left-hand side of (88) must be identically zero for any possible value of $\widetilde{\boldsymbol{\delta}}$. This means that all the coefficients of the matrix $\left(\widetilde{W}^e Y - \widetilde{H}^e\right)$ must be zero, i.e., Eq. (91) must hold:

$$\widetilde{W}^e Y = \widetilde{H}^e \tag{91}$$

4.3.3 Uncertain Inequalities

Uncertain inequalities are enforced, through the row-wise max operator, for the constraint-specific worst-case manifestation of $\widetilde{\boldsymbol{\delta}}$ within the polyhedral uncertainty set, as indicated by Eq. (92)-(93).

$$\max_{\boldsymbol{\delta}}\left(\widetilde{W}_j^{\boldsymbol{i}} Y - \widetilde{H}_j^{\boldsymbol{i}}\right)\widetilde{\boldsymbol{\delta}} \leq \tilde{h}_j^i - \tilde{T}_j^i \boldsymbol{x} \tag{92}$$

$$s.t\ \tilde{L}\widetilde{\boldsymbol{\delta}} \leq \tilde{\boldsymbol{l}} \tag{93}$$

Since the left-hand side of Eq.(92) is a linear program with respect to the perturbation vector $\widetilde{\boldsymbol{\delta}}$, it is possible to prove using the duality theorem of linear programming that $\boldsymbol{x}$ is feasible for Eq. (92) if and only if the dual linear program defined by Eq.(94)-(96) has a feasible solution Λ_j (where vector Λ_j, the jth row of matrix Λ, is the vector of dual variables introduced for constraint j) [50]:

$$\min_{\Lambda_j} \tilde{\boldsymbol{l}} \Lambda_j \tag{94}$$

$$s.t\ \tilde{L}^T \Lambda_j \geq \widetilde{W}_j^i Y - \widetilde{H}_j^i \tag{95}$$

$$\Lambda_j \geq 0 \tag{96}$$

Thus, Eq. (92) can be replaced with Eq. (95)-(96), guaranteeing the validity of the original uncertain constraint (92) for any possible manifestation of $\widetilde{\boldsymbol{\delta}}$ through the existence of a feasible solution Λ_j to its dual linear program (94)-(96):

$$\min_{\boldsymbol{x},Y,\Lambda} \tilde{\boldsymbol{c}} \begin{bmatrix} \boldsymbol{x} \\ Y\widehat{\mathbb{E}}[\boldsymbol{\delta}] \end{bmatrix} \tag{97}$$

$$s.t. \tag{98}$$

$$\tilde{T}^e \boldsymbol{x} = \widetilde{\boldsymbol{h}}^e \tag{99}$$

$$\widetilde{W}^e Y = \widetilde{H}^e \tag{100}$$

$$\tilde{\boldsymbol{l}} \Lambda \leq \widetilde{\boldsymbol{h}}^i - \tilde{T}^i \boldsymbol{x} \tag{101}$$

$$\tilde{L}^T \Lambda \geq \widetilde{W}^i Y - \widetilde{H}^i \tag{102}$$

$$\Lambda \geq 0 \tag{103}$$

Eq. (97)-(103) define the tractable robust counterpart reformulation of the original AARO problem, which is a fully defined deterministic MILP with a finite number of variables and constraints. It can, therefore, be handled with commercially available MILP solvers. The size of matrixes Y and Λ is respectively $[(i + 2s + 2n + j) \cdot kt \text{ x } t]$ and $[c \text{ x } lk]$, where i is the number of dispatchable units, s is the number of storages, n the number of networks, j the number of microgrid goods, k the number of uncertain parameters, t the number of timesteps, c the number of uncertain constraints and l the number of uncertainty set constraints per each uncertain factor k. It is apparent how the size of the robust counterpart MILP rapidly grows with the number of time steps, number of uncertain data (energy demand profiles and non-dispatchable production units) and installed units.

4.4 Uncertainty set definition

The general polyhedral uncertainty set is represented by a set of linear inequalities (Eq. (78)). Although some examples of advanced formulations of uncertainty sets have been proposed in the literature (e.g. Lorca et al. [64] proposed a dynamic uncertainty characterization accounting for the inter-temporal correlation of wind generation forecast errors, Ning and You [65] presented a data-driven uncertainty set construction method, combining different polyhedral uncertainty set to reduce the volume of the uncertainty space), most of the robust optimization works in the literature resort to the budget uncertainty set formulation originally proposed by Bertsimas and Sim in [63], which corresponds to setting instantaneous error thresholds and cumulated error norms (uncertainty budget). In this thesis, I consider a polyhedral uncertainty set featuring an extended budget uncertainty set, determined on the basis of the energy-related considerations arising from a thorough statistical analysis of the historical forecast error profiles.

In the traditional budget uncertainty set, instantaneous uncertain deviations from forecasts of each uncertain parameter $k \in \boldsymbol{\mathcal{K}}$ are bounded by maximum upwards and downwards error boxes which are time-dependent, to represent the variability of forecast accuracy with the hour of the day:

$$\delta_{k,t}^{+} \leq \overline{\delta}_{k,t} \qquad \forall k \in \boldsymbol{\mathcal{K}}, t \in \boldsymbol{\mathcal{T}} \qquad (104)$$

$$\delta_{k,t}^{-} \leq \underline{\delta}_{k,t} \qquad \forall k \in \boldsymbol{\mathcal{K}}, t \in \boldsymbol{\mathcal{T}} \qquad (105)$$

Furthermore, the cumulated absolute error is constrained over the simulation window. In our uncertainty set formulation, the cumulated error is bounded over periodic intra-day time windows $\mathcal{T}_i \subseteq \boldsymbol{\mathcal{T}}$, to model the realistic distribution of the cumulated daily forecast error at different times of the day and to avoid unnecessary over-conservativeness of the worst-case scenarios. Then, in addition to the usual limit on the overall absolute error in Eq. (106) norm constraints are enforced also for strictly positive and strictly negative errors, setting thresholds for maximum energy demand/production overestimate and underestimate. These norms are generally more restrictive than the cumulated absolute error norm since uncertain parameters tend to fluctuate above and below their forecasted value. In virtue of the distinction introduced within the model between positive and negative forecast errors, imposing a specific norm on each signed error component leads to a resulting bound on the cumulated error value which is significantly more restrictive than what would be obtained from the absolute error norm (Eq.(106)) with only one of the error components different from zero.

$$\sum_{t\in\mathcal{T}_i}\left|\delta_{k,t}^{+}+\delta_{k,t}^{-}\right|\leq\Gamma_k^{abs} \qquad \forall k\in\boldsymbol{\mathcal{K}},\forall\,\mathcal{T}_i \qquad (106)$$

$$\sum_{t\in\mathcal{T}_i}\delta_{k,t}^{+}(t)\leq\Gamma_k^{+} \qquad \forall k\in\boldsymbol{\mathcal{K}},\forall\,\mathcal{T}_i \qquad (107)$$

$$\sum_{t\in\mathcal{T}_i}\delta_{k,t}^{-}(t)\leq\Gamma_k^{-} \qquad \forall k\in\boldsymbol{\mathcal{K}},\forall\,\mathcal{T}_i \qquad (108)$$

Finally, I propose the adoption of ramp limitations on error variations from one timestep to the following: since errors on energy profiles (on a relatively coarse time resolution mesh) are generally autocorrelated and do not abruptly move within the uncertainty space, this constraint helps in representing a realistic continuous error trajectory:

$$\left|\delta_{k,t}-\delta_{k,t-1}\right|\leq\overline{\Delta\delta}_k \qquad \forall k\in\boldsymbol{\mathcal{K}},t\in\boldsymbol{\mathcal{T}} \qquad (109)$$

If the error is split into its positive and negative components, in order to properly enforce the limitation on the instantaneous error variation imposing constraint (109) on the net forecast error δ is not sufficient, since the ramp constraint on signed components $\delta^{+}$and δ^{-} (which are the ones actually affecting the recourse) could be bypassed by considering both components different from zero at the same time. Therefore, the uncertainty ramp constraint must be enforced also on the separate components

$$\left|\delta_{k,t}^{+}-\delta_{k,t-1}^{+}\right|\leq\overline{\Delta\delta}_k \qquad \forall k\in\boldsymbol{\mathcal{K}},t\in\boldsymbol{\mathcal{T}} \qquad (110)$$

$$\left|\delta_{k,t}^{-}-\delta_{k,t-1}^{-}\right|\leq\overline{\Delta\delta}_k \qquad \forall k\in\boldsymbol{\mathcal{K}},t\in\boldsymbol{\mathcal{T}} \qquad (111)$$

Constraint (109) is on the other hand still relevant, since the constraint on net uncertainty variation might conversely be violated for example by considering simultaneous and opposite variations for its signed components. The fact that to be properly enforced the ramping constraint has to be imposed three times, in addition to the coupling between different time instants that it introduces in the problem, makes the ramping constraint particularly computationally expensive.

It is important to remark that in this work forecast errors $\boldsymbol{\delta}$ are preferentially expressed in absolute (energetic) terms, instead of percentage deviations from nominal. This is more adequate for uncertain parameters, such as the PV power generation forecast, which forecasted value varies in a wide range across the simulation period. In this case, the percentage error at low forecasted generation output is on average sensibly higher than at high forecasted values. This characteristic of forecast error is not properly modeled by imposing an uncertainty budget on percentage variations.

4.5 Limitations of the Affine Decision Rules

Decision rules should include all possible corrective measures that could be implemented when operating an actual MES. Indeed, the more flexible the decision rules are, the less conservative the optimal robust solution will be, with a positive effect on the overall performance. Ideally, assuming a fully flexible functional expression of corrective measures $\Delta\boldsymbol{x}^{\delta}$, the optimal recourse policies could be effectively used for the real-time control of the system. However, plain affine decision rules not accounting for second stage

binary variables are not sufficiently flexible to reproduce the actual corrective measures that one could use in practice, leading in turn to over-conservative scheduling solutions.

According to the analysis developed in this thesis, based on extensive tests on real-world case studies, the major limitations of purely affine decision rules are the following:

1) Inaccurate modeling of battery charge/discharge efficiency in the recourse laws;
2) Over-conservative decision rules for units with multiple outputs (e.g., CHP and CCHP engines);
3) Impossibility to consider recursive start-up/shut-down of quick-start units (e.g., gas boilers);
4) Over-conservative management of storage units and units with dynamic constraints (e.g., ramp-up/down).

To the best of the author's knowledge, no previous work has highlighted limitations 1, 2 and 4 of AARO, while several recent papers can be found addressing limitation 3, by proposing integer decision rules (e.g., [66]), or resorting to fully adjustable mixed-integer recourse (without defining decision rules, e.g., [67][68]). On the other hand, assuming plain affine decision rules allows deriving a tractable formulation of the robust counterpart, as done in Paragraph 4.3, by reformulating the infinite number of constraints into a finite number exploiting linear programming duality. If binary second stage variables were included, the nonconvex structure of the constraints would prohibit the use of duality results, calling for more sophisticated (and computationally intensive) approaches [66].

4.5.1 Improper modeling of recursive battery efficiency

It is worth noting that the recursive net storage power variable $sp_{s,t}^{\delta}$, composed of charge and discharge variables $dp_{s,t}^{\delta}$ and $cp_{s,t}^{\delta}$ each penalized by the corresponding discharge/charge efficiency (Eq. (58)), may underestimate the storage efficiency in recursive charge/discharge operations. In the deterministic problem formulation, the optimality of the solution implies that flux components $cp_{s,t}$ and $dp_{s,t}$ are never positive at the same time, since this would introduce an unnecessary energy loss in the charging / discharging processes. This is also true for the first stage decisions of the proposed AARO formulation. On the other hand, the AARO formulation might require that both $cp_{s,t}^{\delta}$ and $dp_{s,t}^{\delta}$ are different from zero at the same time t in the recourse. This occurs whenever the battery must change the direction of the net exchange in the recourse with respect to the first stage (nominal) operation. Figure 10 shows the recursive net energy flow sp^{δ} exchanged with the battery as a function of the data perturbation δ, as it is represented by purely linear decision rules (Figure 10 – left) and as it should be represented accounting for integer recurse (Figure 10 – right). In the example shown in the figure, the nominal (first stage) solution is to discharge the battery (net nominal power flow $sp^{\delta}(\delta = 0)$ is positive), while the optimal recourse decision is to decrease sp^{δ} as the perturbation δ increases (e.g., overproduction of electricity from intermittent RES). Above a certain value of δ, sp^{δ} turns negative, indicating that the recourse decision is to change the direction of battery exchange (the unforeseen intermittent production increase is high enough to start charging the battery). The top plots also show the recursive storage charge and discharge power components $dp^{\delta}$and cp^{δ}. Since both must be positive and linear between δ = 0 (nominal solution) and the maximum value of the perturbation $\bar{\delta}$, storage losses ε^{δ} occurring as coa nsequence of purely linear decision rules are overestimated, since the loss term

is applied on both the charge and discharge components and not on the net exchange. The bottom-left plot shows the AARO model representation of recursive energy loss ε^{δ} as function of δ, compared to the real case loss $\varepsilon^{\delta}_{real}$ (reaching zero when the net exchange flow $sp^{\delta} = 0$). Figure 10 – right shows how this issue could be overcome adopting a conditional linear decision rule able to selectively act on a single charge/discharge power component $dp^{\delta}$and cp^{δ}. In order to do so it would be necessary to adopt piecewise linear decision rules featuring binary recourse variables and optimized break points (see e.g., [69]) which would substantially increase the computational cost of the problem. It must also be noted that since the decision rules depend on the history of the perturbation $\tilde{\boldsymbol{\delta}}$, the identification of the breakpoints is not easy.

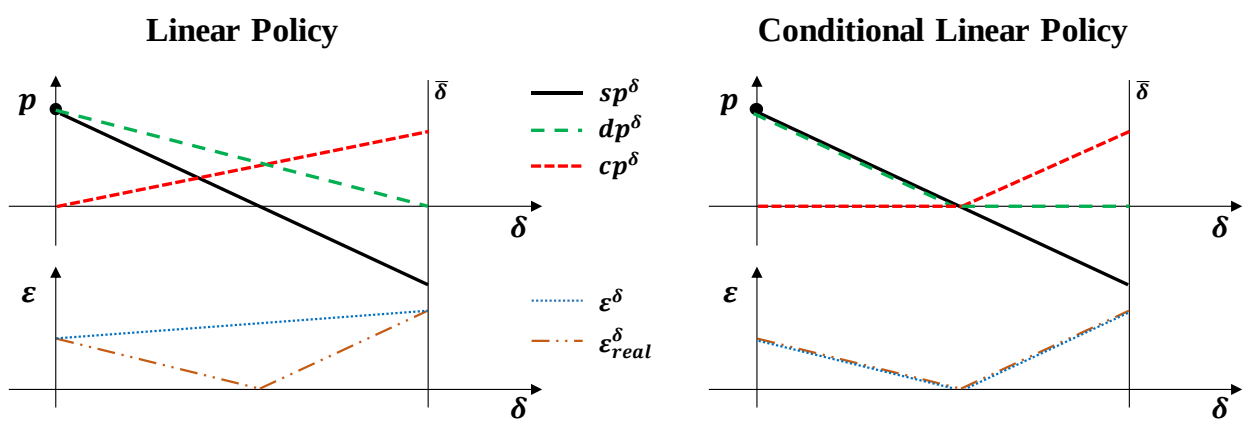

Figure 10: Plot of the net energy flow exchanged with the battery (sp^{δ}) and energy loss ε^{δ} as functions of the data perturbation δ. Top-left plot shows the charge and discharge power components of the battery $dp^{\delta}$and cp^{δ} in the AARO model. The bottom-left plot shows the energy loss ε^{δ} compared to the real case. The right-hand plots show the correct solution which requires a conditional linear decision rule.

4.5.2 Over-conservative decision rules for poly-generation units

Another relevant impact of the absence of conditional recourse is setpoint overcorrection for cogeneration units (e.g., CHP engines) when the two or more demands of the output energy are uncertain (e.g., electricity and heat). As a simple example to show this issue, in this Paragraph is simulated with the AARO MILP model the case of a single CHP engine (one-degree-of-freedom CHP unit) supplying heat and electricity to an islanded system affected by uncertainty of both heat and electricity demands. Due to the lack of storage systems and dynamic constraints for the engine (e.g., ramp-up/down constraints), the engine decision rule should depend only on the current uncertainty realizations (i.e., $Y^{+}_{ICE,th,t,\tau} = 0 \; for \; all \; t \neq \tau$). Temporal indexes are therefore omitted in the following descriptions. The engine load must, therefore, be adjusted on the basis of the current pair of actual energy demands ($\tilde{d}^{\delta}_{th}, \tilde{d}^{\delta}_{el}$), without being influenced by the past forecast errors. Figure 11 shows four possible forecasted combinations of thermal and electric demands (denoted with points A_0, B_0, C_0, D_0) and, around each forecasted point, the boxes defined by all possible uncertain perturbations. Points A_1, B_1, C_1, C_2, … D_7 within the boxes represent examples of possible energy demand realizations. The part-load operating curve of the ICE can be well approximated with a linear function between the minimum and the maximum load, linking thermal and electric power output (see, e.g.,

[70]). The optimal operating point of the engine (falling on the engine operating line) identified by the AARO model for each demand combination are denoted with A'_1, B'_1, C'_1, C'_2, … D'_7.

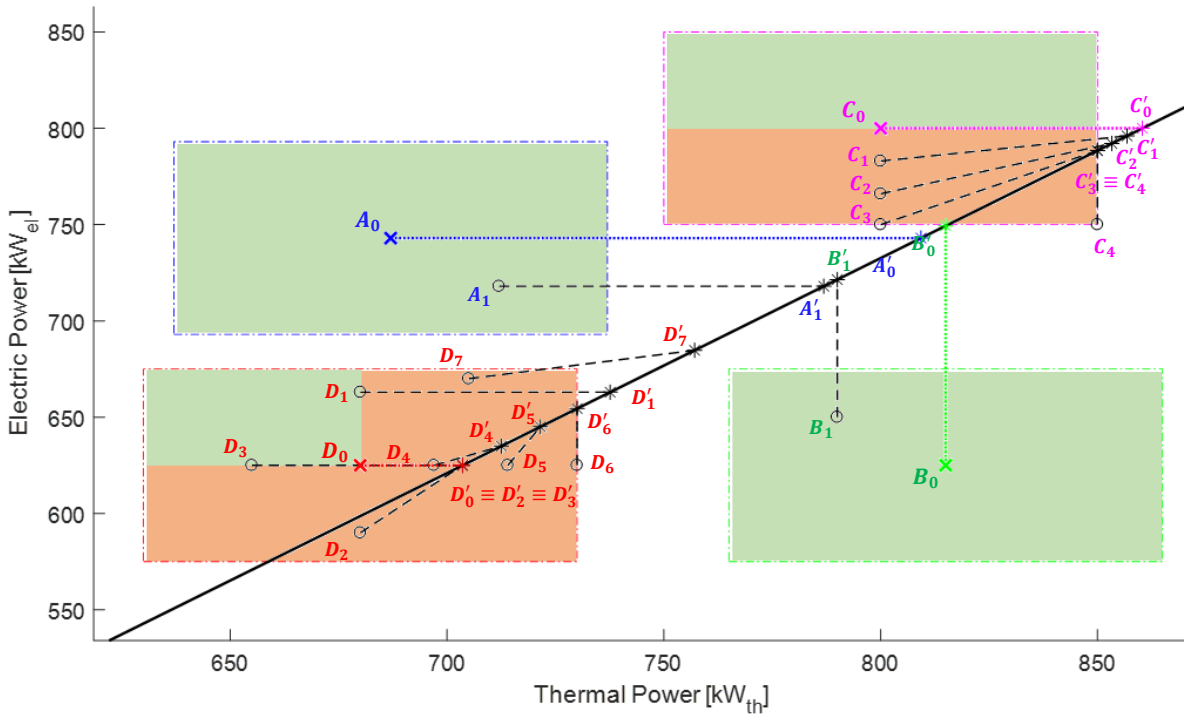

Figure 11: Plot of the energy demand and ICE operating points (nominal and corrected) in the power-heat diagram. The points have been obtained by solving the AARO model. For demand points falling in the red regions, the affine decision rules are over-conservative (the engine load is higher than required to meet the demands and the excess production is wasted).

For any possible point (i.e., realization) within the uncertainty boxes, the operating point of the engine is required to provide electricity and heat production higher than or equal to the corresponding demand. To compensate both electricity and heat demands for any potential uncertain realization within the uncertainty box around point A_0, it is sufficient to follow an affine decision rule depending only on the electric demand deviation $\delta\tilde{d}_{el}$ (i.e., $Y^{+}_{ICE,el} = -Y^{-}_{ICE,el} = \frac{1}{\tilde{m}_{ICE,el}}$, $Y^{+}_{ICE,th} = Y^{-}_{ICE,th} = 0$), corresponding to the *electric-driven* operating mode (the engine follows the electric load regardless of the thermal load). This is due to the fact that in the nominal solution the engine generates more heat than required in any potential scenario associated with A_0, Excess thermal power is wasted. Following the electrical load variation ensures that for any possible combination of perturbations $[\delta\tilde{d}_{el}, \delta\tilde{d}_{th}]$ heat demand manifestation $\tilde{d}^{\delta}_{th}$ is met. The opposite occurs for the potential combinations of heating and electricity demands around point B_0, where the decision rule adjusts the engine load only on the basis of heat demand perturbation $\delta\tilde{d}_{th}$ (i.e., $Y^{+}_{ICE,el} = Y^{-}_{ICE,el} = 0$, $Y^{+}_{ICE,th} = -Y^{-}_{ICE,th} = \frac{1}{\tilde{m}_{ICE,th}}$,), corresponding to the *thermal-driven* operating mode. In both cases A_0 and B_0, the affine decision rules meet the combination of thermal and electric demands with the minimum possible engine fuel consumption and thus are energetically and economically optimal.

In the case of points C_0 and D_0 (in Figure 11), the uncertainty box around the demand pairs crosses the operating map of the engine indicating that there is not a prevailing demand that always univocally sets the engine load (while the other is automatically met). In the ideal decision rule, if the combination of the two demands falls above the engine part-load linear curve, the engine should operate in the *electric-driven* mode, while if it falls below the engine should operate in the *thermal-driven* mode. However, implementing such ideal decision rule requires the use of binary (conditional) variables which are not allowed in the plain AARO framework used here. This impossibility of switching from electric to thermal driven corrections leads to over-conservative solutions as shown for points C_1, C_2, C_3, and D_2, D_7 represented in Figure 11.

Specifically, in the decision rules associated with nominal point C_0, $Y^-_{ICE,th}$ must be zero because if the load were reduced proportionally to any potential thermal demand reduction, the uncertain electric load $\tilde{d}^{\delta}_{el}$ might not be met. As for $Y^-_{ICE,th}$, the optimal decision rule features $Y^-_{ICE,th} = 0$ since the nominal engine thermal production is sufficient to meet any possible positive perturbation of thermal demand $\delta\tilde{d}^+_{th}$ (having $Y^-_{ICE,th} > 0$ would cause an unnecessary over-correction of the engine load with consequent increase fuel consumption). The fact that $Y^-_{ICE,th} = 0$ does not allow decreasing the engine load on the basis of the thermal demand (i.e., adopting the thermal-driven mode) when the realization of uncertain demands lies below the engine map. In this case, the ideal decision rule (which minimizes the fuel consumption of the engine) should switch from electric-driven to thermal-driven ($Y^+_{ICE,th} = \frac{1}{\tilde{m}_{ICE,th}}$, $Y^-_{ICE,el} = 0$) but such switch is not possible under the AARO framework. The optimal affine decision rule found in our robust AARO model performs an affine mapping of $\delta\tilde{d}^-_{el}$ into the segment of engine loads defined by points C'_0 and C'_3 which preserves feasibility under any possible realization of the uncertain demands. This affine map is shown by the segments connecting the demand points C_1, C_2, C_3 with the corresponding engine operating points C'_1, C'_2, C'_3 in Figure 11. Compared to the ideal decision rule (thermal-driven), the engine loads are higher than necessary, leading to the dissipation of both electricity and heat. The decision rule is thus certainly suboptimal.

For point D_0, the decision rule associated with positive perturbations of the two demands must include affine positive coefficients associated with both independent demand perturbations (i.e., $Y^+_{ICE,el} = \frac{1}{\tilde{m}_{ICE,el}}$, $0 < Y^+_{ICE,th} < \frac{1}{\tilde{m}_{ICE,th}}$), to guarantee feasibility in the two opposite cases: $\delta\tilde{d}^+_{el} = 0$, $\delta\tilde{d}^+_{th} > 0$, and $\delta\tilde{d}^+_{el} > 0$ and $\delta\tilde{d}^+_{th} = 0$. In particular, for $\delta\tilde{d}^+_{th}$, the optimal decision rule is an affine map of δd^+_{th} into the segment of engine loads defined by points D'_0 and D'_6. Such decision rule leads to a thermal production greater than uncertain thermal demand $\tilde{d}^{\delta}_{th}$ whenever $0 < \delta\tilde{d}^+_{th} < \delta\bar{d}^+_{th}$ (load overcorrection) as shown in Figure 11 for points D_4 and D_5. Thermal excess production is zero only when $\delta\tilde{d}^+_{th}$ is equal to its maximum value (point D_6). Moreover, if both demands have simultaneous positive perturbations (both demands are higher than forecasted, e.g., point D_7), both affine corrections depending on electric and thermal load increase will be applied at the same time, leading to an overall increase of the engine load higher than necessary (engine load overshooting). In turn, the load overshoot may also imply a limitation on the maximum nominal (first stage) engine load which is tighter than that required by the potential perturbation amplitudes (represented

by the dashed box). The engine load is not optimally corrected also for $\delta\tilde{d}_{el}^{-} > 0$ (i.e., when there is a negative deviation of the electric demand from its forecast) since $Y_{ICE,el}^{-}$ must be zero: if the engine load was decreased proportionally to the electric demand, the thermal production might not be sufficient to meet the thermal demand in all points falling in the triangle below the ICE part-load curve. The result is that, in case of electric demand reductions, the engine load not altered, dissipating any excess production according to an over-conservative strategy.

In summary, for all uncertain demand pairs falling within the green regions of Figure 11, the engine load is correctly adjusted, while for the demand combinations within the red regions the engine load correction is suboptimal since it is associated to unnecessary energy dissipation.

4.5.3 Use of quick-start units

The absence of second stage binary variables does not allow considering the potential start-up/shut-down of quick-start units in the recourse, to deal with uncertain perturbations. Plain affine or piece-wise linear decision rules only allow for load adjustments in the recourse, limiting unit commitment decisions to the first stage and imposing that all required units, even if their contribution is needed only for extreme uncertainty realizations, must always be in operation. Normally, this involves dispatching them at minimum load, with negative effect on system performance. On the other hand, unlike large power plants, boilers, gas turbines, and internal combustion engines can generally be quickly switched on/off according to the actual needs, implying the possibility of real-time adjustments of commitment decisions. Accounting for this kind of flexibility would lead to significantly more efficient operating solutions. A potential modification to the AARO formulation presented in this Chapter is discussed in 5.5.2 and tested in Chapters 5 and 6.

4.5.4 Dynamic Constraints

The state evolution of units featuring dynamic constraints (e.g. storage systems, units with load ramping limitations) must be constrained also in the second stage (recourse) as a function of the uncertainty realization. In particular, such constraints on the state variables must hold under any possible uncertainty realization and this may lead to inefficient utilization of these units. An example of the inefficient management of storage systems is shown in Figure 12 for a system composed of solar PV panels and a battery. While the demand uncertainty is neglected, the PV production is assumed to be uncertain with a maximum positive variation of $\delta\overline{up}_{PV}$. The figure shows how a deviation δup_{PV} in the PV array power generation is managed by the decision rules of the AARO model. The battery charge power recursive correction $\Delta cp_{BESS}^{\delta}$, computed according to the optimal decision rules based on the observed $\delta up_{PV,t}$ history, causes a storage content deviation $\Delta C(\delta up_{PV})$ (solid blue line). Instead $\Delta C^{\delta}(\delta\overline{up}_{PV})$ (dashed blue line) represents the storage content deviation that would follow a consistent maximum forecast error occurring in all timesteps. As this line reaches the maximum battery capacity, the PV production must be curtailed/wasted. While in an optimal strategy PV generation should be curtailed only when the storage unit is fully charged, the AARO formulation is not able to represent this conditional recursive action, and curtailment is triggered also when it would not be necessary. This correction is not optimal as energy is wasted without reaching the maximum battery state of charge, decreasing the capacity of the storage to compensate net demand increases in later

timesteps. Depending on the specific problem characteristics (e.g., if a threshold on the maximum energy dissipation is imposed), the first stage (nominal) solution could also be negatively affected by the limited flexibility of the decision rules. Analogous considerations can be done, for example, on the lower bound on the charge level and on the ramping constraints of the generators.

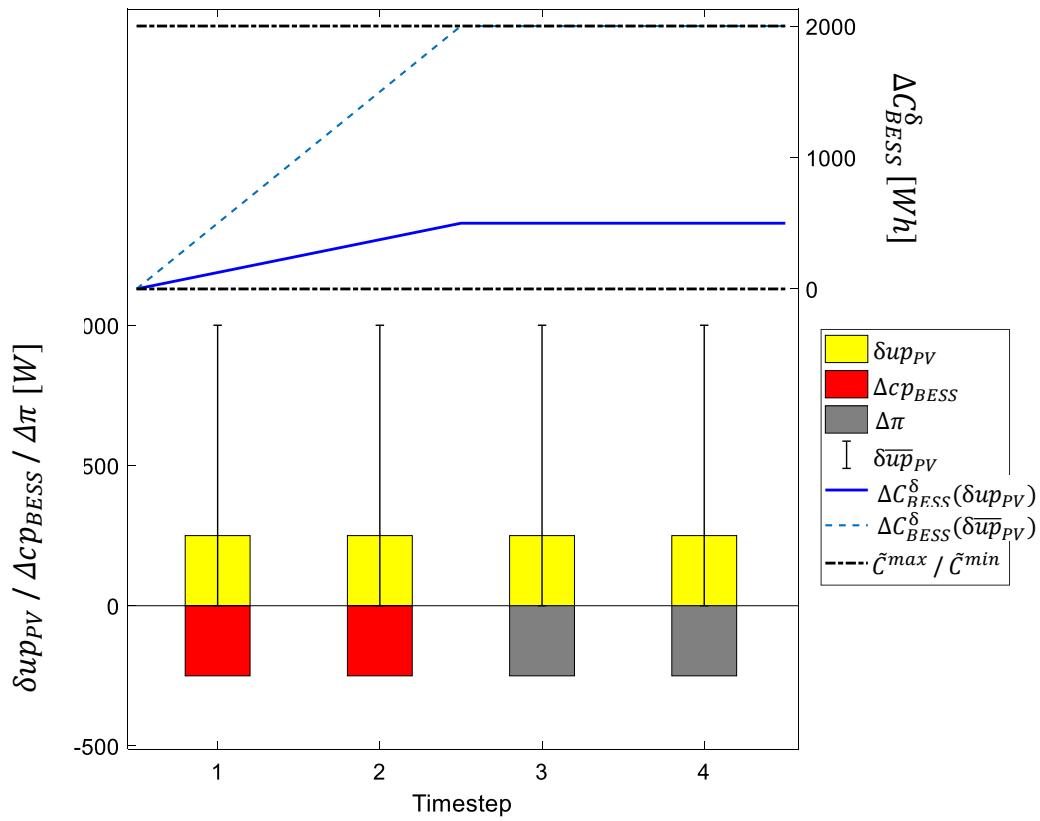

Figure 12: Example of inefficient PV production curtailment due to limits of the affine decision rules.

4.6 Model Adjustments

This paragraph proposes potential model adjustments that can be implemented according to the characteristic of the considered application, in order to improve the computational effectiveness of the formulation: due to the extremely large size of the tractable robust counterpart problem, computation time is often a barrier to the practical adoption of the AARO formulation.

4.6.1 Partial-past recourse

The general form of the recourse coefficients matrix $Y_{i,k,t,\tau}$ presented in the previous section requires non-anticipativity of the decision rules (i.e., the recourse matrices $Y_{i,k}$ are triangular lower) and the decision rule depends on all full history of past realizations of the uncertain parameters (e.g., the storage charge/discharge rate at time *t* can be adjusted on the basis of the energy demand forecast errors occurred in all previous timesteps). For certain applications with limited dynamic behavior (i.e., with no or relaxed ramping constraints and with no or limited storage capacity), the optimal corrective actions at a given time *t* depend

essentially on the uncertainty realizations occurred in the latest timesteps. Indeed, if the system has no storage units and no time linking constraints, each time instant is independent of the others: thus, the optimal decision rules are functions only of the current perturbation (i.e., the recourse coefficient matrix $Y_{i,k}$ is diagonal). Lorca et al [71] already explored the possibility of simplifying the form of recursive policies to improve computational performance, showing how less general versions of the affine policies can yield good results in terms of overall performance while sensibly reducing problem complexity.

In light of these considerations, to reduce the number of variables of the robust problem, the idea of partial-past recourse is here introduced, which limits the number of recourse coefficients by defining a recourse temporal depth $\overline{\tau}$, representing the lower bandwidth of matrix $Y_{i,k}$:

$$Y_{i,k,t,\tau} = 0 \quad \forall\, \tau < \overline{\tau}, \tau > t \qquad\qquad \forall i, k \in \boldsymbol{\mathcal{K}}, t \in \boldsymbol{\mathcal{T}} \tag{112}$$

Of course, adopting the partial-past recourse simplification for problems featuring storage units and slow-ramping generators limits the decision rules space and may lead to significantly more conservative solutions compared to the standard approach (full-past recourse). The practical application of the partial-recourse strategy to real-world problem is discussed in Chapters 5 and 6.

4.6.2 Uncertainty factors aggregation

The energy demand profile and the production of the corresponding non-dispatchable generators (e.g., electricity demand and PV production) can be considered a separate uncertain parameter. Alternatively, they can be aggregated, in order to consider the net energy demand as a single uncertainty factor. It is important to note that, while the two approaches are equivalent in the deterministic scheduling problem formulation, there is a significant difference in the robust formulation. Specifically, handling them as separate uncertain parameters allows defining decision rules which feature separate response coefficients with respect to each of the forecast errors. This increases the degrees of freedom of the recourse actions but, on the other hand, it leads to two important drawbacks:

1) since the two factors are considered to be independent one from the other, the worst-case condition (maximum deficit of renewable production and maximum peak of energy demand) may lead to over-conservative solutions;
2) a larger size of the uncertain parameters set $\boldsymbol{\mathcal{K}}$ leads to a substantial increase in the number of dual variables necessary for the AARO problem reformulation, which may imply impracticable computational times.

To avoid these drawbacks, I propose to group all uncertain factors affecting the net demand of any given energy form into a single uncertain net demand. Its uncertainty can be characterized by combining the uncertainty sets of all uncertain parameters affecting it. It is important to notice that, although for the reasons explained it is convenient to deal with a single aggregated uncertain parameter, it is fundamental to preserve the independent uncertainty characterization referred to all individual uncertainty factors that contribute to net demand uncertainty. This is due to the fact that a given net demand might result from very different combination of load demand and non-dispatchable generation: a scenario of low demand and absent non-

dispatchable generation might correspond, in terms of net demand value, to a scenario of high load demand and high non-dispatchable generation. It is apparent how, according to which scenario yields the same value of net demand, the associated uncertainty is extremely different. In this thesis uncertainty factors are therefore always characterized independently, and the uncertainty set of aggregated uncertain parameters is constructed composing the independent uncertainty sets of each uncertainty factor.

To preserve the conservativeness of the formulation accounting for each uncertainty factor separately, the maximum positive and negative deviation of net demand of each form of energy $j \in \boldsymbol{\mathcal{D}}$ at time t must be computed as the sum of maximum upwards/downwards deviations of each factor $k \in \boldsymbol{\mathcal{K}}$ affecting net demand j. Since non-dispatchable generators production potential contributes with a minus sign to the identification of net demand, their upwards deviation bounds will contribute to the definition of the downwards deviation bound of net demand, and vice-versa:

$$\begin{aligned} \overline{\delta}\tilde{d}_{j,t}^{net} &\leq \overline{\delta}\tilde{d}_{j,t} + \sum_{l \in \boldsymbol{\mathcal{ND}}_j} \underline{\delta} up_{l,t} \\ \underline{\delta}\tilde{d}_{j,t}^{net} &\leq \underline{\delta}\tilde{d}_{j,t} + \sum_{l \in \boldsymbol{\mathcal{ND}}_j} \overline{\delta} up_{l,t} \end{aligned} \qquad \forall j \in \boldsymbol{\mathcal{D}}, t \in \boldsymbol{\mathcal{T}} \qquad (113)$$

Where $\boldsymbol{\mathcal{ND}}_j$ is the subset of non-dispatchable generators $\boldsymbol{\mathcal{ND}}$ producing energy form $j \in \boldsymbol{\mathcal{D}}$.

Similarly, each uncertainty budget $\Gamma_{d_j^{net}}$ for net demand d_j^{net} should be computed, to preserve the same conservativeness of the independent uncertainty characterization, as the sum of each relevant uncertainty budget:

$$\begin{aligned} \Gamma_{d_j^{net}} &\leq \Gamma_{d_j} + \sum_{l \in \boldsymbol{\mathcal{ND}}_j} \Gamma_l \\ \Gamma_{d_j^{net}}^{+} &\leq \Gamma_{d_j}^{+} + \sum_{l \in \boldsymbol{\mathcal{ND}}_j} \Gamma_l^{-} \\ \Gamma_{d_j^{net}}^{-} &\leq \Gamma_{d_j}^{-} + \sum_{l \in \boldsymbol{\mathcal{ND}}_j} \Gamma_l^{+} \end{aligned} \qquad \forall j \in \boldsymbol{\mathcal{D}} \qquad (114)$$

On the other hand, it is important to remember that the parameters characterizing the uncertainty set of each uncertainty factor are obtained in this thesis from a statistical analysis of forecast errors (see Paragraph 5.2). Instantaneous deviation boxes and cumulated error budgets are associated with a given confidence interval on the history of forecast error observations. When composing the independent errors into a single error manifestation, summing the percentiles of the independent observations yields a conservative uncertainty space, since it is unlikely that all uncertain quantities hit their maximum deviation from forecast at the same time. To limit the conservativeness of net demand uncertainty set, error propagation techniques can thus be adopted. Specifically, error propagation theory states that for the sum of independent uncertain variables x_i characterized by standard errors e_i, the standard error of the sum can be obtained by adding in quadrature the standard errors of all uncertain variables x_i [72]:

$$z = x_1 + x_2 + \cdots \tag{115}$$

$$e_{\overline{z}} = \sqrt{e_{\overline{x_1}}^2 + e_{\overline{x_2}}^2 + \cdots} \tag{116}$$

Although inappropriate from a strict mathematical point of view (a detailed accounting of the interaction between confidence interval goes beyond the scope of this work), in evaluating the model performance on the test cases described in the next Chapter we explore the application of the described error propagation techniques to the definition of net demand uncertainty set:

$$\overline{\delta}\tilde{d}_{j,t}^{net} \leq \sqrt{\overline{\delta}\tilde{d}_{j,t}^2 + \sum_{l \in \boldsymbol{\mathcal{ND}}_j} \underline{\delta} up_{l,t}^2} \qquad \forall j \in \boldsymbol{\mathcal{D}}, t \in \boldsymbol{\mathcal{T}} \tag{117}$$

$$\ldots$$

$$\Gamma_{d_j^{net}} \leq \sqrt{\Gamma_{d_j}^2 + \sum_{l \in \boldsymbol{\mathcal{ND}}_j} \Gamma_l^2} \qquad \forall j \in \boldsymbol{\mathcal{D}} \tag{118}$$

$$\ldots$$

5 DAY-AHEAD OPERATION SCHEDULING

In this Chapter, the two formulations of the scheduling problem proposed in the previous Chapters are numerically compared, examining three real-life case studies: an off-grid sub-Saharan electric microgrid and two grid-connected CHP applications: a Hospital and a University Campus. The comparison is developed by producing actual demand and RES production forecast profiles, resorting to different forecasting techniques based on the available dataset, to serve as inputs for the system nominal scheduling operation. Daily nominal scheduling is assumed to be determined 24-hours in advance, based on day-ahead forecasts. Actual system operation is then evaluated accounting for the real demand and RES generation profiles, tackling the real-time dispatch problem according to a two-layers EMS structure: the first layer defines the strategic day-ahead scheduling decisions, such as unit commitment schedule and nominal storage usage profile, based on either the deterministic or the robust problem formulation; the second layer adopts the strategic decisions taken by the first layer and manages real-time unbalances according to different proposed algorithms. The nature of the second layer algorithm and its interaction with the first layer depend on the problem formulation adopted in the first layer. Specifically, two different second layer approaches are proposed. Firstly, rule-based second layers, which define adjustments to the nominal scheduling plan according to pre-defined decision rules, are evaluated. At this stage, the optimal decision rules yield by the AARO formulation are compared with heuristic dispatch algorithms, specifically developed for each case study to adapt the deterministic scheduling solution. Secondly, a more homogeneous MILP-based second layer algorithm is proposed, based on the Shrinking Horizon approach and featuring a deterministic second layer problem formulation, with the addition of constraints to enforce the strategic decisions taken by the first layer. Two operating modes are considered in this second comparison: Fixed Unit Commitment Mode, in which the day-ahead commitment plan defined by the first layer cannot be changed by the second layer, and Modifiable Unit Commitment Mode, in which the commitment status of quick-start units can be changed by the second layer with respect to the first layer plan.

This Chapter and Chapter 6 analyze and discuss the advantages and differences related to tackling the UC and ED problem resorting either to the robust approach presented in Chapter 4 or to the deterministic approach featuring reserve constraints described in Chapter 3. The two formulations are compared by means of an extensive numerical testing campaign, under different sets of assumptions on the characteristics of the deployed EMS and for a variety of case studies and system designs.

To effectively compare the proposed formulations, and to properly assess their performance when deployed in real-life systems, a substantial effort was put in defining simulation work-frames representative of realistic management conditions, and in proposing architectures for EMS overseeing system operation compatible with practical on-field implementation. Real dataset of demand and renewable generation potential, from on-field measurements collected by our industrial partners in real-life MES and microgrids, are used in defining the case studies.

All the EMSs proposed in this work operate based on the structure depicted in Figure 13: based on forecast information, a nominal scheduling solution is identified by resorting to one of the MILP scheduling problem

formulations. Real forecast profiles, produced adopting various forecasting techniques based on the available information, are used as input for the first layer problem solution. The actual system performance, as forecast errors are in turn observed, is evaluated by introducing a lower level management algorithm, which introduces real-time adjustments to the nominal first layer scheduling solution based on the manifestation of the actual demand and RES generation profiles. The impact of forecast errors on performances and the suitability of the scheduling problem formulation as confronted with the inputs non-deterministic nature is therefore accurately accounted for.

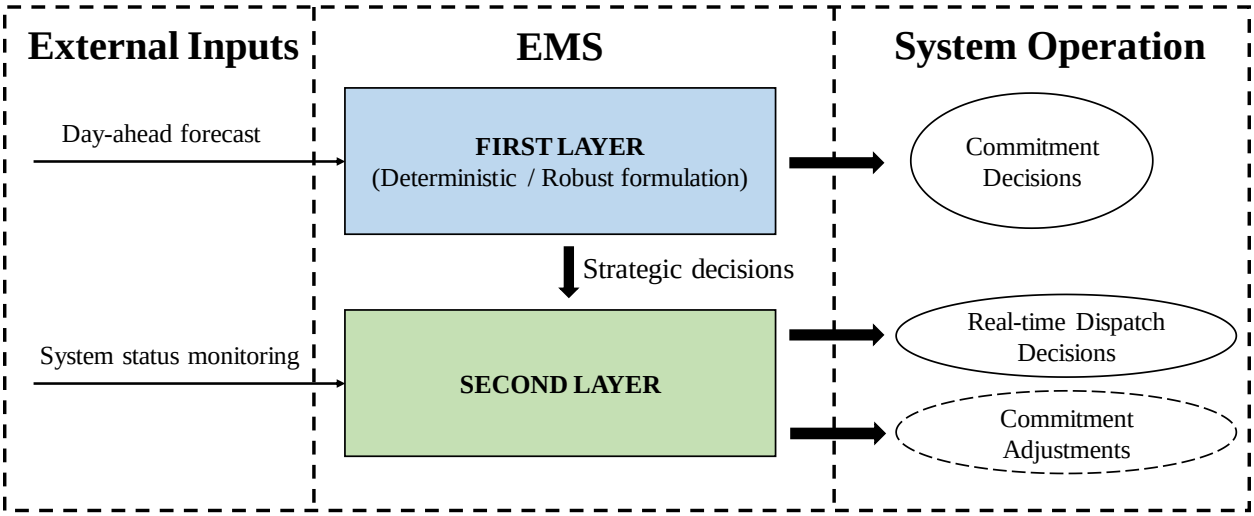

Figure 13: two layers EMS general structure

In this Chapter, the robust and the deterministic approaches are applied to systems operating according to a day-ahead scheduling optimization: based on the forecasts of demand and non-dispatchable production for the upcoming day and the corresponding uncertainty, the commitment plan of all units and the corresponding nominal dispatch solution are identified by the EMS first layer. During the rest of the day, the EMS second layer takes care of adjusting the reference dispatch solution, accounting for the strategic decisions taken by the first layer. The second layer defines the setpoint of all units and, when possible, introduces corrections in the Unit Commitment schedule identified by the first layer, to account for the actual manifestation of uncertain parameters. This kind of day-ahead scheduling approach is commonly adopted in systems with a medium or low level of automation, where the start-up sequence of most units is overseen by an operator based on a predefined commitment schedule that it is unpractical to frequently modify.

Three different second layer algorithms are considered in this Chapter, reflecting different assumptions on the system management strategy and control capability:

1) Rule-based second layer algorithm (Paragraph 5.4);
2) MILP-based second layer algorithm with no real-time commitment adjustments (Paragraph 0);
3) MILP-based second layer algorithm with real-time commitment adjustments (Paragraph 0).

5.1 Test Cases Definition

The numerical testing campaign is performed on three different test cases:

- an electric sub-Saharan off-grid microgrid;
- a Combined Heat and Power (CHP) generation system for a grid-connected hospital;
- a CHP generation system for a grid-connected university campus.

All test cases are representative of actual existing systems. The profiles of demand and non-dispatchable generation potential for the islanded microgrid and the hospital [73] are based on actual on-field measurements, provided by industrial partners operating real systems, while load profiles for the campus are reconstructed based on physical models [74]. The key data relative to each case study are summarized in Table 1 (specifying type and characteristics of internal energy demands and accounted uncertainty sources) and Table 2 (listing the installed units in the alternative designs considered for each case study). For the on-grid Campus test case, peak power and daily demand are relative to the three seasons represented in the dataset (respectively winter, summer, and mid-season).

Table 1: test case characteristics

Test Case	**Energy Provided**			**Uncertainty Factors**
	Energy	**Peak Power [MW_p]**	**Daily Demand [MWh/day]**	
Off-grid Micro-Grid	Electricity	1.1	14.2	Electric Demand
On-grid Hospital	Electricity	1.9	35.3	Electric + Thermal Demand, PV production
	Heat	4.6	83	
On-grid Campus	Electricity	2.8 / 3.7 / 2.4	26.1 / 28.9 / 22.5	Electric + Thermal Demand, PV production
	Heat	10.3 / 0 / 3.5	66.4 / 0 / 13.4	

The system design considered for the off-grid microgrid corresponds to the typical hybrid microgrid architecture adopted for medium/large off-grid villages. The diesel generators provide the necessary reserve to compensate for PV fluctuations and ensure system stability. For the Hospital and University Campus case studies, several different system designs have been considered, accounting for various combinations of installed RES capacity, generators technologies, and storage sizes. The performance of the deterministic and robust formulations is therefore compared in a wide set of realistic configurations, to derive results as general as possible. Table 2 lists type and size of the installed units in all alternative designs considered for each case study.

Table 2: design configurations and installed units for the three case studies

	Quick-Start	Microgrid	Hospital							Campus		
CONFIGURATION / **UNITSS**			**HA**	**HB**	**HC**	**HD**	**HE**	**HF**	**HG**	**CA**	**CB**	**CC**
Diesel generator [kW_{el}]	Y	2 x 550	-	-	-	-	-	-	-	-	-	-
Natural gas CHP engine [kW_{el} / kW_{th}]	N	-	1 x 1900 / 1770	1 x 1900 / 1770	2 x 1000 / 1040	2 x 1000 / 1040	-	1 x 1050 / 1080	-	1 x 960 / 1000	-	1 x 2050 / 1900
Natural gas Boiler [kW_{th}]	Y	-	3 x 1700	3 x 1700	2 x 1270	1 x 1270	-	-	-	1 x 3960	1 x 4170	1 x 5900
PV field [kW_{el}]	-	1 x 1440	-	-	-	1 x 1000	1 x 1000	1 x 2000	1 x 1500	1 x 3150	1 x 3150	-
Heat Pump [kW_{th}]	Y	-	-	1 x 2070	1 x 2070	2 x 2070	2 x 1050	3 x 2070	-	1 x 1670	-	1 x 1550
ORC CHP unit [kW_{el} / kW_{th}]	N	-	-	-	-	-	1 x 1000 / 4830	-	1 x 1000 / 4830	2 x 60 / 350	1 x 515 / 2570	-
Biomass Boiler [kW_{th}]	N	-	-	-	-	-	1 x 1680	-	1 x 1680	-	-	-
Thermal Storage [kWh_{th}]	-	-	1 x 1274	1 x 1274	1 x 1274	1 x 10000	1 x 10000	1 x 10000	1 x 10000	1 x 21140	1 x 28400	1 x 4626
Lithium-Ion Battery [kWh_{el}]	-	1 x 3600	-	-	-	-	-	-	-	-	-	-

Some of the units reported in Table 2 are characterized by dynamic limitations in terms of minimum-up time and upwards/downwards load ramping. Table 3 summarizes the dynamic constraints considered for each generator technology.

Table 3: dispatchable generators dynamic constraints

	Diesel generator	Natural gas CHP engine	Natural gas Boiler	Heat Pump	ORC CHP unit	Biomass Boiler
Min Up Time [h]	2	6	2	-	24	4
Ramp limit [%/h]	-	-	-	-	25%	50%

Unitary charge/discharge efficiency (no charge/discharge losses) and a self-discharge rate of 0.5%/h is considered for the thermal storage (Thermal Energy Storage System, TESS), while Lithium-Ion batteries (Battery Energy Storage System, BESS) are characterized by 97% charge/discharge efficiency and no self-discharge rate. For both grid-connected MES (campus and hospital), hourly price profiles of purchased/sold electric energy are considered in accordance with the Italian electric energy market [75].

5.2 Forecast Profiles and Uncertainty Characterization

As already mentioned, forecast profiles were generated for each case study by following different forecasting methodologies, according to the available data and the characteristics of the uncertain parameters. Specifically:

- An autoregressive SARIMA model has been used for the electric load forecast of the off-grid microgrid (see Paragraph 7.2.1);
- A simple forecast based on clear sky radiation has been produced for the Somalian PV arrays, in virtue of the very low PV production variability (see Paragraph 7.2.1);
- Artificial Neural Networks (ANN) were trained to predict thermal and electric load forecast of the Hospital, according to the method described in [76];
- A Moving Average was performed to estimate electric and thermal load forecast for the Campus;
- PV production for the CHP test cases was computed via the ANN described in [77].

Table 4: historical data and forecast production

Study Case	**Available data / temporal resolution**	**Testing Set**	**Forecasting technique**		**MAPE [%]**	**MAD [kW]**
Off-grid microgrid	3 months, 1 min	10 days	PV	Clear-sky	16.9%	32.8 kW
			Electric Load	SARIMA	4.9%	29.3 kW
CHP Hospital	6 months, 1 h	21 days	Electric Load	ANN	3.9%	59.4 kW
			Thermal Load		4.9%	170 kW
			PV (p.u.)		58.9%	34 W/kW
CHP Campus	3 months, 1h	17 days	Electric Load	Moving Average	30%	185 kW
			Thermal Load		41%	660 kW
			PV (p.u.)	ANN	24.9%	42.3 W/kW

Table 4 shows the available data and specific forecasting technique used in each case. The performance of the alternative formulations was evaluated on a subset of the available dataset (*testing set*).

The parameters defining the uncertainty sets have been determined based on a statistical analysis of the forecast accuracy, encompassing the available dataset of forecast errors. The values of vector $\tilde{\boldsymbol{l}}$ defining the uncertainty space $\mathcal{U}$ (Eq. (78)) are set to meet the 99.5th (0.5th) percentile of forecast errors observations over the entire time series. Expected forecast errors, which appear in the objective function of the robust formulation (Eq. (97)), are calculated as the average of historical positive/negative forecast error components. For the rural microgrid test case, for which a larger forecast error dataset is available due to the lower profiles temporal resolution, error boxes and expected forecast errors are defined differently in each hour of the day, while for the Hospital and the Campus case studies they are defined uniformly in consecutive 3 hrs time windows. Intra-day and cumulated norms are imposed on 8 windows lasting 3 hours each.

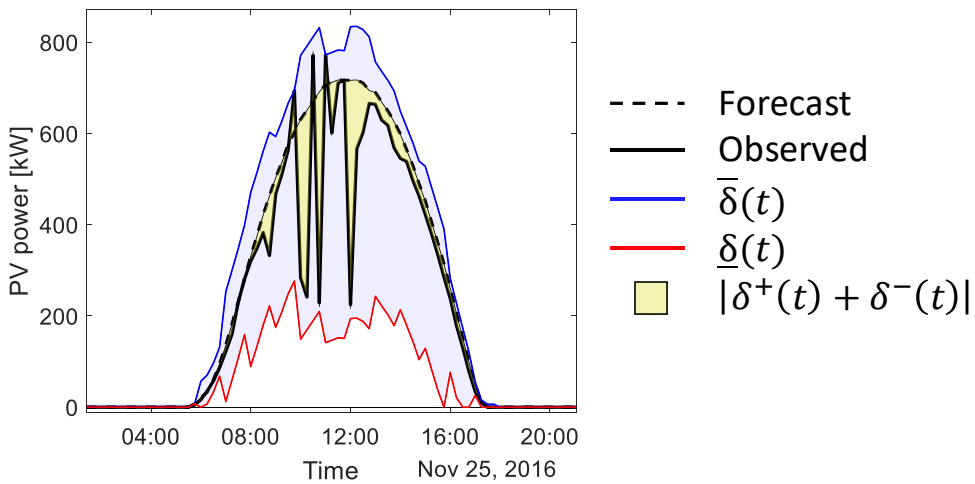

Figure 14: uncertainty space for PV production

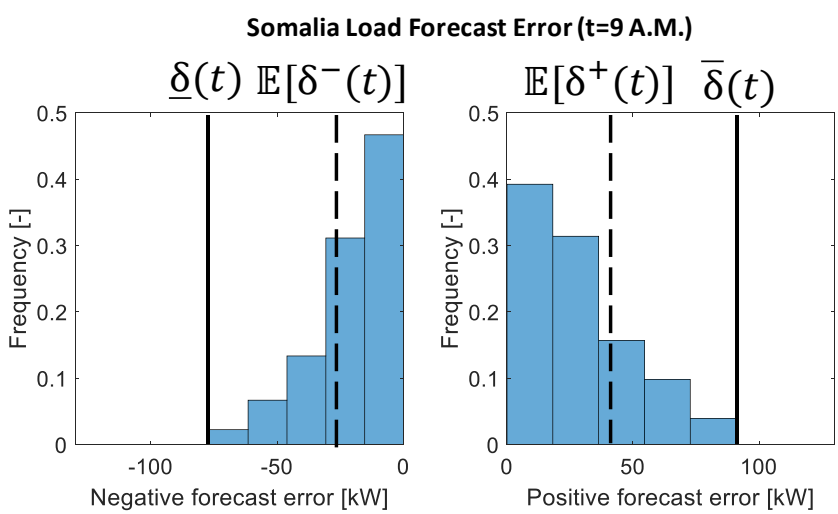

Figure 15: Error probability distribution for the forecast of the electric load of the Somalian Microgrid at 9 A.M.. The figure shows also the upper bounds of the uncertainty box and the positive and negative expected values.

5.3 Deterministic Problem Formulation

The performance of the robust approach is compared with an equivalent deterministic formulation of the optimal management problem, corresponding to a certain ($\boldsymbol{\delta} = \mathbf{0}$) and non-recursive ($\Delta \boldsymbol{x}^{\delta} = \mathbf{0}$) version of the MILP detailed in Chapter 4. This is, in turn, a simplified version of the more general model presented in Chapter 3, adapted to present a homogeneous comparison between the two formulations based on coherent modeling assumptions. Namely, the presented case studies only account for units with linear part-load curves, which could not be represented in the affinely adjustable modeling framework. Nevertheless, this is an assumption normally made in real-life systems, since the units are often accurately represented by linear curves in their typical operating range. Reserve constraints described in Paragraph 3.5 are used to impose a degree of conservativeness to the deterministic solution. While a fixed set of power deviations is considered in each test case, according to the accuracy of the forecast profiles, the energy reserve duration T^{res} is used as controllable parameter to tune the deterministic formulation conservativeness.

5.4 Rule-based Second Layer EMS

As an initial comparison, the direct use of the AARO decision rules in the EMS second layer is compared to the adoption of ad-hoc rule-based dispatch strategies developed to correct the deterministic scheduling plan, adjusting the dispatch profiles according to the observed net demand profiles. Each day is considered separately from the others, enforcing cyclic constraints on the nominal day-ahead solutions. Nominal UC plan and dispatch profiles are determined in both cases by the EMS first layer at the beginning of the day, based on the day-ahead forecasts of demand and non-dispatchable production and the corresponding uncertainty. Then, a different adjustment algorithm is followed by the second layer, according to the formulation adopted for the EMS first layer:

- If the AARO formulation is adopted in the first layer, the second layer setpoint adjustments are computed by following the optimal decision rules yield by the first layer solution;
- If the deterministic formulation is adopted in the first layer, the second layer setpoint adjustments are based on a rule-based balancing strategy specifically developed for each case study.

When adopting the AARO formulation, the UC plan determined by the first layer solution is never modified, since it already ensures sufficient generation capacity to cover for any net demand scenario and since the second layer corrections are based on the decision rules. In the off-grid electric microgrid case study, the nominal UC plan is never modified also when adopting the deterministic formulation, since the stability of the electric system would be immediately compromised by insufficient generation capacity giving no margin for the recursive start-up of diesel generators. Solution conservativeness must, therefore, be enforced only by means of adequate reserve constraints. Conversely, in the CHP systems temporary discrepancies between demand and generation can be tolerated since the thermal inertia of the heating distribution system and of the thermal loads (e.g. buildings) delays the effect of insufficient generation commitment. Therefore, the deterministic first layer formulation for the Hospital and the Campus case studies does not enforce reserve margins on thermal generation capacity, and the rule-based second layer algorithm can modify, in addition to all setpoints, also the unit commitment of quick-start units (e.g. boilers, heat pumps).

The simulations of the off-grid microgrid test case are performed with a temporal resolution of 30 minutes and therefore represent a more challenging problem in terms of computational complexity. For this reason, the off-grid microgrid test case is used to evaluate four alternative AARO formulations featuring the ad hoc modifications presented in Paragraph 4.6. The effectiveness of the proposed modifications is assessed both in terms of solution quality and average problem solution time. The following robust model formulations (summarized in Table 5) are considered:

- Formulation **R0** consists of the standard AARO formulation with piece-wise affine decision rules, featuring a basic budget uncertainty set (Eq. (104)-(106), $\mathcal{T}_i \equiv \boldsymbol{\mathcal{T}}$) and full-past recourse (e.g. recourse matrixes Y_i diagonal lower) [54]. Uncertainty on energy demands and non-dispatchable production (i.e., PV production) is accounted for separately, with an independent characterization of the two uncertainty sets;
- Formulation **R1** includes the full uncertainty set characterizations proposed in this thesis (Section 4.4), represented by equations (104)-(109);
- Formulation **R2**, in addition to the enhancements of formulation **R1**, considers an uncertain net energy demand (energy demand minus the energy production from non-dispatchable production) and the associated uncertainty set obtained as the worst-case combination of the demand and production uncertainty sets, as discussed in Section 4.6.2;
- Formulation **R3,** in addition to the modifications introduced in **R2**, features the partial-past recourse approach discussed in Section 4.6.1 to limit the computational time. In particular, the recourse temporal depth $\overline{\tau}$ is limited to 6 hours ahead of operating time.

Table 5: alternative robust model formulations

Name	R0	R1	R2	R3
Extended Uncertainty Characterization (Paragraph 4.4)		✓	✓	✓
Uncertain Net Demand (Paragraph 4.6.2)			✓	✓
Partial-past recourse (Paragraph 4.6.1)				✓

5.4.1 Rule-based second layer algorithm for off-grid microgrid

The rule-based second layer correction logic developed for the off-grid microgrid monitors the status of the system, namely generators load and BESS State of Charge (SOC), and decides how to share the net demand forecast error among all the units accounting for the deviation of the actual BESS SOC from its expected trajectory (from day-ahead optimization) and for the technical limitations of each unit. The block-flow scheme of the algorithm is reported in Figure 16.

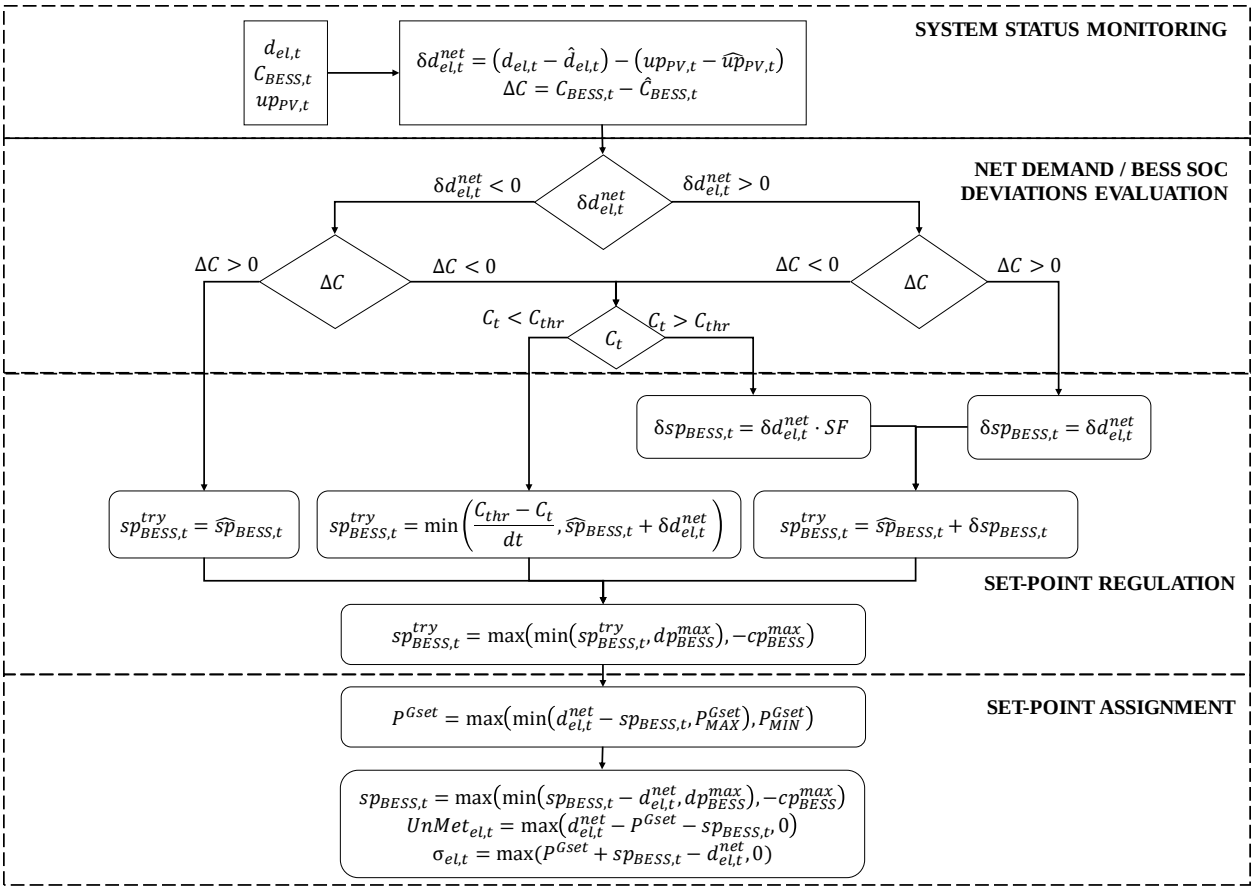

Figure 16: rule-based real-time correction algorithm for the off-grid microgrid.

At each timestep, two main parameters are computed: the deviation of actual net demand from its forecasted value $\delta d_{el,t}^{net}$ and the deviation of BESS energy content from its nominal value ΔC.

- If net demand is higher than anticipated ($\delta d_{el,t}^{net} > 0$), and the BESS charge is above its reference trajectory ($\Delta C > 0$), the battery compensates the entire net demand increase;
- If net demand is higher than anticipated ($\delta d_{el,t}^{net} > 0$) and BESS charge is lower than nominal but above a lower capacity threshold ($\Delta C < 0$ & $C \geq C_{thr}$), the BESS covers a fraction of the net demand deviation, decreasing as ΔC increases according to the split factor SF:

$$SF = \frac{C - C_{thr}}{C_{nom} - C_{thr}} \tag{119}$$

- Similarly, if net demand is lower than anticipated ($\delta d_{el,t}^{net} < 0$) and BESS charge is lower than nominal but above C_{thr} ($\Delta C < 0$ & $C \geq C_{thr}$), part of the nominal excess production is used to charge the BESS, according to a different split factor:

$$SF = 1 - \frac{C - C_{thr}}{C_{nom} - C_{thr}} \tag{120}$$

- As the BESS charge falls below the capacity threshold C_{thr} ($C < C_{thr}$), defined as 90% of the nominal charge, the algorithm, the BESS power is set to restore the threshold capacity;

- Finally, if net demand is lower than expected ($\delta d_{el,t}^{net} < 0$) but the battery capacity is above its reference trajectory ($\Delta C > 0$), the BESS nominal power is not modified, and the entire production surplus is used to reduce the load of generators.

Once the BESS power has been determined (enforcing all limitations due to max charge/discharge power and SOC), the total genset production is computed as the difference between the net demand and the corrected BESS power. Once again, limitations due to ramp rates and min/max generator load are accounted for:

$$P^{Gset} = \max\left(\min\left(d_{el,t}^{net} - P^{BESS}, P_{MAX}^{Gset}\right), P_{MIN}^{Gset}\right) \tag{121}$$

An auxiliary linear program distributes the total genset production among all the available generation units, imposing all technical constraints and additionally considering a small penalty in the OF for set-point variation, so to avoid unnecessary ramping.

Finally, the BESS set-point is adjusted to avoid unmet demand or PV curtailment, which might occur due to technical constraints affecting the generators setpoint calculation.

5.4.2 Rule-based second layer algorithm for grid-connected multi-energy systems

Since in the on-grid case studies the connection with the national grid guarantees that the electric demand can always be met, a priority-based thermal-driven balancing algorithm is adopted for the Hospital and Campus CHP systems.

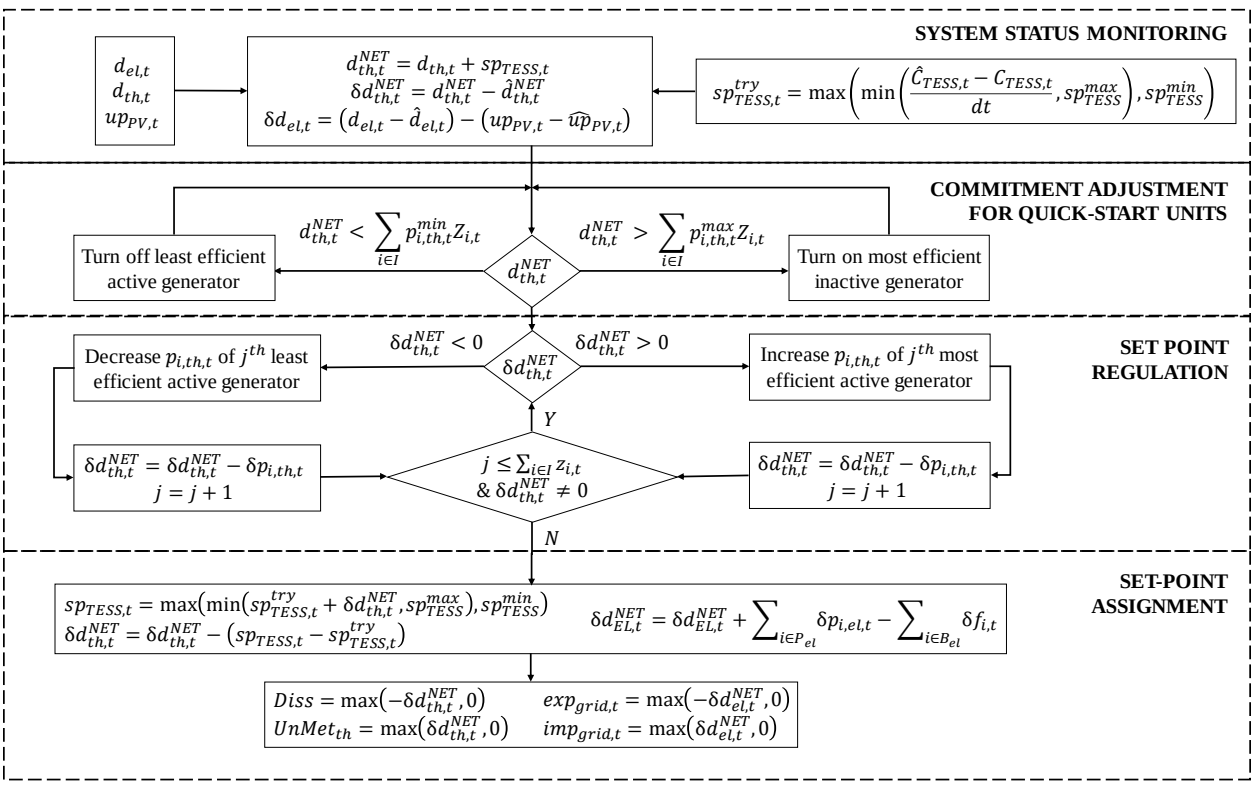

Figure 17: Heuristic real-time correction algorithm for the grid-connected MES.

This approach represents a balancing strategy often used by MES operators, according to the idea that starting from the optimal plan defined by the first layer, the most efficient units should be used to balance deviations of thermal demand from forecast, to minimize the new fuel consumption. The block-flow diagram of the logic is shown in Figure 17.

Based on the system status and the observed thermal demand, if the committed generation capacity is either not sufficient or excessive, the on/off status of quick-start units (such as boilers and heat pumps) is modified, accounting for all technical constraints on the commitment variables (e.g. minimum up/downtime). Then, the thermal net demand variation is distributed among the generation units according to an efficiency raking list, aimed at prioritizing the use of the most efficient units. TESS charge/discharge profile is preferentially not modified with respect to the reference trajectory defined by the first layer unless the thermal demand deviation cannot be compensated by acting only on the generation units (because of technical constraints such as ramping limits or limitations in unit commitment adjustments). If so, the thermal storage contributes to balance the system, deviating from its nominal trajectory. TESS capacity deviations are accounted for in the energy balance of following time-steps, so to restore the expected storage level evolution as soon as the required generation capacity is available. Electric system unbalances are compensated by adjusting the exchange with the national electric grid.

5.4.3 Off-Grid Electric Microgrid Results

Table 6 shows the expected (day-ahead estimates) and actual (real-time operation) overall diesel consumption across the testing period, for the robust and the deterministic first layer formulations considered. Real-time adjustments are computed following the optimal affine decision rules if the AARO formulation is adopted in the EMS first layer, or the rule-based algorithm described in Paragraph 5.4.1 if the deterministic formulation is adopted instead. To account for the storage level daily variations introduced by the second layer, which violate the cyclic constraint imposed on storage charge in the first layer, the daily BESS charge deviation is accounted for as an equivalent fuel saving (or consumption), assessed as the fuel that would be consumed to produce that amount of energy with diesel generators at the average generation efficiency attained during the day.

Table 6: comparison between robust and deterministic solutions

Simulation Mode		Expected Operating Cost [€]	GAP [%]	Actual Operating Cost [€]	GAP (increase wrt omniscient) [%]	Service Interruptions		Avg. Sol. Time [s]
						Unserved Energy [kWh]	Service Reliability [%]	
OMNISCIENT (lower bound)		12605		14020		0	100	6.4
DETERMINISTIC with/without Spinning Reserve	**No reserve**	12609	0.0%	12772*	-8.9%*	5000	88.5	7.6
	T^{res}= 1h	13672	8.5%	14634*	4%*	1568	96.4	6.8
	T^{res}= 2h	14291	13.4%	15624*	11%*	670	98.5	6.5
	T^{res}= 3h	15010	19.1%	16573*	18%*	53	99.5	6.3
ROBUST	**R0**	13838	9.8%	16515	18%	0	100	406
	R1	13597	7.9%	15943	14%	0	100	778
	R2	13618	8.0%	16097	15%	0	100	175
	R3	13710	8.8%	16191	16%	0	100	48

As a reference, Table 6 reports also the optimal performance computed according to a deterministic formulation with no reserve constraints in case of perfect forecast (i.e., in case the day-ahead forecast exactly matches the actual demand and PV production profiles), denoted with "Omniscient". Since in this case the day-ahead UC and ED deterministic MILP has a perfect knowledge of the future profiles and can plan the optimal solution without restrictions, its performance can be considered as a "lower bound" to benchmark the performance of the other approaches. Indeed, compared to the omniscient MILP planning, the AARO and the deterministic approaches need to resort to their respective real-time dispatch adjustment strategies to compensate forecast uncertainty. The distance of each scheduling solution from the global optimum is expressed as a percentage gap with respect to the Omniscient solution. An omniscient benchmark is defined both for the nominal (first layer) solution (associated with the forecast profiles) and for the actual dispatch solution (associated with the real profiles of demand and non-dispatchable generation).

Results show how both the introduction of reserve constraints and the adoption of the robust formulation cause an increase in the expected diesel consumption with respect to a deterministic solution without spinning reserve constraints. This difference represents the cost of adapting the nominal dispatch solution to ensure margins for real-time corrections, to compensate forecast errors. For the deterministic formulation, the expected operating cost grows rapidly with the energy reserve duration $\boldsymbol{T^{res}}$, increasing by 10% as the energy reserve is increased from 1 to 3 hours. This is mainly due to tighter limitations on storage usage, which must maintain a higher level of nominal SOC to provide its reserve contribution and allow for safe operation without active diesel generators. In turn, the increased solution conservativeness has the effect of increasing PV curtailment. On the other hand, the nominal operating cost associated with the most efficient robust formulation (**R1**) is about 10% less than the most conservative deterministic model. The robust formulation is therefore significantly more cost-effective in identifying an efficient yet conservative nominal dispatch.

The introduction of the proposed uncertainty set characterization (**R1**) leads to an overall recursive fuel consumption reduction of about 3.5% with respect to the standard budget uncertainty set (**R0**), while almost doubling the average computation time. The increase in problem complexity is mainly due to the introduction of ramp constraints on $\boldsymbol{\delta}$ components (Eq.(109)), which introduce a strong coupling between different time instants. Aggregating the demand and PV uncertainty factors (formulation **R2)** has a dramatic effect on computation time, allowing to identify the optimal solution more than four times faster than formulation **R1.** This is due to the significantly lower number of dual variables in the tractable robust counterpart (from about 96000 to 47000). On the other hand, aggregating the uncertain factors reduces the degrees of freedom of the decision rules, slightly worsening performances: **R2** attains an actual (real-time operation) diesel consumption which is about 1% higher than **R1**. Finally, the combination of uncertainty aggregation and partial-past recourse (formulation **R3**) further reduces the number of dual problem variables (27000), leading to a reduction in computational time of an order of magnitude with respect to **R1** without significantly affecting the solution quality.

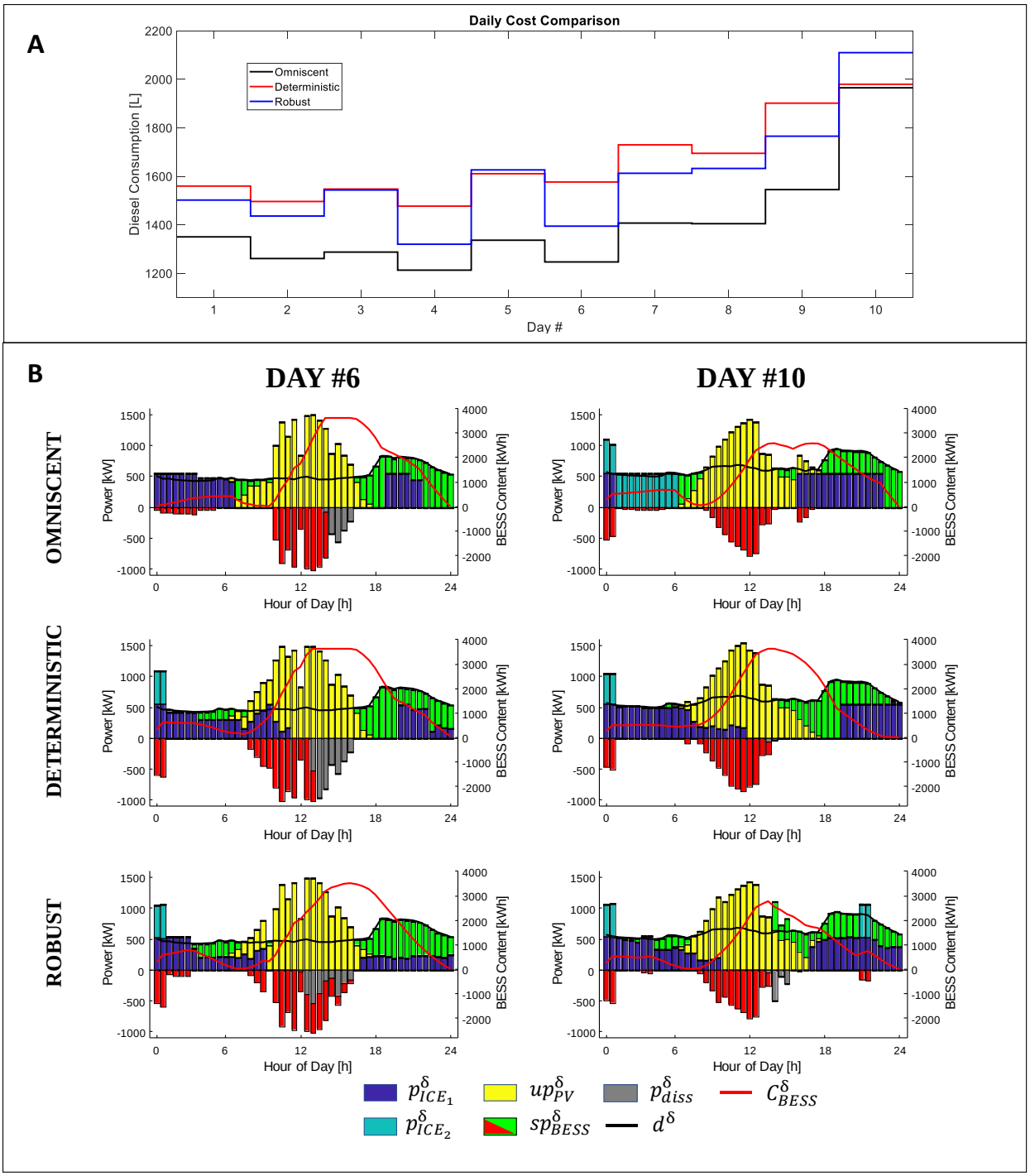

*Figure 18: comparison of actual total diesel consumption between omniscient, deterministic (Tres=3h) and robust (R1) formulations over the 10 simulation days (**A**). Omniscient simulation has perfect foresight on actual demand and PV profiles and does not account for reserve constraints. Dispatch profiles for the three models are shown for day 6 (**B**) and day 10 (**C**).*

Compared with the robust formulation, deterministic day-ahead UC shows significant limitations in terms of reliability. It is important to notice that unserved energy is also associated with an avoided energy generation, which would increase the overall diesel consumption of the deterministic formulations leading to service interruptions (marked with an asterisk in Table 6). Although adopting higher reserve margins

reduces the occurrence of service interruptions, none of the deterministic models systematically avoids unmet demand during the 10 days simulated. The most conservative model ensures 99.5% service reliability. This is a significant limitation with respect to the AARO approach, which is not only reliable for the uncertainty manifestations observed in the simulations but also for any other potential uncertainty manifestation encompassed by the uncertainty set.

Figure 18-A shows a comparison between the omniscient, the robust (**R1**) and the deterministic (T^{res}=3) formulations, in terms of daily diesel consumption, for the simulated days. Detailed dispatch profiles corresponding to the actual system operation (actual demand and PV production) are also shown in two representative days: day 6 (Figure 18-B-left), during which the robust formulation attains the largest saving with respect to the deterministic solution, and day 10 (Figure 18-B-right), when conversely the deterministic solution attains a lower cost. Inefficiencies in the decision rules reduce the advantage of the robust formulation over the deterministic formulation as the actual fuel consumption is computed. Premature and unnecessary PV curtailment (grey bars) can be observed in the robust dispatch profiles of both day 6 and day 10 due to the limitation of plain affine decision rules highlighted in Paragraph 4.5.4. In day 6 though PV curtailment is close to the minimum necessary to avoid violating the constraint on maximum storage capacity, although distributed across the BESS charging phase instead of being activated only after reaching the upper BESS SOC limit.

5.4.4 Grid-Connected CHP Systems Results

For the sake of brevity, only the best AARO formulation (i.e., **R1**) has been applied to the grid-connected MESs. Due to the low temporal resolution of the problem considered in this case study (1h), the computational time is already limited and there is no need of introducing the simplifications of versions **R2** and **R3**. As for the deterministic simulations, no reserve margins are included in the MILP since the rule-based real-time dispatch algorithm can modify the commitment decisions of quick-start units to meet thermal demand increase. In each design configuration, the robust and deterministic performances are compared with the deterministic omniscient solution (e.g. deterministic model featuring no reserve constraints and with a perfect vision on future uncertain profiles). which provides the operating cost lower bound.

Table 7 reports the results obtained in terms of daily average expected and actual operating costs, reliability and unserved energy demand for the considered design configurations of the Hospital and Campus. In all considered cases, the AARO formulation computes a higher expected operating cost (day-ahead) compared to the deterministic model. However, for all designs except design HE (where the advantage of the deterministic is minor), the robust approach leads to lower actual operating costs, thanks to the better day-ahead commitment and to the effective dispatch adjustment prescribed by the optimal decision rules. The advantage of the robust approach is considerable for the designs featuring PV panels (i.e., hospital designs HD to HG and campus designs CA and CB) because its affine decision rules can compensate electric net demand variations by adjusting not only the exchange with the national electric grid but also the load of the CHP engines. Furthermore, the robust model consistently avoids thermal outages (i.e., unmet thermal demand).

Table 7: results summary for the MES systems serving the hospital and the campus.

HOSPITAL						
Design	Simulation Mode	Expected Operating Cost [€]	Actual Operating Cost [€]	GAP [%]	Unserved Thermal Energy[kWh]	Service Reliability [%]
HA	OMNISCENT	68586			0	100%
	DETERMINISTIC	68418	69048	0.7%	0	100%
	ROBUST	68607	68943	0.5%	0	100%
HB	OMNISCENT	59682			0	100%
	DETERMINISTIC	59157	61383	2.9%	0	100%
	ROBUST	59745	60879	2.0%	0	100%
HC	OMNISCENT	59262			0	100%
	DETERMINISTIC	58821	60606	2.3%	0	100%
	ROBUST	59262	60207	1.6%	0	100%
HD	OMNISCENT	54054			0	100%
	DETERMINISTIC	53634	56007	3.6%	0	100%
	ROBUST	54075	54999	1.8%	0	100%
HE	OMNISCENT	177702			0	100%
	DETERMINISTIC	176757	177849	0.1%	0	100%
	ROBUST	176778	177891	0.1%	0	100%
HF	OMNISCENT	93429			0	100%
	DETERMINISTIC	92463	96033	2.8%	0	100%
	ROBUST	92799	94542	1.2%	0	100%
HG	OMNISCENT	171381			0	100%
	DETERMINISTIC	170310	171990	0.4%	214	99.4%
	ROBUST	170478	171927	0.3%	0	100%
CAMPUS						
Design	Simulation Mode	Expected Operating Cost [€]	Actual Operating Cost [€]	GAP [%]	Unserved Thermal Energy[kWh]	Service Reliability [%]
CA	OMNISCENT	20160			0	100%
	DETERMINISTIC	17205	21855	8.4%	0	100%
	ROBUST	17490	20955	4.0%	0	100%
CB	OMNISCENT	33210			0	100%
	DETERMINISTIC	30285	33345*	0.4%*	1970	94.6%
	ROBUST	31755	34695	4.5%	0	100%
CC	OMNISCENT	32925			0	100%
	DETERMINISTIC	31485	34740	5.5%	0	100%
	ROBUST	31710	33525	1.8%	0	100%

Instead, the deterministic formulation incurs in outages in the case of Design HG of the Hospital case study and design CB of the Campus case study. These two are the most critical design configurations due to the

presence of a CHP ORC featuring tight ramp constraints in design HG, and due to the undersized generation capacity in design CB. In these cases, a robust management of the thermal storage is essential to meet the unforeseen peak in thermal demand. In addition to ensuring operation feasibility without service interruptions, the robust approach also achieves economic advantages as high as 1.8% compared to the deterministic approach in the designs considered for the Hospital case study. This advantage further increases up to 4.1% in the Campus case study, where forecast profiles are more subject to uncertainty and the considered designs feature undersized generation capacity combined with large thermal storage systems (to meet the peak demand), as well as units with slow dynamics (slow ramp rates, long minimum up-times, and no quick-start units).

To meet demand and production perturbations from forecasts, the deterministic approach often relies on the real-time control algorithm to change the commitment status of quick-start units (i.e., boilers and heat pumps). This is shown in Figure 19, reporting the expected (day-ahead) and actual (real-time) production profiles during one of the simulated days in the case of Hospital design HC. In each timestep, two sets of stacked bars (representing the energy production/consumption of each unit) are shown: the left stacks indicate the expected (day-ahead) solution while the right stacks denote the actual (real-time) dispatch. Frequent on/off cause not only a reduction of the units' lifetime but also an increase in pollutant emissions (in case of the combustion-based units). In comparison, the AARO formulation (which cannot implement real-time commitment adjustments) identifies a day-ahead UC which is adequate to meet any demand and RES production forecast error. The actual dispatch profiles identified by the three solution approaches (Omniscient, Deterministic and Robust) are also shown for the same case study in Figure 20-B, while Figure 20-A shows a comparative summary of the daily operating cost for each approach in the simulated days.

Finally, Figure 21 shows the actual dispatch profiles associated with the three problem formulations for two Campus design configurations. In the case of Design CA, relevant differences in the commitment decisions can be observed between the deterministic and the robust solutions, both in the day-ahead and real-time operation. Since the forecast of thermal demand underestimates the actual profile, several adjustments in the commitment decisions are made by the real-time correction algorithm. On the other hand, the commitment solution found by the robust model already accounts for the potential increase in thermal demand, planning more accurately the discharge profile of the thermal storage. Thanks to this "robust" planning, the robust solution leads to a daily operating cost 7% lower than the deterministic solution. The difference shown for Design CB is even more relevant since, in this design configuration, the thermal generation capacity is undersized with respect to the peak thermal demand. Therefore, the correct management of the storage unit is essential to avoid unmet thermal demand (black bars in Figure 21).

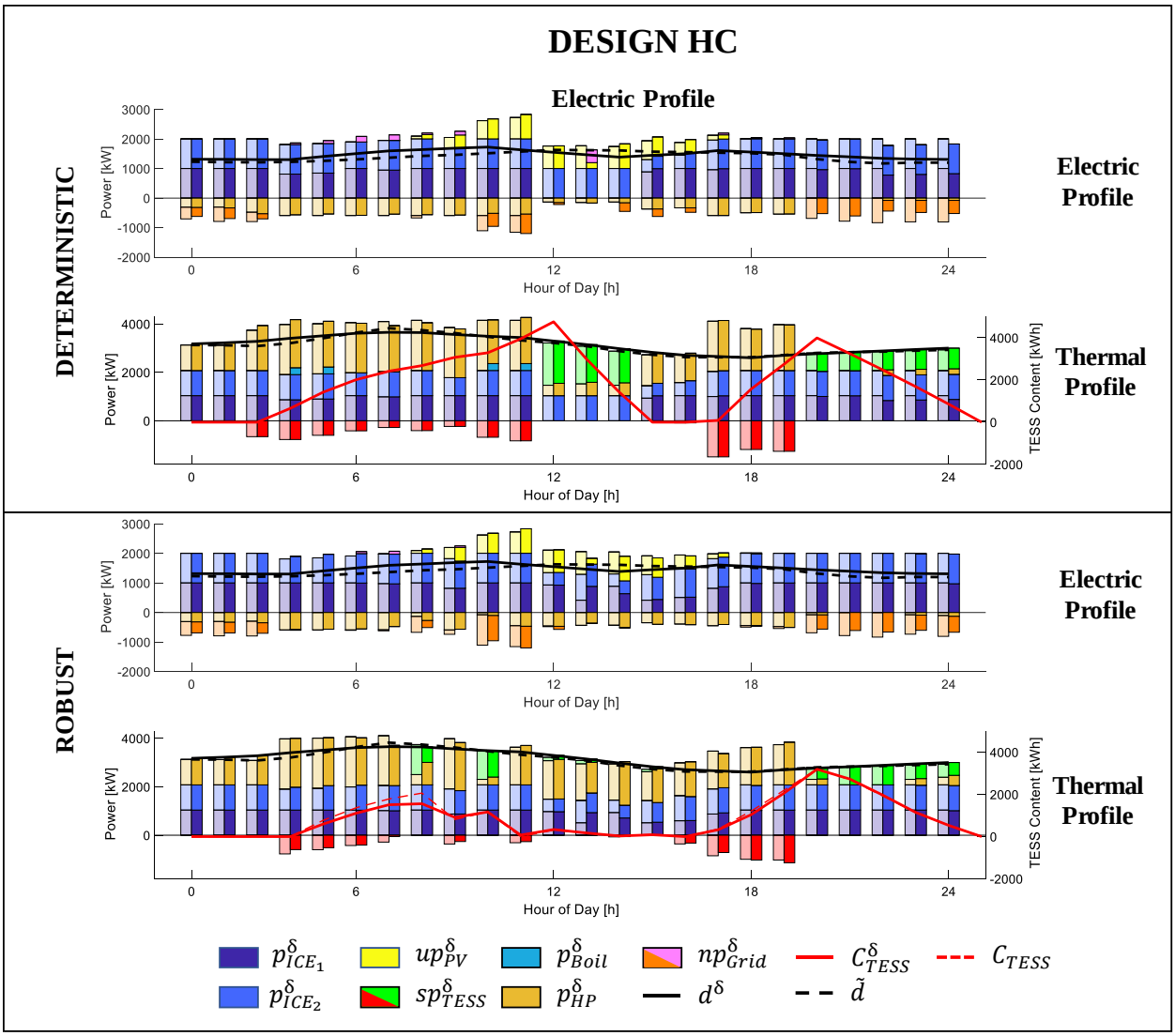

Figure 19: comparison of nominal (left stacks) and actual (right stacks) dispatch profiles, for one simulated day of operation of Hospital design HC.

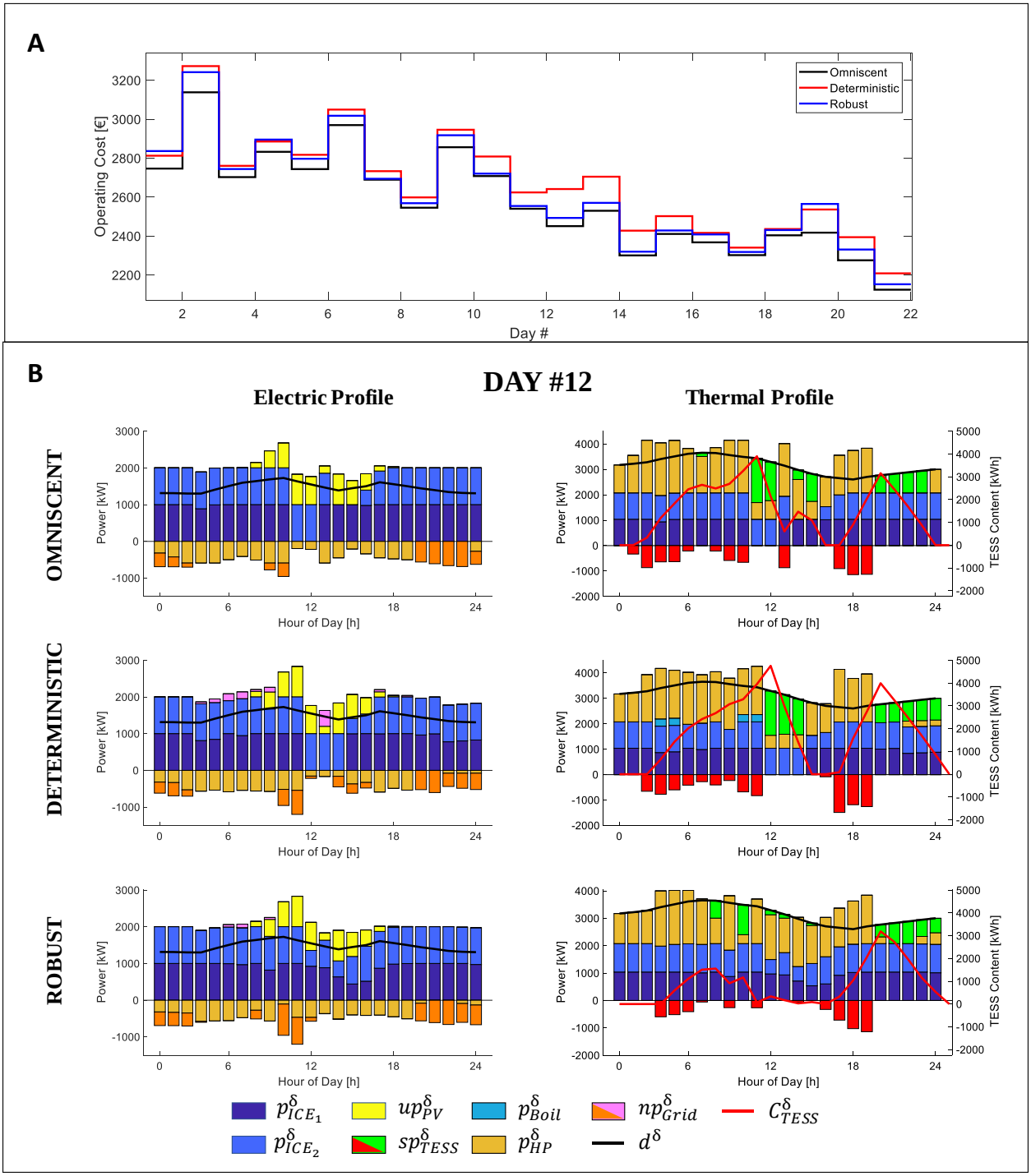

Figure 20: operating cost comparison throughout all simulation days between omniscient, deterministic and robust approaches (top), for case study HC. The detail of the dispatch solution is shown below for day 12, in which the robust model attains the maximum advantage over the deterministic formulation.

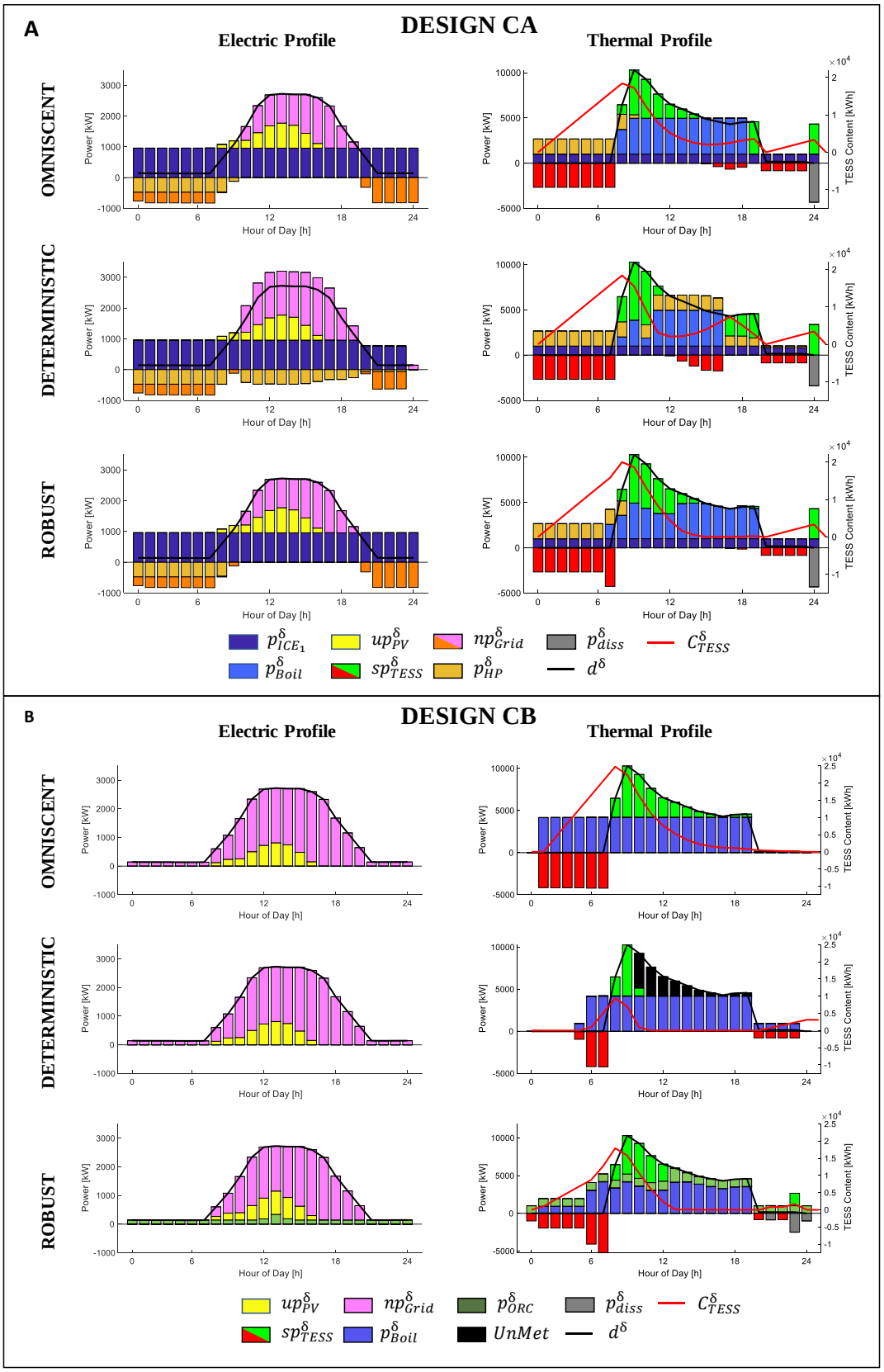

Figure 21: real-time electric and thermal dispatch profiles of Omniscient, Deterministic and Robust formulations for Campus Designs A (top) and B (bottom).

5.5 MILP-based Second Layer EMS

The second layer algorithms proposed in the previous Paragraphs have the merit of being readily implementable in a real-life EMS, as they allow to rapidly take adjustment decisions only based on the observed values of demand and non-dispatchable production and on the reference solution of the predictive first-layer problem. The complex calculations involved in the solution of a MILP cannot be performed on a Programmable Logic Controller (PLC), which is the control unit overseeing the operation of a microgrid. They must, therefore, be carried out on an external platform (typically an industrial computer), which in turn communicates with the PLC. The second layer algorithms depicted in the previous Paragraph have therefore the merit of being completely detached from the platform on which the first layer MILP is solved, and the real-time system management can be fully and independently overseen by the system PLC without a critical reliance on the communication with the first layer platform, avoiding any potential problem arising from communication delays or glitches in the MILP solution process. This represents a control architecture which is commonly adopted nowadays in applications overseen by our industrial partners. Similarly, the management architecture featuring a direct implementation of the decision rules yield by the adjustable robust formulation of the scheduling problem could in principle be implemented on a PLC. Nevertheless, relying on the heuristic second layer subordinates the overall actual system performance to the effectiveness of the considered second layer logic, affecting the comparison between the proposed first layer formulation approaches. Furthermore, as explained in Paragraph 4.5, the recourse policies yield by the robust formulation are prone to inefficiencies and their direct use for real-time management penalizes the performance of the robust approach.

A new comparison based on a uniform and sounder real-time dispatch strategy is therefore presented in this Paragraph. As seen in the case of the second layer algorithms developed in the previous Paragraph, second-layer control logics are often based on tracking the reference evolution of the system yield by the first layer predictive solution. This proves to be an effective strategy as long as the forecasts considered in the first layer are accurate, at least in terms of overall energy demand/production: if so, the strategic management determined by the first layer solution continues to be valid also in the presence of fluctuant deviations of demand and non-dispatchable generation from forecast. Based on this consideration, we introduce in this Paragraph a MILP-based second layer algorithm, which in each timestep solves a deterministic UC and ED problem on the remaining fraction of the day inheriting some of the decisions taken by the first layer. This solution approach is commonly referred to as *Shrinking Horizon* (SH) approach: in the first problem timestep, the second layer problem can observe the actual demand and renewable generation values, while future time-steps are still associated to the forecast profiles considered by the first layer (Figure 22).

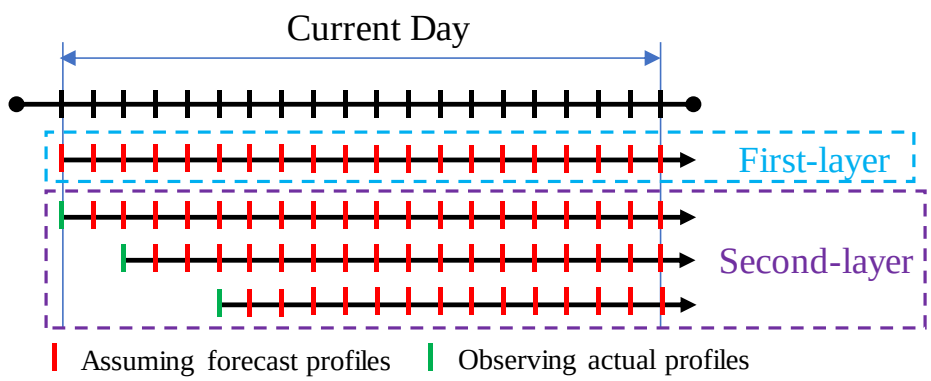

Figure 22: Shrinking Horizon second layer algorithm

The Shrinking Horizon strategy is more appealing in terms of system performance and proves useful to compare the effectiveness of the two first-layer formulations based on a coherent real-time adjustment algorithm, which can account for the peculiarities of both formulations. Nevertheless, it must be stressed that:

1) The assumption of knowing exactly the value of demand and non-dispatchable generation potential for the present timestep, although reasonable, might not be always accurate, especially for simulations with coarse temporal resolution;
2) Relying on the solution of a MILP problem for real-time management implies the necessity of more frequent interactions between the MILP solution platform and the system PLC, which in turn poses the problem of communication robustness and speed.

The simulations presented in this Paragraph and in the following therefore envision a more advanced EMS architecture, which deployment requires frequent interactions between the platform for MILP solution and the PLC for real-time management. Furthermore, particularly in the simulations of CHP systems with hourly temporal resolution, very short-term forecasting techniques might be required to accurately estimate the actual values of uncertain parameters during the following hour.

5.5.1 Second Layer MILP Formulation

A deterministic formulation is adopted for the second layer MILP solved in the SH instances, both because of computational time issues and because of the underlying idea that the solution yield by the robust formulation, which is consistently feasible for many potential different scenarios, should not be frequently updated. First and second layer must exchange information, to ensure that the solution conservativeness identified by the first layer is preserved by the second layer decisions, which might otherwise introduce excessive modifications in the dispatch profiles with respect to what originally planned by the first layer. To this end, two types of constraints are added in the second layer problem, according to whether the first layer formulation is deterministic or robust (Figure 23):

- For simulations adopting the deterministic formulation in the first layers featuring reserve constraints, coherent reserve constraints accounting for the same energy reserve duration T^{res} are enforced in the second layer problem;

- For simulations adopting the robust formulation in the first layers, the recursive storage capacity $C_{s,j}^{\delta,FL}$ identified by the optimal first layer correction policies and associated with the first timestep of the current second layer solution instance is computed, based on the history of observed forecast errors: $C_{s,j}^{\delta,FL}$ sets a conservative lower bound for the first timestep capacity evolution determined by the deterministic second layer, which does not feature reserve constraints.

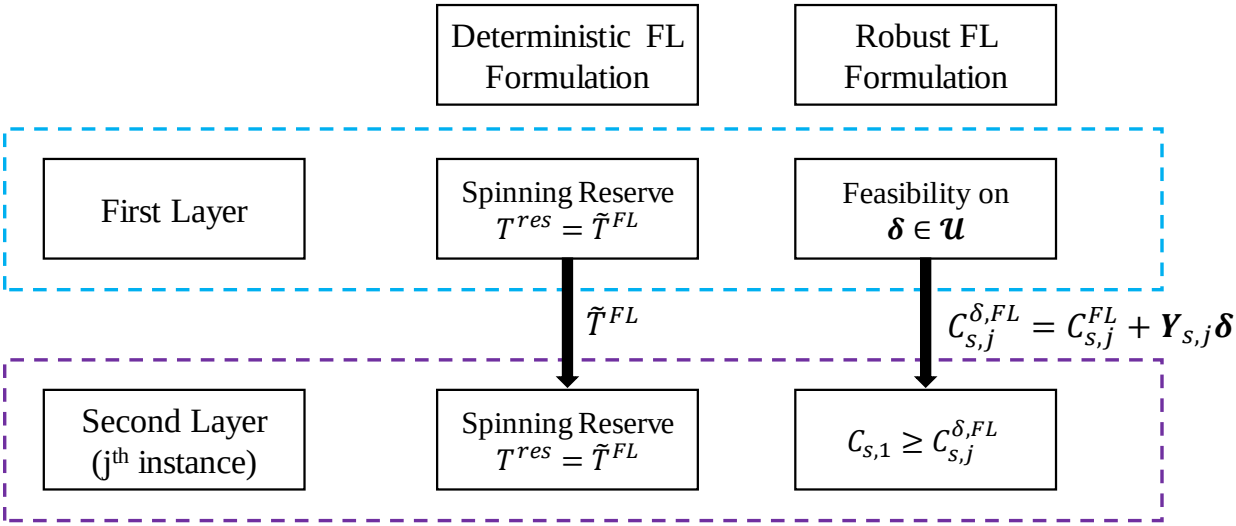

Figure 23: approach to uncertainty of first and second EMS layer in the deterministic and robust work-frame. When the first layer features the deterministic problem formulation, accounting for spinning reserve constraints with $T^{res} = \tilde{T}^{FL}$, coherent reserve constraints are enforced in each jth solution instance of the second layer deterministic problem. When the first layer features the robust formulation, the optimal first layer storage recourse policy is applied to the observed forecast errors, to determine a robust lower bound for the first timestep of the deterministic second layer j^{th} solution instance.

While it is apparent how adopting the same reserve constraint of the deterministic first layer in the second layer ensures that a coherent conservativeness is enforced by the two solution stages, it is worth explaining the strategy adopted for the robust simulations. The main inefficiencies in the recursive policies are related to unnecessary dissipation of renewable generation potential and to the ineffective adjustment of setpoints due to the rigid decision rules structure. Both inefficiencies lead to a recursive storage state of charge trajectory which is more conservative than required. On the other hand, following the recourse policies is associated with a guarantee of feasibility, as long as the manifestation of uncertainty is encompassed by the uncertainty set $\boldsymbol{\mathcal{U}}$. Therefore, by introducing a lower bound on storage capacity that is consistent with the robust decision rules, the second layer can avoid the inefficient decisions taken in the recourse of the first layer while ensuring that storage capacity is enough to provide the reserve contribution accounted by the robust dispatch solution.

To effectively enforce in the second layer same exact conservativeness of the robust first layer solution, the management trajectory defined by recursive laws should be preserved for all dynamic units, including slow ramping generators. On the other hand, in the test cases presented in the previous paragraphs the main components playing a fundamental effect in ensuring service reliability are storage systems. Furthermore, bounding the storage trajectory already affects the management of all other units, pushing the second layer

towards a solution which tends to be coherent with the first layer decisions. Therefore, we limit the constraints transfer between the two layers to the lower bound on storage capacity evolution, while allowing a more efficient redistribution of all units' load (optimized by the second layer MILP) with respect to what prescribed by the recourse laws. If ramping constraints of non-flexible units prove to be an issue in ensuring service continuity, the recursive management of non-flexible units could be enforced in the second layer according to the same approach proposed for storage systems.

Adopting the deterministic second layer allows to properly account for all simplifications which might have been introduced in the first layer. This is the case for storage charge/discharge efficiency. Including its effect in the robust formulation introduces the overestimate of recursive energy losses detailed in Paragraph 4.5.1, which would hinder the economic effectiveness of storage usage in the recourse. On the other hand, the storage has typically a fundamental role in balancing renewables fluctuations, while the additional costs connected to its inaccurate modeling would push towards recursive solutions that are less effective in the real world. The solution adopted is, therefore, to include storage efficiency only in the nominal energy balance, where its effect is accurately quantified, and to assume unitary charge/discharge efficiency in the recourse. By doing so, the actual trajectory of the storage according to the recourse laws might tend to "drift" towards lower state of charges, as the additional losses not accounted in the recursive energy balance of the robust formulation manifest in the physical system. This is normally not an issue, for two reasons:

1) The entity of the "drift" is proportional to the integral of storage setpoint difference introduced by the recourse; therefore, for time instants that are not far from the solution horizon starting time and for limited differences in the exchange profile variation, the drift will be moderate;
2) Recourse laws tend to underestimate the recursive trajectory of the battery (see Paragraph 4.5.1): the unaccounted energy losses are therefore partially balanced by the reduction in recourse inefficiencies that follows the introduction of formal set-point optimization in the second stage.

Another feature introduced in the second-layer MILP is a weight on time-dependent cost indexes, reducing in time. The weight has the effect of giving a preferential importance in the optimization to the time-steps which are closer to the current solution time, and in particular to the first time-step, which constitutes the only certain cost index of the problem since it is associated to the current uncertainty manifestation: time-dependent cost indexes are therefore associated with a linearly decreasing coefficient, equal to 1 for cost indexes occurring in the first timestep and reducing to 0.8 for cost indexes relative to the last timestep.

To limit the impact of daily storage charge variations on the overall solution, the simulations of presented in this Paragraph assume continuity of the simulation time span, enforcing a continuous actual storage charge trajectory across the simulation of consecutive days by imposing the final actual storage charge of one day as the initial condition for the following. Similarly, all relevant information related to the dynamic constraints for dispatchable units (commitment status, ramp constraints, minimum up/downtime) is transferred from one day to the following. The total simulation timespan is therefore treated as a unique consecutive period. A final storage charge target is enforced both in the first- and second-layer problems, substituting the cyclic condition assumed for the simulations in the previous Paragraph. While the first layer can

generally meet the final capacity constraint, the second layer problem might be forced to deviate from it, either because of insufficient generation resources with respect to the actual demand profile or because of excess production availability that, instead of being dissipated, are stored to be used in the following day in virtue of the final storage charge valorization (Eq.(33)). Therefore, the final capacity constraint is expressed as a soft equality constraint, introducing a penalty cost for negative deviations of the final storage charge with respect to the target:

$$C_{s,T} \geq \tilde{C}_{s,end} - C_s^{dev}$$
$$C_s^{dev} \geq 0 \tag{122}$$

$$c_s^{Cdev} = C_s^{dev} c_s^{\Delta C^{end}} \tag{123}$$

Positive deviations (e.g. a final storage charge higher than what prescribed) are not penalized, since they are already avoided unless they are required to avoid unnecessary dissipation of energy excess production (due for example to a unit minimum load constraints, to the operating strategy decided for poly-generation units, or to ramp-down constraints of slow units).

5.5.2 Robust and Deterministic Model Adaptations for Quick-Start Units

As already mentioned, two operating modes are explored for the MILP-based second layer algorithms:

1) *Fixed Unit Commitment*: in this operating mode, the commitment of the units can only be set in the first stage; in the case of day-ahead commitment optimization, this is equivalent to setting an operation schedule for the machines at the beginning of the day. In many real-life large-size CHP microgrids, where units are started-up manually by operators, univocally setting a non-modifiable sequence of commitment changes is an actual requirement;
2) *Modifiable Unit Commitment*: in this operating mode, it is possible to change at any moment the commitment status of quick-start units, either in the first or second EMS layer; units are still subject to all constraints involving their binary variable value and evolution (e.g. minimum up/downtimes, start-up consumption penalties, start-up ramp up limits, etc.).

In the definition of the second layer problem, machines are therefore divided into two groups: *quick-start* units, which commitment status is not bounded by the decisions taken by the first layer routine, and *non-flexible* units, for which due to complex or long start-up / shut down procedures, or due to the impossibility of automatically control their commitment status from the PLC, the status binary variable is forced through appropriate constraints to the same profile identified in the first layer. Table 8 specifies the assumption made for each dispatchable generation technology.

Table 8: units division in Non-Flexible (NF) class and Quick-Start (QS) class

Unit	Natural gas CHP ICE	Natural gas Boiler	Heat Pump	ORC CHP unit	Biomass Boiler	Diesel ICE
Class	NF	QS	QS	NF	NF	QS

The second layer can, in any case, modify the load of all units, within the limits of their technical characteristics and accounting for the past evolution of their dynamic constraints up to the current timestep (continuity in load ramps, minimum up/downtimes with respect to the last start-up/shut-down, etc.).

When considering the modifiable unit commitment operating mode, some changes must be introduced in the deterministic and robust formulations. Specifically, the deterministic reserve constraint defined by Eq.(47) must be modified to include the potential contribution of quick-start units. The machines set $\boldsymbol{\mathcal{M}}$ is therefore partitioned in set of "slow" units $\boldsymbol{\mathcal{M}}^{S}$ and set of quick-start units $\boldsymbol{\mathcal{M}}^{QS}$. Reserve contribution from slow units is still defined by Eq.(48), while reserve contribution of quick-start units is determined based on the value of their binary status variable $z_{i,t}$, modifying Eq.(48) to distinguish between the contribution to be considered when the unit is in operation and when it is off:

$$p_{i,j,t}^{res} = \min\left(\tilde{p}_{i,j}^{max}, \left(p_{i,j,t} + \widetilde{ru}_{i,j}^{lim}\right)z_{i,t} + \widetilde{in}^{max,SU}\left(1 - z_{i,t}\right)\right) \qquad \forall t \in \boldsymbol{\mathcal{T}} \qquad (124)$$

As already mentioned, the plain AARO formulation of the commitment and dispatch problem cannot account for the recursive start-up of units with minimum load and bounded up/downtimes, because of the impossibility of including binary recourse (Paragraph 4.5.3). A modification of the robust formulation is therefore proposed to indirectly consider the contribution of quick-start units, introducing for machines $i \in \boldsymbol{\mathcal{M}}^{QS}$ the additional input recourse variable $\Delta f_{i,t}^{QS,\delta}$, that can be different from zero only when the unit is off, and that can bypass the constraint on minimum load. $\Delta f_{i,t}^{QS,\delta}$ is associated to the recursive energy production $p_{i,j,t}^{QS,\delta}$:

$$0 \leq \Delta f_{i,t}^{QS,\delta} \leq \widetilde{in}^{max,SU}\left(1 - z_{i,t}^{QS}\right) \qquad \forall\, i \in \boldsymbol{\mathcal{M}}^{QS}, t \in \boldsymbol{\mathcal{T}} \qquad (125)$$

$$\Delta p_{i,j,t}^{QS,\delta} = \Delta f_{i,t}^{QS,\delta}\widetilde{m}_{i,j} \qquad \forall\, i \in \boldsymbol{\mathcal{M}}^{QS}, t \in \boldsymbol{\mathcal{T}}, j \in \boldsymbol{\mathcal{O}}_i \qquad (126)$$

The uncertain energy balance of Eq.(66) is consequently modified to include the described contribution from quick-start units:

$$\begin{aligned}\tilde{d}_{j,t}^{\delta} + \textstyle\sum_{b\in\boldsymbol{\mathcal{B}}_j} f_{b,t}^{TOT\delta} + \sum_{b\in\boldsymbol{\mathcal{B}}_j^{QS}} \Delta f_{b,t}^{QS,\delta} + p_{j,t}^{diss,\delta} = \textstyle\sum_{i\in\boldsymbol{\mathcal{M}}_j} p_{i,j,t}^{\delta} + \\ \textstyle\sum_{i\in\boldsymbol{\mathcal{M}}_j^{QS}} \Delta p_{i,j,t}^{QS,\delta} + \sum_{l\in\boldsymbol{\mathcal{ND}}_j} \widetilde{up}_{l,t}^{\delta} + \sum_{s\in\boldsymbol{\mathcal{S}}_j} sp_{s,t}^{\delta} + \sum_{n\in\boldsymbol{\mathcal{N}}_j} np_{n,t}^{\delta}\end{aligned} \qquad \forall\, j \in \boldsymbol{\mathcal{D}}, t \in \boldsymbol{\mathcal{T}} \qquad (127)$$

The relation between quick-start production $\Delta p_{i,j,t}^{QS,\delta}$ and quick-start consumption $\Delta f_{i,t}^{QS,\delta}$ only accounts for the slope of the machine linear part-load curve, since it must be associated with a null machine production when the machine is not recursively activated. The accounted machine efficiency is therefore different from the load-dependent production efficiency that is associated with a linear part-load curve with intercept $\tilde{q}_{i,j}$ different from zero. Specifically, if $\tilde{q}_{i,j}$ is negative (representing a generation efficiency decreasing with load) the recursive generation efficiency is overestimated. On the other hand, the purpose of the recursive generation term is including in the robust formulation the idea of integer recourse for quick-start units. It must be noted that $\Delta f_{i,t}^{QS,\delta}$ can only be positive (additional cost), since the nominal fuel consumption associated with machines in hot standby is necessarily zero. The economic effect of the start-up penalty associated with each unit is paid in all time-steps where the unit is potentially expected to operate, representing a "stand-by" cost (Eq.(128)). The optimality of the solution will, therefore, push towards scheduling plans that use quick-start units as little as possible, minimizing the accounting of potential changes on nominal unit commitment.

$$c^f = \left(f_{i,t}^{TOT} + \mathbb{E}[\Delta f_{i,t}^{\delta}]\widetilde{w}^{\Delta} + \mathbb{E}\left[\Delta f_{i,t}^{QS,\delta}\right] + z_{i,t}^{QS} f_{i,t}^{SU}\right) \tilde{c}_{fuel,i,t} \qquad \forall\, i \in \boldsymbol{\mathcal{M}}^{QS}, t \in \boldsymbol{\mathcal{T}}, j \in \boldsymbol{\mathcal{O}}_i \quad (128)$$

5.5.3 Off-Grid Electric Microgrid Results

Fixed Unit Commitment Mode

Table 9 shows a comparison of the overall system performance associated with different deterministic and robust formulations of the scheduling problem solved in the EMS fist layer. An omniscient deterministic simulation, with perfect vision on the actual profiles of demand and non-dispatchable generation and featuring no reserve constraints, is always considered as the operating cost lower bound. Four deterministic formulations associated with increasing level of conservativeness are compared: a purely deterministic formulation with no reserve constraints, and three formulations with reserve constraints characterized by different energy reserve durations T^{res}. Robust simulations are performed adopting formulations **R2** and **R3** **(**Table 5**)**, both featuring uncertainty factors aggregation and, in the case of **R3**, partial past decision rules with a recourse temporal depth $\overline{\tau} = 6h$. In addition to the standard version of the two models, resorting to the conservative uncertainty aggregation approach represented by Eq. (113)-(114), the alternative versions **R2*** and **R3*** are evaluated, respectively equivalent to **R2** and **R3** in terms of scheduling problem formulation but adopting the non-conservative approach for the aggregate uncertainty set characterization described by Eq. (117)-(118).

Table 9: formulations performance comparison for the off-grid microgrid test case in the Fixed Unit Commitment Mode

Simulation Mode		Expected Operating Cost [€]	Actual Operating Cost [€]	GAP [%]	Unserved Energy [kWh]	Service Reliability [%]	Solution Time [s]
OMNISCIENT		14021			0	100.0%	21
DETERMINISTIC	No Res.	12913	13264	-5.4%	5576	94.5%	21
	T^{res}= 1h	13523	14201	1.3%	3487	96.5%	22
	T^{res}= 2h	14197	15140	8.0%	2643	97.4%	22
	T^{res}= 3h	14703	15928	13.6%	752	99.3%	22
ROBUST	R2	13282	14738	5.1%	0	100.0%	5516
	R3	13327	14803	5.6%	0	100.0%	1026
	R2*	13081	14397	2.7%	0	100.0%	4297
	R3*	13143	14575	4.0%	0	100.0%	830

It is important to remark that the results in Table 9, although referred to the same profiles of load and PV production of the simulations presented in Table 6, are not exactly comparable due to (i) the simulation mode, which enforces continuity between consecutive days in the BESS energy content and commitment constraints and imposes targets for the storage energy content at the end of the day, and (ii) the accounting of BESS charge / discharge efficiency, which was not considered in the previous simulation to evaluate the theoretical performance of decision rules as opposed to a fixed heuristic strategy.

In the fixed day-ahead dispatch operating mode, the introduction of the MILP-based second layer algorithm does not solve the reliability issues observed in Paragraph 5.4 for the deterministic simulations for with

heuristic real-time corrections. As already observed, increasing energy reserve duration T^{res} contributes in decreasing service interruptions but at the same time negatively affects performances (also in virtue of the higher share of served energy). The most conservative deterministic formulation (T^{res}=3h) attains a reliability of 99.3% while leading to an overall operating cost 13.6% above the omniscient benchmark. Conversely, both robust formulations **R2** and **R3**, which now interact with the second-layer algorithm described in Paragraph 5.5.1 for real-time dispatch instead of directly adopting recursive decision rules, attain full reliability while leading to operating costs respectively 5.1% and 5.6% above the global optimum. As expected, the partial-past formulation **R3** has a slightly worse performance with respect to its full-past equivalent **R2**. Nevertheless, partial past reduces computational times by a factor of 5. The overall computational time for the robust formulations is still two orders of magnitude higher than for the deterministic formulations, indicating the dramatically higher complexity of the tractable robust counterpart reformulation with respect to the purely deterministic model. The less conservative characterization of the aggregate uncertainty set introduced in formulations **R2*** and **R3*** significantly improves performances, limiting the conservativeness of the robust scheduling solution and resulting in an actual operating cost for formulation **R2*** which is only 2.7% above the global optimum.

Figure 24 compares dispatch profiles for one day yield adopting the deterministic formulation with T^{res}=3h and with robust models **R2** and **R2***. The day is characterized by an optimistic PV generation forecast for the second part of the day. In the deterministic solution, this causes the premature depletion of the BESS energy content, which is not enough to cover the electrical load in the last hour of the day. Instead, the decision rules of the robust dispatch solution account for the potential decrease in BESS charge due to the PV forecast overestimate: the dashed blue line represents the storage charge trajectory computed by applying the decision rules identified by the EMS robust first layer for storage charge/discharge power, setting a lower bound for the second layer battery management only in the first timestep of each second layer problem. Once again, it is useful to stress that recourse non-anticipativity was not violated in instructing the second layer with the recursive robust storage trajectory, as the lower bound is provided only for the first timestep of each SH instance, which can count on all the error observations required to compute it. The unit commitment defined by the robust first layer, which anticipates an ICE starting hour in the evening with respect to the deterministic dispatch, ensures that the second layer can count on enough generation capacity to follow this SOC trajectory, compensating the deviation due to the reduced PV output and ensuring safe operation until the end of the day. The recursive capacity trajectory is only a conservative lower bound, and this allows the second layer algorithm to deviate from it in the second part of the day when the decision rules would introduce an unnecessary PV curtailment due to the reasons explained in Paragraph 4.5.4.

The difference between **R2** and **R2*** is apparent in the more conservative countermeasures that formulation **R2** implements in the evening to prevent BESS charge depletion, committing for one hour an additional ICE with respect to **R2*** potentially expecting a more significant loss in PV output. Conversely, it is interesting to notice how, due to the definition of the energy reserve constraint in the deterministic formulation, the deterministic dispatch solution tends to be conservative in dispatch when the BESS SOC is low,

postponing the switching off of the ICE with respect to the robust formulation and therefore increasing the nominal PV curtailment due to BESS saturation.

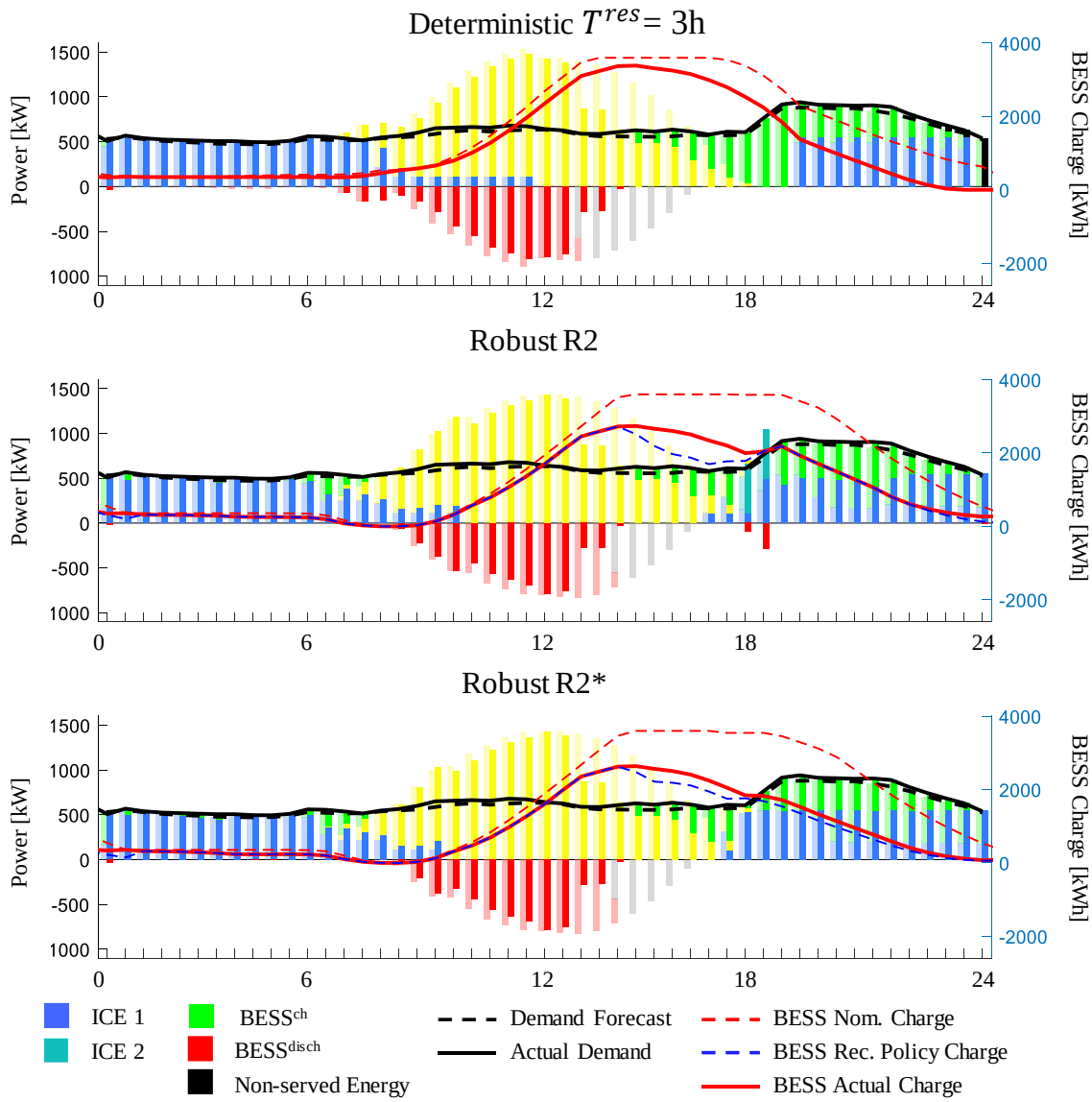

Figure 24: dispatch profiles comparison between deterministic formulation with T^{res}=3h and robust formulations R2 and R2. Bars represent energy output from indicated sources. Transparent bars define nominal dispatch, solid bars actual dispatch.*

Modifiable Unit Commitment Mode

Table 10 shows the performance comparison between the first-layer formulations in the modifiable unit commitment operating mode. In additions to the formulations described for the *Fixed Unit Commitment Mode*, adaptations **R2*^{QS}** and **R3*^{QS}** of formulations **R2*** and **R3*** are introduced, featuring the modification accounting for quick-start units presented in Paragraph 5.5.2.

Allowing the EMS second layer to modify the commitment status of the diesel generators lets the real-time dispatch algorithm, which monitors the actual storage charge evolution following the actual net demand manifestation, to correct the inadequate generation capacity allocation of the deterministic first layer, leading to 100% service reliability also when no reserve constraint is imposed in the first layer problem. Imposing a reserve constraint which accounts for the potential quick start of diesel generators does not worsen performance, since generators do not have to be conservatively committed to contribute to the reserve requirements but it appears to be effective in anticipating the need for recursive start-ups, slightly improving performances with respect to the formulation with no reserve constraints. The difference with respect to the global optimum is in any case below 1% for both deterministic formulations.

Table 10: formulations performance comparison for the off-grid microgrid test case in the Modifiable Unit Commitment Mode

Simulation Mode		Expected Operating Cost [€]	Actual Operating Cost [€]	GAP [%]	Unserved Thermal Energy [kWh]	Service Reliability [%]	Solution Time [s]
OMNISCIENT		14021			0	100.0%	20
DETERMINISTIC	No Res	12578	14151	0.9%	0	100.0%	20
	T^{res}= 1h	12578	14073	0.4%	0	100.0%	20
ROBUST	R2*	13078	14588	4.0%	0	100.0%	4257
	R3*	13116	14663	4.6%	0	100.0%	827
	R2*^{QS}	12824	14407	2.8%	0	100.0%	5598
	R3*^{QS}	12869	14534	3.7%	0	100.0%	1415

Robust formulations **R2*** and **R3***, which do not account for the potential ICEs quick-start, benefit from the increased freedom granted to the second layer dispatch algorithm, which can limit the excessive solution conservativeness improving performances. The second layer is still conditioned by the recursive storage trajectory defined by the first layer and, consequently, the overall performance of the two formulations is significantly worse than the deterministic formulations. It is important to keep in mind though that the robust scheduling solutions are always more conservative than the deterministic solutions, accounting for all potential uncertainty manifestations encompassed by the uncertainty set. In some extreme uncertainty manifestations, the deterministic scheduling might lead to service interruptions despite the capacity of recursively start-up ICEs, because of non-conservative BESS management.

The introduction of the adaptation for quick-start units featured by formulations **R2*^{QS}** and **R3*^{QS}** is effective in leading to the definition of a less conservative storage trajectory, reducing the boundaries on storage management imposed by the robust first layer to the second layer algorithm. The performance of the two formulations is, therefore, closer to the global optimum, with an overall operating cost of formulation **R2*^{QS}** which is only 2.8% worse than the omniscient benchmark. The adaptation, on the other hand, increases the computational time of both formulations with respect to their corresponding versions **R2*** and **R3***.

5.5.4 Hospital Results

The performances of the different formulations in the grid-connected Hospital test case were already observed to be quite similar in the case of day-ahead dispatch with heuristic real-time management (Paragraph 5.4.2), and relatively close to the global optimum. The introduction of a more sophisticated second-layer dispatch algorithm reduces even further the performance differences between deterministic and robust formulations, pushing all solutions towards the omniscient benchmark. Nevertheless, relevant differences in the capacity of avoiding service discontinuities are still observable in the fixed unit commitment operating mode between the two approaches to the formulation of the first layer problem.

Fixed Unit Commitment Mode

Table 11 shows the results for all Hospital design described in Section 5.1, under the assumption of fixed day-ahead unit commitment. As explained in the previous Paragraphs, the omniscient deterministic simulation (with perfect vision on the actual demand and renewable generation profiles) sets the cost lower bound. Four deterministic simulations, one without generation reserve constraints and three with increasing levels of energy reserve duration T^{res}, are performed. Robust formulation **R2** is considered for the simulations, featuring the full uncertainty set characterization presented in Chapter 4, full-past recourse and conservative uncertainty aggregation, since the size of the dataset used for the statistical uncertainty set characterization is reduced with respect to the off-grid microgrid case study. Due to the lower temporal resolution of load and renewable generation profiles, the possibility of partial-past decision rules is not explored in this test case.

For most of the designs, even without the possibility of adapting the commitment of units during the day, introducing an adequate level of reserve in the deterministic formulation is sufficient to achieve very high service reliability. It is important to keep in mind that low and isolated values of unserved thermal energy are not an issue in thermal systems since simulations do not account for the thermal inertia of buildings and heating distribution systems that smooth out the actual effect of insufficient thermal generation on the thermal energy users. For this reason, values of unmet thermal demand can be observed also in some of the simulations featuring a robust first layer, since the conservativeness of the uncertainty set was tuned according to a confidence level of 97.5% on the forecast error observations to avoid excessive solution conservativeness. Not all potential uncertainty manifestations are therefore encompassed by the uncertainty set, and the solution robustness might be compromised in extreme forecast error scenarios. Nevertheless, the entity of the service interruption is always dramatically lower when the EMS first layer features the robust formulation. This is true also for the most critical design configurations from the point of view of reliability, namely HD and HF. In both designs, it is convenient to use the large thermal storage to limit the use of heat pumps during the central hours of the day, when electricity is more expensive.

Table 11; formulations performance comparison for the Hospital test case in the Fixed Unit Commitment Mode

Design	Simulation Mode		Expected Operating Cost [€]	Actual Operating Cost [€]	GAP [%]	Unserved Thermal Energy [kWh]	Service Reliability [%]	Solution Time [s]
HA	OMNISCIENT		33605			0.00	100.0%	18
	DETERMINISTIC	No Res.	32756	33102	-1.5%	16513	98.1%	17
		T^{res}= 1h	32883	33527	-0.2%	5550	99.4%	18
		T^{res}= 2h	32967	33762	0.5%	176	100.0%	19
		T^{res}= 3h	32941	33733	0.4%	76	100.0%	19
	R2		32887	33686	0.2%	46	100.0%	3887
HB	OMNISCIENT		29791			0	100.0%	27
	DETERMINISTIC	No Res.	28814	30075	1.0%	5625	99.4%	28
		T^{res}= 1h	28856	30243	1.5%	1717	99.8%	30
		T^{res}= 2h	28898	30315	1.8%	390	100.0%	34
		T^{res}= 3h	29025	30347	1.9%	390	100.0%	30
	R2		29033	30273	1.6%	98	100.0%	5004
HC	OMNISCIENT		29302			0	100.0%	20
	DETERMINISTIC	No Res.	28458	29601	1.0%	2109	99.8%	20
		T^{res}= 1h	28502	29605	1.0%	62	100.0%	21
		T^{res}= 2h	28691	29692	1.3%	0	100.0%	23
		T^{res}= 3h	28758	29773	1.6%	0	100.0%	25
	R2		28597	29785	1.6%	0	100.0%	2111
HD	OMNISCIENT		26790			0	100.%	23
	DETERMINISTIC	No Res.	25923	26918	0.5%	16075	98.2%	20
		T^{res}= 1h	25924	26953	0.6%	8244	99.1%	20
		T^{res}= 2h	25932	27074	1.1%	6181	99.3%	21
		T^{res}= 3h	25899	27199	1.5%	4697	99.5%	21
	R2		26064	27561	2.9%	621	99.9%	9282
HE	OMNISCIENT		55141			0	100.00%	39
	DETERMINISTIC	No Res.	53609	55197	0.1%	2618	99.7%	38
		T^{res}= 1h	53642	55234	0.2%	0	100.0%	40
		T^{res}= 2h	53613	55182	0.1%	0	100.0%	37
		T^{res}= 3h	53615	55183	0.1%	0	100.0%	35
	R2		53559	55131	0.0%	0	100.0%	3157
HF	OMNISCIENT		47740			0	100.0%	29
	DETERMINISTIC	No Res.	45138	47182	-1.2%	18865	97.8%	30
		T^{res}= 1h	44890	47601	-0.3%	11721	98.7%	30
		T^{res}= 2h	44928	47776	0.1%	8058	99.1%	29
		T^{res}= 3h	44943	47854	0.2%	6626	99.2%	25
	R2		45469	48140	0.8%	249	100.0%	1099
HG	OMNISCIENT		52756			0	100.0%	20
		No Res.	51035	52927	0.3%	1469	99.8%	20

	DETER-MINIS-TIC	T^{res}= 1h	51014	52879	0.2%	0	100.0%	21
		T^{res}= 2h	51020	52879	0.2%	0	100.0%	21
		T^{res}= 3h	51021	52872	0.2%	0	100.0%	21
	R2		50860	52760	0.0%	0	100.0%	735

On the other hand, under the assumption of non-modifiable unit commitment, it is critical to correctly account for the actual capacity of the storage to cope with substantial increases in load thermal demand, otherwise without the support from committed heat pumps the storage capacity might not be enough to prevent service interruptions. The conservativeness imposed on the deterministic formulation through the adoption of increasing energy reserve durations has limited effectiveness in preventing insufficient generation capacity allocation. This is due to the fact that, since deterministic reserve constraints always account for the nominal storage trajectory, they do not properly account for persistent underestimates of the thermal demand profile, which induce severe modifications in the actual storage trajectory with respect to the reference nominal trajectory required to provide the accounted generation reserve. Conversely, the robust formulation, in virtue of the accurate tracking of storage trajectory evolution defined by the recursive decision rules, is able to optimally plan the commitment schedule of dispatchable generators to the minimum hours required to ensure sufficient support to the TESS in case of prolonged thermal load increase with respect to forecast. Figure 25 shows a comparison of the dispatch profiles of two deterministic solutions characterized by increasing energy reserve durations, and of the robust solution for one day and for design configuration HD. The nominal solution aims at minimizing the operating hours of heat pumps, that support the CHP engines in supplying the thermal load. As the energy reserve duration increases, the deterministic nominal solution identifies a nominal storage charge trajectory reaching higher values, to provide the reserve necessary to keep the heat pumps switched off during the central hours of the day. The most conservative deterministic solution (T^{res}=3h) turns on two heat pumps in the morning, aiming at a high thermal storage charge to supply the demand between 10 to 18 with no heat pumps in operation. The actual storage charge trajectory is on the other hand consistently lower than the reference trajectory, and the committed generation resources are not enough to compensate its deviation from nominal level, necessary to provide the necessary generation reserve. This results in five hours of insufficient thermal supply, from 14 to 18. Furthermore, it is important to consider that higher TESS charge levels are associated to higher energy losses due to thermal storage self-discharge, which is proportional to the storage temperature (and therefore to the storage energy content). The commitment strategy defined by the robust solution is significantly different. The recursive storage trajectory defined by the optimal decision rules (indicated by the blue dotted line) accounts for the capacity of the system to manage the deviation of the TESS charge trajectory from nominal and provides a correct reference for the actual storage charge defined by the EMS second layer. Since the overall thermal demand deviation from forecast is particularly high (extreme uncertainty manifestation), in this particular day the robust formulation fails as well in committing sufficient generation capacity, and the actual storage charge trajectory falls below the reference defined by the decision rules in the hours from 11 to 16, resulting in a brief service interruption at 15. This is on the other hand due to the relaxed definition of the uncertainty set and could be avoided by tuning the confidence in the statistical analysis leading to the definition of the uncertainty set parameters.

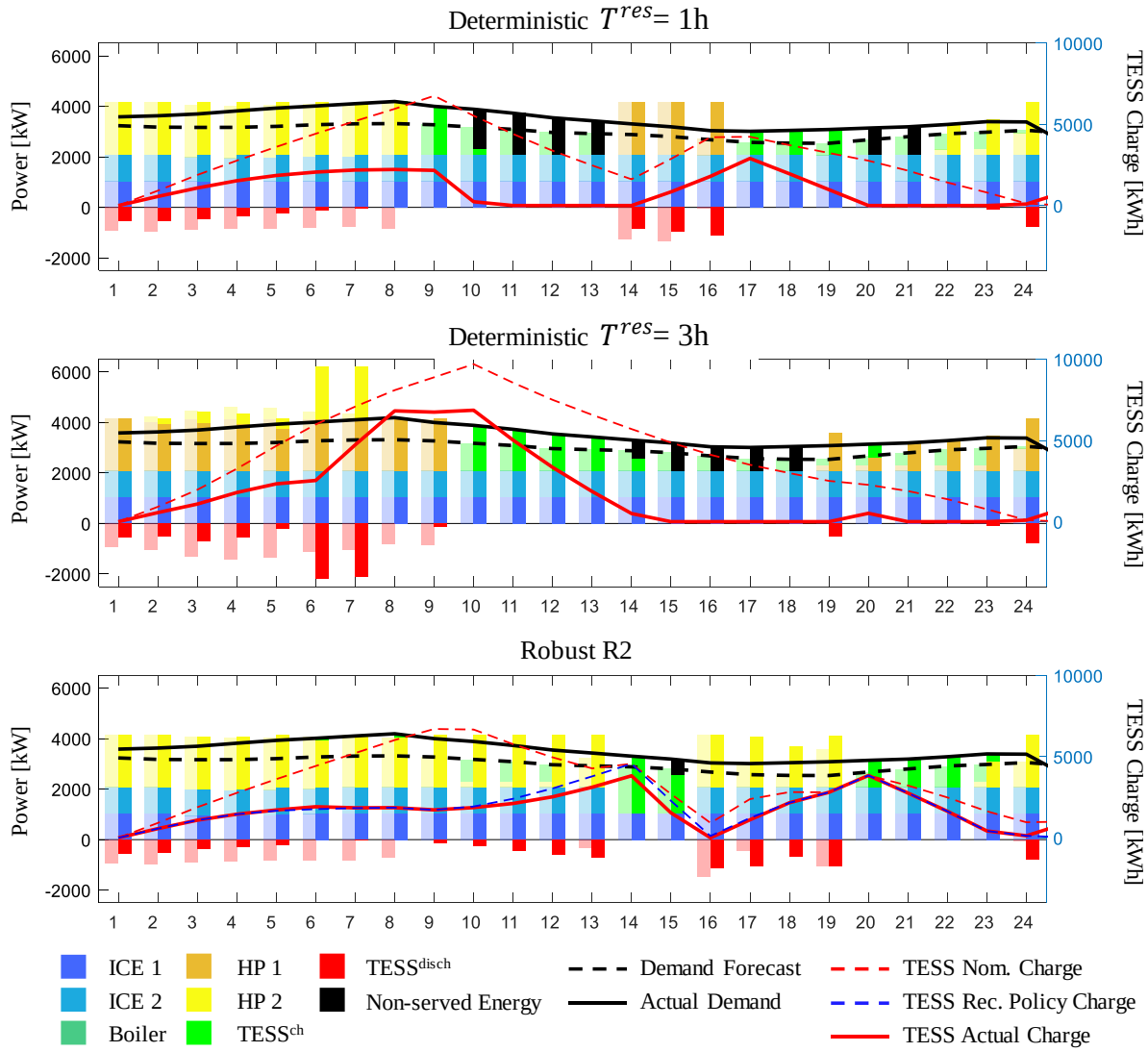

Figure 25: dispatch profiles comparison between deterministic formulation with Tres=1h, deterministic formulation with Tres=3h and robust formulation, for one day of design HD simulations

Modifiable Unit Commitment Mode

In this operating mode, robust simulations are performed both with the already described **R2** formulation and with its adaptation **R2^{QS}**, featuring the simplified accounting of quick-start units contribution proposed in Paragraph 5.5.2. If the EMS second layer is allowed to modify the commitment status of quick-start units with respect to the commitment plan defined by the first layer, full reliability is always achieved by both methods, as shown in Table 12. Erroneous commitment schedules identified by the deterministic formulation in the first layer, like the example described above, can be recursively fixed during real-time operation. Featuring a reserve constraint in the deterministic formulation results to be unnecessary, and even if it is included it does not worsen performances since it can correctly account for the reserve contribution of quick-start units also when their nominal commitment status is off, representing the actual possibility of

turning them on if needed. Design HG does not feature quick-start units and therefore is not reported in Table 12.

Table 12; formulations performance comparison for the Hospital test case in the Modifiable Unit Commitment Mode

Design	Simulation Mode		Expected Operating Cost [€]	Actual Operating Cost [€]	GAP [%]	Unserved Thermal Energy [kWh]	Service Reliability [%]	Solution Time [s]
HA	OMNISCIENT		33605			0	100.0%	89
	DETERMINISTIC	No Reserve	32673	33587	-0.1%	0	100.0%	122
		$T^{res} = 1h$	32671	33588	-0.1%	0	100.0%	85
	ROBUST	R2	32866	33656	0.2%	0	100.0%	3008
		$R2^{QS}$	32729	33662	0.2%	0	100.0%	3248
HB	OMNISCIENT		29791			0	100.0%	19
	DETERMINISTIC	No Reserve	28779	29991	0.7%	0	100.0%	19
		$T^{res} = 1h$	28759	29953	0.5%	0	100.0%	20
	ROBUST	R2	28996	30020	0.8%	0	100.0%	7025
		$R2^{QS}$	28896	30086	1.0%	0	100.0%	751
HC	OMNISCIENT		29302			0	100.0%	20
	DETERMINISTIC	No Reserve	28463	29431	0.4%	0	100.0%	20
		$T^{res} = 1h$	28464	29428	0.4%	0	100.0%	21
	ROBUST	R2	28608	29535	0.8%	0	100.0%	2444
		$R2^{QS}$	28491	29580	1.0%	0	100.0%	894
HD	OMNISCIENT		26790			0	100.0%	20
	DETERMINISTIC	No Reserve	25878	26963	0.6%	0	100.0%	19
		$T^{res} = 1h$	25891	26973	0.7%	0	100.0%	21
	ROBUST	R2	26005	27295	1.9%	0	100.0%	10024
		$R2^{QS}$	25954	27451	2.5%	0	100.0%	5104
HE	OMNISCIENT		55241			0	100.0%	23
	DETERMINISTIC	No Reserve	53587	55345	0.2%	0	100.0%	24
		$T^{res} = 1h$	53587	55346	0.2%	0	100.0%	25
	ROBUST	R2	53541	55202	-0.1%	0	100.0%	3408
		$R2^{QS}$	53506	55169	-0.1%	0	100.0%	3371
HF	OMNISCIENT		47740			0	100.0%	31
	DETERMINISTIC	No Reserve	44751	47998	0.5%	0	100.0%	30
		$T^{res} = 1h$	44753	48013	0.6%	0	100.0%	29
	ROBUST	R2	45316	48100	0.8%	0	100.0%	1222
		$R2^{QS}$	45308	48062	0.7%	0	100.0%	1192

As already seen for the off-grid microgrid case study, once commitment integer recourse is introduced both robust formulations tend to identify an optimal dispatch strategy which is slightly suboptimal compared to the deterministic formulations.

In the case of the formulation **R2** this is due to an excessive conservativeness of the first layer solution, that does not account for the potential contribution of quick-start units and imposes to the second layer a sub-optimal recursive thermal storage trajectory which limits its effectiveness. Nevertheless, the performance of formulation $\mathbf{R2^{QS}}$ is pretty much aligned with model **R2** in all considered designs, with the exception of some design configurations for which $\mathbf{R2^{QS}}$, even if slightly lowering nominal operating cost, is associated to a moderately higher actual operating cost. The effect can be considered significant (in the sense that the difference is above the convergence gap assumed in the first layer problem solution) in the case of design HD, where $\mathbf{R2^{QS}}$ increases by 0.6% with respect to **R2** the actual operating cost gap from cost benchmark. The performance difference is due to an increase in fuel consumption costs of the $\mathbf{R2^{QS}}$ solution that is not balanced by the corresponding increase in revenues associated with energy trading with the grid. Accounting for the contribution of all dispatchable generators, total thermal energy production in the two solutions is equivalent, with a minor reduction (-0.3%) of total thermal generation for $\mathbf{R2^{QS}}$ due to a decrease in thermal losses from the TESS, which is operated at a lower average state of charge. Nevertheless, the dispatch solution identified by $\mathbf{R2^{QS}}$ is characterized by more frequent changes in the reference commitment (21 changes for $\mathbf{R2^{QS}}$ versus 10 for **R2**), and by the preferential use of the natural gas boiler with respect to the heat pumps to correct the nominal energy production schedule. The first difference leads to an increase in start-up costs for $\mathbf{R2^{QS}}$ while the second, which is the major cause for the cost difference, depends on how the second layer must adapt to the recursive TESS trajectory imposed by the first layer. Ultimately, the differences are attributable to the misrepresentation of generation efficiency for quick start units described in Paragraph 5.5.2, and to the fact that, and to the inexact calculation of the stand-by cost for the heat pumps which is always valorized (in the absence of an accurate accounting of how electricity would be provided) at the purchase price from the grid, although the heat pumps are almost always supplied by electric energy produced internally either from the CHP engines or from the PV field.

5.5.5 Campus Results

As shown in Table 4, forecast profiles for the Campus case study are characterized by a significantly lower accuracy. Consequently, the effect of uncertainty on the definition of the scheduling plan is more significant than for the Hospital test case.

Fixed Unit Commitment Mode

Table 13 shows the results for the fixed day-ahead unit commitment operating mode, for each of the three Campus designs considered. Approaching the optimal dispatch problem without accounting for the recursive start-up of quick-start units results extremely challenging when adopting the deterministic dispatch problem formulation. Due to forecast uncertainty, it is necessary to impose very high energy reserve duration in the deterministic formulations to reach sufficiently high levels of service reliability. In any case, 100% service reliability is never attained by the deterministic formulations.

Table 13: formulations performance comparison for the Campus test case in the Fixed Unit Commitment Mode

Design	Simulation Mode		Expected Operating Cost [€]	Actual Operating Cost [€]	GAP [%]	Unserved Thermal Energy [kWh]	Service Reliability [%]	Solution Time [s]
CA	OMNISCIENT		22062			0	100.0%	30
	DET	No Res	18821	21569	-2.2%	35356	89.4%	41
		$T^{res} = 2h$	18972	22133	0.3%	24610	92.6%	46
		$T^{res} = 4h$	20132	23142	4.9%	20528	93.8%	40
		$T^{res} = 6h$	20097	23585	6.9%	5752	98.3%	39
	ROBUST		19902	23085	4.6%	0	100.0%	1194
CB	OMNISCIENT		34899			0	100.0%	27
	DET	No Res	31623	33785	-3.2%	46496	86.0%	35
		$T^{res} = 2h$	31737	34950	0.1%	6524	98.0%	34
		$T^{res} = 4h$	32430	35449	1.6%	6989	97.9%	33
		$T^{res} = 6h$	32441	35462	1.6%	7347	97.8%	30
	ROBUST		32515	35740	2.4%	0	100.0%	629
CC	OMNISCIENT		38777			0	100.0%	36
	DET	No Res	37841	38415	-0.9%	17900	94.6%	36
		$T^{res} = 2h$	37975	38947	0.4%	1094	99.7%	35
		$T^{res} = 4h$	38234	39199	1.1%	1094	99.7%	31
		$T^{res} = 6h$	38307	39283	1.3%	807	99.8%	34
	ROBUST		37448	38833	0.1%	0	100.0%	891

An example of dispatch profiles is given in Figure 26, for Campus design CB. The day shown falls during mid-season, and therefore does not pose challenges in terms of covering thermal demand peaks. On the other hand, the day is characterized by a large underestimate of daily thermal demand in the forecast. As conservativeness is increased in the deterministic formulation, the response of the deterministic approach is to increase the storage charge to its maximum in the morning, expecting it to be enough to supply the thermal load for the whole day. This minimizes the boiler operating hours, operating it at a higher load an increasing generation efficiency. Eventually, thermal storage charge is completely depleted due to the demand underestimate, and a large fraction of thermal demand is not supplied. In the presented example, increasing energy demand reserve was not effective at all in reducing the entity of non-served thermal energy, which slightly increases due to the higher thermal losses deriving from the high TESS state of charge. The solution identified by the robust formulation establishes that the most effective way of ensuring service continuity is increasing the boiler operating hours, adopting a thermal load following strategy and using the TESS to switch off the boiler only when safe to do so.

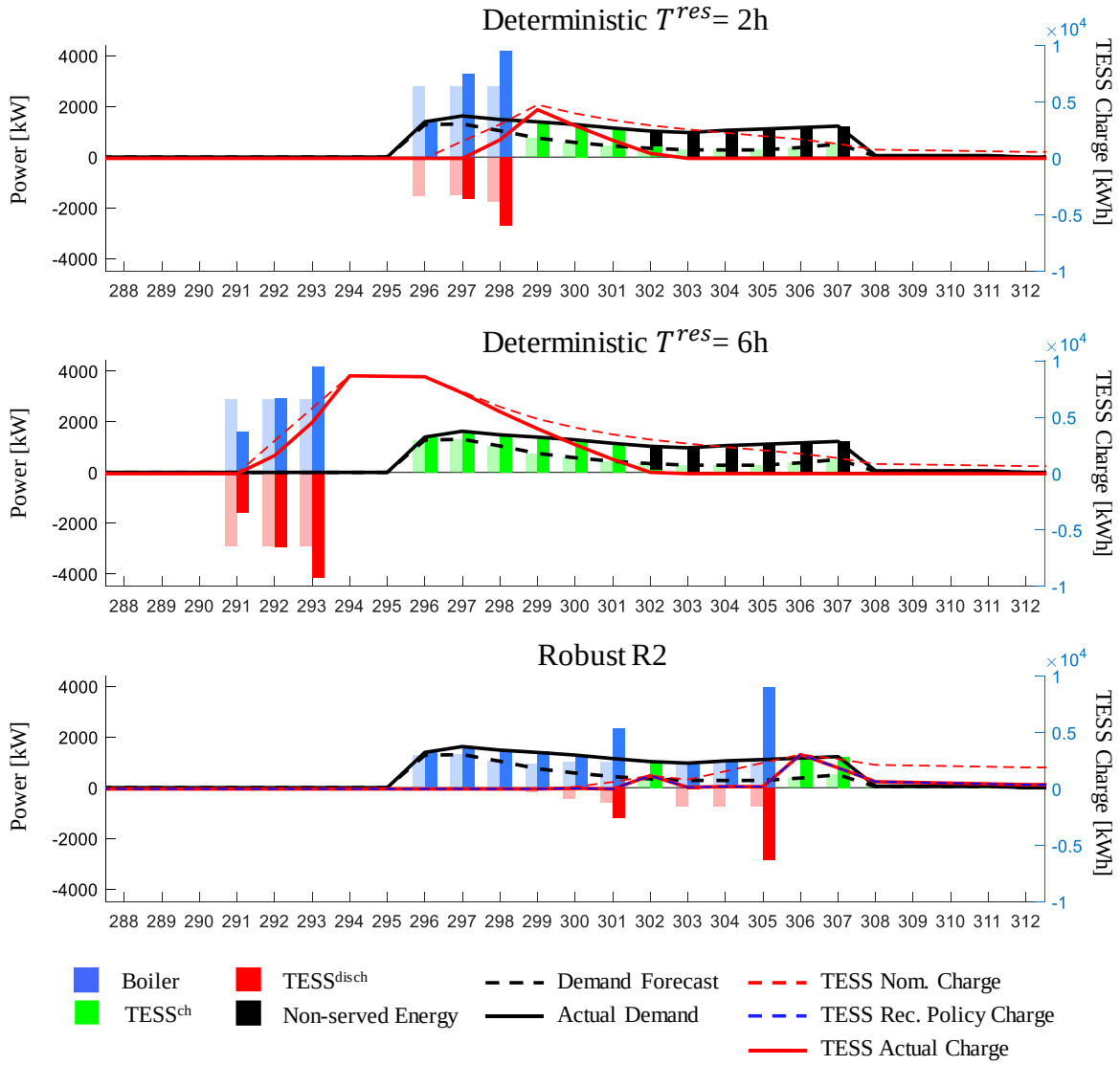

Figure 26: dispatch comparison for a mid-season day of Campus case study, in the case of design CB

Modifiable Unit Commitment Mode

The introduction of real-time adjustments in the commitment status of quick-start units effectively solves the reliability problems affecting the deterministic formulation. A low energy reserve duration (2 hours) is enough to reach 100% service reliability in all three designs. Despite the availability of integer recourse, reserve constraints are in any case necessary to avoid the service interruptions for design CB, which were observed also in the simulations adopting the heuristic corrective layer.

Table 14: formulations performance comparison for the Campus test case in the Modifiable Unit Commitment Mode

Design	Simulation Mode		Expected Operating Cost [€]	Actual Operating Cost [€]	GAP [%]	Unserved Thermal Energy [kWh]	Service Reliability [%]	Solution Time [s]
CA	OMNISCIENT		22062				100.0%	30
	DET	No Res	18814	22593	2.4%	0	100.0%	37
		Eres 2	18812	22585	2.4%	0	100.0%	39
	ROBUST	No QS	19877	23264	5.5%	0	100.0%	1093
		QS	19724	23181	5.1%	0	100.0%	839
CB	OMNISCIENT		34899				100.0%	27
	DET	No Res	31592	35293	1.1%	847		37
		Eres 2	31578	35327	1.2%	0	100.0%	34
	ROBUST	No QS	32478	35689	2.3%	0	100.0%	656
		QS	32133	35684	2.2%	0	100.0%	629
CC	OMNISCIENT		38777			0	100.0%	36
	DET	No Res	38069	39249	1.2%	0	100.0%	29
		Eres 2	38067	39257	1.2%	0	100.0%	32
	ROBUST	No QS	37448	38833	0.1%	0	100.0%	945
		QS	37448	38833	0.1%	0	100.0%	43254

In designs CA and CB, the robust formulations (with and without the modification accounting for quick-start units) leads to a worse performance with respect to the deterministic formulation, with no differences in service reliability. The gap between the two is higher for design CA, which is characterized by a less restrictive total thermal generation capacity with respect to load peaks and by smaller storage size.

5.6 Conclusions

In this Chapter, the adoption of the two MILP formulations of the optimal scheduling problem proposed in Chapter 3 and Chapter 4 is assessed for systems operating according to a two layers EMS based on a day-ahead nominal scheduling definition. Three test cases are characterized, encompassing off-grid and grid-connected systems with different levels of forecast accuracy.

Firstly, a comparison between the formulations is based on one hand on the direct adoption in the EMS second layer of the optimal decision rules identified by the robust first layer, and on the other on the definition of rule-based algorithms to correct the deterministic nominal dispatch acting, when possible, also on the commitment status of quick-start units. According to this EMS architecture, the performance comparison between the two formulations for the off-grid microgrid case study indicates that the robust formulation, mainly in virtue of the better commitment decisions that allow to limit renewables curtailment, attain both a better nominal and recursive performance with respect to the conservative deterministic formulations considered. Furthermore, despite the introduction of reserve constraints, none of the deterministic formulations manages to consistently avoid service interruptions, while all robust formulations considered are associated with 100% service reliability. For the CHP case studies, reliability is less of an issue for the

deterministic formulations, due to the possibility introduced in the second layer management algorithm of modifying the commitment of quick-start units, as it is normally done in real systems. Nevertheless, compared to a priority-based thermal-follow strategy, recursive laws identified by the robust formulation, which allow to identify a synchronized response to fluctuations of thermal and electric net demands and to modify the nominal thermal storage trajectory, lead to an overall result which is often slightly better than the deterministic formulation.

Secondly, a comparison based on more advanced second layer dispatch strategies was presented. A *Shrinking Horizon* algorithm incorporating directives to ensure service reliability from the first layer was presented, under two different operating modes: *Fixed Unit Commitment Mode*, in which the second layer algorithm cannot modify the commitment schedule defined by the first layer, and *Modifiable Unit Commitment Mode*, in which the second layer algorithm can adjust the commitment status of quick-start units. In the fixed unit commitment operating mode, the same reliability issues observed for the microgrid case study when adopting a rule-based second layer are confirmed, indicating that if the status of generators has to be univocally set at the beginning of the day the robust formulation can ensure full reliability at a cost close to global optimum. If on the other hand modifications to the day-ahead commitment are allowed, the second layer can effectively adapt the deterministic solution to reach globally optimal performance, while it is penalized by the imposition of recursive storage trajectory boundary associated to the robust first layer solution. In the Hospital test cases, in the *Fixed Unit Commitment* operating mode the two formulations perform quite similarly in most design configurations, with the exception of a few critical designs where the introduction of reserve constraints in the deterministic formulation is ineffective in reaching 100% service reliability. Conversely, in the *Modifiable Unit Commitment* operating mode reliability issues are solved in all designs, and the performance granted by deterministic EMS first layer is on average better than for the case of robust formulation, although in both cases costs are very close to global optimum (often less than 1% gap). In the Campus case study, which is characterized by lower forecast accuracy, in the *Fixed Unit Commitment* operating mode the deterministic formulation is never able to ensure full reliability despite the introduction of very high energy reserve durations in the reserve constraints, while the robust formulation is associated to full reliability and lower costs. Once again, as *Integer Recourse* is accounted reliability issues are solved, and the deterministic formulation attains a better performance than the robust formulation.

In conclusion, from the extensive numerical simulation campaign conducted, it is apparent how the robust formulation is indeed the optimal choice when dealing day-ahead scheduling optimization in systems that cannot modify the commitment plant of the units during real-time operation. Furthermore, directly applying the recursive laws in CHP systems as opposed to simpler priority-based thermal-follow dispatch strategies might yield some advantages. If advanced second layer dispatch algorithms are accounted for, including the possibility of integer recourse, the robust formulation tends to be excessively conservative in the management of CHP systems, and the deterministic scheduling problem formulation proves to be effective in identifying the optimal system management.

6 OPERATION SCHEDULING ACCORDING TO ROLLING HORIZON APPROACH

In this Chapter, the comparison between deterministic and robust scheduling problem formulation presented in Chapter 5 is extended for the off-grid microgrid case study, to account for a more advanced nominal scheduling definition strategy based on the Rolling Horizon approach. The EMS first layer problem solution is periodically updated during the day, incorporating newly generated forecast profiles that exploit the observations of the uncertain parameters collected during real-time operation. The case study complexity is increased by accounting for the installation of a wind farm, which significantly increases the uncertainty associated to RES generation, and of a biomass Organic Rankine Cycle, representing a cheaper but less flexible alternative to diesel generation. The study temporal resolution is lowered to 15 minutes, allowing to account for delays in the actuation of the start-up command for generators. The adoption of a variable resolution time-mesh is proposed to deal with the computational complexity increase of the robust problem formulation, deriving from doubling the number of timesteps, which would otherwise lead computational times unfeasible for the application (more than 2 days for each instance). Under the new case study assumptions, the robust formulation ensures a significant margin over the deterministic formulation, despite the possibility of frequently updating the nominal scheduling plan to account for actual system evolution. The best robust formulation considered leads to an overall operating cost across the testing period which is 13% lower than the best deterministic formulation, and which is only 2% above the operating cost lower bound associated to an omniscient deterministic simulation.

The comparison between the deterministic and robust formulations presented in Chapter 5 is carried out assuming an EMS architecture based on day-ahead scheduling optimization: the solution of the EMS first layer problem, which defines the nominal unit commitment schedule and the reference capacity trajectory of storage systems, is solved once at the beginning of the day, while during the rest of the day the second layer is responsible for introducing the necessary corrections to the dispatch profiles of all units and, if possible, to the commitment status of quick-start units. Under this operating assumption, all decisions passed down by the first layer to the second layer (reference recursive storage trajectory, commitment of non-flexible units) are not updated during the day to keep track of the actual system evolution. Furthermore, forecast profiles are only defined at the beginning of the day, without exploiting the updated information collected during real-time operation. The short-term updated forecast could still be used to improve the performance of EMSs featuring a MILP-based second layer also in the case of day-ahead nominal dispatch. Finally, the first layer planning horizon is always limited to the upcoming day, imposing periodic boundary conditions to the storage state of charge and the commitment status of the units without considering the foreseen system conditions for the following day, which might affect the optimality of the end-of-day system status. On the other hand, resorting to the day-ahead scheduling approach is necessary for systems where the start-up of units is overseen by operators and not autonomously managed by the system PLC, either because of the technical nature of the PLC – unit interconnection or because of complex start-up procedures, which call for external supervision. In turn, this normally implies the need to communicate the

commitment schedule to the system operator in advance (especially in the presence of non-flexible units) and makes it less practical to introduce changes in the scheduled start-up sequence.

In fully automated systems, where the actuation of operating decisions is autonomously taken care of by the system PLC, the EMS can rely on more sophisticated scheduling approaches. A common strategy adopted in real-life systems to overcome the limitations of day-ahead scheduling is to tackle the optimal management problem according to the Rolling Horizon approach (Figure 27).

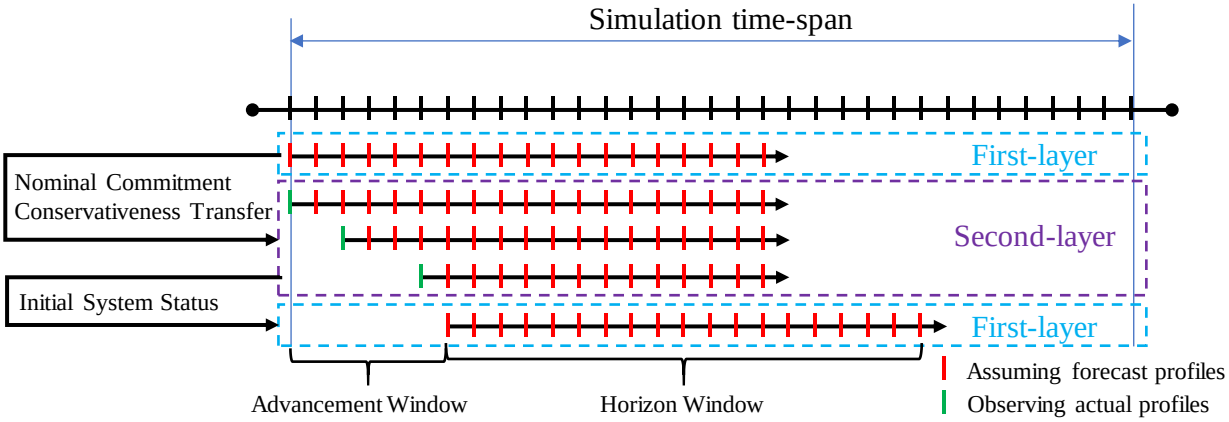

Figure 27: EMS based on Rolling Horizon approach: the EMS first layer solution is periodically updated after the Advancement Window. A Shrinking Horizon approach is still adopted in the second layer. The last second layer solution instance sets the initial condition for the following first layer instance.

The approach consists in solving the optimal dispatch problem over a given future *Horizon Window* of fixed duration (e.g. 24 hours) and implementing only a first fraction of the optimal solution, corresponding to the *Advancement Window*. Then, a new instance of the first layer problem is solved pushing forward the horizon window, accounting for the actual system status at the end of the advancement window and incorporating, if available, any newly generated forecast profile.

In this Chapter, a comparison between the deterministic and robust formulations is presented for the case study of the off-grid microgrid, according to the Rolling Horizon approach. The scheduling problem is solved with a future horizon window of 24 hours, and the solution is updated according to an advancement window of 3 hours. The two operating modes of fixed and modifiable unit commitment in the second layer described in the previous Chapter are both explored.

6.1 Case Study Definition

It is apparent how the possibility of frequently updating the first-layer solution theoretically reduces the utility of resorting to a robust problem formulation in the EMS first layer, as already proven in Chapter 5 when allowing the second layer to recursively modify the unit commitment plan. As a matter of fact, this additional capacity of the second layer was enough to attain full reliability and better performances with the purely deterministic scheduling formulations, for the off-grid electric microgrid study case presented in Chapter 5 under the assumption of day-ahead nominal scheduling. Nevertheless, uncertainty in the off-grid case study depicted in Chapter 5 was limited, and the set of generators only accounted for quick-start diesel

generators. Furthermore, due to the temporal resolution of 30 minutes, it was not possible to properly account for the generators start-up delay, which is the time necessary to implement the start-up command once it is identified by the management algorithm.

Some modifications are therefore introduced in the case study definition for the present Chapter comparison. An updated dataset relative to the Garowe microgrid was provided by the industrial partner ENGIE Eps, referring to the period from January to March 2018. With respect to the data considered in Chapter 5, relative to year 2016, the microgrid has observed a significant increase in the electric load, which maintains the same daily shape but reaches load peak in the evening which is almost twice as high as before. A comparison of a typical daily demand profile for the two years is shown in Figure 28. Energy demand associated with the evening load peak is remarkably consequently more significant with respect load during the central hours of the day, when PV generation is available. The evolution of the demand curve, therefore, increases decoupling between PV generation and energy consumption, enhancing the importance of correct storage management.

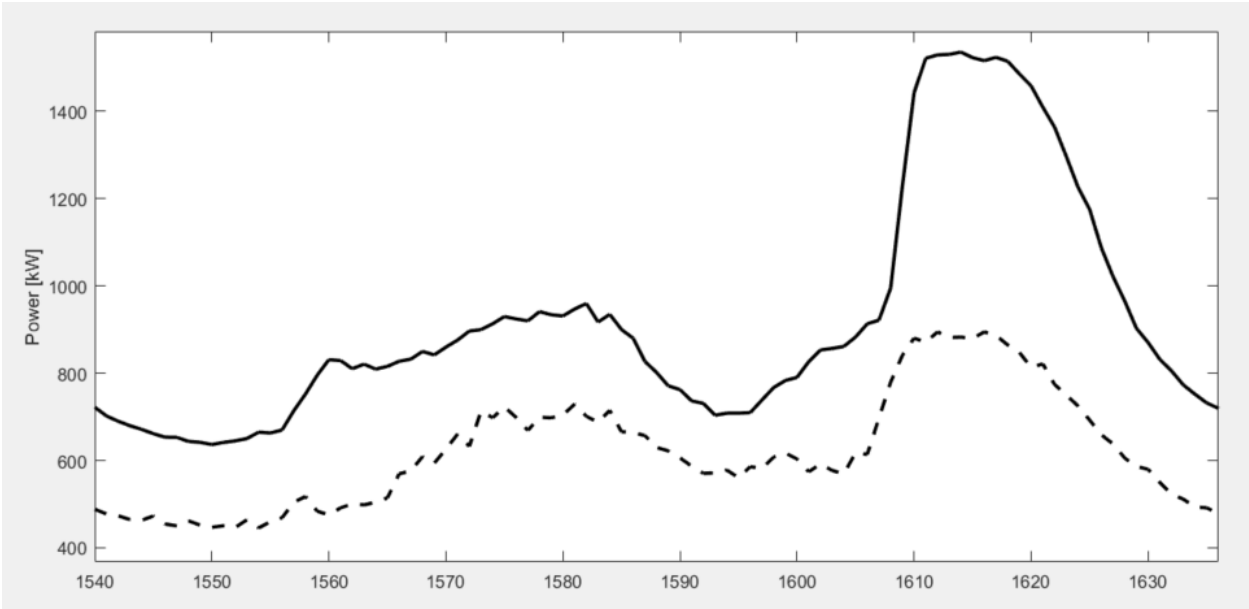

Figure 28: comparison of a typical daily load profile for the Garowe microgrid, in the year 2016 (dashed) and in the year 2018 (solid)

To increase renewable penetration, some wind turbines have been installed in 2018 in Garowe, contributing to the non-dispatchable renewable generation capacity. Wind generators are characterized by much more fluctuant and less predictable power output, increasing the relevance of uncertainty in the dispatch problem. The actual size of the installed wind farm is limited and does not constitute a significant change in the design assumptions of Chapter 5. Starting from the measured wind data, a synthetic production profile for a potential wind farm of 1500 kW_p was therefore produced. Power production is computed from the measured wind speed data according to the wind-power curve of wind turbine generator Vestas225 (Figure 29).

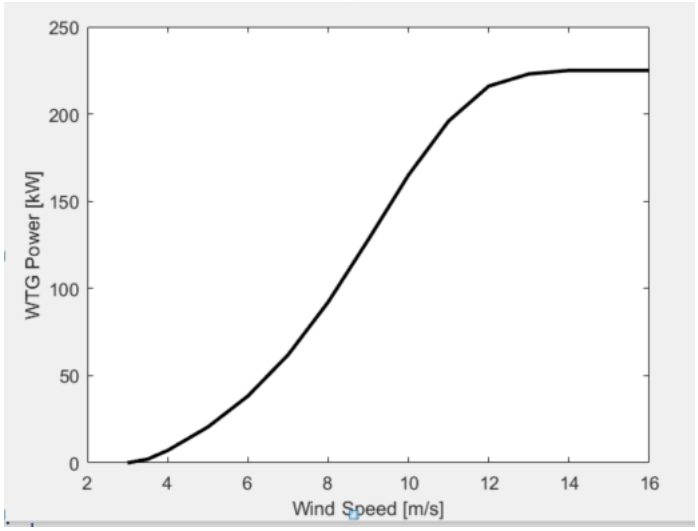

Figure 29: WTG Vestas225 wind-power curve

To further increase the complexity of the operation problem, and in the perspective of lowering the environmental impact of the system which now exclusively relies on dispatchable diesel generators, a 1 MW biomass-fueled Organic Rankine Cycle power plant is introduced in the system, supporting the two 550 kW diesel generators considered for the previous design. The ORC plant represents a non-flexible generation unit, characterized by load ramp constraints, long start-up delays and reduced possibility of modifying its commitment status. A summary of the dynamic load and commitment assumptions on the dispatchable generators is indicated in Table 15.

	Start-up delay [min]	Min Down Time [h]	Min Up Time [h]	Operating load ramping [%/min]	Start-up load [%]
Biomass ORC	120	2	4	1%/min	40%
Diesel ICE	15	0	1	No limit	No limit

Table 15: dynamic constraints for dispatchable generators

A 2220 kWh – 1C Lithium-Ion battery is assumed as the electric storage unit. The updated case study design composition is summarized in Table 16.

Unit	Diesel ICE	Biomass ORC	PV field	Wind Farm	Li-ion BESS
# x Size	2 x 550 kW_{el}	1 x 1000 MW_{el}	1 x 1440 kW_p	1 x 1500 kW_p	1 x 2200 kWh

Table 16: system design composition

6.2 Introduction of Variable Time Mesh

To account for the effect of start-up delays, and to limit the smoothing effect of temporal aggregation on renewable power output and load, the time step duration of the simulations presented in this Chapter is lowered to 15 minutes. The increase in number of time-steps due to the finer temporal resolution, if no modifications are introduced with respect to the formulations introduced in Chapter 5, leads to prohibitive computational times for most robust formulations: as an example, robust formulation **R2**, even accounting for the aggregation of uncertainty factors, is does not reach a convergence gap of 1% after 2 full days.

Introducing significant limitation in the recourse temporal depth τ allows to attain a solution in a few hours, which is still too slow for the proposed operating work-frame. This issue is overcome by the adoption of a variable time mesh for the dispatch problem. Only for the robust simulations, the 15 minutes temporal resolution is considered only for the timesteps falling within the advancement window, while timesteps that are farther from the advancement window, and that are therefore less relevant for the identification of the fraction of dispatch solution which will actually be implemented, are aggregated into longer timesteps, as shown in Figure 30.

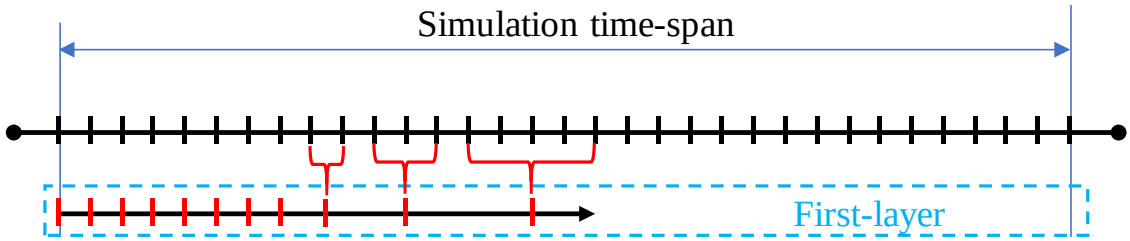

Figure 30: variable time mesh definition

Aggregation involves both forecast profiles and uncertainty set parameters and is performed by averaging the quantities referred to the independent timesteps that are aggregated. The variable time mesh defined in Table 17 is considered in the calculations.

Table 17: variable time mesh definition for the present simulations

Timestep duration	15 min	30 min	1h	3h
Horizon window span	0-3 h	3-9h	9-18	18-24
# of timesteps	12	12	9	2

The total simulation timestep number is consequently reduced from 96 to 35, leading to solution times for a single instance of a few minutes, compatibly with the RH approach.

6.3 Wind Forecast and Uncertainty

While for the electric load and the PV field the same forecasting techniques described in Chapter 5 have been used in the simulations presented in this Chapter, forecasts profiles had to be produced for the expected wind speed profiles, which in turn determine the wind farm power output. The only data available for the task in the dataset is the observed wind speed. Although highly variable from day to day, wind speed pattern exhibits, in the considered simulation period, a daily periodicity, attributable to the geographical characteristics of the site, as shown in Figure 31. In particular, two peaks occurring in most of the days can be identified, one in the central part of the day and one in the evening.

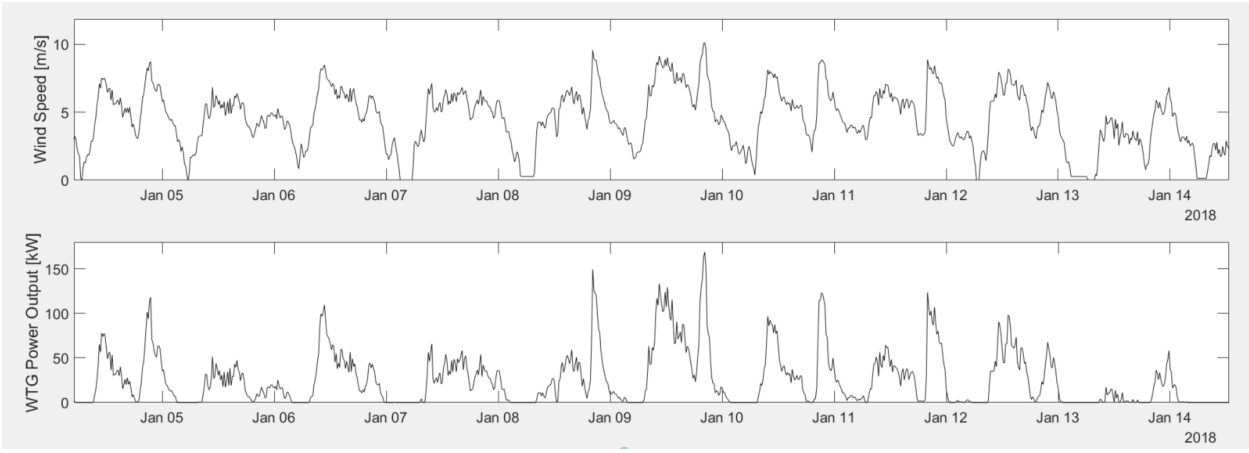

Figure 31: wind speed pattern and consequent WTG production for a single Vestas225 turbine

A SARIMA model was therefore adopted to produce an autocorrelated seasonal estimate of wind speed production. The estimate is updated at each new instance of the RH algorithm (every three hours), accounting for the observed wind speed profiles during the advancement window. As shown in Figure 32. the envelope of predictions relative to the first three hours of each RH instance is characterized by an acceptable accuracy.

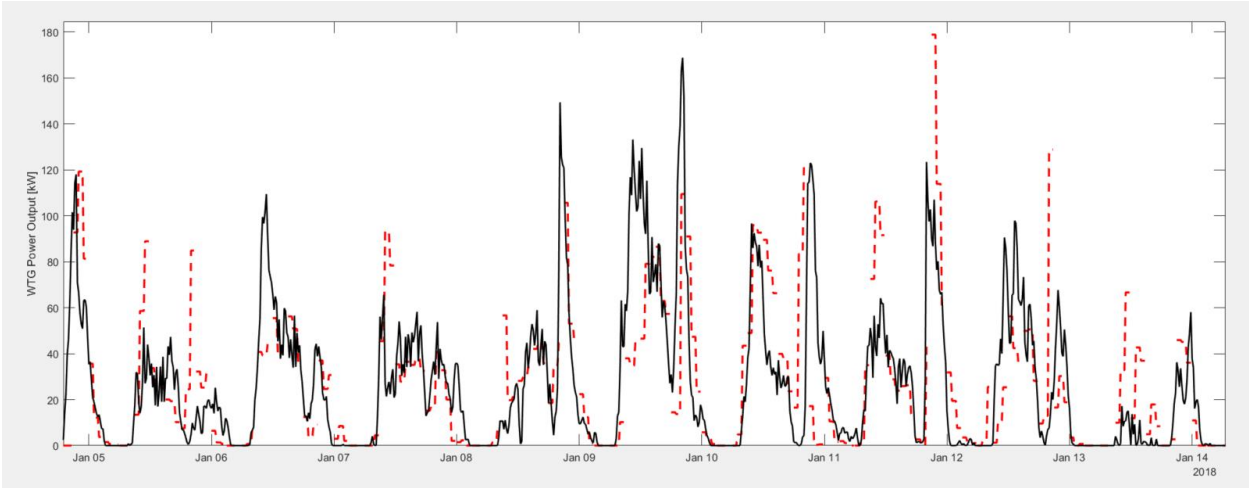

Figure 32: comparison of actual WTG production profile vs envelope of the first three hours of forecasts generated at the beginning of each RH instance

Forecast uncertainty tends to decrease quite rapidly for time instants that are further from the initial solution time, where the autocorrelation components of the SARIMA model is more relevant. The statistical error characterization leading to the definition of the uncertainty set for the robust formulation was therefore performed, for the uncertainty characterization of wind forecast, considering not only the hour of the day but also the temporal distance from the horizon starting time.

6.4 Simulation Results

Fixed Unit Commitment Mode

Table 18 shows the simulation results in the fixed unit commitment operating mode. It must be highlighted that the unit commitment is fixed only in the three hours advancement window, while every three hours the EMS can update the commitment schedule of all units, in accordance with the technical limits posed by start-up delays and minimum up / downtimes. The nominal solution is updated every three hours accounting for the actual system evolution, which is normally quite different from the expected nominal solution of the previous RH instance. Therefore, nominal solution profiles present significant discontinuities in terms of storage charge profile, which make the nominal operating cost estimate not significant. For this reason, Table 18 only reports the actual system operating cost.

Simulation Mode		Actual Operating Cost [€]	GAP [%]	Unserved Electricity [kWh]	Service Reliability [%]	Solution Time [s]
Omniscient		13092		0	100.0%	1008
DETERMINISTIC	T^{res}= 1h	14777	13%	2526	99.7%	459
	T^{res}= 2h	15123	16%	0	100.0%	710
	T^{res}= 3h	15613	19%	0	100.0%	1221
ROBUST	R2*	13582	4%	0	100.0%	6598
	R3* (τ = 6h)	13611	4%	0	100.0%	3792
	R3* (τ = 3h)	13685	5%	0	100.0%	2516

Table 18: formulations performance comparison in the Fixed Unit Commitment Mode

In accordance with the analysis developed in Chapter 5, increasing the energy reserve duration has a negative effect on the performance of the deterministic formulation, although allowing to attain an increase in service reliability. Under the Rolling Horizon assumption with an advancement window of 3 hours, the deterministic model that accounts for a storage reserve duration of 3 hours is virtually fully protected against uncertainty. It is apparent though how in the considered case study the proposed definition of spinning reserve constraints is very inefficient in terms of performance: the operating cost of the least conservative deterministic formulation to attain full reliability is 16% above the global optimum, despite the possibility of frequently redefining the nominal solution granted by the RH approach. With reference to the energy summary shown in Table 19, it is possible to see how the deterministic formulation with T^{res}= 3h with respect to the less conservative and more performing formulation with T^{res}= 1h, relies more heavily on diesel generators to provide the spinning reserve, increasing diesel consumption and the energy generation share covered by diesel ICEs, which are associated to a generation cost which is sensibly higher than the ORC. At the same time, the more conservative storage management causes an increase in renewable power curtailment, which further penalizes the overall economic performance. Finally, when considering T^{res}= 3h diesel generators are more frequently started up (Table 20), implying higher components wearing.

ENERGY SUMMARY				
Load demand	[MWh]	229.55		
RES available energy	[MWh]	88.39		
Max theoretical RES covering	[%]	38.5%		
DISPATCH COMPARISON		T^{res}= 1h	T^{res}= 3h	R2*
RES generation	[MWh]	85.62	81.57	86.74
RES curtailment	[MWh]	2.77	6.82	1.65
Actual RES covering	[%]	37.3%	35.4%	37.7%
ORC Generation	[MWh]	135.44	139.44	140.98
Generation share from ORC	[%]	59.0%	60.5%	61.3%
Diesel Generation	[MWh]	8.45	9.37	2.33
Generation share from Diesel	[%]	3.7%	4.1%	1.0%

Table 19: energy summary for the simulations featuring the indicated first layer formulations

	Tot up-time fraction			Number of SU		
Unit \ Method	T^{res}= 1h	T^{res}= 3h	R2*	T^{res}= 1h	T^{res}= 3h	R2*
ORC	70.3%	78.3%	86.4%	13	13	11
ICE1	12.2%	32.9%	8.0%	15	25	10
ICE2	2.8%	0.8%	0.0%	6	1	0

Table 20: total up-time as a fraction of total simulation time span and number of unit start-ups for the simulations featuring the indicated first layer formulations

Conversely, the robust formulation R2*, thanks to the effective recursive storage planning already accounted in Chapter 5, manages to minimize renewables curtailment, reaching a total renewable penetration which is very close to the theoretical maximum covering. At the same time, R2* very seldom uses diesel generators with respect to the deterministic formulations, limiting their operating hours to the periods where the contribution of the ORC and BESS is not enough to cover for the load peak (Figure 33). In turn, the diesel generation share when the robust formulation is adopted in the EMS first layer reduces to 1% of the total energy generation.

Finally, Table 18 also shows how introducing partial past in the robust formulation is associated with a performance reduction much less significant than in the case of day-ahead scheduling optimization. In Chapter 5, decision rules were used to define the storage trajectory for the whole day and reducing the degrees of freedom of the recourse policies had a deeper impact on the optimality of the recursive storage trajectory. Under the RH framework, the first fraction of the solution can always count on a full recourse, as long as the recourse temporal depth τ does not exceed the advancement window. For the two versions of **R3*** presented in Table 18, which account for a temporal depth respectively of 6h and 3h, featuring partial past only affects the strategic decisions beyond the advancement window, which can to a certain extent be corrected at the following RH instance. The reduction in computational time granted by the partial past, therefore, comes at a very low price in terms of performance reduction.

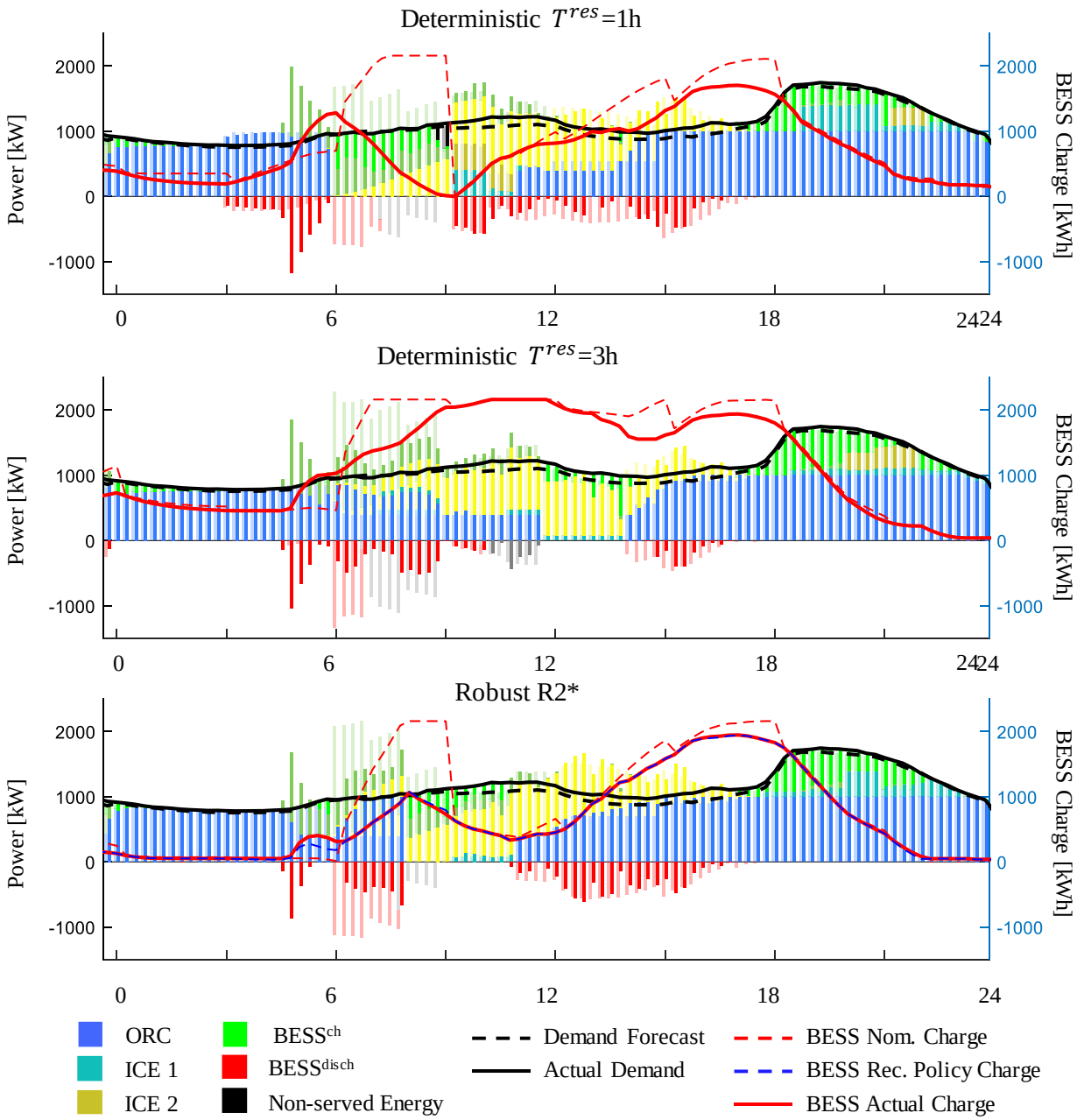

Figure 33: dispatch profiles comparison for the indicated first layer formulations

Modifiable Unit Commitment Mode

Introducing the possibility for the EMS second layer to modify the commitment plan defined by the first layer has to deal with the accounting in the present simulation of the generators start-up delay, set to 15 minutes. Considering the quick start units as readily available in the reserve constraints is therefore not exactly realistic, when compared to the actual capabilities of the units. As a consequence, all deterministic models, which collapse on the same solution in virtue of the mentioned modification, do not attain full reliability, as the start-up delay compromises the system ability to respond to instantaneous net demand fluctuations. It is important to remember that the deterministic second-layer in the SH solution instances

during the RH advancement time still account for the nominal forecast introduced in the first layer, and therefore continue, in case of optimistic renewable generation forecasts, to expect a contribution from renewables that might never manifest. Conversely, the robust formulation **R2*** can effectively guide, through the recursive storage trajectory constraint, the identification of the second layer commitment for ICEs, avoiding service interruptions and exploiting the advantage of a more flexible recursive generators management.

Simulation Mode		Actual Operating Cost [€]	GAP [%]	Unserved Electricity [kWh]	Service Reliability [%]	Solution Time [s]
Omniscient		13092		0	100.0%	1008
DETERMINISTIC	T^{res}= 1h	15230	16%	3897	99.6%	459
	T^{res}= 2h	15232	16%	3858	99.6%	710
	T^{res}= 3h	15160	16%	4229	99.5%	1221
ROBUST	R2*^{QS}	13357	2%	0	100.0%	5219
	R3*^{QS} (τ = 6h)	13439	3%	0	100.0%	3792
	R3*^{QS} (τ = 3h)	13525	3%	1972	99.7%	5427

Table 21: formulations performance comparison in the Modifiable Unit Commitment Mode

6.5 Conclusions

In this Chapter, the comparison between the deterministic and robust formulations of the scheduling problem developed in Chapter 5 is further expanded, for the off-grid microgrid case study, accounting for a management strategy according to the Rolling Horizon approach, while considering a Shrinking Horizon MILP-based second layer. The microgrid case study is updated according to a new dataset relative to the year 2018, and the microgrid design is modified to introduce a wind farm and a non-flexible ORC power plant. Forecast profiles are produced for the wind farm according to a SARIMA model, generating an updated wind forecast profiles at the beginning of every RH instance. A proper accounting of the units start-up delay is also introduced, to consider the technical actuation time of generators start-up command.

The time-resolution of the study is decreased to 15 minutes. Adopting without any modifications the robust formulations described in Chapter 5 would lead to impractical computational times. For this reason, a variable time mesh is considered in the scheduling problem of the robust simulations, increasing the duration of timesteps that are further away from the initial solution time, and therefore less relevant for the identification of the scheduling solution in the advancement window.

Due to the relevant increase in the dispatch problem uncertainty introduced by accounting for wind generation, the performance of the robust formulation under the assumptions of both *Fixed Unit Commitment* and *Integer Recourse* is remarkably better than for the simulations featuring a deterministic first layer. Furthermore, while the introduction of *Integer Recourse* has a positive effect on performance in the robust simulations, in the deterministic simulations it leads to consistent service interruption regardless of the energy reserve duration imposed, due to the start-up delay introduced for the ICE generators.

7 TWO LAYERS DETERMINISTIC EMS FOR REAL-TIME CONTROL OF HYBRID OFF GRID ELECTRIC MICROGRIDS

This Chapter proposes a two layers EMS suited for on-field implementation in a hybrid off-grid electric microgrid. The level of system modeling detail accounted for in the first layer scheduling problem formulation is increased with respect to the previous Chapters, to better account for non-linearities in the units part-load curves and in the power-dependent efficiency of electric storage units. A rule-based second layer algorithm, tracking the reference capacity trajectory defined by the first layer and conceived for direct implementation on the system PLC, is proposed and numerically tested, lowering the temporal resolution of the study to 1 minute. A response filter is introduced in the second layer to decouple high and low-frequency net demand variations, and properly redistribute the variation between genset and storage to avoid abrupt generators ramping. The proposed predictive EMS (P-EMS) is compared with the current EMS deployed in the site that provided the dataset of load and RES generation profiles and with an improved heuristic EMS (H-EMS) developed by the industrial partner ENGIE Eps. Accounting for the current system design, both P-EMS and H-EMS yield a significant improvement in system performance, cutting fuel consumption by more than 20% and leading to a relevant reduction in PV curtailment. The difference between the two new management algorithms is nonetheless little, due to the limited operating degrees of freedom offered by the deployed equipment. The two algorithms are thus compared envisioning a partial revamping of the site, identifying the optimal battery and PV field size associated with each EMS. The optimal solution, associated to the P-EMS ensures safe system operation consuming 25% less diesel by investing in a larger battery and reaching a renewable penetration above 65%, while at the same time reducing the overall system annuity (comprising both investment and operating costs) 6.5% lower than the optimal solution associated to the H-EMS.

In the previous Chapters the comparison between the two MILP formulations of the predictive UC and ED problem for multi-good microgrids and multi-energy systems developed in the present thesis (Deterministic Formulation, Chapter 3, and Affinely Adjustable Robust Formulation, Chapter 4) has shown how the AARO formulation can deal more effectively with uncertainty when (i) commitment decisions are not updated frequently (e.g. fixed day-ahead unit commitment) (ii) changes in the defined scheduling either imply high costs or are limited by technical aspects and (iii) when forecast uncertainty is very high. On the other hand, the differences between the performance of the two methods when considering second-layer strategies compatible with direct implementation on a PLC drastically reduce when the dispatch solution can be frequently updated without consequences, by introducing integer recourse, as shown in Paragraph 5.4.3 where the robust formulation is associated to a dramatic increase in computational times and to a slight worsening of the objective function with respect to an equivalently conservative deterministic formulation. Adopting a Rolling Horizon strategy (Chapter 6) is an effective way of introducing the possibility of updating the generators commitment status while not renouncing to the compatibility of the second layer dispatch algorithm with direct PLC implementation. It must also be remembered that adopting the robust formulation introduces significant limitations in terms of modeling flexibility with respect to the general deterministic formulation described in Chapter 3, mainly related to the inability of accounting for system

non-linearities by means of piece-wise functions. For these reasons, in the following Chapters, specifically focused on PV-ICE-BESS off-grid microgrids that feature fast dispatchable generators, are managed with a Rolling Horizon approach updating the ICE commitment status, and are located in geographical areas where PV production is typically very predictable, a deterministic formulation derived from the general model presented in Chapter 3 will always be implemented, introducing a more detailed modeling of some system non-linearities.

This Chapter presents a two-layer EMS for the optimal management of off-grid electric microgrids. Similarly to the EMS architecture described in Paragraph 5.4, the proposed EMS features a MILP-based first layer, which establishes a reference for the strategic management of the microgrid resources and defines the units commitment schedule based on the forecasts of demand and non-dispatchable generation. The real-time dispatch of all units is then corrected by a second layer heuristic algorithm, which accounts for the optimal decisions established by the upper level while continuously adjusting operating set points to deal with the observed real-time values of demand and non-dispatchable generation. With respect to the heuristic dispatch logic presented Paragraph 5.4, the second layer algorithm developed in this Chapter is conceived to operate at a higher frequency (e.g. every minute or less) and features a response filter to avoid unnecessary abrupt ramping of the generators. First-layer decisions are periodically updated according to a Rolling Horizon approach, as described in Chapter 6.

The performance of the developed Predictive EMS (P-EMS) is compared with a Heuristic EMS (H-EMS), developed and being evaluated for deployment by the industrial partner ENGIE – EPS. Simulations are performed on a minute time-scale. The algorithms and simulation results presented in this Chapter have been published in the Journal Renewable Energy [78].

7.1 Microgrid Architecture

The developed algorithm addresses the optimal management of a hybrid microgrid, featuring a Photo-Voltaic (PV) field, a Battery Energy Storage System (BESS), and an arbitrary number of dispatchable generators (Figure 34). The PV array and the BESS stack are independently connected to the AC bus by means of dedicated inverters. Furthermore, we assume that generation and consumption units are physically located close to one another, justifying the single-node approach.

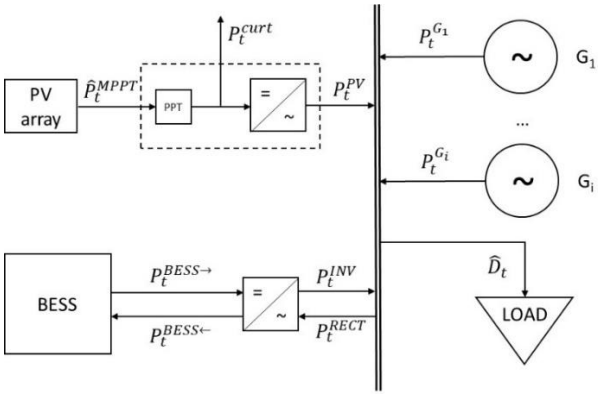

Figure 34: microgrid architecture

7.2 Hierarchical EMS Structure

A schematic description of the two-layer Predictive EMS (P-EMS) is provided in Figure 35. The identification of the set-points to be sent to each unit local controller is conceptually divided into two consecutive stages. The first layer performs a MILP-based deterministic optimization of strategic system management, minimizing operating cost over the following 24 hours. To this end, the *forecast generation module* described in section 7.2.1 provides expected load and PV production profiles for the next 24 hours, with a time resolution of 15 minutes. The solution of the first layer problem defines the UC schedule of all generators, and the optimal trajectory of the BESS SOC.

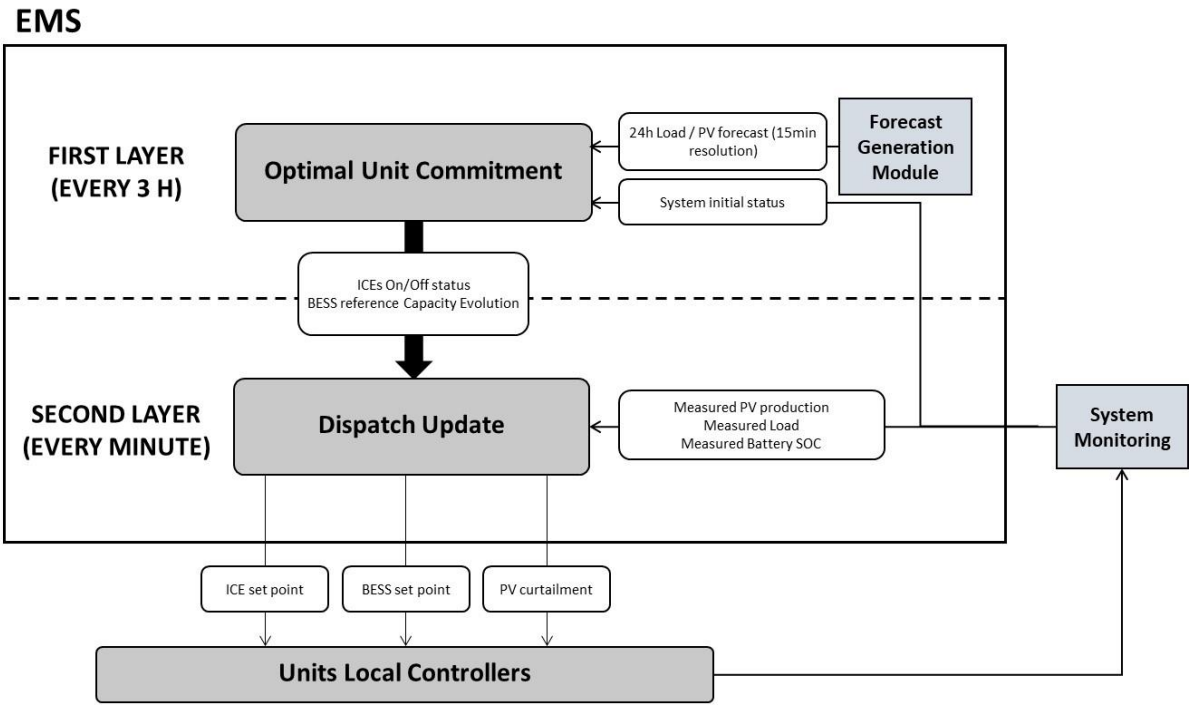

Figure 35: EMS flowchart

The second layer receives from the upper level the switching commands for generators start-up / shut down, as well as the BESS SOC reference trajectory. Additionally, it has access to the current system status which is constantly monitored. As the actual value of net demand is observed, dispatch of all units is updated to account for deviations from the forecasted profiles, and new set-points are sent to each unit local controller.

7.2.1 Forecast Generation Module

The *forecast generation module* (FGM) provides forecasted load and PV production profiles as input for the solution of the first-layer predictive problem. Forecasting methodologies for load and PV power have been extensively studied in literature [79][80], either relying on regressive methods, machine learning techniques or hybrid models. Every approach requires a sizeable set of historical data to tune the model parameters in agreement with prior power measurements and weather forecast, therefore, the procedure is strongly site dependent. The output of the FGM must be a deterministic forecast profile, as the UC is solved

considering reserve margins. The forecast methods selected for the present case study are described in Paragraph 7.5.2.

7.3 First Layer: Optimal Unit Commitment

The first-layer Unit Commitment (UC) problem is tackled according to a version of the general MILP deterministic formulation described in Chapter 3, here briefly discussed. Spinning reserve constraints are enforced in the problem formulation (Eq.(47)), to increase its conservativeness and allow for real-time corrections to the nominal dispatch profiles. Solution conservativeness is controlled acting on the reserve duration T^{res} (Eq.(50)) liming the spinning reserve contribution provided by the BESS. The general formulation of the first layer problem, suitable for a genset including different technologies and sizes of dispatchable generators, is here discussed.

The objective function is to minimize the overall operating cost over the simulation horizon, comprising both physical and virtual cost terms introduced in Chapter 3:

- Generators fuel cost $\tilde{c}_i^f$ and O&M cost
- BESS O&M cost $sp_{BESS,t}^{disch}\tilde{c}_{BESS}^{OMxTP}$
- Virtual generator set-point variation cost $c_{i,t}^{\Delta P}$
- Virtual curtailment cost
- Virtual valorization of residual terminal storage charge $C_{BESS,T}v_{BESS}^{C}$

$$\sum_{t\in T}\left[\sum_{i\in GenSet}\left(\tilde{c}_i^f + c_i^{OM} + c_{i,t}^{\Delta P}\right) + c_{BESS}^{OM} + c_t^{diss}\right]\widehat{\Delta t} - C_{BESS,T}v_{BESS}^{C} \tag{129}$$

7.3.1 Modeling Assumptions

Generators

Piece-wise linear (PWL) part-load curves are defined for each generator i, according to the approach described in Paragraph 3.4.1. Since it is common for generators to be characterized by a generation efficiency monotonically decreasing with load (convex part-load curve, Figure 39), the modeling approach based on defining a set of linear lower bounds to fuel consumption is adopted. For the described application, the decision of adopting this modeling approach in place of the more formal definition of piece-wise function described in Paragraph 3.4.1 does not introduce implicit dissipation in the energy balance, since all machines are single-output and do not consume internal microgrid goods. On the other hand, if slow ramping units are installed, ramp constraints should be enforced on machine output to avoid a potential by-pass of ramp-down constraints. A start-up fuel consumption penalty $\widetilde{in}^{SU}$ is considered for generators, entirely allocated in the time-step during which start-up occurs

The set-point variation cost included in the objective function is defined by two cost segments, one defining a cost dead-band for small setpoint deviations (below 5%) and one introducing a penalization proportional to the setpoint deviation excess with respect to the defined dead-band threshold.

Battery

The battery is modeled as an "energy tank" (Paragraph 3.4.3), varying its charge level according to the power exchange with the AC bus, net of the losses introduced by the battery itself and by the inverter/rectifier. Energy content is bounded by maximum and minimum BESS SOC, while charge and discharge power are limited by inward / outward battery power rating. A binary variable is introduced to avoid simultaneous charge/discharge, to avoid implicit dissipation.

With respect to the simple single tank model of Chapter 3 though, storage power exchange with the AC bus, must account for both battery charge/discharge efficiency and inverter/rectifier efficiency:

$$sp_{BESS,t}^{disch} \cdot \tilde{\eta}_{BESS}^{disch}(sp_{BESS,t}^{disch}) \cdot \tilde{\eta}^{inv} = p_t^{INV} \qquad \forall\, t \qquad (130)$$

$$sp_{BESS,t}^{ch} = p_t^{RECT} \cdot \tilde{\eta}_{BESS}^{ch}(sp_{BESS,t}^{ch}) \cdot \widetilde{\hat{\eta}^{rect}} \qquad \forall\, t \qquad (131)$$

Where p_t^{INV} and p_t^{RECT} represent the DC-AC and AC-DC conversion fluxes to/from the AC bus, $\hat{\eta}^{inv}$ / $\hat{\eta}^{rect}$ are respectively the inverter/rectifier efficiency, and $\tilde{\eta}_{BESS}^{disch}$ / $\tilde{\eta}_{BESS}^{ch}$ are BESS discharge/charge efficiency.

As indicated, battery efficiency is, in turn, a function of the battery power itself. Eq. (130)(131) are therefore formulated through a piece-wise linear approximation, similarly to what described for dispatchable units. This modeling approach is equivalent, in the general formulation of Chapter 3, to define a virtual good ("stored electric energy") for which there is no internal demand, and that can be stored in the BESS with unitary charge/discharge efficiencies. The inverter-rectifier is then represented by two mutually exclusive machines (Eq.(18)), consuming/producing the good "stored electric energy" and delivering/withdrawing from the AC bus electric energy (Figure 36).

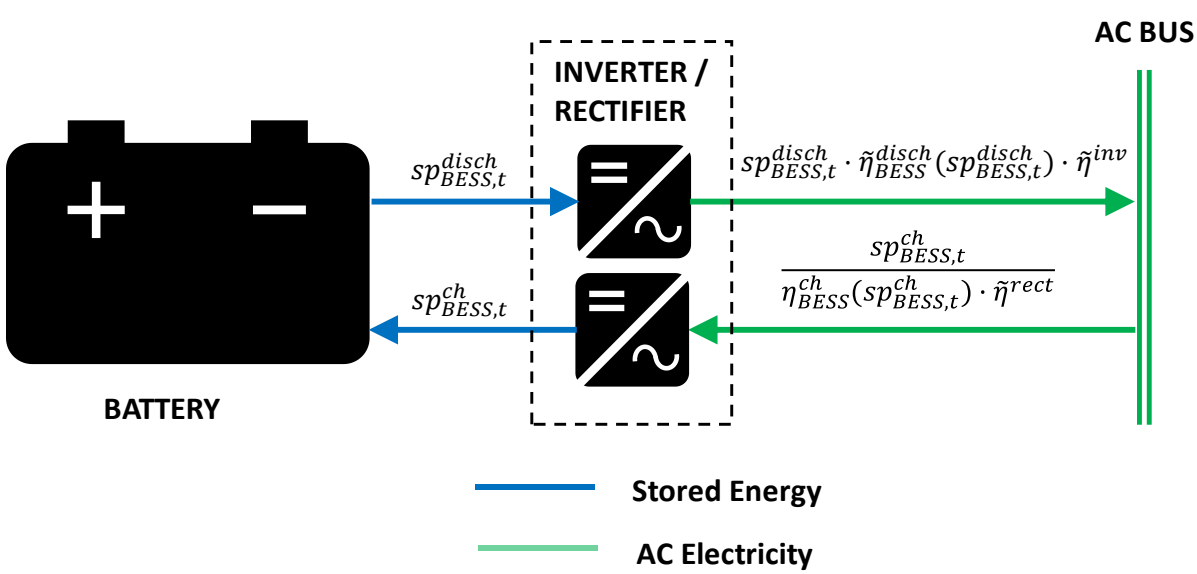

Figure 36: modeling of variable storage charge-discharge efficiency through the definition of the auxiliary microgrid good "Stored Energy", exchanged with the AC bus via two mutually exclusive machines with non-linear part load curve representing the BESS Inverter / Rectifier.

Photovoltaic Array

PV power output is upper bounded by the PV nominal production at Maximum Power Point $\tilde{p}_t^{MPP}$, a function of panel characteristics and environmental condition at time t (see Eq.(26)). The PV array might, on the other hand, operate at Reduced Power Point (RPP), regulating the array voltage to produce a smaller fraction of its maximum potential. For the sake of simplicity, the profiles of $\tilde{p}_{PV,t}^{MPP}$ already incorporate the effect of charge controller and inverter efficiencies. Generation potential is split in $p_{PV,t}$, delivered on the AC bus and p_t^{curt}, which represents the power reduction with respect to maximum production potential:

$$\widetilde{up}_{PV,t}^{MPP} = up_{PV,t} + up_t^{curt} \qquad \forall\, t \in \boldsymbol{\mathcal{T}} \qquad (132)$$

Energy balance and Spinning Reserve

With reference to the system architecture of Figure 34, not accounting for the possibility of planned load shedding in the EMS first layer and assuming a single non-dispatchable load, the generic nominal energy balance (Eq.(42)) on the AC bus is given by:

$$\sum_{i \in GenSet} p_{i,t} + p_t^{INV} - p_t^{RECT} + up_{PV,t} = \hat{d}_t \qquad \forall\, t \in \boldsymbol{\mathcal{T}} \qquad (133)$$

While the generic reserve constraint in Eq.(47) becomes:

$$\sum_{i \in GenSet} p_i^{res} + p_{BESS,t}^{res} \geq \left(1 + \Delta\tilde{d}^{\%}\right)\tilde{d}_t - \left(1 - \Delta\widetilde{up}_{PV}^{\%}\right)P_t^{PV} \qquad \forall\, t \in \boldsymbol{\mathcal{T}} \qquad (134)$$

Where $\Delta\tilde{d}^{\%}$ and $\Delta\widetilde{up}_{PV}^{\%}$ are respectively set to 25% and 90%. Reserve contribution p_i^{res} from dispatchable generators is calculated according to Eq.(48), while BESS reserve power (Eq. (49)) accounts for the stored energy conversion efficiency at maximum discharge power:

$$sp_{s,t}^{res} \leq \widetilde{sp}_s^{max} \cdot \tilde{\eta}_{BESS}^{disch}(sp_{BESS,t}^{disch}) \cdot \tilde{\eta}^{inv} \qquad (135)$$

Energy reserve duration is defined according to Eq.(50).

7.3.2 First layer output

The first layer problem provides an optimal reference for the strategic evolution of the battery energy content which is then tracked during real-time operation when the set-points of all units need to be continuously rearranged based on the actual values of demand and PV production. Generators commitment schedule is fully defined by the first layer, and it is not modified by the second layer. First layer solution is updated after an advancement period of 3 hours, according to a Rolling Horizon approach, to account for the actual system evolution with respect to the nominal planning and to incorporate updated forecast information.

7.3.3 Second Layer: Dispatch Update

During real-time operation, as the actual net demand is observed, corrective actions must be taken on the set-points to maintain the system balanced. A primary control level takes care of very-short-term variations (in the order of milliseconds), stabilizing the frequency by redistributing instantaneous deviation among all machines in operation, following their droop curve [81]. This level of control is not explicitly modeled in the present work. Then, a secondary control level recalculates the nominal operating condition of all

machines and shifts their droop curves to guide the equilibrium towards a new set-points arrangement. The purpose of the proposed EMS second layer is to continuously identify the updated near-optimal dispatch to be implemented by the secondary controller.

A conceptual scheme of the dispatch update algorithm is depicted in Figure 37. The second layer receives inputs from the first layer and from on-field measurement and incorporates a PI controller to track the reference battery capacity trajectory. Starting from the periodic call to the PI controller (**Step 0**), at a given time step the dispatch update is performed in four consecutive steps:

Step 1: the PI controller evaluates the difference between reference and actual BESS charge to generate a cumulated genset production variation signal $\Delta\bar{P}_t^{gset}$: Shifting a fraction of power generation from BESS to genset (or vice-versa) allows to gradually restore the optimal BESS SOC trajectory, with a responsiveness that depends on the PI settings. A new reference aggregate genset power $\bar{P}_t^{gset*}$ is thus calculated from the PI correction signal and the nominal aggregate genset power $\bar{P}_t^{gset}$. $\bar{P}_t^{gset*}$ must be within maximum and minimum generation limits associated with the operating generators. An updated reference BESS power $\bar{P}_t^{BESS*}$ is calculated accordingly from reference BESS power $\bar{P}_t^{BESS}$, to account for the load shift introduced by the PI controller.

$$\bar{P}_t^{gset*} = max\left(min\left(\bar{P}_t^{gset} + \Delta\bar{P}_t^{gset}, \tilde{P}_t^{gset,min}\right), \tilde{P}_t^{gset,max}\right) \tag{136}$$

$$\bar{P}_t^{BESS*} = \bar{P}_t^{BESS} - \left(\bar{P}_t^{gset*} - \bar{P}_t^{gset}\right) \tag{137}$$

Step 2: the net demand variation with respect to nominal scenario $\Delta\tilde{d}_t^{net}$ is tentatively allocated entirely to the BESS, as a deviation from its updated nominal value $\bar{P}_t^{BESS*}$, leading to the definition of BESS actual setpoint:

$$P_t^{BESS} = \max\left(\min\left(\bar{P}_t^{BESS*} + \Delta\tilde{D}_t^{net}, \tilde{P}^{BESS,min}\right), \tilde{P}^{BESS,max}\right) \tag{138}$$

As indicated in Eq.(138), the physical limitations on maximum power exchange with the battery (e.g. maximum charge/discharge power, maximum/minimum SOC constraints) are accounted for, although not explicitly indicated in the equation for the sake of clarity.

Step 3: as the BESS dispatch power is set, the remaining load fraction is distributed among the active generators, curtailing a fraction of the PV if necessary. In the simulations presented in this Chapter, to simplify the accounting of maximum / minimum power limits and ramp constraints for all generators, this step is solved formulating a simplified non-predictive dispatch LP for the present timestep, with generators commitment status and BESS power exchanged set as constraints. In addition to fuel cost, the objective function includes the ramp penalty cost $c_{i,t}^{\Delta P}$ with respect to actual operating condition in the previous timestep. If the algorithm is actually implemented in a PLC that does not have this capability, the redistribution of total genset power among generators can be done on the basis of a cost prioritization list, or fixed sharing coefficients.

Step 4: the updated set-points are sent to each machine local controller, while the PI controller, based on the new measures of BESS charge, generates the genset production variation signal for the following cycle.

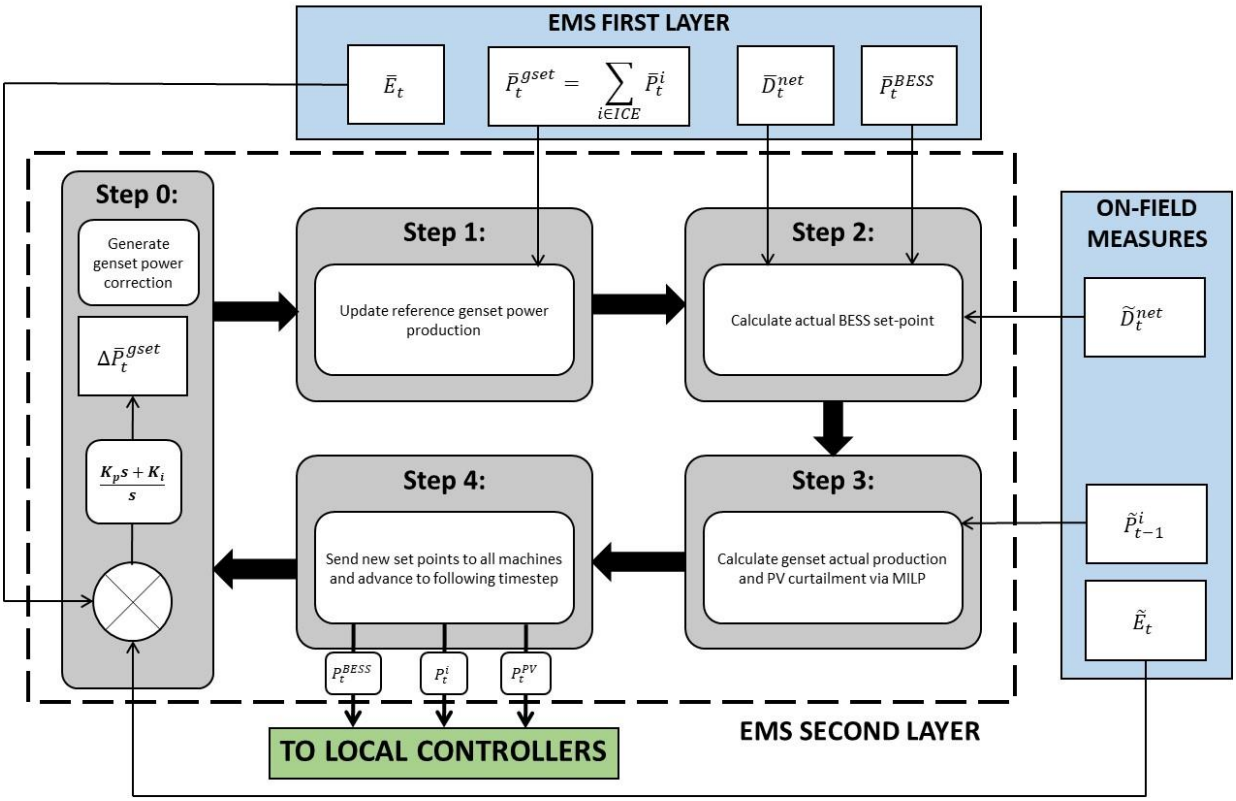

Figure 37: EMS second layer flowchart

The proposed algorithm presents the advantage of relying only on measured data, constituting a non-predictive real-time adjustment method that complements the predictive solution of the upper layer problem. Furthermore, an equivalent response filter is introduced to selectively allocate high-frequency net demand deviation on the BESS, while the genset balances lower frequency systematical deviations without stressing the generators.

For the present calculations, the dispatch update time has been limited to one minute, consistently with the data available. However, the computational time for each control loop iteration is well below 1 s, therefore allowing for a much faster update rate. As mentioned, the LP in *Step 3* might be replaced by a simpler and faster redistribution strategy, since the problem complexity is very limited. The proposed EMS second layer is therefore suited for direct implementation on a central PLC.

7.4 Heuristic EMS

An improved Heuristic EMS (H-EMS) developed by the industrial partner ENGIE – EPS for the management of multi-ICE/BESS/PV systems is used as a state-of-the-art approach for the evaluation of the proposed two-layer P-EMS. This control logic is based on a modified Load Following (LF) strategy [82], stating in its basic version that when a generator is in operation, it is dispatched to follow the net electrical load, and does not contribute to charging the battery unless forced to by its operating constraints (e.g. minimum load, ramp-down limit). Power spinning reserve requirements, analogous to the ones introduced for

the P-EMS in Eq. (47), are enforced on system operation, to cover quick load variations that do not leave enough time to start an additional engine. Since the H-EMS only accounts for the current timestep, no energy reserve duration is considered for the battery (Eq.(49)). The control logic has been specifically developed to be deployed on a standard Programmable Logic Controller (PLC).

The H-EMS computes the set-points of all dispatchable units based on the measurements of net demand and BESS charge level. The battery SOC determines the prioritization between BESS and genset: a high SOC implies that the battery will be dispatched until saturation before a generator is turned on, while a low SOC leads to the preferential usage of diesel engines to cover the load. Generators never directly charge the battery, unless forced to by ramp-rate or minimum load limitations. An upper and lower SOC thresholds are defined, in between which BESS prioritization is cyclically switched, following a hysteresis charge cycle: after hitting the lower threshold, the H-EMS waits until the SOC is restored above the upper threshold before prioritizing again BESS discharge over generators. The battery is also used to smoothen genset set-point variations. A response filter splits high and low frequency of net demand variation, allocating the high-frequency component to the BESS. The number of generators start-up is also limited, imposing a minimum on-time of 20 minutes.

7.4.1 Comparison with HOMER Load Following strategy

This Paragraph presents a comparison of the H-EMS introduced in the previous Paragraph with a similar management strategy implemented in the commercial software HOMER [97], a software developed by the U.S. National Renewable Energy Laboratory (NREL) and globally considered a standard for the design of microgrids. With respect to the Load Following strategy implemented in HOMER, the modifications introduced in the H-EMS aim at limiting excessive stressing of the diesel generators, both in terms of frequent start-up/shut-down and abrupt ramping. To this end, the two major innovative features are:

- The introduction of a hysteresis cycle in the very low BESS charge region, imposing an upper threshold on SOC restoration before generators can be turned off;
- A response filter which splits, whenever possible, the high and low-frequency components of net demand variations respectively between the battery and the genset.

Table 22: performance comparison between H-EMS and HOMER LF

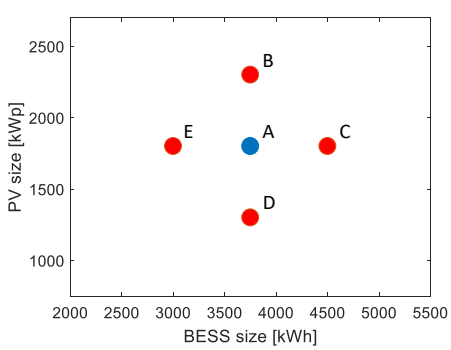

Case	BESS [kWh]	PV [kWp]	H-EMS		HOMER-LF	
			cons. [10^3 L]	Startup #	cons. [10^3 L]	Startup #
A	3750	1800	563.0	1062	561.9	3029
B	3750	2300	544.1	1032	541.6	2753
C	4500	1800	513.3	1060	511.7	3027
D	3750	1300	660.6	1135	665.0	3277
E	3000	1800	614.4	1062	615.7	3029

Spinning reserve requirements are accounted for in the H-EMS coherently with HOMER, imposing a dispatchable generation potential which is proportional to PV output and demand. A minimum on-time period for generators is also considered.

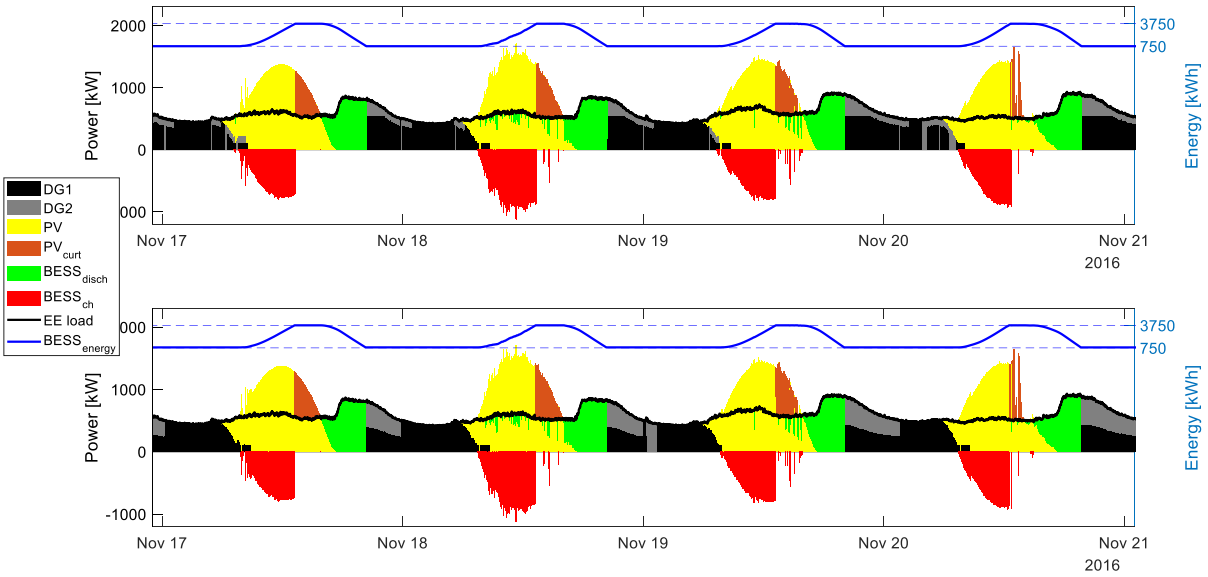

Figure 38: comparison between dispatch profiles of HOMER LF (above) and H-EMS (below)

The details of the H-EMS adaptations developed by EEPS cannot be thoroughly discussed here for IP reasons. Nevertheless, since its performance is used as a comparison to assess the effectiveness of the proposed predictive management algorithm, a comparison with HOMER LF was performed. To fairly compare the two dispatch logics, the response filter included in the H-EMS was switched-off as this option is not available in HOMER. Five different system architectures were considered, comprising the optimal design identified in Paragraph 7.6.3 and four neighboring configurations representative of a sensitivity analysis on PV / BESS size. Since HOMER requires yearly profiles for the simulations, an equivalent yearly dataset was created duplicating the available profiles.

As reported in Table 22, differences in fuel consumption between the two management logics are limited, suggesting a substantial consistency between dispatch decisions. This is confirmed by the dispatch profiles in Figure 38: most of the time, the operating conditions of the generators (on-off status and load) is very similar. On the other hand, a difference can be observed in the number of start-ups, about 60% less for the H-EMS, demonstrating the effectiveness of the load-following corrections implemented in the H-EMS.

7.5 Case Study Definition

7.5.1 Microgrid Characteristics

The algorithms developed are applied to the management the off-grid microgrid deployed in Garowe, Somalia [83]. Installed units comprise of:

- Four 630 kVA/500 kW ICE;
- Six PV arrays, for a total field nominal power of about 1 MW_p;
- A 1440 kWh lead-acid BESS, composed of two battery packs, connected to the AC bus through a 250 kVA bidirectional inverter.

The microgrid is currently managed by a central PLC, which controls ICEs on-off status and all power set-points. The BESS follows a daily cycle, charging when exceeding renewable production is available and covering part of the load at night. BESS charge/discharge power is conservatively limited to 120kW by the control system to reduce battery wearing, although the BESS is able to provide up to 200 kW. PV field production can be controlled by a Reduced Power Point Tracker, if the combined production from PV and ICEs is greater than the load and the BESS has either reached its maximum SOC or is already charging at maximum power. In any case, the operation of all the components must comply with spinning reserve requirements, selected as the maximum between the PV production, which may suddenly drop, and an instantaneous load increase $\Delta\hat{d}^{res}$, set to 250 kW based on the analysis of historical data:

$$\Delta d_t^{net\ reserve} = max\{\Delta\hat{d}^{res}, \hat{P}_t^{MPP}\}; \tag{139}$$

The sum of maximum potential load increase of all active ICEs, plus BESS reserve contribution which is set to 200 kW, must always balance the reserve requirement. This control logic does not consider several aspects included in the EMSs presented, such as the ICE efficiency reduction at partial load, the actual power potential of the BESS, and the smoothing of the ICE setpoint variation.

Actual measures of diesel consumption were used to identify the ICE characteristic curve (Figure 39-left), corresponding to a specific consumption increasing at partial load (Figure 39-right). BESS has been characterized based on nameplates information, while load, PV MPP, and PV actual production minutely profiles are available as part of on-field measures dataset.

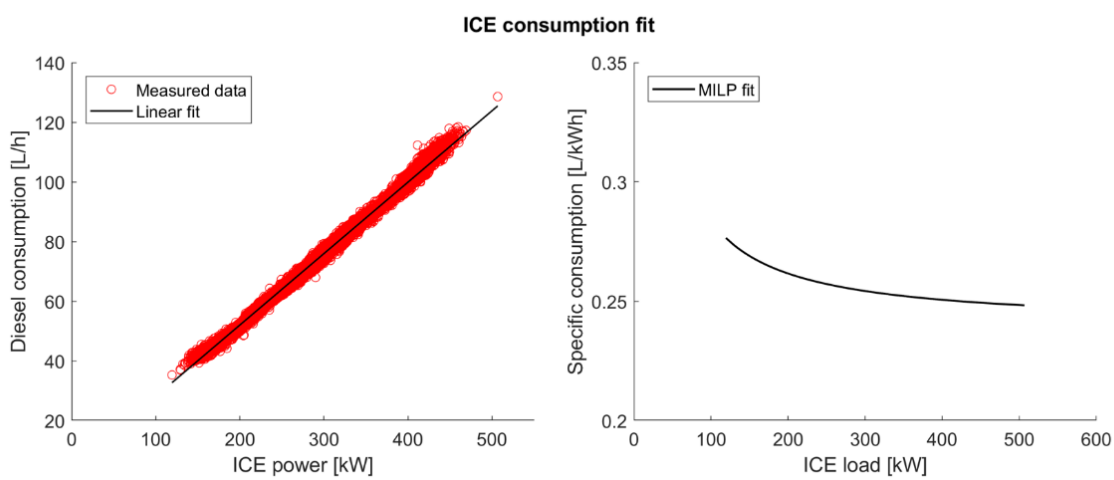

Figure 39: ICE diesel consumption measures and fitting curve

Simulations were based on a dataset of real on-field measurements for electrical load and PV generation potential, provided by the industrial partner ENGIE – Eps, spanning the time period between September

15th 2016 and November 30th 2016. A first fraction of the dataset (up to October 19th 2016) had to be discarded because of the gaps in the measured load profiles due to the frequent acquisition system faults. Out of the remaining dataset (last two weeks of October), some days had also to be excluded as they are used for the training of the load forecasting methodology. The month of November was therefore selected as test period for operating cost evaluation.

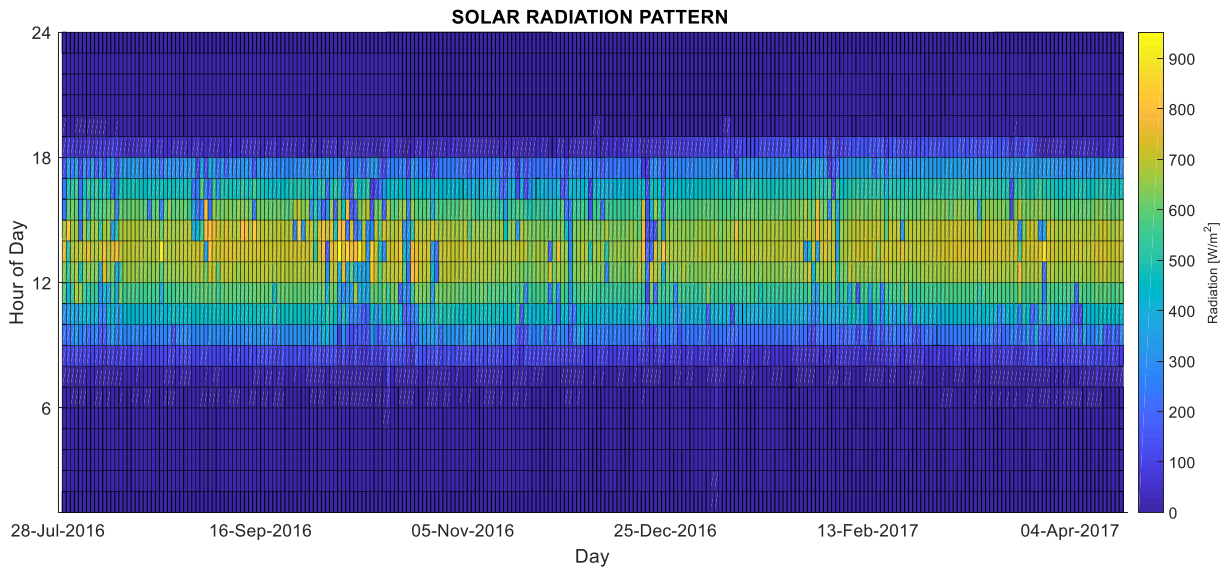

Figure 40: solar radiation pattern for the time period in between July 28th 2016 and April 16th 2017

About the seasonal variation of the considered loads and PV power generation, the PV generation potential measured in Garowe for the period going from July 28th 2016 to April 16th 2017 is shown in Figure 40. Although a minor seasonal effect on radiation can be observed, the variability of the average daily energy production is within the range of ± 10% of its average value as a consequence of the location which is pretty close to equator (latitude 9 N). Furthermore, the number of "rainy days" during the same period, defined as days in which the overall PV production is below 70% of the average value, are limited to 3 out of 263.

7.5.2 Forecasting Methods

7.5.2.1 Load forecast

Among the several techniques used for load forecasting [79], Seasonal Autoregressive Integrated Moving Average (SARIMA), already applied to electric demand forecast for microgrid management [84][85][47], has been used in this study. This method is suitable for forecasting electricity consumption as the demand pattern presents a daily periodic behavior; no exogenous variables are considered in this case, due to the lack of temperature and irradiation forecast. The identification and tuning of the SARIMA model follows the Box-Jenkins methodology [86], then, the final model is univocally identified by Akaike information criteria (AIC) minimization [87]. The selected model is a SARIMA(2,0,1)(0,1,1)$_{96}$, whose coefficients have been evaluated with the Econometric Toolbox in Matlab (R2017b). The available dataset consists of samples of consumed active power measured on minute base, averaged every 15 minutes to have the same temporal resolution of the first-layer problem. Load forecast is updated every time a new instance of the

UC problem is solved, incorporating the new load measures in the training set. Forecast accuracy is quantified in terms of Mean Average Percentage Error (MAPE) and Skill Score (SS) index, which compares the forecast Root Mean Squared Error (RMSE) to the RMSE of a persistent forecast, that assumes a future profile equal to the previous day observations. The SARIMA model performs a MAPE of 3.74% and a SS of 0.392 for the whole test period. A sample of load forecast profiles is shown in Figure 41.

$$MAPE = \frac{1}{n}\sum_{i=1}^{n}\frac{\left|Y_{test,i} - Y_{forecast,i}\right|}{Y_{test,i}} \cdot 100\,; \tag{140}$$

$$SS = 1 - \frac{RMSE_{forecast}}{RMSE_{persistent}}; \tag{141}$$

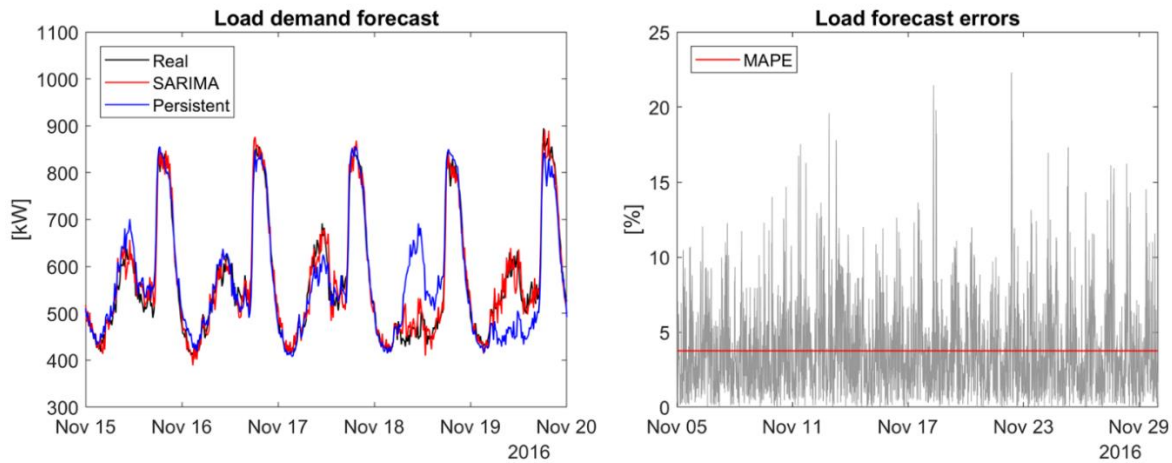

Figure 41: Load demand forecasted profiles with SARIMA compared to a persistent method (right) and mean and instantaneous errors of SARIMA method (left)

7.5.2.2 PV forecast

Due to the absence of irradiation and ambient temperature forecast data, a proper method for PV output forecasting such as [88], could not be implemented in the considered test case. PV production has therefore been estimated based on the historical data according to the peculiarity of the site. In sunny days, PV production closely follows the theoretical clear-sky profile. PV production tends, on the other hand, to rapidly fluctuate in changeable weather days, accounting for about 20% of the total time. Two different reference profiles have been defined, assuming to know in advance if the next day will be sunny or not. It is important to note that the selection of clear or variable weather can be updated every time the forecast is updated. In the case of variable weather, a similarity with known real and forecast data from previous work has been assumed. In particular, the quantiles distribution of forecast error between fitted and real Garowe data has been set as close as possible to the one resulting from a validated PV forecast method [88], scaling the clear-sky profile by a constant coefficient. The fitted profiles are shown in Figure 42.

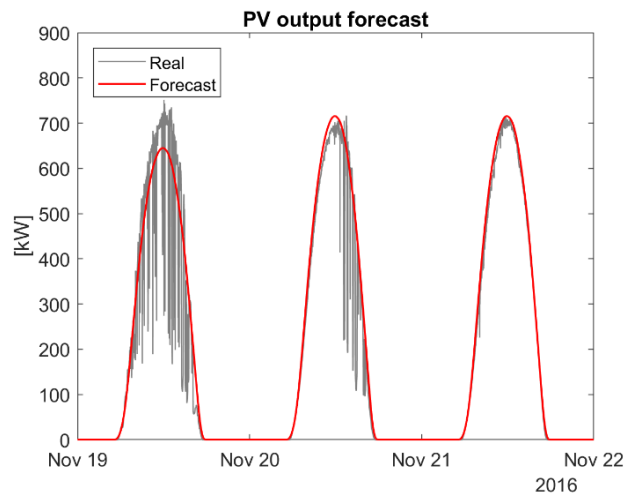

Figure 42: PV forecast generated versus actual production profile

7.5.3 Economic Performance Indexes

System economic performance is evaluated in terms of annuity [89], an equivalent cost index that accounts for both operating cost and investment/replacement cost of components:

$$Annuity = \sum_{i \in Component} \frac{(Inv_i \times DR)}{1 - (1 + DR)^{-LT_i}} + \sum_{i \in GenSet} c_i^f \tag{142}$$

Where Inv_i is the component investment, calculated according to its size and to its technology-specific cost c^{tech} (Table 23), DR is the investment discount rate, set to 10%, LT_i is the component lifetime, c_i^f is the yearly diesel cost for each ICE. Yearly diesel cost is computed by accounting for fuel consumption rate in each simulation time-step and prorating the total consumption over the year according to the simulation time-span T^{sim}.

$$c_i^f = \sum_t in_{i.t}\, \hat{c}^{diesel} \cdot \frac{8760\ [h]}{T^{sim}} \tag{143}$$

Diesel cost $\hat{c}^{diesel}$ is assumed to be 1 €/L.

The annuity corresponds to constant cash flow in terms of year-zero euros that would need to be paid each year to cover for investment, replacement and operating costs indefinitely. It allows to evaluate and compare the cost of systems that include many components with a different lifetime. It is important to note that the lifetime of BESS and ICEs is respectively expressed in terms of lifetime throughput $\widehat{LTTP}$ and lifetime operating hours $\widehat{H}_i$. The actual component lifetime is, therefore, a consequence of the dispatch profile itself.

Based on the annuity, it is possible to define the Levelized Cost of Electricity as:

$$LCOE = \frac{Annuity}{Total\ Demand\ Served} \tag{144}$$

Costs and lifetimes assumptions, reported in Table 23, have been obtained by private communication with companies working in the sector and are consistent with the technical reports from IRENA [7][90]; the PV investment cost includes inverters and installation cost, while the balance of plant (BOP) cost has been considered separately from the cost of BESS modules, due to their different lifetimes. Considering that the focus of this work is on the operation strategies on one-month time span, the effect of aging on the performance of PV panels and BESS modules is neglected.

Table 23: Specific investment cost and lifetime for each component technology.

	PV	**ICE**	**BESS modules[1]**		**BESS converter**	**BESS BoP**	
			Li-ion	**Lead acid**		**Li-ion**	**Lead acid**
c^{tech}	1000 €/kWp	160 €/kWp	270 €/kWh	110 €/kWh	80 €/kW	200 €/kWh	70 €/kWh
LT	20 y	50000 h	$5500 \cdot \Delta\hat{E}^{max}$ kWh	$1000 \cdot \Delta\hat{E}^{max}$ kWh	20 y	20 y	

7.6 Simulation Results

First, a comparison between the presented P-EMS and H-EMS with respect to the current microgrid management systems was performed, adopting the system design deployed in Garowe, described in Paragraph 7.5.1. Then, a partial change in microgrid design is evaluated, reducing the number of engines from four to two, and exploring a grid of BESS and PV field sizes to assess the overall economic performance of each configuration.

7.6.1 Hierarchical Control Testing

As previously mentioned, the advancement time for the RH first-layer solution is set to 3 hours, as opposed to a future foresight of 24 hours. References profiles for the lower level, established by the first layer with a 15 min temporal resolution, are linearly interpolated to a minute by minute discretization, before being passed down to the second layer. The PI controller modulates the genset overall production to track the nominal BESS charge trajectory as load and PV production deviate from forecast. Accurate and updated forecast, as well as reference trajectory correction, contribute to allowing for efficient rescheduling of BESS SOC restoration. PI controller tuning allows to set the desired responsiveness to SOC deviations:

1) If the priority is to be protected against outages and/or PV curtailment is limited→ aggressive PI
2) If SOC restoration can wait for new first layer solution instance → weak PI

An example of first vs. second layer dispatch is shown in Figure 43. In the example, load demand forecast is accurate, while PV production has been significantly overestimated. The genset, therefore, compensates for the supply deficit, gradually increasing its output to cover the energy demand and to restore BESS trajectory. Starting from 16:30, the real SOC is higher than the reference trajectory, therefore the genset modulates downwards its power production with respect to the first-layer set-points. The PI response, in this case, is slow: a more aggressive PI would have restored BESS capacity faster, stressing the machines and potentially anticipating self-restoration of capacity trajectory due to PV output increase or load demand

[1] BESS lifetime throughput is evaluated as number of cycles from minimum to maximum SOC

overestimate. The energy reserve constraints enforced in the upper layer ensure in any case that demand can be satisfied.

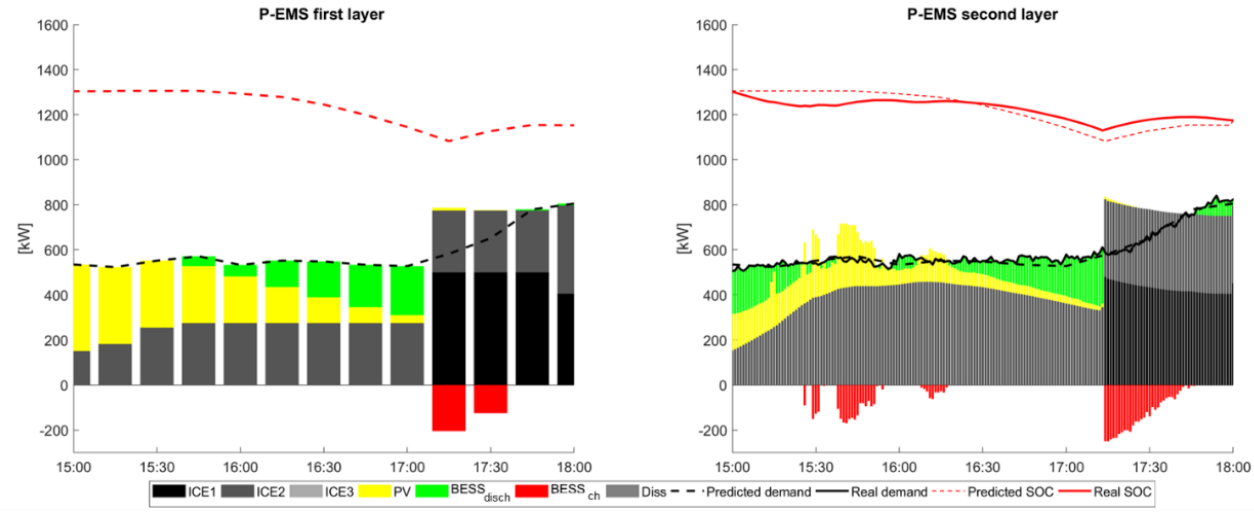

Figure 43: Comparison between UC and real-time dispatch

7.6.2 Garowe Current Design

Figure 44 shows a comparison of the dispatch profiles yield by the H-EMS (center) and P-EMS (bottom) EMSs, compared to the real operation of the microgrid (top). Time resolution is 1 minute. It is clear how both alternative management strategies more effectively schedule the unit commitment of ICEs, minimizing the number of active engines to provide spinning reserve and consequently increasing their average load factor. Fuel consumption is cut by more than 20%, PV curtailment reduced by a factor of 8 increasing the renewable penetration from 18,8% to more than 31% (Table 24).

The economic performance of the two approaches is very close, with slightly lower fuel consumption for the P-EMS by 1.2%. This is mainly due to the system design featuring a small lead-acid battery of limited power and capacity. This implies that the optimal microgrid management strategy is relatively straightforward. Furthermore, the small battery size limits the system dynamic behavior, reducing the extent to which the predictive feature of the P-EMS can be exploited. As a matter of fact, the performance of H-EMS and P-EMS falls, respectively, within 1.9% and 0.8% above the global optimum, calculated by solving a minutely MILP with perfect future foresight over each day (corresponding to a total diesel consumption of 62700 L).

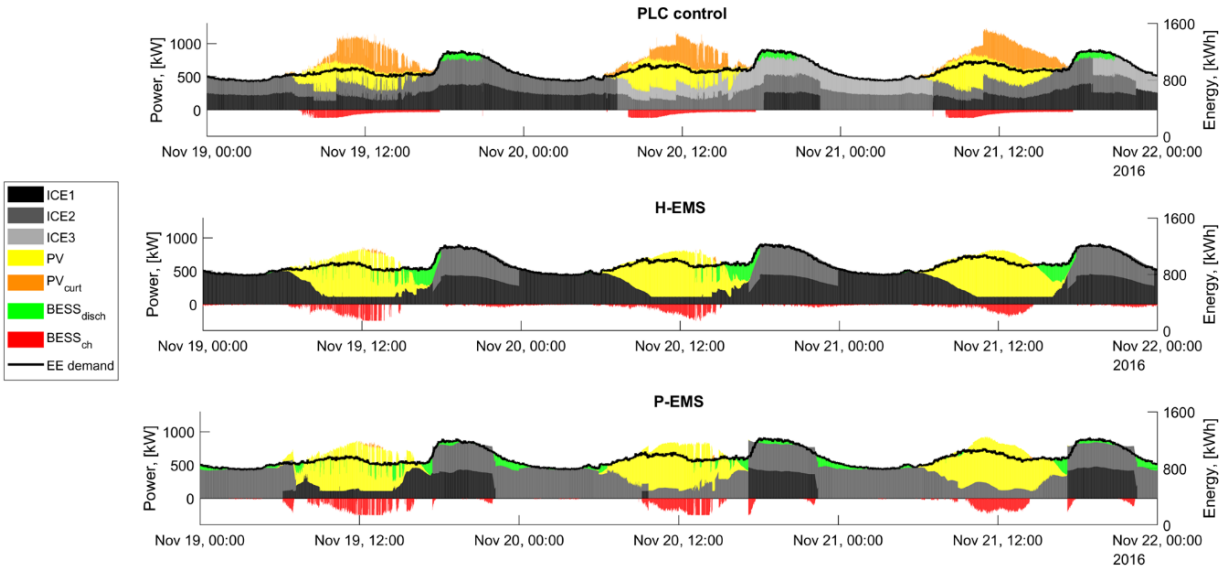

Figure 44: dispatch profiles identified by current dispatch system (top), H-EMS (center), and P-EMS (bottom)

Table 24: results summary on simulations of Garowe reference case

ENERGY SUMMARY				
Load demand	[MWh]	355.2		
RES available energy	[MWh]	120.8		
Max theoretical RES covering	[%]	34.02		
DISPATCH COMPARISON		**Real Case**	**H-EMS**	**P-EMS**
RES generation	[MWh]	66.6	112.2	114.5
RES curtailment	[MWh]	54.2	8.61	6.3
Actual RES covering	[%]	18.8	31.6	32.2
Diesel generation	[MWh]	296.8	249.2	246.7
Total diesel consumption	[10^3 L]	74.7	63.9	63.2
ECONOMIC COMPARISON		**Real Case**	**H-EMS**	**P-EMS**
Annuity	[k€/month]	86.5	76.2	75.7
LCOE	[€/MWh]	239.3	210.3	209.1

A few differences can still be noted in the dispatch profiles yield by the two algorithms:

1) The P-EMS distributes the battery utilization on a longer time span, serving for peak shaving and securely operating the system with only one diesel engine at higher load factor more often than the H-EMS;
2) Both EMSs are effective in smoothing ICE ramps, which is a remarkable advantage in terms of machines wearing mitigation. On the other hand, since an indirect filter is adopted in the MILP formulation and PV curtailment is not included as a smoothing option, the filtering effect doesn't

work in the P-EMS when the BESS is either full or empty. This effect is not present in the H-EMS, which incorporates an actual response filter.

7.6.3 New Design

System design and management algorithm are closely related: systems featuring non-controllable units and components with marked dynamic behavior, such as batteries or machines with limiting ramping constraints, can better benefit from the adoption of the P-EMS. At the same time, both EMS seem capable of securing the operation of the microgrid using less generation resources than what currently installed in Garowe.

A new design with partial modification to the Garowe microgrid architecture was therefore developed to assess the actual potential of the proposed P-EMS; the new design leads to a micro-grid with higher flexibility and dispatchability which requires an effective dispatch strategy making it the optimal case study to investigate the effectiveness of the proposed management algorithm. To create the new design, The following assumptions were made: (i) the current ICE models are maintained, but the number of engines is reduced from four to two, (ii) lead acid batteries are replaced with lithium-ion which is a more flexible technology in terms of power exchange as well energy capacity and it is commonly adopted in large microgrids, and (iii) a potential expansion of the PV field is also considered. Estimate of the yearly operating cost is based on the month of November, assumed representative of typical year conditions in virtue of the limited location seasonality (see Paragraph 7.5.1). Parameters of the design study are BESS capacity and PV field nominal power.

A grid of potential PV – BESS sizes is explored. Figure 45 shows the annuity for the systems within the range of sizes considered. It can be seen how:

- The optimal PV field size is respectively 2 times and 1.8 times larger than the current installed capacity in Garowe, when adopting P-EMS and H-EMS;
- The optimal BESS size if the P-EMS is adopted is 1.5 times larger than for the H-EMS case, reflecting a steeper gradient in fuel consumption reduction at higher BESS sizes, consequence of the ability of the P-EMS to extract value from a smart BESS management;
- The range of BESS sizes that can effectively be exploited from an economic point of view is broader as the size of the PV field increases for both dispatch methods;
- The economic performance of the P-EMS is better in most of the PV-BESS size plane, mainly due to the difference in diesel consumption (Figure 46). On the other hand, when decreasing PV field capacity, as seen for the current Garowe design, both strategies lead to comparable results, that reflect similar dispatch profiles.

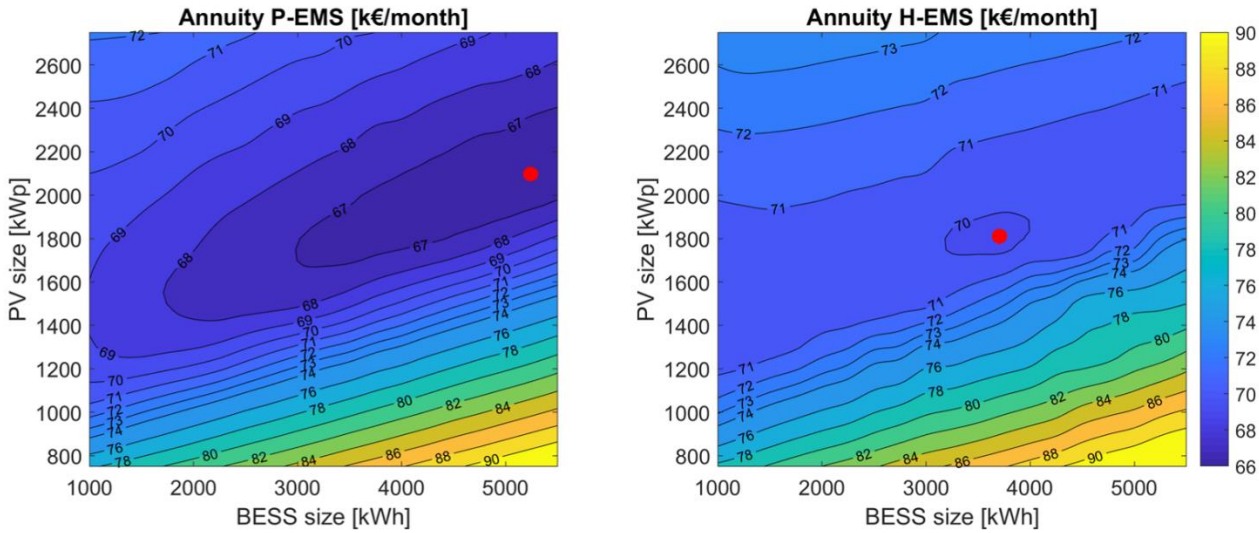

Figure 45: system annuity as function of PV field peak power and BESS capacity if the P-EMS (left) or the H-EMS (right) is adopted; the red points indicate the optimal design configurations.

As PV field size increases, so does renewable penetration, reducing the overall diesel consumption (Figure 46). Savings are more relevant when the PV field is small with respect to BESS capacity, while they tend to stabilize at larger PV field nominal power, where storage capacity is saturated by the daily PV production. The same holds for large batteries, which result to be oversized with respect to a given renewable energy production.

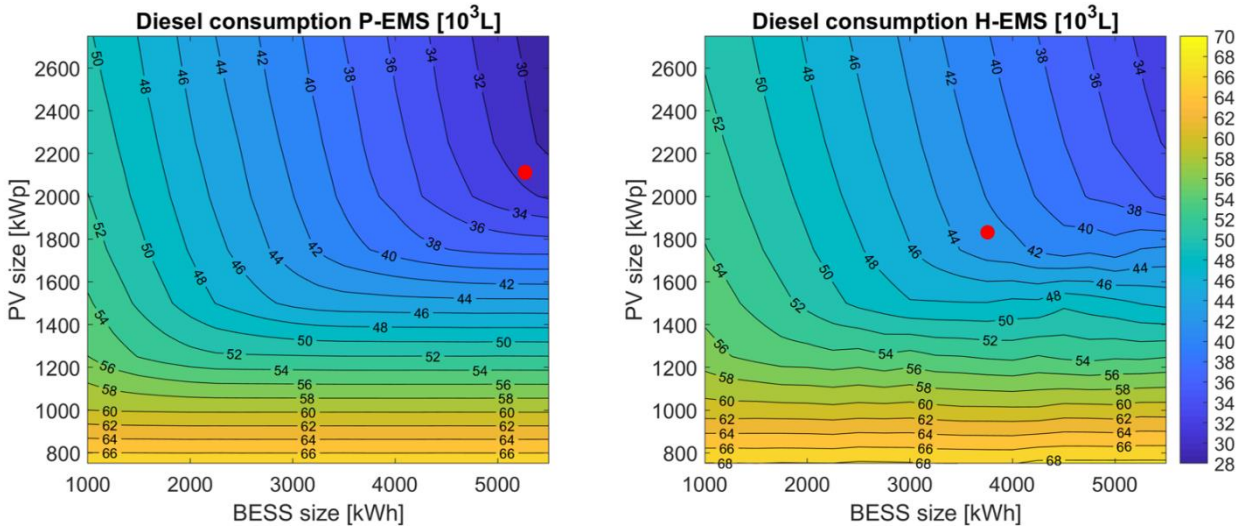

Figure 46: diesel consumption as function of PV field peak power and BESS capacity if the P-EMS (left) or the H-EMS (right) is adopted; the red points indicate the optimal design configurations.

The relative cost share of each component in the two optimal architectures is shown in Table 25. Diesel consumption is the main cost index in both P-EMS and H-EMS cases, respectively accounting for 50% and 60% of the annuity. P-EMS optimum spends almost 1.5 times more than H-EMS optimum in BESS: extensive BESS usage grants a fuel consumption reduction of about 25%, which outbalances the additional BESS

capital investment and leads to a system annuity for the optimal P-EMS system which is 6.5% lower than the optimal H-EMS system. Fuel saving, which is due to both PV curtailment reduction and higher ICEs efficiency as a consequence of the higher load factor (Figure 47), also reflects in improved environmental performance. From this analysis, it can be concluded that the P-EMS outperforms H-EMS in terms of LCOE and CO_2 emissions.

Table 25: annuity indexes summary for optimal H-EMS and P-EMS architectures

Annuitized cost indexes	**H - EMS**		**P - EMS**		**P - EMS to H - EMS Δ%**	**Weight on Δ% annuity**
	k€/month	annuity %	k€/month	annuity %		
PV CAPEX	9.86	14.1	11.26	17.2	14.2	2.0
BESS CAPEX	8.68	12.4	11.33	17.3	30.5	3.8
BESS Converter CAPEX	0.74	1.1	0.61	0.9	-17.6	-0.2
BoP CAPEX	6.04	8.6	8.45	12.9	39.9	3.4
ICE CAPEX	1.58	2.3	1.35	2.1	-14.6	-0.3
ICE OPEX	42.98	61.5	32.35	49.5	-24.7	-15.2
ANNUITY [k€/month]	**69.88**		**65.35**		**-6.5%**	
LCOE [€/MWh]	**196.7**		**186.9**			

Table 26: energetic performance comparison between H-EMS and P-EMS optimal architectures

ENERGY SUMMARY				**P - EMS to H - EMS Δ%**
Load demand	[MWh]	355.2		0.0
RES available energy	[MWh]	211.5	241.7	14.3
Max theoretical RES covering	[%]	59.5	68.1	14.5
DISPATCH COMPARISON		**H -EMS**	**P - EMS**	
RES generation	[MWh]	192.4	231.1	20.1
RES curtailment	[MWh]	19.1	10.6	-44.5
Actual RES covering	[%]	54.2	65.1	20.0
Diesel generation	[MWh]	168.9	128.2	-24.1
Total diesel consumption	[10^3 L]	43.0	32.3	-24.7

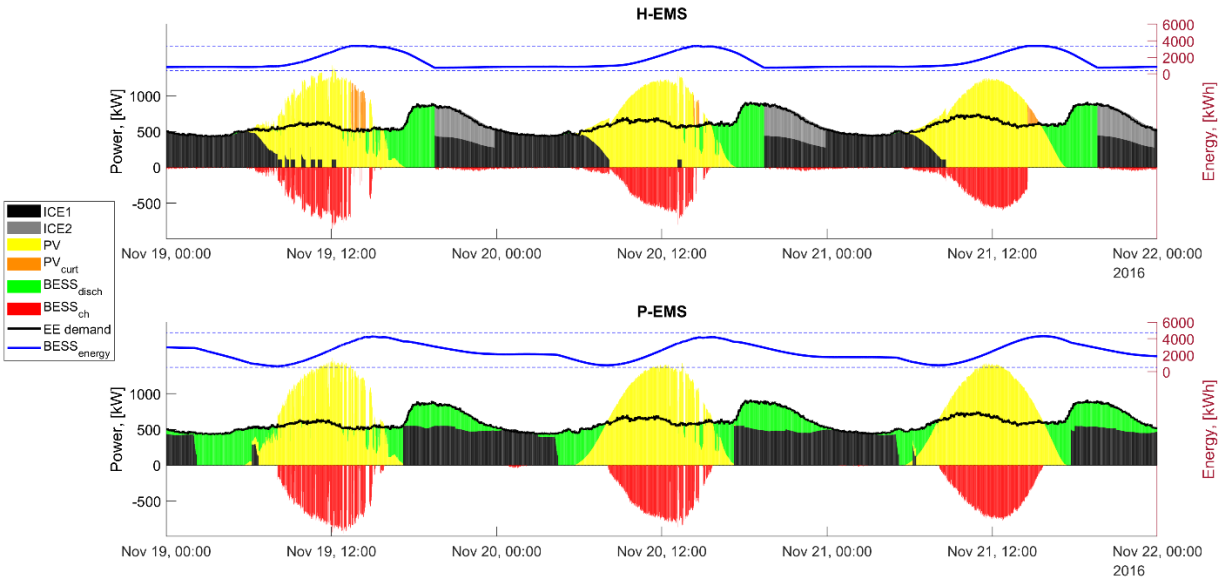

Figure 47: optimal designs dispatch profiles

7.7 Conclusions

This Chapter proposes and numerically evaluates a new two-layer EMS for the economic dispatch and control of off-grid PV-ICE-BESS microgrids. The first layer of the algorithm optimally solves the predictive unit commitment problem over a horizon window of 24 hours via a deterministic Mixed Integer Linear Programming formulation of the optimal UC and ED problem. The generators on/off status and the reference BESS charge trajectory are defined in this stage. Spinning reserve constraints are adopted to account for electric demand and PV production uncertainties. A Rolling Horizon approach is adopted to update the first layer solution every 3 hours. The EMS second layer performs an on-line set-point update for all active units, based on the measured values of uncertain parameters and on the BESS SOC set by the upper layer. The algorithm is suited for an on-field implementation, deploying the first layer of the EMS on a support industrial PC, which communicates with the system PLC on which the second layer is run.

The performance of the new algorithm is numerically tested on data from a microgrid located in Garowe, Somalia. The performance improvement yielded by the Predictive EMS (P-EMS) is assessed with respect to the control system currently deployed in the microgrid and to a new improved heuristic version (H-EMS). Results show a significant reduction in diesel consumption (about 15%) allowed by the two new control algorithms with respect to current consumptions. On the other hand, limitations intrinsic in the system architecture limit the advantage of a predictive optimization (P-EMS), which reduces the fuel consumptions with respect to H-EMS by only about 1%.

Finally, a new design for Garowe microgrid is evaluated, replacing lead-acid batteries with lithium-ion and the overall system cost is explored as function of BESS capacity and PV field nominal power. Two distinct analyses are carried out under the assumption of deploying respectively the P-EMS or the H-EMS. The two EMSs are associated to very different optimal designs, with the P-EMS pushing towards a larger investment

in the storage system that brings about a fuel consumption reduction by about 25% because of both reduced PV curtailment and higher ICEs load factor. The optimal P-EMS system scores a total annuity of 65.35 k€/month, 6.5% lower than the H-EMS optimal system. The adoption of the proposed control algorithm, if deployed within an appropriately sized microgrid, therefore leads to an energy production that is both cheaper and greener.

8 DESIGN OPTIMIZATION OF RURAL OFF-GRID MICROGRIDS

This Chapter proposes a MILP-based design optimization algorithm for hybrid off-grid microgrid, developed for application in the context of regional electrification planning. The deterministic scheduling problem formulation is adapted, introducing binary investment variables for discrete components selection from a generation and storage technology catalogue. The typology and size of all microgrid components is identified by solving a deterministic design and operation problem over a reference period, representative of the typical year in terms of renewable generation potential and load profiles for the microgrid site. The actual operating cost associated to the optimal design is then validated by means of a realistic simulation of its operation spanning the entire typical year, according to a Rolling Horizon approach with limited future foresight (24-hours ahead). The proposed predictive design algorithm (PA) is compared with a heuristic design and operation algorithm (HA) developed at the MIT Universal Energy Access Lab, in collaboration with whom the project has been developed. The comparison is carried out solving several instances of the microgrid design problem, accounting for various compositions of microgrid loads (categorized according to a library of consumer classes), and a wide range of microgrid sizes in terms of overall yearly energy demand. Results show how the PA with respect to the HA allows to attain savings in the overall microgrid cost (comprising both investment and operating costs) between 2-3% in the case of small systems that do not feature a dispatchable generator, while the advantage increases to 7-8% for microgrids large enough to include in the optimal design a diesel generator. At the same time, the microgrids designed according to the PA are associated to a higher level of service reliability, as well as to a higher share of renewable penetration in systems featuring diesel generators.

The deterministic model for dispatch optimization presented in Chapter 3 considers a fixed system architecture, in terms of characteristics of the installed units. On the other hand, the design analysis performed in Chapter 7 on the architecture of the Garowe off-grid microgrid demonstrated how the optimal operating performance attainable by a microgrid is strongly affected by the flexibility provided by its design, which in turn determines the investment cost necessary to construct it. In general, the effective selection and sizing of the components comprising a microgrid cannot prescind from the definition of its management logic, without which it is not possible to account for an accurate estimate of the operating costs following the adoption of a specific design. Simulating system operation over a reference time period allows to evaluate the fitness of candidate solutions, and consequently guide the design selection process. This is particularly important in the case of off-grid systems, where the requirements of ensuring reliable system operation, attaining high renewable penetration and limiting the final energy cost for its users make the design definition stage particularly critical.

This Chapter presents a MILP formulation of the discrete design optimization problem: starting from the model introduced in Chapter 3 binary investment variables are introduced, to activate / deactivate the presence of candidate microgrid components, discretely selected from a catalog listing different models of generators, battery modules and PV panels. Optimization aims at minimizing system annuity, the equivalent cost index accounting for both investment and operating costs introduced in the previous Chapter. An explicit dependency of annuitized investment cost for generators and batteries on their operation profile is

introduced in the MILP design problem formulation, to correctly account for the effect of wearing on the lifetime of these components and on the impact that it has on design decisions. Optimal design and operation are identified at the same time, simulating the microgrid operation over a reference period and allowing for the simultaneous and interdepended optimization of both. The algorithm is suited for the inclusion of seasonal operation constraints in the design stage, such as minimum reliability thresholds and seasonal diesel availability. Finally, the operating cost estimated in the solution of the design problem is validated, introducing realistic assumptions on forecast availability for dispatch optimization. The yearly operation of the optimal design is thus evaluated following a Rolling Horizon (RH) approach and solving an operation problem equivalent to the formulation adopted for the first-layer of the EMS proposed in Chapter 7, to identify the optimal dispatch solution corresponding to the selected design. The effect of uncertainty on system operation is not accounted for in this Chapter, as the capacity of the predictive algorithm to deal with uncertainty has already been proven in the previous Chapters.

The algorithm has been developed as part of the collaboration with the MIT Universal Energy Access Laboratory, as a potential alternative to the heuristic sizing and operation methodologies under study. These algorithms are meant to be integrated into the software REM (*Reference Electrification Model*) [91], a comprehensive tool for the definition of regional electrification planning in developing countries. The software manages the definition of electrification clusters within a partially electrified region, evaluating on- and off-grid electrification options for groups of users. A detailed microgrid design is finally identified for all off-grid clusters and stand-alone users. The performance of the new MILP-based design algorithm is thus compared to the heuristic algorithm (HA) used at the time (2016) for off-grid microgrid optimization, in a preliminary and simplified version of the REM. The dispatch logic implemented in the HA is the Advanced Battery Valuation (ABV) strategy described in [92]. Design and operation are optimized using the two algorithms for a large number of rural microgrids of different sizes, in the work-frame of sub-Saharan African regions electrification. Solutions are compared both in terms of overall cost, service quality and renewable penetration, demonstrating the superiority of the proposed algorithm with respect to all comparison parameters. The algorithm and results presented in this Chapter have been published on the Journal Applied Energy [89].

8.1 Microgrid Design optimization algorithms

As already mentioned, the identification of the optimal microgrid design, as well as the definition of an effective operation strategy, is a critical stage to ensure the competitiveness of off-grid systems and to minimize the Levelized Cost of Electricity (LCOE) for their users. Design and operation strategy are interdependent: selecting the microgrid configuration based on an erroneous estimate of how it will be dispatched can lead to sensibly sub-optimal actual performances as shown by Mazzola in [44]. A few approaches commonly adopted in the field of electrification planning for the identification of optimal off-grid microgrids design are summarized in Table 27.

Table 27– brief classification of the literature approaches to microgrid design optimization

<table>
<tr><th>Model type</th><th>Design identification (layer 1)</th><th colspan="2">Dispatch strategy (layer 2)</th></tr>
<tr><td>Analytical</td><td>Analytical expression</td><td colspan="2">Simulation not performed</td></tr>
<tr><td rowspan="4">two-layers</td><td rowspan="4">Grid search
(GA, PSO, Pattern Search)</td><td rowspan="3">Heuristic</td><td>LF</td></tr>
<tr><td>CC</td></tr>
<tr><td>ABV</td></tr>
<tr><td colspan="2">MILP</td></tr>
<tr><td>single layer</td><td colspan="3">MILP</td></tr>
</table>

Off-grid LCOE can be estimated using *analytical models* that do not simulate the system operation over a period but only require assumptions on overall energy demand and technological performances of components [93], or that include also additional lumped factors, such as population density [94]. These models present the advantage of requiring very short computation time, and for this reason, they are the preferred method for estimating the cost of off-grid systems in preliminary electrification planning studies. On the other hand, they do not explicitly address the design and dispatch problem, which can lead to misleading LCOE estimates. This limitation can be overcome with more complex simulation-based design algorithms that select the size of components based on the simulated performance of candidate solutions over a reference period.

A broad range of different *two level models* has been proposed in the literature [95]. Most of the approaches decouple design and dispatch problems, resorting to the performance evaluation of fixed architecture systems as fitness parameter to guide the exploration of the design space [96]. Adopting heuristic dispatch logics is a fast and realistic way of simulating the microgrid operation. They comprise of a set of predetermined rules that control the system based on its status and on the characteristics of the installed equipment and have the merit of being easily deployable in real systems given the state of the art in commercially available hardware. The two most acknowledged heuristic dispatch strategies for hybrid off-grid microgrids are Cycle-Charging (CC) and Load Following (LF) (see Paragraph 7.4.1). CC and LF are implemented in the widely known simulation-based microgrid design optimization software HOMER [97], developed by the U.S. National Renewable Energy Laboratory (NREL) and globally considered a standard for the design of microgrids. Alternative and more advanced heuristic strategies are proposed by Li [92]: among them, the Advanced Battery Valuation (ABV) strategy attains a good performance without equipment oversizing and does not require the calibration of the diesel activation/deactivation threshold present in the CC approach. Even more advanced second-layer control strategies, best suited for complex system architectures, rely on Mixed Integer Linear Programming [98], as discussed in extent in this thesis.

As a drawback, the two-layers models complicate the introduction of seasonal and yearly constraints, and in general limit the possibility of accounting for interactions between adjustments to the dispatch strategy and selection of the optimal components. The fitness of design solutions that do not enforce the requirements on overall system performance can be penalized ex-post, but trying to adjust the structure of the operational management logic to avoid the penalization would require an iterative process between the first and second layer that would severely limit the effectiveness of the search space exploration. For the same

reason, an accurate accounting of wearing cost for components whose lifetime is influenced by their yearly dispatch is of difficult implementation in algorithms that separate design and dispatch optimization processes.

On the other hand, integrating design and dispatch optimization in a *single level model* leads to the formulation of a complex problem, that can be tackled via MILP. The most famous software for design optimization relying on this technique is DER-CAM [99], developed at Lawrence Berkeley National Laboratory since early 2000. The software is oriented towards design and operation evaluation for complex CHP and trigenerative grid-connected microgrids in developed countries and includes the evaluation of the thermal behavior of buildings. A much simpler model is presented by Ferrer-Martí [100] for the optimization of spatially distributed off-grid microgrids featuring solar panels and wind turbine generators. The model optimizes number and location of installed units and electrical connections between consumption points but does not consider the installation and management of dispatchable generators. In [101] the design of a distributed multi-node CHP system featuring dispatchable and non-dispatchable DERs is optimized via a MILP in both on-grid and off-grid scenarios. Although partial load operation is allowed for dispatchable units, a constant efficiency is assumed for the machines. The effect of components wearing on their lifetime is also not accounted for. Most importantly, the model does not deal with the non-deterministic nature of renewable energy production, nor performs a re-evaluation of the microgrid performance with limited future foresight.

8.2 Hybrid Microgrid Architecture

The developed design optimization model is limited to off-grid hybrid microgrid featuring the general architecture shown in Figure 48 [102].

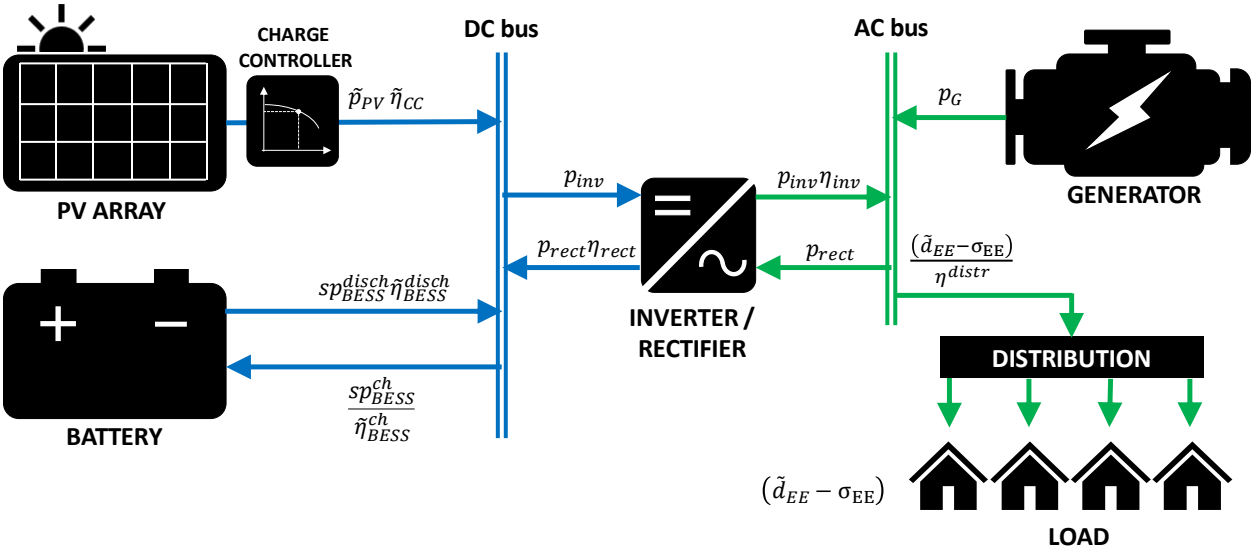

Figure 48: hybrid microgrid architecture

A photovoltaic (PV) array and a battery energy storage system (BESS) are connected to the direct current (DC) bus, which can bi-directionally exchange energy with the alternate current (AC) bus via an

inverter/rectifier. The microgrid load and a dispatchable generator are directly connected to the AC bus. Network losses are only accounted for in the connection between the AC bus and the load, by means of an average distribution loss efficiency η^{distr}, increasing the perceived demand on the AC bus. Network losses between the generation and storage units are neglected, as the components are assumed to be close to one another. The efficiencies of the PV array charge controller and of the inverter/rectifier are also accounted for.

Two power balances are imposed on the AC and DC buses, which are connected by an inverter / rectifier allowing for bi-directional power conversion. In the model formulation introduced in Chapter 3, this is equivalent to consider AC and DC power fluxes as distinguished virtual goods, with the inverter/rectifier acting as a connector linking the two bus balances, according to conversion efficiencies $\tilde{\eta}_{inv}$ / $\tilde{\eta}_{rect}$. The electrical load is modeled as a non-dispatchable AC load, split in high and low priority components $\tilde{d}_{HP,t}$ and $\tilde{d}_{LP,t}$, associated to different unmet penalties:

$$\begin{cases} p_{PV,t}\tilde{\eta}_{CC} + dp_{BESS,t}\tilde{\eta}_{BESS}^{disch} - \frac{cp_{BESSt}}{\tilde{\eta}_{BESS}^{ch}} - p_{inv,t} + p_{rect,t}\tilde{\eta}_{rect} = 0 \\ p_{G,t} + p_{inv,t}\tilde{\eta}_{inv} - p_{rect,t} = \frac{(\tilde{d}_{HP,t}-\sigma_{HP,t})+(\tilde{d}_{LP,t}-\sigma_{LP,t})}{\tilde{\eta}_{distr}} \end{cases} \quad \forall t \qquad (145)$$

where:

- Power injected by the PV array on the DC bus is equal to the power produced by the panels (p_t^{PV}) multiplied by the efficiency of its charge controller ($\tilde{\eta}^{CC}$);
- Power injected by the battery on the DC bus is equal to the power discharging from the battery ($sp_{BESS,t}^{disch}$) multiplied by the battery discharging efficiency ($\tilde{\eta}_{BESS}^{disch}$);
- Power withdrawn from the DC bus by the battery is equal to the power charging the battery ($sp_{BESS,t}^{ch}$) divided by the battery charging efficiency ($\tilde{\eta}_{BESS}^{ch}$);
- p_t^{RECT} is the power withdrawn from the AC bus and injected by the rectifier (with efficiency $\tilde{\eta}^{rect}$) on the DC bus;
- P_t^{inv} is the power withdrawn from the DC bus and injected by the inverter (with efficiency $\hat{\eta}^{inv}$) on the AC bus;
- $p_{G,t}$ is the power production by the generator;
- $(\tilde{d}_{HP,t} - \sigma_{HP,t})$ and $(\tilde{d}_{LP,t} - \sigma_{LP,t})$ are respectively the high priority and low priority served loads: $\tilde{d}_{HP,t}$ / $\tilde{d}_{LP,t}$ is the reference high / low priority energy demand of microgrid users, $\sigma_{HP,t}$ / $\sigma_{LP,t}$ is the high / low priority unmet load, and $\tilde{\eta}_{distr}$ is the efficiency of the distribution network.

Starting from:

- Reference aggregate demand profiles, defined by the single profiles of all customers within the boundaries of an electrification cluster and
- Per-unit PV generation potential profile characterizing typical radiation conditions of the location

the objective of the design optimization is to minimize the sum of annuitized investment cost and operation costs (*annuity*), which in turn determine the Levelized Cost of Electricity (LCOE) for the microgrid users. The design is defined by the number, size, and typology of installed components, namely:

- Technology and size of the dispatchable generator;
- Technology and number of PV modules constituting the PV field;
- Technology and number of BESS modules constituting the system electrochemical storage;
- Size of the inverter/rectifier

Components selection is based on an equipment catalog, listing technical and economic characteristics of different type of options for each component class. A uniform modeling approach is adopted for the alternative PV and BESS technologies, which are therefore characterized based on a standard set of model parameters. Details of the considered modeling approach are presented in Paragraph 8.4.2. Similarly, the catalog includes various models of generators of different sizes, each associated with a specific characteristic curve and technical parameters. Because of the relatively simple customizability of inverter/rectifiers, the size of this component can be varied continuously and is not selected from a discrete list. A variable specific installation cost is on the other hand considered, to account for economies of scale.

Table 28: information included in the generation catalog for each component class

Unit	Technical parameters	Cost parameters
GENERATORS (ICE)	• Rated power • Load-fuel curve • Max / min load • Lifetime operating hours • Start-up penalty	Machine cost Installment cost Yearly O&M
BESS	• Module capacity • Module max / min SOC • Charge/discharge efficiency • Max charge /discharge current • Nominal voltage • KiBaM model parameters • Lifetime energy throughput	Module cost Installment cost Yearly O&M
PV	• Module rated power • Lifetime • Per-unit generation potential profile	Module cost Installment cost Yearly O&M
INV/REC	• Inverter / rectifier efficiency • Inverter / rectifier size ratio • Lifetime	Specific cost curve Installment cost Yearly O&M

Table 28 summarizes the information contained in the catalog. The only generation technology considered in the calculations are diesel internal combustion engines. A limited subset of the operating constraints described in Chapter 3 is therefore implemented, but the design model is in principle extendible to include any type of generation technology, by adding if necessary additional operating constraints, as per the

general formulation of Chapter 3. The catalog could, therefore, be extended according to the exposed guidelines, to account for additional generation / storage technologies.

8.3 Microgrid design optimization

The MILP-based design optimization algorithm (hereafter referred to as *Predictive Algorithm*, PA) described in this Chapter has been developed to serve as an alternative sizing method to the heuristic sizing routine (*Heuristic Algorithm*, HA) developed at MIT Universal Energy Access Laboratory [103]. Both algorithms, given a certain aggregate load profile and the local renewable generation potential, define an optimal configuration of generation and storage systems that aims at minimizing the system annuitized total cost.

Both PA and HA are based on a two-step approach. First, a "*design sub-problem*" selects the optimal generation and storage technologies and sizes, evaluating the system operation over four weeks representative of the whole typical year. Considering only a subset of the typical year timespan is necessary to limit the problem size and therefore the computational time. Additionally, often only average seasonal data are available for a given location, allowing for the characterization of typical seasonal weeks. If the location shows significant seasonal variability in radiation and/or demand patterns, typical weeks and their corresponding weights on the objective function would need to be determined by a more accurate clustering process, similarly to what is done in [104]. In the case study under analysis, the low seasonality of demand profiles within the region simplifies the selection process of the characteristic weeks, which were therefore equally spaced within the year covering the four seasons. Second, the "*operation sub-problem*" tests the selected design over the entire typical year, accurately estimating the yearly system operating cost and components wearing. The results obtained from both sub-problems are finally combined to provide the resulting system annuity and LCOE estimate.

The HA relies on an iterative search of the design space, based on the fitness of each candidate system configuration. Both in the "*design"* and "*operation"* sub-problems, dispatch decisions are based on the heuristic and non-predictive Advanced Battery Valuation strategy [15], and the design space exploration is therefore decoupled from the dispatch decisions taken in the operation sub-problem that simply evaluates the performance of a fixed-architecture candidate solution.

Conversely, the PA solves the "*design sub-problem*" optimizing at the same time design and dispatch decisions. The optimization problem is formulated as a single MILP, constituting an adaptation of the optimal dispatch MILP described in Chapter 3. Binary investment variables, in addition to operating set-points of all units, constitute the variables of the optimization problem. The problem encompasses the entire design reference period, and therefore the optimization algorithm has an omniscient vision of future profiles of solar radiation and load. This approach has the advantage of allowing for the easy and effective inclusion of constraints over specific time spans, like minimum annual system reliability or daily/weekly fuel consumption limits. In two-layers algorithm (e.g. the HA), seasonal constraints are accounted for a-posteriori, discarding or penalizing the design solutions that do not enforce them without accounting for potential modifications in the dispatch strategy that could avoid violating the constraints. On the other hand, in single-

layer algorithms, the dispatch profile that set design fitness is associated to an unrealistic perfect knowledge of load and radiation profiles across the whole design reference period, which result in an optimistic evaluation of actual operating costs. This unrealistic assumption is made less critical by the introduction in the design sub-problem of two types of reserve constraints:

- *Spinning reserve* constraints (Eq.(47)-(49)), which impose to account for generation margins that allow compensating net demand fluctuations;
- Capacity reserve margins, which introduce a slight oversizing of critical components (e.g. I/R, PVCC) that increases the design solution conservativeness.

Table 29: general scheme of the main differences between HA and PA approaches in the solution of design and operation sub-problems

		HA	**PA**
Design sub-problem	**Output**	Optimal equipment sizing	Optimal equipment sizing
	Considered period	Four representative weeks	Four representative weeks
	Equipment typology and size	Optimized	Optimized
	Method of optimization	Grid search	MILP ("*one shot"*)
	Objective function	Minimization of system annuity	Minimization of system annuity
	Dispatch strategy	Pre-determined prioritization rules among resources, applied to actual operating conditions	Optimized
	Additional notes	Dispatch decision rules are independent from design decisions	Accurate BESS and ICE wear cost are included in the optimization and power reserve is enforced
	Output	Investment decisions	Investment decisions
Operation sub problem	**Considered period**	Full year (8760 hours)	Full year (8760 hours)
	Equipment typology and size	Fixed by the design sub-problem	Fixed by the design sub-problem
	Method of optimization	Rule based, applied to actual operating conditions	MILP (*Rolling Horizon*)
	Objective function	None. Rule based.	Minimization of operational cost, including BESS and ICE wear cost
	Dispatch strategy	Pre-determined prioritization rules among resources, applied to actual operating conditions	Optimized
	Additional notes	none	Power reserve is enforced
	Output	Yearly dispatch profiles	Yearly dispatch profiles, now with updated dispatch assuming perfect 24-hour forecast

The second layer of the PA overcomes the initial assumption, evaluating the actual yearly performance by solving a realistic "*operation sub-problem"* adopting a rolling horizon (RH) approach: the actual hourly dispatch strategy is optimized only based on near future (24 hours) forecast of RES energy production and load consumption, which can be estimated with good confidence. The additional dispatch update that would be needed to adapt the dispatch solution to the actual net demand manifestation is not explicitly modeled in this work, since it has already been extensively proven that, with adequate reserve margins, the predictive

solution is capable of dealing with forecasts uncertainty. Both MILP were formulated in MATLAB, using the toolbox YALMIP [105].

A scheme of the main differences among the two methods and the two sub-problems is reported in Table 29.

8.3.1 Design objective function

The objective of the design optimization is to minimize the overall system cost, comprising both investment costs (sustained every time a component is purchased / replaced), and operating costs. Due to inhomogeneity of cost indexes temporal distribution, an equivalent parameter accounting for differences in the discount rate to be applied must be considered. To this end, the concept of *annuity* is adopted as problem objective function. Annuity represents an equivalent fixed amount of money that the investor would have to spend each year to purchase, operate and maintain the microgrid, for an indefinite amount of time. It is equivalent to a Net Present Costs calculated over an infinite investment evaluation horizon and distributed homogeneously across the investment lifetime. The annuity cash flow, expressed in year zero currency, is therefore composed of by yearly operating cost $OPEX$ and the sum of all components investment /replacement cost $CAPEX_i$ annuitized according to annuity factor AF_i.

$$Annuity = \sum_i [CAPEX_i \cdot AF_i] + OPEX \tag{146}$$

The yearly operating costs is estimated based on dispatch profiles associated to the solution of the design optimization problem. Operating cost is considered representative of all future years, therefore neglecting the effect of wearing on components performance as well as potential changes in the shape of demand profiles. Accounting for these changes would require performing simulations of the operation on multiple years, which would in turn increase the size of the design problem and its computational complexity. Operating costs include fuel cost for all generators, operation and maintenance costs for each microgrid component, and a virtual penalization for non-served energy:

$$OPEX = \sum_i O\&M_i + \sum_t \left[\sum_g f_{g,t} + c_t^{UM} \right] \cdot K^{prorate} \tag{147}$$

Purchase/replacement costs is annuitized according to the annuity factor AF_i, accounting for

- yearly discount rate $\widetilde{dr}$, representing the expected return on invested capital (considering inflation rate, equity / debt cost, and investment risk) and according to which cash flows sustained in different years are made comparable;
- frequency at which the investment cost is sustained, to replace the component at the end if its lifetime LT_i.

The annuity factor yielding the annuitized investment cost fraction for component i is therefore calculated as:

$$AF_i = \frac{\widetilde{dr}}{1-(1+\widetilde{dr})^{LT_i}} \tag{148}$$

For some components, like PV panels or the I/R, lifetime is constant. For other components, as generators and batteries, lifetime depends on the component usage pattern, that affects its wearing process. In the case of generators, lifetime is defined as the total amount operating hours $\widetilde{H}_o^{G,MAX\ LT}$. Actual lifetime duration is therefore calculated according to the actual generator yearly operating hours $H_o^{G,year}$:

$$LT^{ICE} = \frac{\widehat{H}_o^{ICE,MAX\ LT}}{H_o^{ICE,year}} \tag{149}$$

The lifetime of BESS system is expressed as Life-Time Through-Put (LTTP), that is the overall energy which can flow through the battery before it needs to be replaced. LTTP is in turn proportional to number of battery modules n^{BESS}, life-time energy throughput that can be provided by a single module during its lifetime $\widehat{E}^{BESS,MAX\ LT}$. Lifetime duration is then calculated based on the actual BESS yearly energy output $E^{BESS,year}$:

$$LT^{BESS} = \frac{n^{BESS}\widehat{E}^{BESS,MAX\ LT}}{E^{BESS,year}} \tag{150}$$

It is worth noting that this link between dispatch decisions and component lifetime (and therefore system annuity) is fully accounted for by the PA method in the solution of the "*design sub-problem",* while the HA approach simply accounts for it in the calculation of the annuity, and considers battery replacement cost when taking dispatch decisions only as a fixed operation and maintenance cost, based on an estimate of the actual BESS lifetime.

The LCOE is finally calculated as the ratio between the equivalent annual cost and the overall demand served. The equivalent annual cost for the system is calculated as the sum of:

- The annuitized investment cost for the selected equipment: size and technology are determined by the "*design sub-problem*", but the annuity factor of ICE and BESS is updated based on their actual yearly usage, determined in the "*operation sub-problem*";
- The annual operating cost associated to the yearly dispatch profiles yielded by the solution of the "*operation sub-problem".* Load shedding cost is not included, since its scope is simply to affect the objective function, ensuring a higher quality of the service, but it does not represent a real cash flow.

8.4 MILP Design Problem Formulation

8.4.1 Annuitization of variable life-time components in PA

In the objective function, the actualization coefficients for ICE and BESS investment cost are a non-linear function of both the investment and operation variables (Eq.(149)-(150)). The actualized non-linear investment cost function is on the other hand convex with respect to its variables in the space of interest. It can therefore be approximated by means of a real variable, lower bounded by a family of linear constraints constituted by a set of lines (or planes) tangent to the original non-linear cost curve (or surface). In the

optimal solution of the MILP, the annuitized cost linear proxy will be as low as possible, and therefore bounded by this set of constraints. The spacing of the tangent points determines the accuracy of the annuitized investment cost proxy and can be controlled arbitrarily by increasing the number of tangent points as shown in Figure 49.

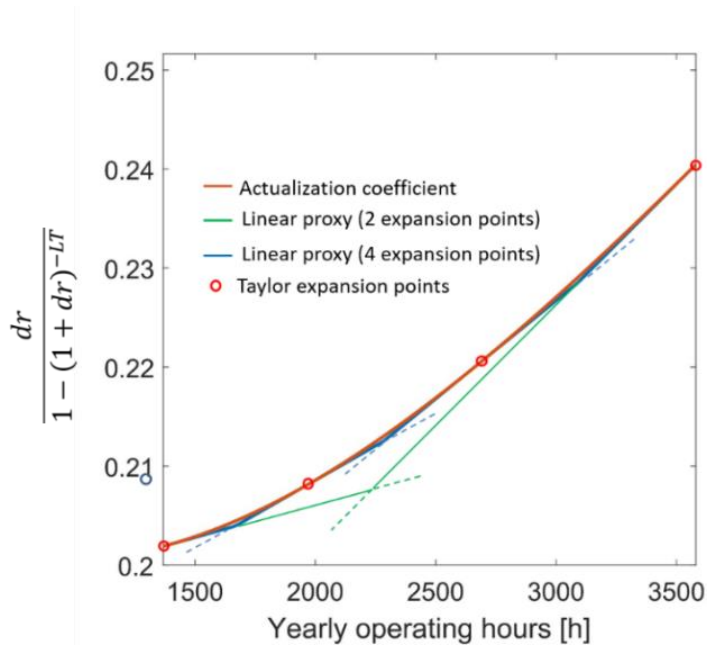

Figure 49: Non-linear ICE actualization coefficient as function of yearly operating hours (orange line) and family of linear coefficients that serve as lower bound with adjustable precision. The linear proxy characterized by 4 expansion points follows more closely the actual value of the actualization coefficient.

The approach is equivalent with the technique explained in Paragraph 3.4.1 for dispatchable generators with convex part-load curve. More details on the specific annuitized investment cost formulation adopted for BESS and generators are provided respectively in paragraphs 8.4.2.3 and 8.4.2.5.

8.4.2 Modeling Assumptions

The following paragraphs describe the adaptations of the general formulation presented in Chapter 3 for the optimal operation problem, specifying how the constraints for each component type have been modified in order to introduce design variables in the PA design problem.

8.4.2.1 Photovoltaic (PV) array

The PV array is formed by a discrete number of modules n_{PV}, selected among one of the technologies listed in the generation catalogue. Each PV technology $i \in \boldsymbol{\mathcal{PV}}$ is associated to a per-unit generation potential profile $\tilde{p}_{i,t}$, representing the specific array power output corresponding to typical yearly ambient conditions (irradiance and temperature) characteristic of the geographical location and technological performance of the module technology. PV excess production can be curtailed with respect to Maximum Power Point (MPP) power, by acting on the PV charge controller, delivering only a fraction of the generation potential on the DC bus. The product of number of installed modules and per-unit production profile determines the MPP generation, constituting an upper bound for PV power $p_{PV,t}$ dispatched on the DC bus:

$$p_{PV,t} \leq \sum_{i \in \mathcal{PV}} \tilde{p}_{i,t} \cdot n_i^{PV} \qquad \forall t \in \mathcal{T} \qquad (151)$$

Technology selection variables I_i^{PV} determines the typology selected for the PV array, bounding the number of installed models according to $\tilde{n}_i^{max}$. A single PV technology can be active at a time:

$$n_i^{PV} \leq I_{PV,i} \tilde{n}_i^{max} \qquad \forall t \in \mathcal{T} \qquad (152)$$

$$\sum_{i \in \mathcal{PV}} I_{PV,i} \leq 1 \qquad (153)$$

PV array annuitized CAPEX is yield by the sum over all PV technologies of the annuitized investment cost, computed as product of number of panels and single panel purchase cost. A technology-specific lifetime $\widetilde{LT}_i$, independent from operating decisions, is considered in the annuitization coefficient:

$$CAPEX_{PV}^{ann} = \sum_{i \in \mathcal{PV}} \frac{\tilde{c}_i^{PV} \cdot n_i^{PV} \cdot \widetilde{dr}}{1 - \left(1 + \widetilde{dr}\right)^{-\widetilde{LT}_i}} \qquad (154)$$

8.4.2.2 PV Charge Controller

The maximum power dispatched on the DC bus determines the size of the PV Charge Controller (PVCC) coupled to the PV array, which might be undersized with respect to PV array peak power. Charge controller size is assumed to be modifiable with continuity, but a minimum size threshold is introduced. The efficiency of the charge controller is assumed not to depend on its size:

$$p^{nom,CHC} \geq p_{PV,t} \cdot \tilde{\eta}_{CC} \qquad \forall t \in \mathcal{T} \qquad (155)$$

$$p^{nom,CHC} \geq \tilde{p}^{min,CC} \cdot \sum_{i \in \mathcal{PV}} I_{PV,i} \qquad (156)$$

PVCC specific investment cost tends to decrease with size, due to economies of scale. Based on the provided catalog of models available on the market, a cost-size interpolant function can be defined. The function can then be approximated via a piece-wise function, according to the methodology shown for machines characteristic curves in Chapter 3. If the range within which the size of the PVCC will fall can be estimated with confidence, a simpler approach consists in considering a linear size-cost curve defined by coefficients $\tilde{m}^{CHC}$ and $\tilde{q}^{CHC}$, obtained as local linearization of the original non-linear interpolant. In this case, annuitized PVCC investment cost is yield by:

$$CAPEX_{PVCC}^{ann} = \left(\tilde{m}^{CHC} \cdot p^{nom,CHC} + \sum_{i \in CAT^{PV}} I_i^{PV} \cdot \tilde{q}^{CHC} \right) \cdot \frac{\widetilde{dr}}{1 - \left(1 + \widetilde{dr}\right)^{-\widetilde{LT}_{CC}}} \qquad (157)$$

A constant PVCC lifetime $\widetilde{LT}_{CC}$, independent from its size, is considered.

8.4.2.3 Battery Energy Storage System (BESS)

The battery stack is constituted of a discrete number of modules n_i^{BESS}, selected from a technology list $i \in \mathcal{BESS}$, associated to different nominal module energy capacity $\hat{E}_i^{mod}$ and State of Charge (SOC) boundaries $\widehat{SOC}_i^{max}$ / $\widehat{SOC}_i^{min}$. Energy content $E_{i,t}$ is therefore bounded by an upper and lower limit depending on technology and number of installed modules:

$$n_i^{BESS} \cdot \hat{E}_i^{mod} \cdot \widehat{SOC}_i^{min} \leq E_{i,t} \leq n_i^{BESS} \cdot \hat{E}_i^{mod} \cdot \widehat{SOC}_i^{max} \qquad \forall t \in \boldsymbol{\mathcal{T}}, i \in \boldsymbol{\mathcal{BESS}} \quad (158)$$

The dynamic evolution of the BESS energy content is given by the usual storage dynamic equation:

$$E_{i,t+1} = E_{i,t} + cp_{i,t} - dp_{i,t} \qquad \forall t \in \boldsymbol{\mathcal{T}}, i \in \boldsymbol{\mathcal{BESS}} \quad (159)$$

To count on a more general battery modeling approach, capable of dealing with multiple battery technologies, The Kinetic Battery Model described in [60] is adopted for all battery technologies, consistently with the commercial design software HOMER [82]. The model is based on a linearization of the internal battery kinetics, and it divides stored energy in two fractions: energy readily available to be exchanged $E_{i,t}^1$, and energy chemically bonded within the battery and therefore not accessible to be exchanged $E_{i,t}^2$. A set of equations describes the dynamic transition of energy from the bounded to the readily available state, as a function of the technology-specific kinetic parameters $\hat{k}_i$ and $\hat{c}_i$.

$$E_{i,t+1}^1 = E_{i,t}^1 \cdot e^{-\hat{k}_i} + E_{i,t} \cdot \hat{c}_i \cdot \left(1 - e^{-\hat{k}_i}\right) + E_{i,t+1} \cdot \frac{1}{\hat{k}_i}\left(1 - e^{-\hat{k}_i} + \hat{c}_i \cdot \left(\hat{k}_i + e^{-\hat{k}_i} - 1\right)\right) \qquad \forall t \in \boldsymbol{\mathcal{T}}, i \in \boldsymbol{\mathcal{BESS}} \quad (160)$$

$$E_{i,t}^2 = E_{i,t} - E_{i,t}^1 \qquad \forall t \in \boldsymbol{\mathcal{T}}, i \in \boldsymbol{\mathcal{BESS}} \quad (161)$$

The kinetic BESS internal state evolution in turn also affects maximum charge /discharge power:

$$cp_{i,t} \leq \frac{\hat{c}_i \cdot n_i^{BESS} \cdot \hat{E}_i^{mod} + E_{i,t}^1 \cdot e^{-\hat{k}_i} + E_{i,t} \cdot \hat{c}_i \cdot \left(1 - e^{-\hat{k}_i}\right)}{\frac{1}{\hat{k}_i}\left(1 - e^{-\hat{k}_i} + \hat{c}_i \cdot \left(\hat{k}_i + e^{-\hat{k}_i} - 1\right)\right)} \qquad \forall t \in \boldsymbol{\mathcal{T}}, i \in \boldsymbol{\mathcal{BESS}} \quad (162)$$

$$dp_{i,t} \leq \frac{E_{i,t}^1 \cdot \hat{k}_i \cdot e^{-\hat{k}_i} + E_{i,t} \cdot \hat{c}_i \cdot \hat{k}_i \cdot \left(1 - e^{-\hat{k}_i}\right)}{\left(1 - e^{-\hat{k}_i} + \hat{c}_i \cdot \left(\hat{k}_i + e^{-\hat{k}_i} - 1\right)\right)} \qquad \forall t \in \boldsymbol{\mathcal{T}}, i \in \boldsymbol{\mathcal{BESS}} \quad (163)$$

Although originally developed for lead-acid batteries, by tuning the kinetic parameters the KiBaM can be used to represent a wide range of different battery technologies. Specifically, by setting high kinetic constants the entire energy content of the battery is collapsed in readily available energy, tracing back to the "single-tank" model described in Chapter 3, suitable for example for lithium-ion batteries.

As already mentioned, the lifetime of each battery stack is determined by its lifetime energy throughput, which represents the maximum energy flow that the stack can sustain before having to be replaced (Eq.(150)). The annuitized BESS investment cost is, therefore, a non-linear function of the number of installed modules n_i^{BESS} and the yearly usage $E_i^{BESS,year}$.

$$CAPEX_{BESS,i}^{ann} = \frac{n_i^{BESS} \tilde{c}_i^{BESS} \widetilde{dr}}{1 - \left(1 + \widetilde{dr}\right)^{-\frac{n_i^{BESS} \hat{E}_i^{LTTP}}{E_i^{BESS,year}}}} = f\left(n_i^{BESS}, E_i^{BESS,year}\right) \qquad \forall i \in \boldsymbol{\mathcal{BESS}} \quad (164)$$

Where:

- $\tilde{c}_i^{BESS}$ is the module cost for battery technology $i \in \boldsymbol{\mathcal{BESS}}$;

- $\hat{E}_i^{LTTP}$ is the energy lifetime throughput for battery technology $i \in \boldsymbol{\mathcal{BESS}}$;
- $E_i^{BESS,year}$ is the yearly battery throughput, depending on dispatch decisions $dp_{i,t}$:

$$E_i^{BESS,year} = \sum_{t \in T^{des}} (dp_{i,t}) \cdot K^{prorate} \tag{165}$$

The annuitized BESS investment cost function $f\left(n_i^{BESS}, E_i^{BESS,year}\right)$ is on the other hand convex in both variables. The non-linear cost term can therefore be represented through a family of linear constraints, representing tangent planes to the original cost function in a series of points $j \in \boldsymbol{\mathcal{J}}$, and setting a lower bound to $CAPEX_{BESS,i}^{ann}$:

$$CAPEX_{BESS,i}^{ann} \geq \widehat{m}_{j'}^{KP} \cdot \sum_{t \in T} (dp_{i,t}) + \widehat{m}_{j'}^{Kn} \cdot n_i^{BESS} + \hat{q}_{j'}^{K} \cdot I_i^{BESS} \tag{166}$$

Where I_i^{BESS} is the binary investment variable of storage technology $i \in \boldsymbol{\mathcal{BESS}}$. The selection of a single storage technology, coherently with the microgrid architecture shown in Figure 48, is enforced by bounding the summation of storage binary investment variables I_i^{BESS}:

$$\sum_{i \in \boldsymbol{\mathcal{BESS}}} I_i^{BESS} \leq 1 \tag{167}$$

Finally, storage power output is computed by accounting for the potential contribution of all storage technologies:

$$dp_{BESS,t} = \sum_{i \in \boldsymbol{\mathcal{BESS}}} dp_{i,t} \tag{168}$$

$$cp_{BESS,t} = \sum_{i \in \boldsymbol{\mathcal{BESS}}} cp_{i,t} \tag{169}$$

8.4.2.4 Inverter / Rectifier

An Inverter / Rectifier (I/R) must be installed if either a battery stack and/or a PV array is included in the microgrid, to allow for DC/AC and AC/DC conversion respectively represented by the non-negative net flux components $p_{inv,t}$ and $p_{rect,t}$. IR size is determined by the maximum power exchange between the DC and AC buses, accounting for a fixed nominal power ratio $\widetilde{R2I}$ between the inverter and the rectifier operating modes. The most restrictive condition associated to one of the opposite power flows sets the I/R nominal size $p^{nom,IR}$:

$$0 \leq p_{inv,t} \leq \frac{p^{nom,IR}}{\tilde{\eta}_{inv}} \tag{170}$$

$$0 \leq p_{rect,t} \leq p^{nom,IR} \cdot \widetilde{R2I} \tag{171}$$

Inverter / rectifier efficiencies $\tilde{\eta}_{inv}$ / $\tilde{\eta}_{rect}$ and lifetime are assumed to be independent from its size. As seen in the case of PVCC, A non-linear specific cost curve computed from the generation catalog by interpolating the discrete dataset of commercial models, to take into account economies of scale. Piece-wise linearization

can then be used to fully represent the whole non-linear cost curve, or a local linear interpolant can be defined based on the expected I/R size. In this case, the annuitized investment cost is yield by:

$$CAPEX_{IR}^{ann} = (\widetilde{m}^{IR} \cdot P^{nom,IR} + \tilde{q}^{IR} \cdot I^{IR}) \cdot \frac{\widetilde{dr}}{1 - \left(1 + \widetilde{dr}\right)^{-\widetilde{LT}_{IR}}} \tag{172}$$

Where $\widetilde{m}^{IR}$ and $\tilde{q}^{IR}$ are the local linearization coefficients and $\widetilde{LT}_{IR}$ the I/R lifetime.

8.4.2.5 Generators

A discrete list of generators among which to choose must be included in the generation catalog. Each generator is defined by a part-load curve, linking power production and fuel consumption, as described in Paragraph 3.4.1. A simple linear part-load curve was considered in the model, to limit computational complexity. On the other hand, the characteristic curve of diesel Internal Combustion Engines (ICE), which are the main generators of interest, can generally be very well fitted through a linear interpolant (Figure 39). In principle, all constraints for dispatchable machines presented in Paragraph 3.4.1 could be included in the design problem. Nevertheless, due to the coarse temporal resolution normally considered in design studies (1 h timesteps), only a subset of the operating constraints has been included in the formulation:

- maximum and minimum load limits (Eq.(9))
- ramping limits (Eq(10))
- minimum up/down time (Eq.(12)(13))
- start-up additional consumption (Eq.(14))

A binary investment variable I_i^G links the presence of each generator $i \in \boldsymbol{\mathcal{G}}$ to its investment cost, by setting a limit on its on/off variable $z_{i,t}$:

$$\sum_{t \in T} z_{i,t} \leq I_i^G \cdot T^{des} \tag{173}$$

Where T^{des} is the duration in hours of the design sub-problem. As seen for batteries, the annuitized investment cost of each generator is a non-linear function of its investment decision and dispatch profile, i.e. of its yearly operating hours:

$$CAPEX_i^{ann} = \frac{I_i^G \tilde{c}_i^{ICE} \widetilde{dr}}{1 - \left(1 + \widetilde{dr}\right)^{-\frac{\widehat{H}_o^{ICE,MAX\,LT}}{H_o^{ICE,year}}}} = f(I_i^G, H_o^{ICE,year}) \tag{174}$$

Where:

- $\tilde{c}_i^{ICE}$ is the generator investment cost;
- $H_o^{ICE,year}$ is the generator yearly operating hours, defined as:

$$H_o^{ICE,year} = \sum_{t \in T} z_{i,t}\, K^{prorate} \tag{175}$$

Since the annuitized investment cost is a convex function of yearly operating hours, it can be represented through a family of linear constraints, representing tangent lines to the original cost function in a series of points $j \in \mathcal{J}$, and setting a lower bound to $CAPEX_{G,i}^{ann}$:

$$CAPEX_{G,i}^{ann} \geq \widehat{m}_{j'}^{G} \cdot \sum_{t \in T} z_{i,t} \, K^{prorate} + \hat{q}_{j'}^{G} \cdot I_i^G \tag{176}$$

A limit on the number of installable generators (equal to 1 in the considered architecture) is finally enforced by bounding the summation of all generators investment variables:

$$\sum_{i \in \mathcal{G}} I_i^G \leq 1 \tag{177}$$

Finally, generator power output is computed by accounting for the potential contribution of all generators:

$$p_{G,t} = \sum_{i \in \mathcal{G}} p_{i,t} \tag{178}$$

8.4.3 Spinning reserve requirements

The usual reserve constraint on generation capacity is enforced to ensure that the system is able to face instantaneous and unforeseen variations of demand and renewable generation during real operation. It is assumed that granted this margin, the ICE and BESS are capable to handle real-time active net demand variations and frequency regulation according to their droop curve and to a real-time redispatch algorithm. The maximum power contribution in each hour from BESS and active generators must therefore be enough to satisfy the worst-case net demand, accounting for planned service interruptions:

$$\begin{aligned} &\sum_{i \in \mathcal{G}} p_{i,t}^{max} \, z_{i,t} + \sum_{i \in \mathcal{BESS}} sp_{i,t}^{res} \, \hat{\eta}_i^{disch} \hat{\eta}^{inv} \qquad \forall t \\ &\qquad \geq \left(1 + \widehat{\Delta D}^{\%}\right)\left(\widehat{D}_{(t)} - \pi_{(t)}\right) - P_{(t)}^{PV}\left(1 - \widehat{\Delta PV}^{\%}\right)\hat{\eta}^{CHC}\hat{\eta}^{inv} \end{aligned} \tag{179}$$

Where:

- $p_{i,t}^{max}$ is the maximum power that can be provided by the ICE;
- $z_{i,t}$ is the binary variable that defines if the ICE is switched on (1) or off (0);
- $sp_{i,t}^{res}$ is the maximum reserve power that can be provided by the battery stack, defined as the minimum between storage maximum power and storage full discharge power:

$$\begin{aligned} sp_{i,t}^{res} &\leq \frac{E_{i,t}^{1} \cdot \hat{k}_i \cdot e^{-\hat{k}_i} + E_{i,t} \cdot \hat{c}_i \cdot \hat{k}_i \cdot \left(1 - e^{-\hat{k}_i}\right)}{\left(1 - e^{-\hat{k}_i} + \hat{c}_i \cdot \left(\hat{k}_i + \, e^{-\hat{k}_i} - 1\right)\right)} \\ sp_{i,t}^{res} &\leq \left(E_{i,t} - n_i^{BESS} \cdot \hat{E}_i^{mod} \cdot \widehat{SOC}_i^{min}\right) \end{aligned} \tag{180}$$

- $\widehat{\Delta D}^{\%}$ and $\widehat{\Delta PV}^{\%}$ are the percentage variations to be considered for energy demand and PV production respectively, in defining the worst-case net power that serves as spinning reserve requirement. Both are set to 25%.

8.5 PA Operation sub-problem

Since the dispatch strategy in the "*design sub-problem"* can benefit from the unrealistic exact knowledge of future PV and load trends, once the optimal design has been determined (e.g. the optimal investment variables of the PA design problem), the actual yearly operation cost is computed in the "*operation sub-problem*", adopting a more realistic *rolling horizon* (RH) methodology: the dispatch MILP is conservatively solved for a limited future horizon (24 h), for which weather and demand forecasts are known with perfect accuracy. Once the problem is solved, the obtained solution is implemented only for an initial fraction of the time (6 h), then the starting time is moved forward, and the procedure is repeated until the entire time range has been spanned. It is acknowledged that the perfect day-ahead forecast provides some advantage over the actual operation over an uncertain horizon, but we are relying of the good quality of 24 hour ahead forecasts and on its update every 6 hours. The full accounting of the effect of uncertainty on the predictive management of hybrid off-grid microgrid is discussed in detail in Chapter 7.

The objective function of each dispatch MILP is the minimization of the operational cost of the system, comprising fuel cost, cost of non-served energy, and wearing cost of generator and battery, representing a specific O&M cost index. Specific wearing cost is calculated distributing the component annuitized investment cost estimated in the design sub-problem over the corresponding yearly usage, as reported in equation (181). By doing so, wearing cost leads the yearly operation dispatch to converge to a value of BESS and ICE lifetime close to what is found as optimal in the "*design sub-problem"*, tuning the actualized investment cost achieved by the two simulations.

$$c_G^{wear} = \frac{CAPEX_G^{ann}}{\sum_{t \in T^{des}} z_{i,t}\, K^{prorate}} \qquad c_{BESS}^{wear} = \frac{CAPEX_{BESS}^{ann}}{\sum_{t \in T^{des}} (\, dp_{i,t}) \cdot K^{prorate}} \tag{181}$$

Finally, system annuity is re-computed combining sizing information determined by the *design sub-problem* and the optimal yearly dispatch strategy yield by the *operation sub-problem*. All relevant non-linear cost functions (e.g. generator part-load curve, I/R and PVCC specific investment cost) are included in their non-linear form in this last stage. Therefore, all errors introduced by the MILP linearization process can only influence the quality of the optimal MILP solution, not the value of the LCOE itself.

8.6 Heuristic design algorithm (HA)[2]

The HA design approach is based on an exploration of the design space through a direct search method [106], aiming at minimizing system annuity. For each candidate solution, system annuity is estimated by simulating system operation through the reference design period, according to the Advanced Battery Valuation (ABV) strategy described in [92].

ABV follows, time step after time step, a prioritization among the available generation units, to produce the instantaneous load and to charge the battery when considered economically convenient. No information about future load / radiation profiles is exploited, and no spinning reserve is enforced. The dispatch

[2] The heuristic algorithm employed in this paper is the one being used for microgrid optimization in a preliminary and simplified version of the Reference Electrification Model developed by the MIT/Comillas Universal Energy Access Lab. For more information see http://universalaccess.mit.edu.

prioritization list is built according to a specific energy production cost for each source: PV panels have null generation cost (absolute dispatch priority), ICEs specific generation cost is related to their part-load efficiency, whereas the cost of load shedding (which can be considered as an equivalent generation contribution) is set according to the required reliability of the system [92]. The cost of using the battery as a generation unit is weighted relatively to the other generators proportionally to its present state of charge: the closer the battery is to its maximum SOC, the higher its ranking in the prioritization list will be.

The units are dispatched from the least costly up, saturating their generation capacity until the load is satisfied. The effectiveness of the dispatch method versus other well-known heuristic dispatch strategies (Cycle Charge, Load Following) is thoroughly discussed in [92].

The HA looks for an optimal microgrid design by exploring a search space comprising various combinations of PV, BESS and ICE sizes. To enhance convergence and to avoid local minima, a bi-dimensional search for BESS and PV sizes is performed, fixing the ICE size. Starting from a center design point (red dot in Figure 50-left) the algorithm solves the hourly dispatch problem over the design sub-period for 8 surrounding combinations of PV and BESS sizes (blue points). In the following iteration, the center design point is moved to the point with the lowest system annuity among the ones explored thus far. If the new center is different from the previous one, the search radius identifying the neighbors remains unchanged (Figure 50-center) otherwise it is reduced (Figure 50-right). The search continues until the search radius is equal to the grid discretization.

An optimal combination of PV field and BESS sizes is identified for each ICE size considered. The ICE size is in turn varied according to two strategies: starting from the lowest to the highest reasonable ICE size available (the minimum size that can meet peak demand), and from the highest to the lowest. The two strategies stop the search when an annuity minimum with respect to ICE size is found (i.e. the annuity corresponding to optimal PV and BESS sizes increases with respect to the previous ICE size considered). The optimal solutions of the two strategies are then compared, and the one yielding the lowest annuity is selected as optimal design configuration. Finally, the actual optimal system annuity is recomputed exploring the operation throughout the full characteristic year in the *operation sub-problem*, as seen for the PA.

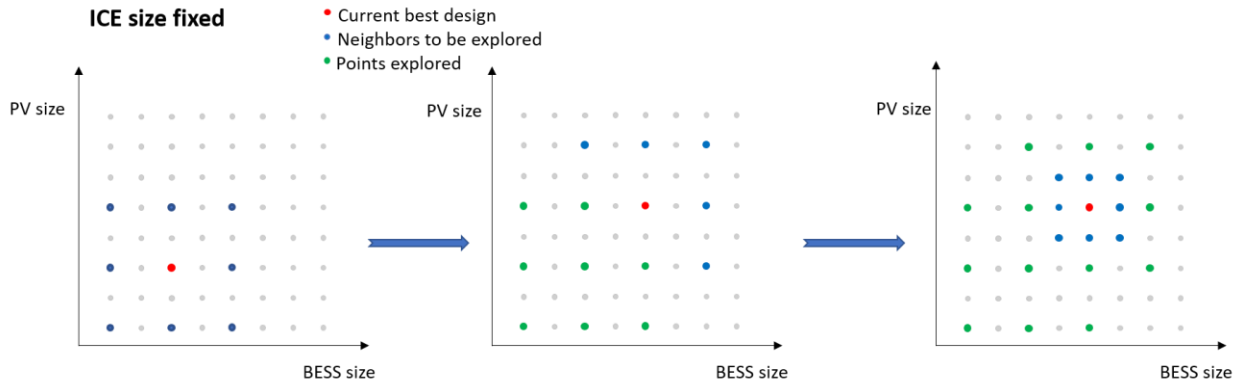

Figure 50: search algorithm for heuristic design

8.7 Comparison of HA and PA design and operation

The two design algorithms were compared in the framework of a test case representative of a rural region in sub-Saharan Africa[3], characterized in terms of local renewable generation potential and typology of non-electrified customers. Specifically, hourly patterns of electricity usage for ten different categories of users were based on a dataset provided by members of the MIT / Comillas Universal Energy Access Lab[4], elaborating the results of a field survey defining typical appliances associated to each class and life habits. Table 30 shows the users categories and the corresponding numerosity within the region. The methodology adopted in defining the energy consumption profiles is described in [107]: based on the rated power of each appliance, verbal descriptions of its usage pattern and considering an aleatory variation respect to the average profile, a library of different reference energy consumption profiles for each customer type has been produced. Examples of class-specific profiles are shown in Figure 51 for six different types of users. The black lines represent the annual average hourly load profiles while the two red dotted lines are the 5th and 95th percentiles, respectively.

Total number of buildings	47251		
Estimated number of currently electrified buildings	6435		
Numbers of non-electrified buildings			
Small residential	31879	Cooperatives	55
Large residential	7967	Government	8
Shops	768	Primary school	31
Banks	43	Secondary school	20
Churches	40	Hospitals	5

Table 30 test case consumers by type in the considered region

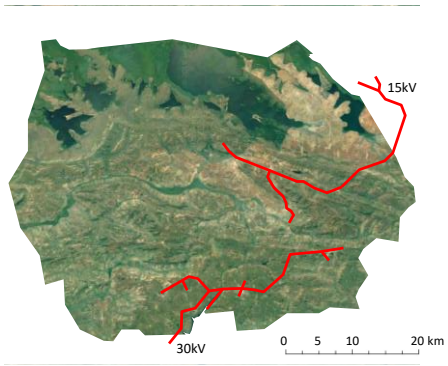

Optimal design and operation for a diverse set of clusters of users, covering a range of aggregate yearly energy demand, were identified using the two design algorithms. Multiple aggregate load profiles were created by preserving on average the same regional ratio between users of different classes and varying the total number of users within the microgrid, their composition, and the random association of each user to a characteristic profile from the profile library. By doing so, each microgrid size interval was characterized through a wide range of potential cases, different in terms of peak power and aggregate load pattern shape, in order to assess the differences between PA and HA approaches under the most general assumptions. Microgrid sizes go from stand-alone systems including only one building to very large systems encompassing a wide fraction of the region.

[3] Due to the existence of a non-disclosure agreement between the author's institution and the local distribution and transmission authority providing the dataset, the exact location of the region adopted as case study is not declared here.
[4] See http://universalaccess.mit.edu

Table 31 shows a comparison between PA and HA optimal component sizing for the 10 synthetic microgrids whereas Figure 52 shows the percentage savings achieved by the PA for all the investigated microgrids.

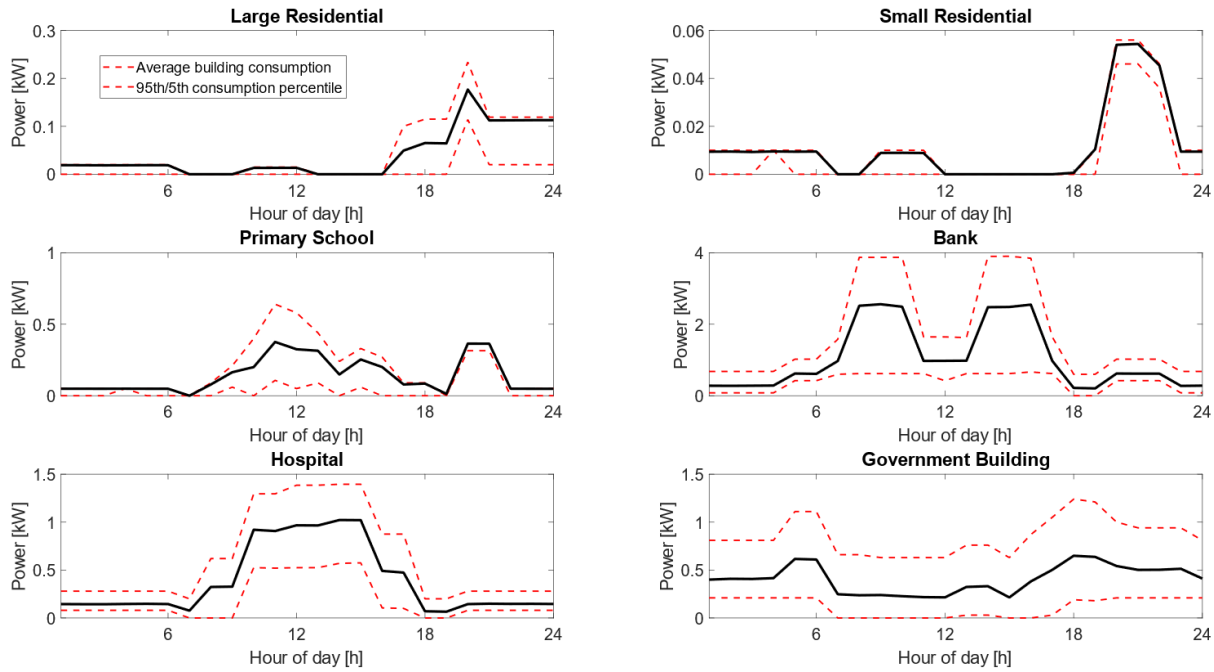

Figure 51: average consumption profile and hourly load variability for different types of users

For microgrids with low annual energy demand no ICE is installed, since the high specific cost of small size ICEs and their low generation efficiency make them not competitive with purely solar electricity generation plus storage. For PV-BESS only systems the annuity reduction attained with PA is between 2% and 4%, due to the relatively straightforward identification of an optimal dispatch strategy for non-complex systems (Figure 52). A transition zone can be observed for annual energy demand of about 75-100 MWh/year, where the architecture of the optimum design that is obtained by the two methods is different. Here, the PA includes an ICE in the system as opposed to a costlier PV-BESS system designed by the heuristic method. As the installation of an ICE becomes feasible, the advantage attained by the PA sharply increases to 6-9%, denoting the better ability of the proposed routine to manage the operational degree of freedom given by the engine, and of exploiting it in conjunction with the buffer capacity of the battery to optimize the ICE fuel consumption and battery wear (we acknowledge the advantage provided by the 24 hour perfect forecast). Finally, at even higher sizes both methods feature an ICE, but the PA consistently opts for a larger PV array, and manages to minimize PV curtailment and to optimize the usage of the smaller ICE by exploiting the flexibility granted by the adoption of a very large BESS.

Table 31: optimal heuristic and predictive microgrid design for different microgrid sizes

			HEURISTIC OPTIMA							PREDICTIVE OPTIMA						
Users	**Yearly Energy kWh**	**Peak-Power kW**	**BESS kWh**	**PV kW**	**ICE kW**	**CAPEX $**	**OPEX $**	**Annu-ity $**	**LCOE $/kWh**	**BESS kWh**	**PV kW**	**ICE kW**	**CAPEX $**	**OPEX $**	**Annu-ity $**	**LCOE $/kWh**
1	157.5	0.09	0.65	0.14	0	115.67	71.95	195.4	1.253	0.57	0.14	0	111.05	71.71	191.0	1.225
4	1027	0.65	4.18	1	0	451.36	85.94	558.3	0.534	3.94	1	0	435.68	84.81	543.8	0.518
12	3041	1.59	10.75	2.75	0	1124.6	112.8	1342	0.421	10.47	3	0	1139.3	112.4	1295	0.418
34	8245	5.04	32.9	8	0	3330.7	195.1	3686	0.436	30.9	7.75	0	3228.3	187.5	3607	0.424
101	24630	14.7	99.8	23	0	9576	436.4	10630	0.417	93.1	22.5	0	9285.5	413.3	10379	0.405
301	75150	44.1	291	70	0	28654	1163	31735	0.407	121	34.25	40	14716	14812	29550	0.393
894	2.31e5	131.3	127.6	62	100	26018	57396	85735	0.365	248.5	84.25	100	32526	46307	78996	0.342
2664	6.85e5	390.7	378.5	180	300	77145	1.62e5	2.45e5	0.353	692.1	231.8	300	91565	1.36e5	2.28e5	0.333
7940	2.08e6	1167	861.9	614	1000	2.22e5	4.93e5	7.26e5	0.346	2266	756.3	750	2.96e5	3.87e5	6.83e5	0.329
40810	1.07e7	6000	2950	3143	6000	1.06e6	2.65e6	3.74e6	0.348	10320	3607	4000	1.40e6	2.09e6	3.49e6	0.327

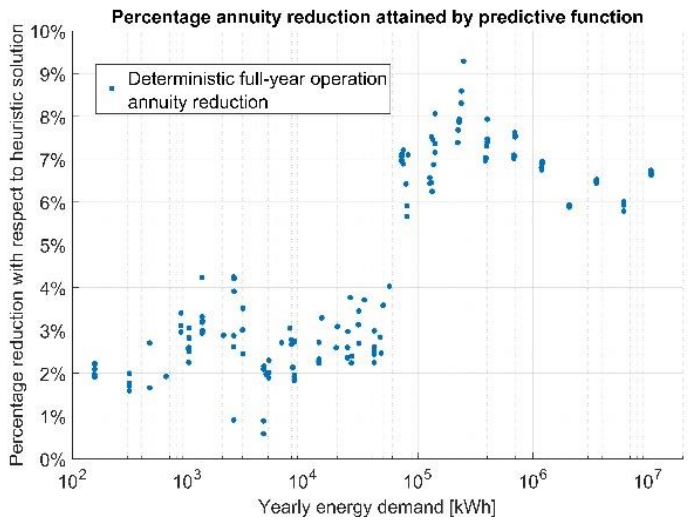

Figure 52: annuity reduction by adopting the predictive design algorithm for various microgrids

Figure 53 shows the LCOE trend and break-up as a function of microgrid size, for the HA and PA approaches (left and right stacks respectively). Economies of scale make larger microgrids cheaper per unit output. On the other hand, connecting users in areas with low density of demand will imply larger distribution networks with higher connection costs. BESS is the main cost for stand-alone and small microgrids while fuel is the major cost index for systems featuring an ICE. Therefore, an optimal dispatch of the engine is a key factor in reducing the total cost of microgrid design, explaining the increase in energy cost relative difference between HA and PA for large systems.

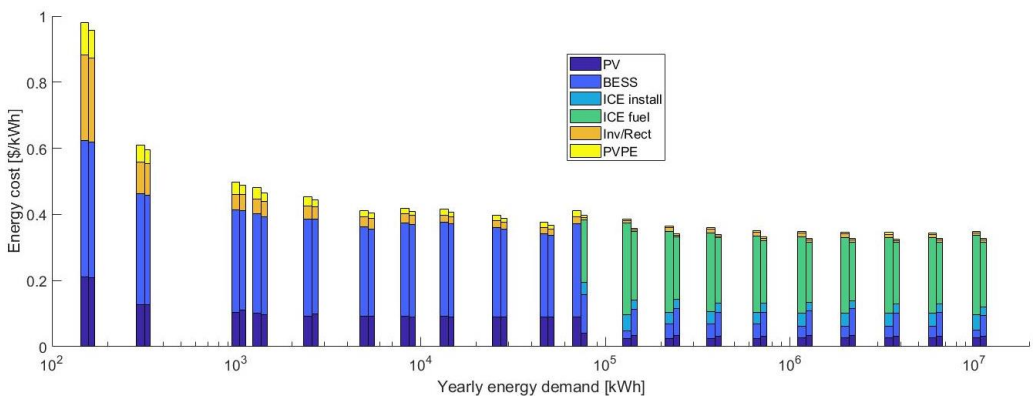

Figure 53: LCOE break-up for microgrid of increasing size, for heuristic (left bar) and predictive (right bar) optimal design

The optimal management of the ICE results in a higher percentage of production from renewable resources for large systems, consistently achieving a percentage of overall energy production from PV which is about 10 percentage points higher for the PA as reported in Figure 54-left. Finally, the predictive approach also results in higher average system reliability for small microgrids supplied by just PV and BESS and reaching a nearly 0% load shedding once an ICE is installed as reported in Figure 54-right. This reflects in an annuity reduction attained by the PA over the HA, which is generally greater than the corresponding LCOE reduction since, differently from the LCOE, the annuity explicitly accounts for the non-served energy penalty.

Including the integrated production planning of additional energy-related goods in addition to electricity, as proposed by the authors in [108], would increase the degrees of freedom exploitable by MILP optimization, and lead to even further energy cost reduction.

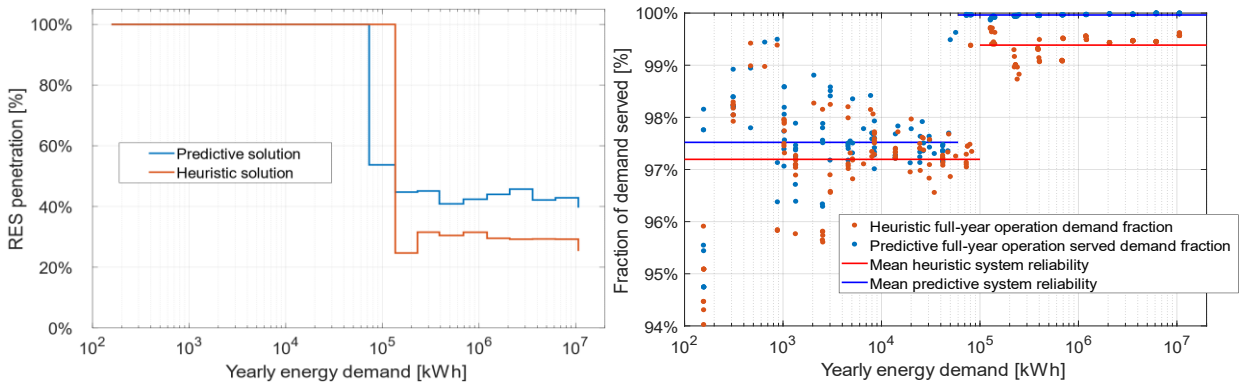

Figure 54: (left) renewable share of energy generation for microgrids of various sizes, (right) fraction of demand served in heuristic (red) and predictive (blue) optimal designs, for various microgrid sizes

8.8 Conclusions

This Chapter proposes a MILP-based approach to the optimal sizing of rural microgrids. The proposed Predictive Algorithm (PA) is based on the solution of a Mixed Integer Linear Program formulation of the Unit Commitment and Economic Dispatch problem accounting for discrete investment variables. The PA is compared with a Heuristic Algorithm (HA) evaluating the system operating profiles according to predefined heuristic dispatch rules and performing a search of the design space to identify the optimal design configuration. Both are applied to the local electrification of rural communities of a Sub-Saharan African region. The comparison between the two algorithm is performed by exploring the design of a large number of different microgrid instances, generated according to a reference library of class-specific loads, and encompassing a wide range of sizes and compositions. The analysis highlights how the main advantages of the PA with respect to HA are:

- The optimal design of PV and BESS is identified by the HA according to a modified pattern search method that may incur in local minima, as well as with the search of the optimal ICE. Multiple launching of the optimization process or examination of all the possible combinations of PV, BESS and ICE generally results in an unacceptable computational time. The PA method modifies the problem formulation with a linear approximation that allows computing the microgrid optimal design and dispatch by solving a *one-shot* MILP problem;
- The HA dispatch strategy is based on a heuristic rule that allows to deal with each time step independently from the others and ignores the consequences of these hourly decisions on the overall yearly performance. As a result, HA cannot develop dispatch strategies that account for component wear or annual constraints, for instance. The only option for HA is to penalize a-posteriori the solutions that do not satisfy these global criteria, potentially discarding optimal design configurations that, with proper dispatch decisions, would be capable of respecting the constraint.

- On the contrary, the PA method considers component design and operation dispatch jointly, as well as the entire optimization horizon. This allows PA to include easily component wearing costs and general constraints like a minimum annual system reliability or maximum fuel consumption. An obvious drawback of PA is that it assumes a perfect knowledge of uncertain events over the period of optimization. However, a realistic performance of the design obtained with PA can be obtained by simulating its operation with a predictive MILP optimization algorithm, following the Rolling Horizon approach. It remains for further research to take advantage of the "anticipative vision of the PA method" to design heuristic operation rules that mimic the optimal behavior observed in the solution given by PA.
- The numerous tests performed with both algorithms designing microgrids show that PA leads to a lower cost of electricity, a higher system reliability and a larger penetration of renewable energy for all the investigated cases. These advantages are more marked for more complex microgrid architectures that include an ICE in addition to PV and BESS, and in the presence of dispatchable loads or multi-commodity systems.

9 CONCLUSIONS

This doctoral thesis deals with the development and numerical evaluation of advanced formulations of the optimal scheduling problem for microgrids and Multi-Energy Systems (MES), based on Mixed Integer Linear Programming (MILP) techniques. The contribution of the thesis is articulated in four consecutive stages:

1. **Definition of versatile general MILP formulations for the predictive optimal scheduling of MES and MEMG.** Two alternative formulations are proposed: Chapter 3 presents a deterministic formulation of the scheduling problem, dealing with forecast uncertainty through the introduction of reserve constraints, while Chapter 4 introduces a more formal and explicit approach to uncertainty based on the Adjustable Robust Optimization theory;
2. **Comparative performance assessment exploring the adoption of the two proposed formulations for the optimal management of real-life systems.** Various architectures of two-layers EMS overseeing nominal operation scheduling and real-time dispatch are presented in Chapter 5 and Chapter 6, for three case studies characterized by means of experimental datasets; system performance is simulated accounting for realistic forecast profiles, generated according to various forecasting techniques; the actual performance of the proposed formulations is therefore assessed when confronted with the non-deterministic nature of the scheduling problem inputs;
3. **Development and numerical assessment of a two-layers MILP-based EMS for hybrid off-grid microgrids.** The EMS presented in Chapter 7 is developed for actual on-field implementation, defining a rule-based second layer algorithm that can be implemented on an industrial PLC; a response filter is introduced in the second layer, decoupling high and low-frequency net demand variations and imposing realistic load ramps on the generators; the effect of the non-linear variation of storage efficiency as function of storage power is also accounted for;
4. **Formulation of a discrete MILP-based design optimization algorithm for hybrid off-grid microgrids.** The design algorithm, presented in Chapter 8 and based on an adaptation of the deterministic optimal scheduling problem formulation, identifies the optimal design configuration solving an optimal design and operation problem over the design reference period, while a second level evaluates the actual performance associated to the identified optimal system architecture by simulating system operation over the entire typical year, following a Rolling Horizon approach;

The proposed definitions of the deterministic formulation Unit Commitment and Economic Dispatch problem are based on the state-of-the-art literature for MILP-based optimal scheduling models. Several innovative contributions are included in the formulations presented by this thesis. In the case of the deterministic formulation, the original enhancements include the definition of a flexible approach to model complex Multi-Energy Systems, and a discussion of alternative modeling techniques for the identified components classes, compatible with the MILP framework, but characterized by different levels of representativeness and computational cost. The Affinely Adjustable Robust formulation proposed in the thesis, with respect to the literature, features an advanced definition of the uncertainty set, the accounting of multiple internal uncertainty factors, and several ad hoc adjustments that can be implemented to reduce computational time,

one of the main drawbacks of adopting the robust formulation. Furthermore, an expedient to account for the recursive contribution of quick-start units without introducing binary recursive variables is proposed and discussed. Finally, a thorough critical examination of the limitations and intrinsic misrepresentations associated to the Affinely Adjustable Robust formulation of the scheduling problem is discussed, by identifying synthetic case studies to highlight limitations in the effectiveness of the recursive robust scheduling solution.

In Chapter 5 the adoption of the two MILP formulations within two-layers EMSs overseeing nominal operation scheduling and real-time dispatch is assessed, in the case of systems operating according to a day-ahead scheduling planning. Different second layer dispatch algorithms are proposed and tested. Three case studies are defined: an off-grid electric microgrid, and two grid-connected CHP systems, a Hospital a University Campus. Multiple system architectures are considered for the CHP systems, exploring various combination of flexible and non-flexible units, and thermal storage sizes.

In the off-grid electric microgrid case study, results show how the robust formulation is able to limit renewables curtailment and attain both a better nominal and recursive performance with respect to the conservative deterministic formulations when the commitment plan for generators must be planned at the beginning of the day. In this operating mode, despite the introduction of reserve constraints and regardless of which second layer algorithm is adopted, the deterministic formulation does not manage to consistently avoid service interruptions, while the robust formulation always grants 100% service reliability. In addition, savings attained in the total operating cost are as high as 10% for the robust formulation, as opposed to the deterministic formulation, for comparable levels of reliability. As the possibility of introducing real-time commitment changes is accounted for the usefulness of the robust formulation is reduced, as the deterministic formulation is able to ensure service continuity at a slightly lower cost (-2.7%) than the robust formulation.

In the Hospital case study, reliability is less of an issue for the deterministic formulations, if adequate reserve constraints are introduced, also in the case of non-modifiable unit commitment plan. Nevertheless, significant service interruptions are observed in this operating mode for particularly challenging system designs. If a simple priority-based strategy is considered to adjust the dispatch profile defined by the deterministic formulation, following the recursive decision rules identified by the adjustable robust formulation can ensure minor operational cost reduction (in the order of 1%) for most of the design configurations explored. Introducing a more advanced MILP-based second layer dispatch algorithm tends to uniform the performance of the two formulations under both assumptions of fixed and modifiable commitment plan.

In the Campus case study, which is characterized by a higher forecast uncertainty and by very large thermal storage sizes, the advantage of the robust formulation versus the deterministic formulation complemented by the priority-based correction logic is significantly higher, with operating cost savings in the order of 4%. As a consequence of higher forecast uncertainty, reliability is never achieved in any of the considered designs even when significantly increasing the nominal deterministic solution conservativeness, while the robust formulation effectively ensures service continuity. When accounting for scheduling plan

modifications, the results obtained for the Hospital are on the other hand confirmed, and the additional flexibility allows the deterministic formulation to attain lower operating costs and avoid the occurrence of non-served thermal energy.

More in general, the analysis developed in Chapter 5 indicates that resorting to the robust formulation for nominal day-ahead scheduling allows to effectively plan the commitment of the units, eliminating the need for real-time modifications to the commitment plan during the rest of the day. This is essential in situations where real-time adjustments to the commitment plan are unpractical or unfeasible, either due to the technical characteristics of the units or to the nature of the management system (e.g. systems with manual start-up of units). Furthermore, the recursive decision rules yield by the robust formulation provide a useful reference for the real-time management of dynamic components, defining a conservative trajectory that, although generally suboptimal, can serve as a useful reference to real-time dispatch algorithms in order to ensure system reliability. Conversely, in systems where the commitment status of units can be easily and rapidly changed and the nominal scheduling solution can be readily adjusted to account for the actual system evolution, the deterministic approach proves to be effective in identifying a less conservative and better performing operating schedule, while effectively coping with forecast uncertainty by means of adequately tuned reserve constraints. This is also true for systems featuring large storage units with high charge/discharge efficiency, that can limit the impact of incorrect nominal scheduling decisions and provide a redundant buffer that reduces the importance of correct unit commitment planning.

In Chapter 6 a more challenging case study for the off-grid electric microgrid is defined, introducing the more uncertain RES generation contribution of a wind farm, and envisioning the installment of a large size non-flexible biomass-fueled ORC power plant for base-load supply. The management problem is tackled according to a Rolling Horizon approach, ensuring the possibility of updating every three hours the nominal scheduling plan, but introducing a delay in the actuation of start-up commands which depends on the generator technology. Because of the increased problem uncertainty and of the more realistic assumption on start-up delays, the robust formulation proves to attain relevant advantages with respect to the deterministic formulation, leading to an overall operating cost 11.6% lower than the best performing deterministic formulation ensuring the same service reliability. Once again, the analysis confirms that when the capacity of the system to respond to forecast errors is reduced, even more so as the forecasts accuracy worsens, the deterministic formulation is not effective in identifying cost-effective and reliable scheduling solutions, while the robust formulation, in virtue of the explicit accounting of recursive dispatch corrections and of the feasibility guarantee over the uncertainty space, manages to combine adequate solution conservativeness while limiting the impact on the operating costs. Simulations also show how the Rolling Horizon approach can be beneficial to the identification of decision rules, which are “reset” at every new robust solution instance and do not have to account for wide combinations of concatenated forecast errors, which due to the feasibility requirement over any potential scenario falling within the uncertainty set tend to limit the optimality of recursive policies in timesteps farther from the initial solution time. The extensive simulation campaigns also demonstrated how, especially in systems characterized by significant uncertainty, the RH approach can preserve di effectiveness of predictive management optimization, while limiting to day-

ahead optimization, even more so if unit commitment adjustments like the one described in the Modifiable Unit Commitment operating modes depicted in Chapter 4 are not implemented.

The deterministic formulation is still used in Chapter 7 to propose a two-layers predictive EMS (P-EMS) for practical implementation in the control system of sub-Saharan off-grid hybrid microgrids, in virtue of its higher modeling flexibility (that allows to account for non-linearities) and very good performance when forecast uncertainty is limited. The EMS is based on the interaction of an upper MILP-based level with a rule-based second level suitable for direct implementation on a Programmable Logic Controller. Its performance is evaluated according to numerical simulations down to the minute temporal resolution on a real-life case study and compared with a heuristic management system (H-EMS) developed by the industrial partner operating the system. Results show how, if the current system design is considered, the two management algorithms attain a similar performance, with a reduction in fuel consumption granted by the P-EMS of only about 1%. As potential modifications to the system design are considered, a remarkable difference is observed between the two algorithms and the optimal system configuration associated to the deployment of the P-EMS scores an overall cost which is 6.5% lower than for the H-EMS, while at the same time reducing diesel consumption by 25%. Results confirm how adopting MILP-based formal scheduling optimization can have a significant impact in reducing costs and increasing penetration from renewable sources, allowing for an effective commitment of generation resources and for the strategic management of batteries to anticipate the availability of RES generation, limiting RES curtailment and maximizing the added value of storage systems.

Finally, an innovative MILP-based design algorithm based on an adaptation of the deterministic formulation of the scheduling problem is proposed in Chapter 8, and compared with a heuristic algorithm developed at MIT. The two algorithms are evaluated for the design of a large number of microgrids ranging different electrical sizes, in the context of regional electrification of a sub-Saharan African region. With respect to the heuristic approach, the MILP-based algorithm proves to be effective both in reducing costs, particularly in larger systems that feature a dispatchable generator, associated with more complex and flexible scheduling. Once again, in addition to remarkable cost reductions, resorting to MILP optimization also allows to attain higher penetration from RES, as well as increasing service reliability for off-grid customers.

9.1 Future works

Future developments of this doctoral thesis involve both the experimental testing of the proposed algorithms, as well as methodological improvements to the optimal problem definition and solution.

Specifically, the Laboratory of Microgrids [109] was inaugurated on September 2018 at the Politecnico di Milano Energy Department. The experimental facility currently features two 25 kW_p PV arrays, a 25 kW_{el} CHP natural gas engine, a 6 kW_{el} water purifier, a recharge station for electric cars and electric bikes, and will be further expanded within 2019 including additional thermal generation and storage units (two 6 kW_{el} electric heat pumps and a 50L thermal storage), an additional PV field. An improved version of the algorithm presented in Chapter 7 including in the management problem the optimal scheduling of the water purifier has already been implemented in the microgrid PLC, and an experimental campaign is currently

undergoing to experimentally validate the numerical results and continue the comparison with more traditional approaches to system management.

The solution approach pursued in this thesis for the AARO problem formulation highlighted how the inclusion of recursive binary variables has the potential of significantly increasing the performance of the formulation, overcoming the modeling limitations highlighted for the current formulation and allowing for the definition of more performing decision rules, which could potentially serve as an increasingly precise reference for real-time system dispatch. To do so, it is necessary to change the solution approach to the problem, renouncing to the definition of the tractable reformulation of the robust counterpart and resorting to cutting planes algorithms for the solution of the problem. The formulation improvements proposed in this work to limit computational time can still be very effective in counterbalancing the computational complexity that a more advanced formulation of the recursive problem will inevitably imply.

Finally, exploring the third option of MILP-based scheduling problem formulation represented by stochastic optimization is necessary to complete the evaluation of methodological instruments to tackle predictive scheduling optimization accounting for forecast uncertainty. Stochastic optimization has been investigated by the research group in the work-frame of design optimization [110], and activities of the MGL are currently focusing on the development of a predictive second layer for the real-time experimental microgrid control according to stochastic Model Predictive Control (MPC) theory.

10 REFERENCES

[1] "Chapter Climate Change 2014 Synthesis Report Summary for Policymakers Summary for Policymakers."

[2] IEA, "World Energy Outlook 2018: Electricity," *Iea*, 2018.

[3] V. Masson-Delmotte *et al.*, "Global warming of 1.5°C."

[4] "Energy use (kg of oil equivalent per capita) | Data." [Online]. Available: https://data.worldbank.org/indicator/EG.USE.PCAP.KG.OE?most_recent_value_desc=true. [Accessed: 06-Jun-2019].

[5] BP, "BP Statistical Review of World Energy."

[6] T. Mai *et al.*, "Electrification Futures Study: Scenarios of Electric Technology Adoption and Power Consumption for the United States."

[7] IRENA, "Renewable Power Generation Costs in 2017," *Int. Renew. Energy Agency*, 2018.

[8] Giorgio, "Electricity Transmission and Distribution HIGHLIGHTS PROCESS AND TECHNOLOGY STATUS."

[9] A. M. Carreiro, H. M. Jorge, and C. H. Antunes, "Energy management systems aggregators: A literature survey," *Renew. Sustain. Energy Rev.*, vol. 73, pp. 1160–1172, Jun. 2017.

[10] International Energy Agency, "Digitalization & Energy," 2017.

[11] S. Diego, "Office of Electricity Delivery and Energy Reliability Smart Grid R&D Program DOE Microgrid Workshop Report."

[12] P. Mancarella, "MES (multi-energy systems): An overview of concepts and evaluation models," *Energy*, vol. 65, pp. 1–17, Feb. 2014.

[13] D. Herman, "EPRI Project Manager Investigation of the Technical and Economic Feasibility of Micro-Grid-Based Power Systems," 2001.

[14] T. Hawaiian Electric Company, "2019 Power Facts."

[15] "ES-2 Hawaiian Electric Companies."

[16] "Electricity Rates by State (May 28, 2019) | ChooseEnergy.com®." [Online]. Available: https://www.chooseenergy.com/electricity-rates-by-state/. [Accessed: 05-Jun-2019].

[17] UN, "Energy for a Sustainable Future. Report and Recommendations.," New York, 2010.

[18] S. C. Bhattacharyya, "Electrification Experiences from Sub-Saharan Africa," in *Rural electrification through decentralised off-grid systems in developing countries*, Springer, London, 2013, pp. 131–156.

[19] S. Mandelli, J. Barbieri, R. Mereu, and E. Colombo, "Off-grid systems for rural electrification in developing countries: Definitions, classification and a comprehensive literature review," *Renew. Sustain. Energy Rev.*, vol. 58, pp. 1621–1646, May 2016.

[20] J. P. Murenzi and T. S. Ustun, "The case for microgrids in electrifying Sub-Saharan Africa," in *IREC2015 The Sixth International Renewable Energy Congress*, 2015, pp. 1–6.

[21] S. Szabó, K. Bódis, T. Huld, and M. Moner-Girona, "Energy solutions in rural Africa: mapping electrification costs of distributed solar and diesel generation versus grid extension Energy solutions in rural Africa: mapping electrification costs of distributed solar and diesel generation versus grid extensi," *Environ. Res. Lett. Environ. Res. Lett*, vol. 6, pp. 34002–9, 2011.

[22] K. Ubilla *et al.*, "Smart Microgrids as a Solution for Rural Electrification: Ensuring Long-Term Sustainability Through Cadastre and Business Models," *IEEE Trans. Sustain. Energy*, vol. 5, no. 4, pp. 1310–1318, Oct. 2014.

[23] P. Del Rıó and M. Burguillo, "Assessing the impact of renewable energy deployment on local sustainability: Towards a theoretical framework," *Renew. Sustain. Energy Rev.*, vol. 12, pp. 1325–1344, 2008.

[24] "5.9 MW cutting-edge wind and solar microgrid – ENGIE Eps." [Online]. Available: https://engie-eps.com/project/5-9-mw-cutting-edge-wind-and-solar-microgrid-somalia/. [Accessed: 05-Jun-2019].

[25] P. Asmus, "Microgrids, Virtual Power Plants and Our Distributed Energy Future," *Electr. J.*, vol. 23, no. 10, pp. 72–82, Dec. 2010.

[26] S. M. Nosratabadi, R. A. Hooshmand, and E. Gholipour, "A comprehensive review on microgrid and virtual power plant concepts employed for distributed energy resources scheduling in power systems," *Renewable and Sustainable Energy Reviews*. 2017.

[27] L. Meng, E. R. Sanseverino, A. Luna, T. Dragicevic, J. C. Vasquez, and J. M. Guerrero, "Microgrid supervisory controllers and energy management systems: A literature review," *Renew. Sustain. Energy Rev.*, vol. 60, pp. 1263–1273, 2016.

[28] E. Planas, A. Gil-De-Muro, J. Andreu, I. Igo Kortabarria, and I. Igo Martínez De Alegría, "General aspects, hierarchical controls and droop methods in microgrids: A review," *Renew. Sustain. Energy Rev.*, vol. 17, pp. 147–159, 2013.

[29] D. E. Olivares *et al.*, "Trends in microgrid control," *IEEE Trans. Smart Grid*, vol. 5, no. 4, pp. 1905–1919, 2014.

[30] A. Engler and N. Soultanis, "Droop control in LV-grids," *2005 Int. Conf. Futur. Power Syst.*, pp. 6 pp. – 6, 2005.

[31] M. F. Zia, E. Elbouchikhi, and M. Benbouzid, "Microgrids energy management systems: A critical review on methods, solutions, and prospects," *Appl. Energy*, vol. 222, pp. 1033–1055, Jul. 2018.

[32] A. Books, "hierarchical power systems control its value in a changing industry."

[33] Q. Li, F. Chen, M. Chen, J. M. Guerrero, and D. Abbott, "Agent-Based Decentralized Control Method for Islanded Microgrids," *IEEE Trans. Smart Grid*, vol. 7, no. 2, pp. 637–649, 2016.

[34] C.-S. Karavas, G. Kyriakarakos, K. G. Arvanitis, and G. Papadakis, "A multi-agent decentralized energy management system based on distributed intelligence for the design and control of autonomous polygeneration microgrids," *Energy Convers. Manag.*, vol. 103, pp. 166–179, Oct. 2015.

[35] T. Logenthiran, D. Srinivasan, and A. M. Khambadkone, "Multi-agent system for energy resource scheduling of integrated microgrids in a distributed system," *Electr. Power Syst. Res.*, vol. 81, no. 1, pp. 138–148, Jan. 2011.

[36] A. L. Dimeas and N. D. Hatziargyriou, "Operation of a Multiagent System for Microgrid Control," *IEEE Trans. Power Syst.*, vol. 20, no. 3, pp. 1447–1455, Aug. 2005.

[37] A. G. Tsikalakis and N. D. Hatziargyriou, "Centralized control for optimizing microgrids operation," in *2011 IEEE Power and Energy Society General Meeting*, 2011, pp. 1–8.

[38] C. Dennis and C. B. Winn, "OPTIMAL DISPATCH STRATEGY IN REMOTE HYBRID POWER SYSTEMS," 1996.

[39] A. Haghrah, M. Nazari-Heris, and B. Mohammadi-ivatloo, "Solving combined heat and power economic dispatch problem using real coded genetic algorithm with improved Mühlenbein mutation," *Appl. Therm. Eng.*, vol. 99, pp. 465–475, Apr. 2016.

[40] M. Nemati, M. Braun, and S. Tenbohlen, "Optimization of unit commitment and economic dispatch in microgrids based on genetic algorithm and mixed integer linear programming," *Appl. Energy*, vol. 210, pp. 944–963, Jan. 2018.

[41] G. S. Piperagkas, A. G. Anastasiadis, and N. D. Hatziargyriou, "Stochastic PSO-based heat and power dispatch under environmental constraints incorporating CHP and wind power units," *Electr. Power Syst. Res.*, vol. 81, no. 1, pp. 209–218, Jan. 2011.

[42] Z. Wu, W. Gu, R. Wang, X. Yuan, and W. Liu, "Economic optimal schedule of CHP microgrid system using chance constrained programming and particle swarm optimization," in *2011 IEEE Power and Energy Society General Meeting*, 2011, pp. 1–11.

[43] M. Marzband, E. Yousefnejad, A. Sumper, and J. L. Domínguez-García, "Real time experimental implementation of optimum energy management system in standalone Microgrid by using multi-layer ant colony optimization," *Int. J. Electr. Power Energy Syst.*, vol. 75, pp. 265–274, Feb. 2016.

[44] S. Mazzola, C. Vergara, M. Astolfi, V. Li, I. Perez-Arriaga, and E. Macchi, "Assessing the value of forecast-based dispatch in the operation of off-grid rural microgrids," *Renew. Energy*, vol. 108, pp. 116–125, Aug. 2017.

[45] A. Bischi *et al.*, "A detailed MILP optimization model for combined cooling, heat and power system operation planning," *Energy*, vol. 74, pp. 12–26, 2014.

[46] J. R. Birge and F. Louveaux, *Introduction to Stochastic Programming*. Springer New York, 2006.

[47] M. Alipour, B. Mohammadi-Ivatloo, and K. Zare, "Stochastic Scheduling of Renewable and CHP-Based Microgrids," *IEEE Trans. Ind. Informatics*, vol. 11, no. 5, pp. 1049–1058, Oct. 2015.

[48] G. Martinez, N. Gatsis, and G. B. Giannakis, "Stochastic programming for energy planning in microgrids with renewables," in *2013 5th IEEE International Workshop on Computational Advances in Multi-Sensor Adaptive Processing (CAMSAP)*, 2013, pp. 472–475.

[49] G. Cardoso *et al.*, "Microgrid reliability modeling and battery scheduling using stochastic linear programming," *Electr. Power Syst. Res.*, vol. 103, pp. 61–69, Oct. 2013.

[50] A. Ben-Tal, L. El Ghaoui, and A. Nemirovski, *Robust optimization*. Princeton University Press, 2009.

[51] D. Bertsimas, D. B. Brown, and C. Caramanis, "Theory and Applications of Robust Optimization," *SIAM Rev.*, vol. 53, no. 3, pp. 464–501, 2011.

[52] I. Yu Zhang, Student Member, IEEE,Nikolaos Gatsis, Member, IEEE, and Georgios B. Giannakis, Fellow, "Robust Energy Management for Microgrids With High-Penetration Renewables," vol. 4, no. 4, pp. 944–953, 2013.

[53] D. Bertsimas, E. Litvinov, X. A. Sun, J. Zhao, and T. Zheng, "Adaptive Robust Optimization for the Security Constrained Unit Commitment Problem," *IEEE Trans. Power Syst.*, vol. 28, no. 1, pp. 52–63, 2013.

[54] M. Zugno, J. M. Morales, and H. Madsen, "Commitment and Dispatch of Heat and Power Units via Affinely Adjustable Robust Optimization," *Comput. Oper. Res.*, vol. 75, pp. 191–201, 2016.

[55] X. Lü, T. Lu, C. J. Kibert, and M. Viljanen, "Modeling and forecasting energy consumption for heterogeneous buildings using a physical–statistical approach," *Appl. Energy*, vol. 144, pp. 261–275, Apr. 2015.

[56] S. Idowu, S. Saguna, C. Åhlund, and O. Schelén, "Applied machine learning: Forecasting heat load in district heating system," *Energy Build.*, vol. 133, pp. 478–488, 2016.

[57] L. Hern Andez, C. Baladr On, J. M. Aguiar, B. En Carro, A. S. Anchez-Esguevillas, and J. Lloret, "Artificial neural networks for short-term load forecasting in microgrids environment," *Energy*, vol. 75, pp. 252–264, 2014.

[58] S. J. Huang and K. R. Shih, "Short-term load forecasting via ARMA model identification including non-Gaussian process considerations," *IEEE Trans. Power Syst.*, vol. 18, no. 2, pp. 673–679, 2003.

[59] R. Lahdelma and H. Hakonen, "An efficient linear programming algorithm for combined heat and power production," *Eur. J. Oper. Res.*, vol. 148, no. 1, pp. 141–151, Jul. 2003.

[60] J. F. Manwell and G. Jon, "Lead acid battery storage model for hybrid energy systems," *Sol. Energy*, vol. 50, no. 5, pp. 399–405, 1993.

[61] R. Simonetti, "Experimental and analytical study of solar-assisted heat pump," Politecnico di Milano, 2019.

[62] R. Simonetti, L. Moretti, L. Molinaroli, and G. Manzolini, "Energetic and economic optimization of the yearly performance of three different solar assisted heat pump systems using a mixed integer linear programming algorithm," *Submitt. to Energy Convers. Manag.*

[63] D. Bertsimas and M. Sim, "The Price of Robustness," 2001.

[64] A. Lorca and X. A. Sun, "Adaptive Robust Optimization With Dynamic Uncertainty Sets for Multi-Period Economic Dispatch Under Significant Wind," *IEEE Trans. Power Syst.*, vol. 30, no. 4, pp. 1702–1713, Jul. 2015.

[65] C. Ning and F. You, "Data-Driven Adaptive Robust Unit Commitment Under Wind Power Uncertainty: A Bayesian Nonparametric Approach," *IEEE Trans. Power Syst.*, vol. 34, no. 3, pp. 2409–2418, May 2019.

[66] D. Bertsimas and A. Georghiou, "Design of Near Optimal Decision Rules in Multistage Adaptive Mixed-Integer Optimization," *Oper. Res.*, vol. 63, no. 3, pp. 610–627, 2015.

[67] B. Hu and L. Wu, "Robust SCUC considering continuous/discrete uncertainties and quick-start units: A two-stage robust optimization with mixed-integer recourse," in *2016 IEEE Power and Energy Society General Meeting (PESGM)*, 2016, pp. 1–1.

[68] L. Zhao and B. Zeng, "An Exact Algorithm for Two-stage Robust Optimization with Mixed Integer Recourse Problems," *Submitt. available http//www.optimization-online.org/DB_FILE/2012/01/3310.pdf*, pp. 1–16, 2012.

[69] D. Bertsimas and I. Dunning, "Multistage Robust Mixed-Integer Optimization with Adaptive Partitions," *Oper. Res.*, vol. 64, no. 4, pp. 980–998, 2016.

[70] M. Zatti, M. Gabba, M. Rossi, M. Morini, A. Gambarotta, and E. Martelli, *Towards the optimal design and operation of multi-energy systems: the efficity project*, vol. 17, no. 10. Environmental Engineering & Management Journal, 2002.

[71] Á. Lorca, X. Andy Sun, E. Litvinov, T. Zheng, O. Research, and X. H. Andy Sun Milton Stewart, "Multistage Adaptive Robust Optimization for the Unit Commitment Problem," *Oper. Res.*, vol. 64, no. 1, pp. 32–51, 2016.

[72] "Data Analysis Toolkit #5: Uncertainty Analysis and Error Propagation," 1995.

[73] M. Zatti *et al.*, "k-MILP: A novel clustering approach to select typical and extreme days for multi-energy systems design optimization," *Energy*, vol. 181, pp. 1051–1063, May 2019.

[74] A. Gambarotta, M. Morini, M. Rossi, and M. Stonfer, "A Library for the Simulation of Smart Energy Systems: The Case of the Campus of the University of Parma," *Energy Procedia*, vol. 105, pp. 1776–1781, May 2017.

[75] "GME - Download - - EXCEL HISTORICAL DATA." [Online]. Available: https://www.mercatoelettrico.org/En/download/DatiStorici.aspx. [Accessed: 14-May-2019].

[76] L. Grippo, A. Manno, and M. Sciandrone, "Decomposition Techniques for Multilayer Perceptron Training," *IEEE Trans. Neural Networks Learn. Syst.*, vol. 27, no. 11, pp. 2146–2159, Nov. 2016.

[77] S. Leva, A. Dolara, F. Grimaccia, M. Mussetta, and E. Ogliari, "Analysis and validation of 24 hours ahead neural network forecasting of photovoltaic output power," *Math. Comput. Simul.*, vol. 131, pp. 88–100, Jan. 2017.

[78] L. Moretti, S. Polimeni, L. Meraldi, P. Raboni, S. Leva, and G. Manzolini, "Assessing the impact of a two-layer predictive dispatch algorithm on design and operation of off-grid hybrid microgrids," *Renew. Energy*, May 2019.

[79] L. Hernandez *et al.*, "A Survey on Electric Power Demand Forecasting: Future Trends in Smart Grids, Microgrids and Smart Buildings," *IEEE Commun. Surv. Tutorials*, vol. 16, no. 3, pp. 1460–1495, 2014.

[80] J. Antonanzas, N. Osorio, R. Escobar, R. Urraca, F. J. Martinez-De-Pison, and F. Antonanzas-Torres, "Review of photovoltaic power forecasting," *Sol. Energy*, vol. 136, pp. 78–111, 2016.

[81] J. M. Guerrero, J. C. Vasquez, J. Matas, L. G. de Vicuna, and M. Castilla, "Hierarchical Control of Droop-Controlled AC and DC Microgrids—A General Approach Toward Standardization," *IEEE Trans. Ind. Electron.*, vol. 58, no. 1, pp. 158–172, Jan. 2011.

[82] T. Lambert, P. Gilman, and P. Lilienthal, "Micropower System Modeling with Homer," in *Integration of Alternative Sources of Energy*, Wiley-IEEE Press, 2006, pp. 379–418.

[83] A. Dolara, F. Grimaccia, G. Magistrati, and G. Marchegiani, "Optimization Models for Islanded Micro-Grids: A Comparative Analysis between Linear Programming and Mixed Integer Programming," *Energies*, vol. 10, no. 2, p. 241, Feb. 2017.

[84] J. Sachs and O. Sawodny, "A Two-Stage Model Predictive Control Strategy for Economic Diesel-PV-Battery Island Microgrid Operation in Rural Areas," *IEEE Trans. Sustain. Energy*, vol. 7, no. 3, pp. 903–913, Jul. 2016.

[85] C. A. Hans, P. Sopasakis, A. Bemporad, J. Raisch, and C. Reincke-Collon, "Scenario-based model predictive operation control of islanded microgrids," in *2015 54th IEEE Conference on Decision and Control (CDC)*, 2015, pp. 3272–3277.

[86] G. E. P. Box and J. M. Jenkins, *Time series analysis, Forecasting and Control*. Holden-Day, Inc., 1990.

[87] T. Ozaki, "On the Order Determination of ARIMA Models," *J. R. Stat. Soc. Ser. C (Applied Stat.*, vol. 26, no. 3, pp. 290–301, 1977.

[88] E. Ogliari, A. Dolara, G. Manzolini, and S. Leva, "Physical and hybrid methods comparison for the day ahead PV output power forecast," *Renew. Energy*, vol. 113, pp. 11–21, Dec. 2017.

[89] L. Moretti, M. Astolfi, C. Vergara, E. Macchi, J. I. Pérez-Arriaga, and G. Manzolini, "A design and dispatch optimization algorithm based on mixed integer linear programming for rural electrification," *Appl. Energy*, vol. 233–234, pp. 1104–1121, Jan. 2019.

[90] IRENA, "Electricity Storage And Renewables: Costs And Markets to 2030," 2017.

[91] "Computer-aided electrification planning in developing countries: The Reference Electrification Model (REM)."

[92] V. Li, "The Local Reference Electrification Model : comprehensive decision-making tool for the design of rural microgrids," Massachusetts Institute of Technology, Boston, 2016.

[93] A. G. Dagnachew, P. L. Lucas, A. F. Hof, D. E. H. J. Gernaat, H.-S. de Boer, and D. P. van Vuuren, "The role of decentralized systems in providing universal electricity access in Sub-Saharan Africa – A model-based approach," *Energy*, vol. 139, pp. 184–195, Nov. 2017.

[94] F. F. Nerini, O. Broad, D. Mentis, M. Welsch, M. Bazilian, and M. Howells, "A cost comparison of technology approaches for improving access to electricity services," *Energy*, vol. 95, 2016.

[95] A. Chauhan and R. P. Saini, "A review on Integrated Renewable Energy System based power generation for stand-alone applications: Configurations, storage options, sizing methodologies and control," *Renew. Sustain. Energy Rev.*, vol. 38, pp. 99–120, 2014.

[96] M. Husein and I.-Y. Chung, "Optimal design and financial feasibility of a university campus microgrid considering renewable energy incentives," *Appl. Energy*, vol. 225, pp. 273–289, Sep. 2018.

[97] "HOMER - Hybrid Renewable and Distributed Generation System Design Software." [Online]. Available: https://www.homerenergy.com/. [Accessed: 31-Jul-2018].

[98] S. Mazzola, M. Astolfi, and E. Macchi, "The potential role of solid biomass for rural electrification: A techno economic analysis for a hybrid microgrid in India," *Appl. Energy*, vol. 169, pp. 370–383, 2016.

[99] Lawrence Berkeley National Laboratory, "Distributed Energy Resources - Customer Adoption Model (DER-CAM) | Building Microgrid." [Online]. Available: https://building-microgrid.lbl.gov/projects/der-cam. [Accessed: 06-Aug-2018].

[100] L. Ferrer-Martí, B. Domenech, A. García-Villoria, and R. Pastor, "A MILP model to design hybrid wind-photovoltaic isolated rural electrification projects in developing countries," *Eur. J. Oper. Res.*, vol. 226, pp. 293–300, 2013.

[101] E. D. Mehleri, H. Sarimveis, N. C. Markatos, and L. G. Papageorgiou, "Optimal design and operation of distributed energy systems: Application to Greek residential sector," *Renew. Energy*, vol. 51, pp. 331–342, 2013.

[102] V. Salas, W. Suponthana, and R. A. Salas, "Overview of the off-grid photovoltaic diesel batteries systems with AC loads," *Appl. Energy*, vol. 157, pp. 195–216, 2015.

[103] "Universal Access Lab - MIT & IIT-Comillas." [Online]. Available: http://universalaccess.mit.edu/#/main. [Accessed: 13-Feb-2018].

[104] P. Gabrielli, M. Gazzani, E. Martelli, and M. Mazzotti, "Optimal design of multi-energy systems with seasonal storage," *Appl. Energy*, vol. 219, pp. 408–424, Jun. 2018.

[105] J. Lofberg, "YALMIP : a toolbox for modeling and optimization in MATLAB," *2004 IEEE Int. Conf. Comput. Aided Control Syst. Des.*, pp. 284–289, 2004.

[106] R. Hooke and T. A. Jeeves, "`` Direct Search'' Solution of Numerical and Statistical Problems," *J. ACM*, vol. 8, no. 2, pp. 212–229, Apr. 1961.

[107] D. Ellman, "The Reference Electrification Model: A Computer Model for Planning Rural Electricity Access," Massachusetts Institute of Technology, Boston, 2015.

[108] M. Astolfi, S. Mazzola, P. Silva, and E. Macchi, "A synergic integration of desalination and solar energy systems in stand- alone microgrids," *Desalination*, vol. 419, pp. 169–180, Oct. 2017.

[109] "Laboratory of Microgrids – GECOS Webpage." [Online]. Available: http://www.gecos.polimi.it/laboratories/laboratory-of-microgrids/. [Accessed: 17-Jun-2019].

[110] M. Zatti, E. Martelli, and E. Amaldi, "A three-stage stochastic optimization model for the design of smart energy districts under uncertainty," *Comput. Aided Chem. Eng.*, vol. 40, pp. 2389–2394, Jan. 2017.